NOTE TO USERS

DESIGN OPTIMIZATION AND VIBRATION CONTROL OF ADAPTIVE STRUCTURES

Aurelio Domínguez-González

A Thesis

in

the Department

of

Mechanical and Industrial Engineering

Presented in Partial Fulfillment of the Requirements

for the Degree Of Doctor Of Philosophy at

Concordia University

Montreal, Quebec, Canada

June, 2004

Your file Votre référence
ISBN: 0-494-09975-5
Our file Notre référence
ISBN: 0-494-09975-5

ABSTRACT

Design optimization and vibration control of adaptive structures

Aurelio Domínguez-González, Ph. D.
Concordia University, 2005

In the present research work the optimization of structures and the vibration suppression are studied. First, a methodology to find the simultaneous size, geometry and topology design optimization of structures using Genetic Algorithms (GAs) is proposed. The methodology considers that the large structures are constructed from the duplication of some basic structures called bays. In order to have realistic optimal designs, the cross-sectional areas are extracted from the standard profiles and the optimization process is performed considered the AISC design standards.

The second part of the work is concerned with the suppression of the vibration in structural systems. A methodology to find the characteristic parameters of the Bouc-Wen model in the attempt to better characterize the hysteresis phenomenon of MR dampers has been proposed. The methodology takes into consideration the effect of each individual term of the Bouc-Wen model over the hysteretic loop to estimate the appropriate values of the parameters. Considering the relationships of the characteristic parameters, a new model based on the Bouc-Wen model is proposed in which the current, the frequency and the amplitude excitation are incorporated as variables. Based on the proposed hysteresis model, a Finite Element Model (FEM) for the MR damper is developed and then integrated to the FEM of the entire structure. Subsequently, an efficient vibration suppression strategy using MR damper was proposed to improve the

vibration performance index of the structure. Finally, the same hysteresis model is employed to investigate the application of MR dampers as translational actuator.

ACKNOWLEDGEMENT

I am grateful to my loving wife, Gaby, for her inspiration and moral support throughout my research work. Her patience was tested to the utmost by a long period of separation. Without her amorous support and understanding I would never have completed my present work. Particularly, I owe to my little kids, Cary and Llello, for their silent prayer for my work at the time when they needed my company most.

I also want to thank my parents, who taught me the value of hard work by their own example. I would like to share this moment of happiness with my brothers, sisters, nephews, nieces and family in law. They rendered me enormous support during the whole tenure of my research.

I am very thankful and indebted to my co-supervisors Dr. Ramin Sedaghati and Dr. Ion Stiharu for their encouragement, constructive instruction and support. They generously provided their time and effort in the guidance and completion of my thesis research. My gratitude is also extended to Dr. Subash Rakheja who has offered helpful and constructive comments in this work.

I acknowledge to my colleague Mrs. Xiao Qing Ma who kindly provided me the experimental data of the MR damper. Also I am thankful to Dr. Yvan Soucy and Canadian Space Agency who generously provide the hardware of the structure. I appreciate the helpful technical support of Mr. Danious Juras. Finally, I would like to thank all who directly or indirectly supported and helped me to complete my thesis.

TABLE OF CONTENTS

LIST OF TABLES

LIST OF FIGURES

NOMENCLATURE

c_0	Damping of the MR damper
$\boldsymbol{C}$	Damping matrix
E	Young Modulus
f	Objective function
$\boldsymbol{F}$	Force vector
$\boldsymbol{F}_{MR}$	Force of MR damper
F_z	Evolutionary force of MR damper
$\boldsymbol{I}$	Identity matrix
k_0	Stiffness of the MR damper
$\boldsymbol{K}$	Stiffness matrix
$\mathbf{M}$	Mass matrix
p	Penalty function
p_r	Probability of reproduction
p_m	Probability of mutation
p_c	Probability of crossover
$\boldsymbol{p}$	Penalty function
r	Radius of gyration
$\boldsymbol{W}$	Diagonal penalty weighting matrix
$\mathbf{x}$	Displacement vector
$\dot{x}$	Velocity vector
$\ddot{x}$	Acceleration vector
α, β, γ, A	Bouc-Wen constants
λ	Slenderness ratio
σ	Stress
ε	Strain
ρ	Density

Subscripts

u	Upper
l	Lower
MR	Magnetorheological
min	Minimum
max	Maximum
0	Initial value of the variable

CHAPTER 1
INTRODUCTION

Finding the best or optimum design is an important and challenging task which is the ultimate goal of all structural or mechanical designers. Conventionally, the intuition, experience and repeated trials and errors are ad-hoc optimization tools employed to reach this goal. The existence of many fine buildings and aerospace achievements is the evidence of these ad-hoc optimization solutions (ASCE 1997). However, in the latter half of past century, considerable advances have taken place in computer methods for analysis and design that can be of substantial aid to the designer in the creative process of designing and finding the true optimum solution. Furthermore, the technological advances in materials have developed new kind of actuators, which are installed and controlled to improve the performance of the structures under changing environments.

1.1. Motivation and objectives

The proposed research involves fundamental investigations in optimization and semi-adaptive vibration control of adaptive structures making use of the MR-dampers. The traditional passive structures cannot modify their response mechanisms and are thus unable to perform successfully when they are subjected to changing load conditions. Such limitations have motivated considerable interest in developing a new class of structures called adaptive structures, which can modify their shapes or mechanical properties in a controlled manner to accommodate unpredictable environmental changes. Fundamental research is conducted and computational and experimental models based on

the mathematical foundation are developed to optimize the designs and control the response of semi-adaptive structures under environmental changes.

The dynamic response control of truss structures has drawn increasing attention due to their possible application to lightweight space structures (Kida et al. 2000). When a space structure becomes large and flexible, a large magnitude of dynamic response occurs, and this negatively affects the precise attitude and shape characteristics of the entire space structural system. The structural optimization is a challenging area. In order to gain appreciation of the complexity of the structural optimization, a very simple topology optimization problem is presented (Anthony et al. 2000).

Figure 1.1 shows a cantilever structure, which has a harmonic excitation of 1 N over the element 1. The structure is a typical application of an antenna boom arm for use on a satellite. The aim is to reduce the transmission of vibrations from the base to the element 40, where the antenna would be mounted in practice; thus, the objective function is to minimize the vibration energy in the end element. In this structure, the design variables are the coordinates of node located at the position (4,1) which can accept variations +/- 0.25 m in both axis.

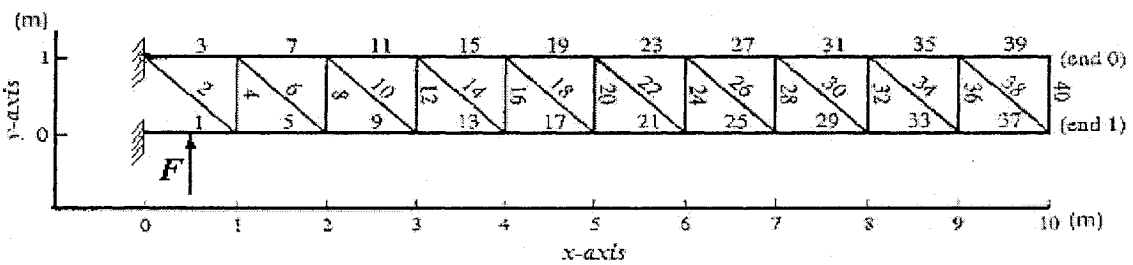

Figure 1.1. 40-elements truss plane structure (Anthony et al 2000).

The Figure 1.2 shows the contour of the objective function against the adjustment of joint (4,1) within the optimization limits. From this plot, it is possible to imagine the complexity of the optimization in structures when all the nodes are included as design variables. Furthermore, the problem is really challenging when semi-active control or active control is added and the positions and number of actuators is taken into account as design variables. In conclusion, the dynamic structural optimization is a high non-unimodal discrete and multi-parametric problem.

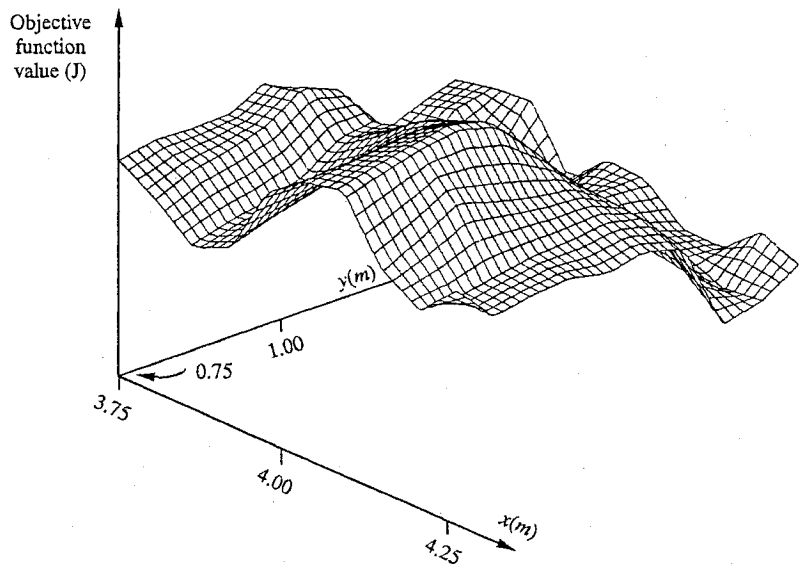

Figure 1.2. Contour plot of the objective function within feasible domain (Anthony et al 2000).

The natural hazards through a combination of strength, deformability and energy absorption must be considered to design structures, which may deform well beyond the elastic limit; for example, in a severe earthquake. They may remain intact only due to their inelastic deform ability, as this deformation results in increased flexibility and energy dissipation. In some cases, this deformation also results in local structural damage, as the structure itself must absorb much of the input energy. One contradictory solution is frequently attained by allowing certain structural damage (Yang et al. 2001).

The implementation of some types of structural protective systems is one alternative solution to prevent the damaging effects of these environmental forces. These protective systems absorb or reflect a portion of the input energy that would otherwise be transmitted to the structure itself. From the energy conservation law the total input energy from the environmental forces is computed by (Uang and Bertero 1988)

$$E = E_k + E_s + E_h + E_d \tag{1.1}$$

where E_k is the absolute kinetic energy, E_s is the recoverable elastic strain energy, E_h is the irrecoverable energy dissipated by the structural system through inelastic or other inherent forms of damping and E_d is the energy dissipated by structural protective systems. The importance of protective systems can be deduced from the above equation since for any energy input, the demand of energy dissipation through inelastic deformation can be reduced by using protective systems. In consequence, many new and innovative concepts for structural protection have been proposed. One of that is the application of magnetorheological (MR) dampers which can function, in passive and semi-active mode (Soong and Spencer 2001).

Semi-active control systems combine the best features of both passive and active control systems, and they appear to offer the greatest likelihood for near-term acceptance of control technology as a viable means of protecting structures (Yang 2001). The control strategy of a semi-active control system is based on the feedback of structural motions. Different control algorithms can be adopted directly from active control systems. However, semi-active control systems are nonlinear due to the intrinsic nonlinearities of

the semi-active devices. The development of efficient control strategies is still an open research topic.

One of the objectives of this research work is to propose new methodologies to find the optimum design of discrete structures for different objective functions. Different drawbacks have been identified for the optimized designs. For example, the final designs may imply many different kinds of profiles or inexistent profile sections on the market. Another problem with the optimization process is related to the number of variables and the possibility to miss the global optimum. The difficulty to find the optimum design is function of the number of design variables, the domain size of the variables, the nature of the variables (continuity and differentiability) and the design constraints. All these factors influence the success of the optimization process; thus, developing a proper methodology is vital to obtain globally optimum designs.

The second objective is to reduce the vibration transmissibility. For this, two approaches are investigated. The first one is to modify the shape of the structure to reduce the transmissibility, which implies the solution of the geometry optimization problem in order to reduce the vibration energy. The second, a more practical and effective approach is to incorporate the MR dampers in the structural system. MR damper is a device that can modify its properties in a few milliseconds due to variations of the current excitation. The low power requirement, the safe manner mode in case of any failure and their fast response make them a promising solution in the future. In order to incorporate the MR damper in vibration suppression applications, an efficient model that simulates accurately the hysteresis behaviour of MR dampers is required.

Another objective of this research is to embed the MR damper in the structural system to suppress the vibration in passive and semiactive mode. To accomplish this, an efficient and accurate finite element should be developed for both the passive bar element and for the MR damper. Also a vibration suppression strategy will be proposed to improve the performance of the structure. Furthermore, the optimum position of the MR damper should be studied to improve its effectiveness. Finally the application of MR dampers as translational actuator is investigated. The principle is to take the vibrational energy from the structure using MR dampers and use that energy to produce actuation actions. This may represents an innovative application of MR-dampers that would eliminate big energy sources and actuators required to correct position errors. The influence of the excitation characteristics as well as the structural stiffness over this lengthening will also be investigated.

1.2. State of art

The topics studied in this research work can be arranged in three themes. The first is concerned with the optimum design of structures by minimizing the weight and structural strength. The second topic deals with the modeling of the hysteresis behaviour of the MR damper in order to be able to apply semi-active control. The last topic deals with the implementation of MR damper in the structure; thus, the structure can work as passive or semi-active system.

1.2.1. Structural optimization of discrete systems

Despite the fact that the structural optimization has achieved extraordinary development in optimization theory and associated algorithms over the last four decades, it is far less

popular in practice. This situation is, at least partly due to the difficulties and complexities of existing structural optimization methods. The structural optimization problem has generally been recognized as a constrained non-convex problem (Anthony et al. 2000). Additionally, the discrete design variables that define the possible profiles to construct the structures convert it to non-smooth problem. Therefore, it is necessary to employ a robust optimization method capable of handling these types of problems while providing global optimum solution. (GAs) have been used as the optimizer due to its capability to catch solutions close to the global optimum and operating with discrete variables. Also, GAs can easily be applied to multi-objective functions.

The application of the optimization techniques in the field of structural engineering dates back to at least 1956 when frame structures were optimized by Heyman (1956) using the linear programming technique. Since then, extensive research has been conducted in the structural optimization field with limited industrial applications. One of the first studies in the Genetic Algorithm (GA) and its application to the structural design optimization was reported by Goldberg et Santami (1986). Keane (1995) studied the optimization of the geometry of a lightweight two-dimensional structure to minimize the vibration transmission. The positions of the joints were used as the optimization variables. Genetic algorithms proved to be an efficient method for highly non-linear problems. After, the optimized design was also verified in practical cases (Keane and Bright 1996). Galante (1996) applied the same technique to optimize the real-world truss structures. He proposed the 'rebirth technique' to escape from local optimums during the optimization process and improve the results of the traditional genetic algorithm.

Anthony et al. (2000) minimized the energy at single frequency, in narrow band and in broad band in structures and proposed a methodology to analyze the sensitivity or robustness of each structure. For this, different random perturbations were generated and the average energy level of each perturbation was determined. Then, the robustness was defined as the spread or width of each statistical distribution, and it was concluded that the optimum structure is not necessarily the most robust one. In the second paper (Anthony and Elliot 2000) of a series of three, they applied active vibration control to reduce the vibration, and they also performed sensitivity analysis. In the third paper (Anthony 2001), they combined the topology design and active vibration control to improve the results. Anthony employed GAs as the optimization technique in the above publications. Prendes et al. (2005) modified the codification of the design variables and the reproduction operation of GAs and applied it to the optimization of complex steel structures. Baumann and Kost (2005) optimized the topology of truss structures by eliminating the uneconomical links using stochastic methods.

The optimal geometry of adaptive truss structures with embedded actuators was investigated by Morutso and Shao (1990). The finite element method has been combined with the sequential programming technique to maximize the structural strength, by changing the angles of the active members. They studied deterministic, probabilistic and dynamical loads. A two-phase method based on the GAs is proposed by Rajeev and Krishnamoorthy (1997) to perform size and topology optimization of truss structures. The result of the optimization process is highly influenced by the penalty functions applied to accommodate the constraints. Coello (2000) has carried out a comprehensive survey of multicriteria optimization techniques. An adaptive penalty function is proposed by

Nanakorn and Meesomklim (2001). Yang and Soh (2002) applied Genetic Programming to optimize truss structures using commercial profiles. The square of the normalized values with respect to the maximum permissible was used as a penalty function. Sandgren and Camerun (2002) used a hybrid method to solve the multicriteria optimization and applied the standard deviation as a penalty function.

In the area of the optimal number of actuators and locations most of the researchers have work only with active elements for vibration control and not many works are in literature. Rao et al. (1991) used genetic algorithms to find the best position of the actuators. The energy dissipated by the active controller was used as cost function. Chen et al. (1994) found the best position by maximizing the cumulative energy dissipated over a finite time interval. The control effort with/without spillover energy was minimized by Lammering et al. (1994). They developed the stiffness matrix for one active and two conventional truss elements, which includes the voltage as variable, and suggested that the optimal position is where there is the largest electric potential. Liu et al. (1997) minimized both the system energy and control effort by solving the discrete-continuous multi-objective programming. They alternatively used Sequential Linear Programming for continuous variables and simulated annealing for the discrete problem. Yan and Yan (2002 a, b) considered the eigenvalues of the "correlative matrix" as a hint for selecting the required number of actuators; then, they applied genetic algorithms to search for the optimal actuator locations. Zimmerman (1993) maximized the energy degree of controllability and suggested that the optimal number and placement are the most repeated solutions in the final sub-optimal structures.

Other researchers have also treated the problem of actuator placement design. Liu et al. (1997) minimized both the system energy and control effort by solving the discrete-continuous multi-objective programming. They alternatively used Sequential Linear Programming technique. Heverly et al. (2001) proposed a hybrid approach that couples a control law and an optimization routine for actuator placement using optimal active control and simulated annealing methods. Herverly et al. (2002) continued the previous research, and applied the methodology to a scaled tailboom model and implemented practical experiments. Umesha et al. (2005) optimized truss structures by decomposing the structure into sub-domains and suboptimization tasks. Each subdomain has independent design variables and a small number of behaviour constraints.

1.2.2. Hysteresis models for MR dampers

Different models have been developed to describe the behaviour of MR damper. These models are classified as the quasi-static and dynamic models. For the quasi-static models, several works have been reported in the literature. Phillips (1969) employed the Bingham model of MR fluids and developed a set of nondimensional variables and the corresponding quintic equation to determine the pressure gradient of MR fluid through a parallel duct. Gavin et al. (1996) used the same approach and developed an axisymmetric model to precisely describe the quasi-static behaviour of the MR damper. They assumed that the yield stress satisfied an inverse power law to account for the radial field distribution. Kamath and Wereley (1996) developed an axisymmetric model and assumed a constant yield stress in the annular gap. Wereley and Pang (1998) developed a similar parallel-plate model with a different set of nondimensional variables.

To consider MR fluid shear thinning/thickening effects, Lee and Wereley (2000) and Wang and Gordaninejad (2000) employed the Hershel-Bulkley model to predict fluid flow in a parallel duct with fixed boundaries. They also developed an axisymmetric model for a circular pipe with constant yield stress.

Although the quasi-static models are capable of describing force-displacement behaviour of the MR damper reasonably well, they are not sufficient to describe the nonlinear force-velocity behaviour of the damper (Yang 2001). To overcome this, different dynamic models have been developed. Stanway et al. (1985) proposed a simple mechanical model, the Bingham model, in which a Coulomb friction element is placed in parallel with a dashpot. A parametric viscoelastic-plastic model based on the Bingham model was proposed by Gamota and Filisko (1991). Ehrgott and Masrri (1992), and Gavin et al. (1996) presented a non-parametric approach employing orthogonal Chebychev polynomials to predict the controllable fluid damper force using the damper displacement and velocity information. Stelzer et al. (2003) employed the Bingham model to simulate a dynamic MR isolator. An and Kwon (2003) combines the Bingham model and the Hodgdon's to predict the mechanical and magnetic behaviour of a commercial MR brake.

The neural network (NN) models perform well given their ability to approximate arbitrary functions. Ideally, a well-trained NN model can approximate an arbitrary function with arbitrary accuracy. Chang and Roshke (1998) developed a neural network model with one hidden layer to emulate the dynamic behaviour of MR dampers. Later, Chang et al. (2002) proposed a NN model to emulate the inverse dynamics of the MR damper. This model is used to calculate voltage signals to be input into the MR damper

so that it can produce desirable optimal control forces. Another model using NN combined with Bingham model was employed by Xu et al. (2003) to apply semi-active control. However, such non-parametric damper models are quite complicated (Yang 2001) and have the disadvantage that their parameters do not have any physical meaning (Smyth et al. 2002).

Another dynamic model was developed by Wereley et al. (1998). This non-linear hysteretic biviscous model is an extension of the nonlinear biviscous model having an improved representation of the pre-yield hysteresis. Yang et al. (2004) proposed a phenomenological model which considers the MR fluid adhesive phenomenon, as well as inertial and shear thinning effects. To accomplish this, he modified the damping constant in the Bouc-Wen model by a monotonous decreasing function with respect to absolute velocity. Choi et al. (2001) have developed a polynomial model that includes the excitation current as variable. The behaviour of the MR dampers was also modeled using a modified LuGre dynamic friction by Canudas et al. (1995) and Jimenez and Alvarez (2002). Recently, Wang et al. (2003) proposed a model based on the symmetric sigmoid function, which considers relationships between the hysteresis phenomenon and the frequency and stroke of the excitation as well as the current excitation. Another model, based on the LuGre model, was proposed by Sakai et al. (2003). It predicts the damping forces based on the inputs of velocity, internal state variable and input voltage, but also it can create an inverse dynamic model to determine the input voltage.

The Bouc-Wen model was initially formulated by Bouc (1971) as an analytical description of a smooth hysteretic model and later generalized Wen (1976). This model has been extensively chosen for its ability to capture, in a continuous fashion, a range of

shapes of hysteresis loops which resemble the properties of a wide class of real nonlinear hysteresis systems (Vinogradov and Pivovarov 1986). Spencer et al. (1997) proposed a phenomenological model for MR dampers based on the Bouc-Wen hysteresis model. This parametric and dynamic model was utilized to describe a wide variety of hysteretic behaviour (Dike et al. 1996a, b; Yang et al. 2001a, b; Yang et al. 2002). The Bouc-Wen model is able to capture the force roll-off in the low velocity region that is observed in the experimental data. Trial and error or some optimization techniques such as Sequential Quadratic Programming (SQP) have already been applied to determine these parameters in such a manner that the error between experimental and simulation results are minimized (Choi et al. 2001; Spencer et al. 1997; Yang 2001; Yao 2002). However, the Bouc-Wen model has some inconveniences. First, the determination of its constant parameters is a complex task that involves very time consuming computation which does not always show good matching between the experimental data and the modeling results. Second, the fact that each set of constant parameters is valid only for single vibration conditions, make the Bouc-Wen model inappropriate for varying excitation environments.

1.2.3. Passive and semi-active control systems

The *passive control systems* alleviate energy dissipation demand on the primary structure by reflecting or absorbing part of the input energy, thereby reducing possible structural damage (Housner et al. 1998). Nonetheless, one limitation is that these systems cannot adapt themselves to change of either external loading conditions or usage patterns.

In the basic passive system, the structure absorbs vibration energy by the inherent capability of structural damping of the material. Thus, complex designs and oversized structures are required to increase the energy absorption capacity of the structure and thus obtain a safe design such that the vibration energy can be absorbed without suffering any structural damage. Anthony et al. (2000a, b, 2001) have shown that the transmissibility of the vibration energy can be reduced by redesigning the shape of the structure, which involves the solution of geometry, size and topology optimization problem. However, the modification of the structures is in many cases restricted by practical aspects such as the market profiles, manufacturing, cost, geometry constraints, etc.

Another type of passive control systems is the vibration isolation system. This system introduces flexibility and energy absorption capabilities, thereby reducing the transmitted energy to the structure. An isolation system should have enough rigidity to support the service loads, adequate flexibility to lengthen the natural period and yield a good isolation effect as well as good energy dissipation capability (Buckle and Mayes 1990). Examples of typical seismic isolation devices are the elastomeric bearing, lead rubber bearings, high damping rubber bearing and sliding friction pendulum bearings (Soon and Constantinou 1994). Many buildings around the world have been constructed with this kind of technique; such as, Los Angeles city Hall, Salt Lake City Building, Yachiyo-Dai House in Japan and west building of the ministry of Post and Telecommunications and the Research Building of the Matumura Construction Company which demonstrated excellent isolation performance during the Great Hanshin earthquake.

The passive supplemental damping devices are another kind of passive control systems. These devices protect the structure from the vibration energy by increasing its energy dissipation capacity. This protective systems function by absorbing a portion of the input energy by the conversion of kinetic energy to heat or through the transfer of energy amount of vibration modes, thereby reducing energy dissipation demands and preventing damage to the primary structure. Some types of these protective systems utilize devices that operate on principles of frictional dampers (Colajanni and Papia 1997; Filiaatrault et al.2000; Levy et al. 2000), metallic yield dampers (Soong and Dargush 1997), viscoelastic dampers (Aprile et al. 1997), viscous fluid dampers (Taylor and Constantinou 1996) and viscous damping walls (Miyazaki and Mitsusaka 1992). Other types of energy dissipative systems incorporate dynamic vibration absorbers, such as tuner mass dampers (TMDs) and tuned liquid dampers. A comprehensive review of the literature on passive protective systems using supplemental damping has been conducted by Soong and Dargush (1997) and Soong and Spencer (2002).

Passive supplemental damping devices have been investigated and developed during the last three decades. The efforts to develop these concepts into real structures have increased significantly, and many of these kinds of devices have been already installed in important buildings in the world; for example, the former World Trade Center in New York, the San Bernardino County Medical Center in California, the Sidney Tower in Australia or the Nagasaki Airport Tower in Japan.

A *semi-adaptive structure* may be viewed as a structure or structural component on which sensors and semi-active control devices are embedded such that their actions are coordinated through a control system imbuing the structure with the capability of

responding spontaneously to external stimuli exerted on the structure in proportion to their magnitudes to compensate for the undesired effects or to enhance the desired effects (Tzou and Anderson 1992). A semi-adaptive structure has the property that can be adjusted in real time but cannot inject energy into the controlled system (Housner et al. 1997). This kind of structures is based on semi-active devices sometimes referred as controllable passive dampers. These devices offer the adaptability of active control devices without requiring large power sources, which represents a valuable characteristic in seismic events when the main power source to the structure may fail. Also, semi-active devices are not at the risk to destabilize the system because they cannot inject energy into the system. Recent studies have indicated that semi-active control systems can achieve significantly better results than passive controls systems; in fact, they may even outperform fully active control systems, demonstrating significant potential for controlling structural responses to a wide variety of dynamic loading conditions (Dyke et al. 1996a, b; Jansen and Dyke 2000; Johnson et al. 2001; Ramallo et al. 2001; Spencer et al. 2000; Yi and Dyke 2000; Yoshioka et al. 2001). The semi-active devices are classified in variable orifice dampers, variable friction dampers, adjustable tuned liquid damper and controllable fluid dampers.

The *variable orifice dampers* change their damping by changing the hydraulic fluid flow resistance using an electromechanical variable orifice as shown in Figure 1.3. This kind of devices was first applied to control the motion of bridges experiencing seismic motion by Feng and Shinozuka (1990). The isolation structural systems using these semi-active devices exhibit superior isolation performance compared with passive isolation systems. Symans et al. (1994) modified a passive fluid damper to develop a

semi-active fluid damper by adding an external bypass loop which contains a controllable valve. This damper needs only a 3.5-watt power supply and can therefore operate on batteries. This type of semi-active devices can significantly increase the energy dissipation capability of structures with low damping (Symans and Constantinou 1997).

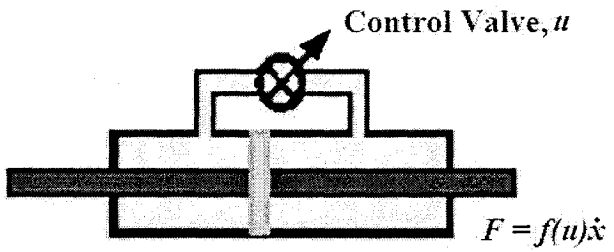

Figure 1.3. Variable orifice damper.

Patten (1998, 1999) has designed a semi-active vibration damper which is comprised of a hydraulic actuator controlled by a motor operated valve. The variable orifice dampers have shown their efficacy since they have been installed mainly in bridges and buildings and reduced the vibration up to 70%.

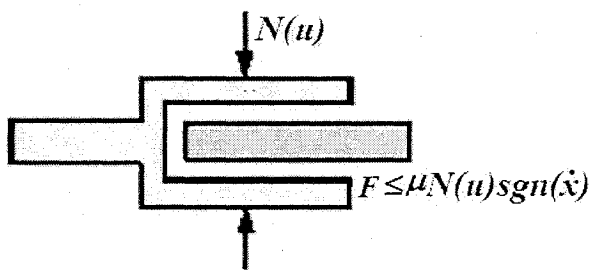

Figure 1.4. Variable friction damper.

The *variable friction dampers* use the surface friction phenomenon to dissipate the vibration energy. This kind of dampers, shown in Figure 1.4, consists of a preloaded friction shaft rigidly connected to the structural bracing. They were studied by Akbay and Aktan (1990, 1991, 1995) where the operation of the brace is controlled by the preload on

the friction interface, which in turn is actively regulated through commands generated by the controller during earthquakes or severe wind excitations.

Feng et al. (1993) employed a semi-active friction controllable fluid bearing in a seismic isolation system. This system has the ability to adapt to changing excitations since the pressure in the fluid can be varied to control the amount of friction at the insulation surface. The semi-active friction damper was modeled as a modulated homogeneous friction (MHF) by Inaudi (1997). A control algorithm is proposed in which the deformation of the damper is used as feedback signal for the controller. The MHF system yields a rate-independent force-deformation cycle for any frequencies.

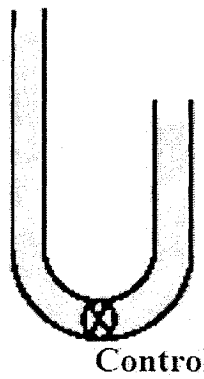

Figure 1.5. Adjustable tuned liquid damper.

The *adjustable tuned liquid dampers* shown in Figure 1.5 are a semi-active control device that utilize the motion of a sloshing fluid or a column of fluid to reduce the response of the structures. They are based on passive tuned sloshing dampers (TSD) and tuned liquid column dampers (TLCD). The TSD use the liquid in a sloshing tank to reduce the resonance of the structural system. Haroum et al. (1994) introduced a hybrid liquid column damper (HLCD). These dampers work by maintaining an optimal damping condition using a variable orifice in the tuned liquid column damper (TLCD). Another device based on TSD was proposed by Lou et al. (1994) where the length of the sloshing

tank could be altered to change the natural frequency of the liquid damper. Yalla et Kareem (2001) drive a ball valve by an electro-pneumatic actuator to modify the cross-section of a tuned liquid column damper (TLSD). Ying et al. (2005) employ a MR-TLCD to reduce the vibration of tall buildings by applying semiactive control

The *controllable fluid dampers* are a class of semi-active devices, consisting of controllable fluids in a fixed-orifice damper as shown in Figure 1.6. Unlike the previous semi-active control devices, which employ electrically controlled valves or mechanisms, controllable-fluid dampers contain no moving parts other than the damper piston. This feature makes them inherently more reliable and maintainable.

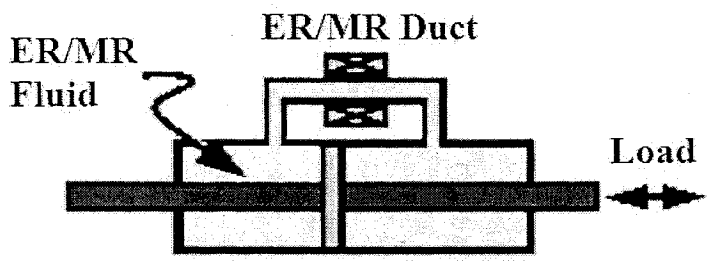

Figure 1.6. Controllable fluid dampers.

Controllable fluid dampers generally utilize either electrorheological (ER) fluid or magnetorheological (MR) fluids. These fluids are unique in their ability to reversibly change from free-flowing, linear viscous fluids to semi-solids with controllable yield strength in only a few milliseconds when exposed to an electric (ER fluids) or magnetic (MR fluids) field. The controllable dampers have recently produced an increased interest in automotive applications (Yao et al. 2002; Stelzer et al. 2003) or structural uses (Onoda et al. 1998; Xu et al 2000; Nagarajaih et al. 2000; Qu et al. 2002; Xu et al. 2003; Yoshida et al. 2003; Zhu et al. 2004; Zhu et al. 2004) A complete description of rheologic fluids, controllable fluid dampers, modeling and applications can be found in (Gavin et al. 1996;

Kamath and Wereley 1996; Makris et al. 1996; Spencer and Sain 1997; Spencer et al. 1997; Yang et al. 2002).

1.3. Present work

The present thesis constitutes a comprehensive study in the area of structural analysis, optimization and control of adaptive structures. Development of new analysis methods, optimization algorithms ad their integration into the design optimization and vibration suppression of adaptive structures and validation of the results by experimental study are among the most significant contributions of this thesis.

In the area of optimization, a new way to solve the problem that is frequently presented during the reproduction operation of the Genetic Algorithms is proposed. This new approach allows controlling the speed of the convergence and evades falling in random search or reaching clones early and thus being trapped in local optimum.

Two new methodologies are proposed in the structural optimization field. The first one solves the optimization problem of real life structures that are built by the repetition of single bays. This new methodology reduces drastically the number of design variables; thus, the search space is significantly smaller compared with the one in the original problem. Furthermore, the computational time is reduced significantly and accurate global solution is found. The second methodology deals with the optimum response of adaptive structures under varying loads. Although this problem was already solved with deterministic methods, the proposed methodology includes practical constraints such as the stroke of the actuator. In addition discrete variables are included in the formulation to determine the optimum position of the active elements.

To simulate the hysteresis phenomenon of MR dampers, a new approach is proposed to determine the characteristic parameters of the Bouc-Wen model. This new methodology uses key information from the experimental data to calculate directly the characteristic parameters, without running any optimization process, to match the simulation and the experimental results with very good accuracy. The characteristic parameters are systematically determined and it has been observed that they tend to follow linear or exponential relations with respect to the excitation current. Furthermore, it was observed that the hysteresis force for the MR damper follows a parabolic pattern with respect to the amplitude and frequency of the excitation. All these relations were incorporated in a new nonlinear hysteresis model for the MR damper. This new model predicts the hysteresis force at any given current, frequency and amplitude excitation which represent a big advantage over the existing models.

Using the new proposed model for MR dampers, the finite element formulation of the MR damper is incorporated into the finite element model of the discrete structure. The developed finite element model was experimentally validated and then employed to study the performance of the proposed vibration suppression strategies in structural systems. Finally the possible application of MR dampers as longitudinal actuators is investigated and the required conditions are stated. This proposed application is based on the concept that it is possible to take the vibrational energy and apply it for actuation actions.

1.4. Overview of the dissertation

This research work is focused to develop a fundamental understanding of optimization of structures and vibration mitigation using semi-active protecting systems. The optimization, the modeling of the hysteresis phenomenon for controllable fluid dampers and the application of this kind of protective devices to structures are the three main topics studied through the thesis.

In the second chapter a brief explanation of FEM is presented and a background about optimization methods for structural optimization is provided. Then, two different approaches are proposed to solve the optimum structural problems. The first approach is based on maximizing the structural strength of the adaptive structures under varying loads in which the position, number and length of the actuator are considered as design variables. In the second approach the optimum design of real life structures are studied. Many practical structures are built from the duplication of some basic bays with standard profiles. Thus, the topology, size and geometry optimization of these kind of structures are accomplished.

The third chapter deals with modeling the hysteresis behaviour of MR dampers. First a background description concerning controllable fluids and dampers is presented and subsequently the main dynamic parametric models proposed to simulate the hysteresis phenomenon are provided. Next, a new methodology to find the characteristic parameters of the Bouc-Wen model is formulated. Finally, a new model, based on the Bouc-Wen model, is proposed. This model considers the amplitude, frequency and current excitation as input variables.

The application of MR damper to reduce the vibration in the structure is studied in Chapter 4. To accomplish that, the FEM model of the bar element and MR damper element with node connections are developed considering the hysteresis model proposed in the previous chapter. Later, the solution of the nonlinear system is briefly presented. Finally the proposed models are validated by comparing the results with the experimental data.

The Chapter 5 deals with the dynamic optimization of passive and semi-active structures. First, the optimization problem to reduce the vibration using the position of the nodes as design variables is performed. After, vibration reduction is achieved with the MR damper embedded in the structure in passive manner and subsequently a strategy of vibration reduction is proposed to improve the performance of the MR damper. Finally a new concept of application of MR damper is introduced. It is shown that it is possible to make use of the vibration energy of the structure and apply this energy in lengthening control actions of a semiactive actuator. Here the influence of the excitation characteristics and the structural stiffness on the lenghtening effect is studied

Finally in Chapter 6, the results and contributions of this research work are summarized and thoughts and suggestions are presented for future work.

CHAPTER 2
STRUCTURAL OPTIMIZATION

The area of structural design optimization has been developing actively during the last three decades due to the natural desire of engineers to design structures that not only satisfy their functional requirements but also perform their functions in an optimal manner. In the present chapter, first the constrained structural optimization problem is stated. Next, the finite element method is briefly explained. Then, the optimization methods for constrained structural problems are discussed. In the end, the methodologies for geometry optimization of adaptive structures and simultaneous topology, size and geometry optimization of real-life structures are proposed.

2.1. Modeling the constrained structural optimization problem

The formulation of an optimum design problem comprises three steps (Arora 1989). First the independent design variables must be precisely identified and defined. Then, the objective function (called the cost function for the minimization problem) must be established. This is a scalar function that must depend explicitly or implicitly on the design variables. Finally, all the constraints of the system need to be specified. Usually constraint expressions involve both the dependent and independent design variables as well as explicit bounds on the variables.

Structural design optimization can be realized in three broad categories (Hafka and Grandhi 1986; Kirsh 1989) namely as size, topology and geometry optimization. The

cross sectional optimization, also known as size optimization, assumes that the elements, nodes, connectivity and locations are fixed while it searches for the optimum shape (cross-sectional area) of the elements. Topology optimization addresses the issues that size optimization ignores; it is concerned with the number and connectivity of the members and joints. On the other side, the geometry optimization looks for the optimum shape of the whole structure; thus, it considers the joints and length of the elements as the design variables. In the present work, the size, topology and geometry optimization of the single bays with which the real life truss structures are constructed has been addressed.

The optimization can be defined as the problem of finding a vector of decision or design variables, which satisfies the constraints and optimizes a vector function whose elements represent the objective functions (Osyezka 1985). These functions form a mathematical description of performance criteria, which are usually in conflict with each other. Hence, the term 'optimize' means finding such a solution, which would give the values of the entire set of objective functions acceptable to the designer. Formally, the optimization problem is stated as:

Find the vector $\boldsymbol{x}^* = [x_1^*, x_2^*, ..., x_n^*]$ which will satisfy the m inequality constraints:

$$g_i(\boldsymbol{x}) \geq 0, \quad i = 1,2,...m, \tag{2.1}$$

the p equality constraints:

$$h_i(\boldsymbol{x}) = 0, \quad i = 1,2,...p, \tag{2.2}$$

and optimize the vector function:

$$f(\boldsymbol{x}) = [f_1(\boldsymbol{x}), f_2(\boldsymbol{x}), ..., f_n(\boldsymbol{x})]^T \tag{2.3}$$

where $\boldsymbol{x} = [x_1, x_2, ..., x_n]$ is the vector of design variables and the optimal solution is denoted by the vector $\mathbf{x}^*$. In the case of n = 1, the problem is called single-objective optimization, otherwise it is known as multicriteria or multiobjective optimization.

2.2. Finite Element Method

To conduct any design optimization problem, it is important to develop efficient analysis and optimization modules. The Finite Element Method (FEM) is a numerical method frequently used to find accurate solution of complex engineering problems. This method was first presented by Turner et al. (1956). They presented the application of simple finite elements for the analysis of aircraft structure. This is considered as one of the key contributions of the FEM. In few years the method gained recognition due to its potential. Today, the method is considered as one of the most powerful numerical techniques to efficiently solve a wide variety of practical problems. One of the main reasons of its spreading use in different fields of engineering is the fast improving in the performance computing power at low cost.

The solution of a general structural problem using FEM consist of the following steps (Rao 1999):

- Discretization of the structure
- Selection of a proper interpolation or displacement model
- Derivation of element stiffness, damping and mass matrices and load vectors
- Assemblage of element equations to obtain the overall equilibrium equations

- Solution for the unknown nodal displacements
- Computation of element strains and stresses

In this section the stiffness and mass matrices will be stated for the truss element in order to use the FEM as analyzer in the optimization process.

2.2.1. Stiffness and mass matrix for truss elements

Truss structures, also called rod or axial bar; consist of flexible truss members under axial forces only and pin-connected at joints. Due to the lightweight and easy assembling, these structures play an important role in the industrialized world and have numerous applications such as bridges, towers, cranes, roof supports, building skeletons, space deployable structures, etc. In this study, a discrete space structure with repetitive bays has been fabricated for experimental study and has been modeled as a space truss structure. Although, a bending moment may occur at the node connections of the element, the truss element has been found to represent the global vibration behaviour of the structure fairly accurate.

The degrees of freedom u_1, u_2 for truss elements in one-dimensional coordinate system are showed in Figure 2.1a.

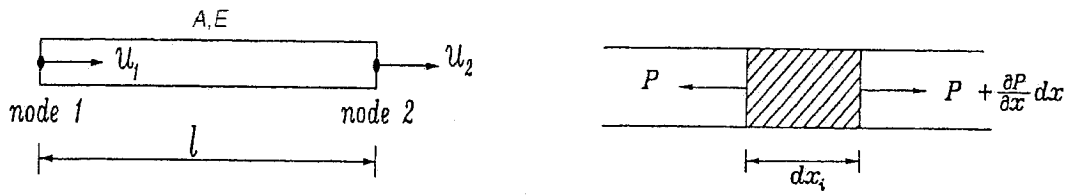

Figure 2.1. a) One-dimensional truss element, b) Free body for truss element

The governing equation to describe the motion of rod is derived by applying Newton's second law to the free body diagram shown in Figure 2.1b (Kwon and Bang 1996)

$$\rho A dx \frac{\partial^2 u}{\partial t^2} = \left(P + \frac{\partial P}{\partial x} dx \right) - P \tag{2.4}$$

where E, A and ρ are the elastic modulus, cross-sectional area and density of the material, respectively. These parameters can be constants or can be function of x for non-homogeneous, non-isotropic and non-isomorphic materials. u is the axial displacement along the rod direction, x and t correspond to the spatial and temporal axes. According to Hooke's law, we can write:

$$\frac{P}{A} = E\varepsilon \tag{2.5}$$

where strain, $\in$ is related to displacement as:

$$\varepsilon = \frac{\partial u}{\partial x} \tag{2.6}$$

substituting the Eqs. (2.6) and (2.5) into Eq. (2.4) yields

$$\rho A \frac{\partial^2 u}{\partial t^2} = \frac{\partial}{\partial x}\left(AE \frac{\partial u}{\partial x} \right) \tag{2.7}$$

Applying the Galerkin's method (Reddy 1993) to Eq. (2.7) we have:

$$\int_0^L \left(\rho A w \frac{\partial^2 \tilde{u}}{\partial t^2} + \frac{\partial}{\partial x}\left(AE \frac{\partial \tilde{u}}{\partial x} \right) \right) w_i dx = 0 \tag{2.8}$$

in which w_i are the weighting functions $\tilde{u}$ is the approximate axial displacement function. The weak formulation of the previous equation can be obtained by integrating it by parts as:

$$\int_0^L \left(\rho A w_i \frac{\partial^2 \tilde{u}}{\partial t^2} + AE \frac{\partial w_i}{\partial x} \frac{\partial \tilde{u}}{\partial x} \right) dx - \left[AEw \frac{\partial u}{\partial x} \right]_0^L = 0 \tag{2.9}$$

It is noted that the first term inside the integral can be identified as stiffness term, the second as the inertia term and the last term defines the essential and natural boundary conditions. At the free end, the natural boundary conditions are $F = AE\,{\partial u}/{\partial x} = 0$ and a the fixed end, the essential boundary condition is $u = 0$.

Let the bar be divided into n units each of length l and let each element has a linear axial displacement field. Thus in a typical two DOF element with end nodes 1 and 2 as shown in Figure 2.1a, the approximate function $\tilde{u}$ is:

$$\tilde{u} = [N]\{d\} = \begin{bmatrix} \frac{l-x}{l} & \frac{x}{l} \end{bmatrix} \begin{Bmatrix} u_1 \\ u_2 \end{Bmatrix} \tag{2.10}$$

in which $N_1 = {l - x}/{l}$, and $N_2 = {x}/{l}$ are the shape functions and $\{d\} = [u_1 \quad u_2]^T$ is the nodal displacement vector.

In Galerkin method, the weighting functions w_i are defined as shape functions N_i. Let us define $[B] = {\partial}/{\partial x}[N] = \begin{bmatrix} -1/l & 1/l \end{bmatrix}$ hence ${\partial \tilde{u}}/{\partial x} = [B][d] = \begin{bmatrix} -1/l & 1/l \end{bmatrix} \begin{Bmatrix} u_1 \\ u_2 \end{Bmatrix}$, thus the axial force at arbitrary x is determined by

$$F = AE\frac{\partial u}{\partial x} \tag{2.11}$$

Now Eq. (2.9) after rearrangement becomes:

$$\sum_{e=1}^{n}\left\{\int_0^l [N]^T \rho A[N]dx\{\ddot{d}^{(e)}\}+\int_0^l [B]^T AE[B]dx\{d^{(e)}\}\right\}=\sum_{e=1}^{n}\left\{[N]^T F\right\}_0^l \tag{2.12}$$

rewritten in short form

$$[M^{(e)}]\{\ddot{d}^{(e)}\}+[K^{(e)}]\{d^{(e)}\}=[P^{(e)}] \tag{2.13}$$

where first and second left terms are known as mass consistent and stiffness matrices and the right term is called the load vector. For truss element they become:

$$\begin{aligned}[K^{(e)}]&=\frac{AE}{l}\begin{bmatrix}1 & -1\\ -1 & 1\end{bmatrix}\\ [M^{(e)}]&=\frac{\rho Al}{6}\begin{bmatrix}2 & 1\\ 1 & 2\end{bmatrix}\end{aligned} \tag{2.14}$$

after proper assembling the Eq.(2.13) can be written as

$$[M]\{\ddot{d}\}+[K]\{d\}=[P] \tag{2.15}$$

where $[M]$ and $[K]$ are $(n\,x\,n)$ global system and mass matrices respectively and $[P]$ is the $(n\,x\,1)$ vector of externally applied concentrated loads and defined as:

$$[M]=\sum_{e=1}^{n}[M^{(e)}];\quad [K]=\sum_{e=1}^{n}[K^{(e)}];\quad [P]=\sum_{e=1}^{n}[P^{(e)}] \tag{2.16}$$

For static problem, the Eq. (2.15) becomes simply:

$$[K]\{d\}=[P] \tag{2.17}$$

2.2.2. Rotational matrix for truss elements and solution of the system

In the previous section the stiffness and the mass matrices were obtained for one-dimensional finite element also called *local coordinates*. For assembling process in order to obtain system stiffness and mass matrices, it is required to transfer first these matrices from local to global coordinates. In this part, stiffness and mass matrices will be computed for the *global coordinates*. The process to transfer the element from local coordinates to global coordinates is called *coordinate transformation* as it can be observed in the Figure 2.2. The coordinate transformation is necessary when the field variable is a vector quantity like displacement and velocity. The coordinate transformation relates the local and global by:

$$\left\{d^{(e)}\right\}^{l} = [R]\left\{d^{(e)}\right\}^{g} \tag{2.18}$$

where the $\left\{d^{(e)}\right\}^{l} = \left[u_i, u_j\right]^T$ is the local displacement vector and $\left\{d^{(e)}\right\}^{g} = \left(u_i, v_i, w_i, u_j, v_j, w_j\right)^T$ is the global displacement vector and $[R]$ is an orthogonal matrix called *rotational matrix* or *rotation.*

The rotation matrix for 2-Dimensional case is a (2x2) matrix determined by the direction cosines as

$$[R] = \begin{bmatrix} l_{ij} & m_{ij} \\ -m_{ij} & l_{ij} \end{bmatrix} \tag{2.19}$$

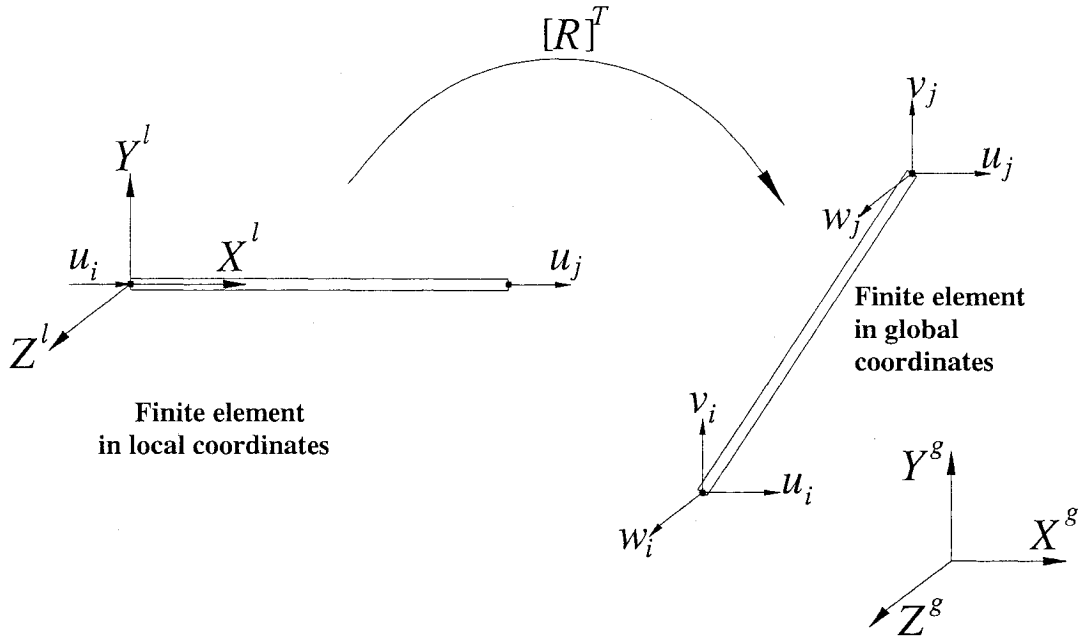

Figure 2.2. Coordinate transformation from the local coordinates to the global coordinates.

where the direction cosines l_{ij} and m_{ij} are calculated using the global coordinates as

$$l_{ij} = \frac{x_j - x_i}{l},\ m_{ij} = \frac{y_j - y_i}{l} \tag{2.20}$$

where (x_i, y_i) and (x_j, y_j) are nodal coordinates measured at global coordinates. The length of the finite element can be calculated by

$$l = \sqrt{(x_j - x_i)^2 + (y_j - y_i)^2} \tag{2.21}$$

For the 3-Dimensional case, the rotation matrix has a (2x6) dimension and it is stated as

$$[\boldsymbol{R}] = \begin{bmatrix} l_{ij} & m_{ij} & n_{ij} & 0 & 0 & 0 \\ 0 & 0 & 0 & l_{ij} & m_{ij} & n_{ij} \end{bmatrix} \tag{2.22}$$

the direction cosines are calculated by

$$l_{ij} = \frac{x_j - x_i}{l},\ m_{ij} = \frac{y_j - y_i}{l},\ n_{ij} = \frac{z_j - z_i}{l} \tag{2.23}$$

and the length of the finite element is computed using the global coordinates as

$$l = \sqrt{(x_j - x_i)^2 + (y_j - y_i)^2 + (z_j - z_i)^2} \tag{2.24}$$

A complete description of how to derive the rotational matrices are developed in (Rao 1999; Kwon and Bang 1986). Since the rotational matrices is valid for any vector, the global force vector can be computed by

$$\{P^e\}^l = [R]\{P^e\}^g \tag{2.25}$$

Now considering Eqs. (2.18), (2.25) and (2.13) the equation in element level be can written as:

$$[M^{(e)}][R]\{\ddot{d}^e\}^g + [K^{(e)}][R]\{d^e\}^g = [R][P^e]^g \tag{2.26}$$

Multiplying both sides of Eq. (2.26) by $[R]^T$ and considering that $[R]^T = [R]^{-1}$, the above equation can be rewritten as:

$$[M]^g\{\ddot{d}\}^g + [K]^g\{d\}^g = [R][P]^g \tag{2.27}$$

where

$$[M]^g = [R]^T[M^{(e)}][R], \quad [K]^g = [R]^T[M^{(e)}][R] \tag{2.28}$$

are the global mass and stiffness matrices for the element. Now that the stiffness, displacement and force have been transformed to global coordinates, they can be assembled to find system mass and stiffness matrices in order to obtain the system governing equation given in Eq. (2.15).

It is noted that the system stiffness matrix in its present form is singular and thus boundary conditions should be applied in order to be able to find the nodal displacement and subsequently strain and stress in elements.

2.3. Optimization methods for constrained structural problems

As mentioned before one of the main components in structural design is the optimization part. The optimization methods are taking an important role in computer methods for designing engineering systems. The optimization methods allow to the designer evaluate more alternatives in order to have better and more cost-effective final designs. There are different classifications for the optimization methods. Here, the optimization algorithms are classified based on gradient and non-gradient methods. Because typical structural optimization problems are nonlinear and constrained (Keane 1995), a lot of effort goes towards the algorithms for constrained problems.

2.3.1. Gradient methods

A one-step solution is in general impossible in the constrained structural optimization problems. The simplest idea to overcome the problem is to take the best solution from a couple of trial solutions. Another pragmatic strategy is to generate a series of intermediate solutions, which converge to the final optimum. Naturally, while traveling from an initial to the optimal solution at each iteration step, two important questions arise: which direction shall be taken for the next step, and how far to go in this direction. The many available algorithms differ in how they get answers to these questions. The main deterministic algorithms are again subdivided with respect to the type of variables (primal and/or dual variables) used in the formulation. Four main sub-classes are as follows:

2.3.1.1. Primal methods

These methods work directly in the n-dimensional space of the optimization variables x. They make no use of Lagrange multipliers and the Kuhn-Tucker (KT) necessary conditions (Pardalos and Rosen 1987). The simplest algorithms are primal, direct search methods. Successful primal methods, which make use of gradient information, are known as *method of feasible directions* or *general reduced gradient methods*.

2.3.1.2. Penalty and barrier function methods

The penalty and Barrier methods work also in the n-dimensional space of the optimization variables (Vanderplats 1984; ASCE 1997). They, however, transform the constrained problem into an unconstrained one. The approach is principally simple and quite robust. An old methodology is known as SUMT (Sequential Unconstrained Minimization Technique), which generates a series of unconstrained sub-problems to finally get a solution near to but not exactly the optimum. That was one of the reasons why the method did not gain popularity. The basic idea, however, came back just recently as interior point method. The mathematical basis has been improved and SUMT has now been put into the frame of so called continuation methods, which generates a series of solutions with increasing penalty factor that allow a controlled approach to the optimum until the solution is accepted or the problem condition collapses. In this context the penalty factor can be understood as a continuation parameter.

2.3.1.3. Dual methods

The dual methods use primarily the dual m-dimensional space of Lagrange multipliers λ. The primal optimization variables x are determined by back substitution (Venkaya 1971; Rozvany 1989). Dual methods split the original optimization problem into two partial problems, which have to be solved sequentially. One is unconstrained and formulated in terms of x, the other is formulated in terms of λ and is only constrained by simple bounds. In the case of equality constraints it is unbounded too. Because of the simply structured sub-problems, methods for unconstrained problems can be applied directly or with minor modifications to handle bounds on variables.

2.3.1.4. Lagrange methods

These methods work in the full $(n+m)$-dimensional space of primal and dual variables x, λ (Rozvany 1989; Venkaya 1971; Xu and Agrawal 2000). They directly tackle the Kuhn-Tucker necessary conditions by solving a sequence of linearized sub-problems. These sub-problems are characterized by a quadratic objective and linear constraints. That's why these kinds of methods are called *SQP-* or *Sequential Quadratic Programming methods*. A simplified variant uses a linear approximation for the objective also and is called *SLP-* or *Sequential Linear Programming*. SQP methods are considered to be one of the most or even the most sophisticated methods from the mathematical point of view. They have been successfully applied for many structural optimization tasks and are available in almost every structural optimization package. However, they appear to be not robust enough for very large problems. Research on the field is still in progress.

2.3.2. Non-gradient methods

Optimization structural problems are characterized by having many variables, highly non-linear relationships between the variables and objective function, and an objective function that has many peaks and troughs. In few words, these kinds of problems are difficult to deal with. The search for methods that can cope with such problems has led to the subject of evolutionary computation. Techniques in this field are characterized by a stochastic approach to the search for improved solutions, guided by some kind of evolutionary control strategy (Fleming and Purshouse 2002; Sarma and Adeli 2000). One of the main characteristics of these methods is that they have the ability or mechanism to escape from local optimums and catch solution close to the global optimum (Yang and Soh 2002). The four main non-gradient methods currently used are as follows:

2.3.2.1. Simulated Annealing (SA)

SA is an stochastic method which is an analogy with physical annealing of a solid (Chen et al. 1994; Liu et al. 1997; Rutenbar 1989). In physical systems, jumps to higher energy actually do happen, but the current temperature T moderates them. At higher temperatures, the probability of large uphill moves in energy is large; at low temperatures the probability is small. The Metropolis algorithm models this with a Boltzmann distribution: the probability of an uphill move of size ΔE at temperature T is $P_r[accept] = e^{-\Delta E/T}$. In practice, this probabilistic acceptance is achieved by generating a uniform random number R in [0,1] and comparing it against the threshold P_r. Only if

$R < P_r$ the is move accepted. Thus, very probable moves can be rejected, and very improbable moves can be accepted at least occasionally.

2.3.2.2. Evolutionary Programming (EP)

EP involves three steps that are repeated until a threshold for iteration is exceeded or an adequate solution is obtained (Fogel 1995; Soh and Yang 2000). First an initial population of trial solutions is randomly chosen. Second, each solution is replicated into a new population. Each of these offspring solutions are mutated according to a distribution of mutation types, ranging from minor to extreme with a continuum of mutation types between. The severity of mutation is judged on the basis of the functional change imposed on the parents. Finally, each offspring solution is assessed by computing its fitness. Typically, a stochastic tournament is held to determine n solutions to be retained for the population of solutions, although this is occasionally performed deterministically.

2.3.2.3. Evolutionary Structural Optimization (ESO)

The ESO method is based on the simple concept that by slowly removing inefficient material from a structure, the residual shape evolves in the direction of making the structure better. Almost all types of constraint such as stiffness, frequency, buckling load constraints can be imposed. The optimization process for ESO requires a rejection criterion which establishes when the finite element result is accepted as part of the final designs or when it is rejected (Xie and Steven 1997).

2.3.2.4. Genetic algorithms (GAs)

Due to efficiency of GAs in capturing the global optimization solution, structural optimization problem studied in this research mainly utilizes the GAs as optimizer. GAs are one form of directed random search as it was stated by Holland (1975). The form of direction is based on Darwin's "survival of the fittest" theories. In GAs an initial population is created randomly or heuristically. Each element of the initial population represents a design and is called chromosome that are typically strings of binary bits. Each bit is called genes. Genes occur at different locations or loci of the chromosomes, and take on certain values which are called alleles. These sets of chromosomes evolve over generations to get new and hopefully better designs. In biological science the term genotype refers to the overall genetic makeup of an individual and is analogous to a structure in structural design. Also, the external characteristics are refered with the phenoype that is analogous to an actual parameter set such as design parameters.

Four differences separate GAs from more conventional optimization techniques (Goldberg and Samtami 1986): 1-Direct manipulation of a coding, 2-Search from a population, not a single point, 3-Search via sampling, a blind search, 4- Search using stochastic operators, non deterministic rules.

The implementation of the GAs usually involves the following cycle: i) Evaluate the fitness of all of the individuals in the population. ii) Create a new population by performing operations such as reproduction, crossover and mutation on the individuals whose fitness has just been measured, iii) Discard the old population and iterate using the

new population. The operations of the second step, which represents the heart of GA, are briefly described.

Reproduction is a process in which individual strings are copied according to their objective values, f (biologist call this function the fitness function). Intuitively, one can think of the function f as some measure of profit, utility, or fitness that we want to maximize. Copying string according to their fitness values means that strings with a higher value have a higher probability of contributing one or more offspring in the next generation. This operator, of course, is an artificial version of natural selection, a Darwinian survival of the fittest among string creatures. In natural populations, fitness is determined by a creature's ability to survive predators, pestilence, and the other obstacles to adulthood and subsequent reproduction. In our unabashedly artificial setting, the objective function is the final arbiter of the string-creature's life or death.

Many reasonable algorithms exist to enable the individuals with the higher fitness values have the higher chance to be selected into the mating pool. The most widely used technique is the proportional fitness selection or *roulette-wheel selection* (Goldberg 1989) that can be represented by the following equation

$$P_r(i) = \frac{f(i)}{\sum_{j=1}^{n} f(i)} \tag{2.29}$$

where i represents the chromosome, P_r the probability of being reproduced and f is the objective function or fitness and n the size of the population. However, the drawback of this technique is that when a very good element emerges in the population, this element will be reproduced many times. This would lead to have clones significantly far from the

global optimum. On the other side when the fitness of the population is too uniform and the convergence is slow because the search may become a random walk.

To address these shortcomings, fitness scaling is often used. The simplest way to scale fitness is linear scaling (Chan 1997)

$$f' = af + b \tag{2.30}$$

here, the scaled fitness f' is scaled by using two coefficients a and b such that the average scaled fitness f'_{avg} equals to the average of raw fitness f_{avg} and the best individual $f_{\max}$ is scaled down to around $2f'_{avg}$. However fitness scaling does not work for all populations.

Another approach is to use a selection with good selection pressure. Selection pressure is the degree to which the better individuals are favoured. For instance, Goldberg and Deb (1991) proposed a scheme that randomly chooses a set of individuals from the population and picks the best for reproduction. However, the important genetic information of a good chromosome can be ignored if it is in competition with better elements.

In this study a new approach is proposed, which considers the Table 2.1 to determine the number of times that one chromosome is reproduced. For example, if the size of the population n is 200 and the probability of reproduction P_r is 0.2; then the number of chromosmes to be copied ($n_r = nP_r$) is 40 elements of the best elements. Thus, the 1st best element is copied six times, the 2nd and 3rd are copied 5 times, and so on until it is completed 40. Therefore, the probability of reproduction can control the speed

of convergence. In Figure 5.1 the effect of the probability of reproduction of 0.2, 0.5 and 0.8 can be appreciated. It is noted that for low probability of reproduction the convergence is slower but may find a better solution. For the high probability, the convergence is fast but the solution falls in a local optimum because the population becomes fastly clones of the best elements.

After reproduction operation, simple *crossover* may proceed in two steps. First, members of the newly reproduced strings in the mating pool are randomly mated. Second, each pair of strings undergoes crossing over as follows: an integer position k along the string is selected uniformly at random between 1 and the string length minus one $[1, n-1]$. Two new strings are created by swapping all characters between positions $k+1$ and n inclusively.

Table 2.1. Number of times to copy the chromosome

n_r	**Times of copying**
2	2
7	3,2,2
16	4,3,3,2,2,2
30	5,4,4,3,3,3,2,2,2,2
50	6,5,5,4,4,4,3,3,3,3,2,2,2,2,2
77	7,6,6,5,5,5,4,4,4,4,3,3,3,3,3,2,2,2,2,2,2
...	...

Mutation is a low probability random operation, which may slightly perturb the design represented by the prodigy. The operator works on a bit-by-bit basis and is governed by the probability of mutation. The mutation operation allows to each bit the to change from 0 to 1 or vice verse. This operator also allows new zones to be explored in the search space.

In optimization problem investigated in this study, the design variables are mainly the position of the actuators, the topology, size and the geometry of the structure. Thus, the cost function may not be continuous and subsequently non-differentiable function. Additionally, it can be highly non-convex function. For the position of the actuators problem, the actuation locations are passive design variables, and they are confined to discrete positions; thus, the gradient-based optimization routines cannot be applied, since the gradients are not meaningful. Considering this, the optimization method should be chosen from the stochastic methods that have the capacity of solving discrete and continuous problems and are able to find the global optimum.

As was mentioned before, GAs has been selected due to its capacity to handle discrete design variables and also catch the global optimum point. Also, the penalty functions can be easily incorporated in GAs which is not the case for deterministic methods. Moreover, their performance in structural optimization applications has been proven in different studies (Keane 1996). In deterministic approaches (Goldberg and Santami 1986) the penalty methods have often been criticized due to steep ridges that they impose on otherwise smooth problems. These ridges can cause difficulty among search techniques, which depend upon a particular shape of local search surface. However, this objection is not relevant to GAs method since they do not depend on

continuity or derivative existence for their operation. In this research, FEM as analyzer engine has been combined with GAs as optimizer engine to find global optimum solution in placement, size, topology and geometry optimization problem. Figure 2.3. describes how GAs and FEM are merged together.

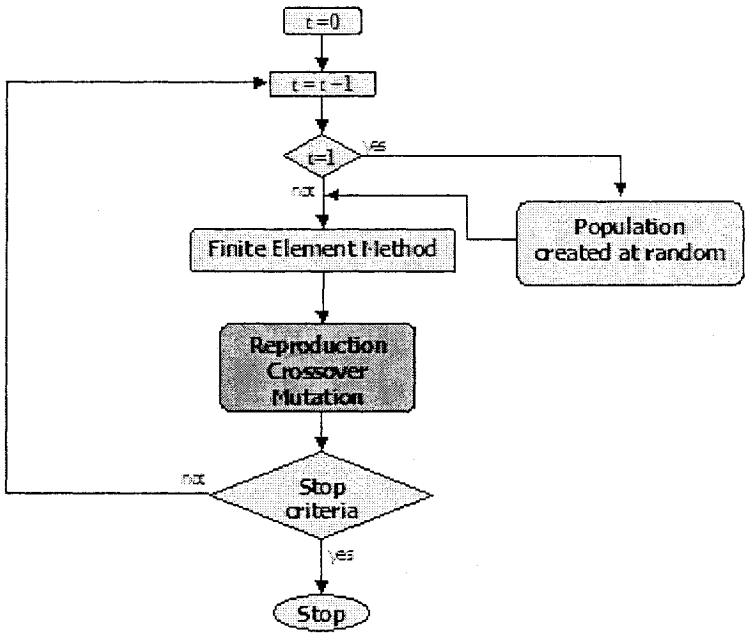

Figure 2.3. Optimization process combining GAs and FEM.

2.4. Geometry optimization of adaptive structures

The traditional space structures cannot modify their response mechanisms when subjected to varying load conditions, which may be different than those considered in the design stage and thus may lead to failure or potential instability of subsystems or components. Such performance limitations of traditional passive structures have motivated considerable interest in developing a new class of structures (adaptive

structures), which can modify their shapes in a controlled manner to accommodate unpredictable environmental changes.

In a recent topology involving optimization of the adaptive structures (Morutsu and Shao 1990) FEM has been combined with the sequential programming technique to maximize the structural strength, by changing the angles of the active members. However, the optimal placement of the active members to accommodate the environmental changes has not been investigated.

Actuator placement on large space adaptive structures is a recent thrust and challenging work in discrete optimization problem. Past practice was based on sequential linear programming method. However, this method may result in a local optimum and has shown some deficiencies and there is no mechanism to climb up the local optimum (Golberg and Santami 1986).

In this research the finite element technique is combined with the modified GAs to search for optimal locations, the minimum number and length of active members simultaneously. The effect of the maximum stroke of the active elements on the optimum location is also investigated. GAs have been employed as the optimizer due to its robustness and flexibility to employ multi-parametric objective functions and discrete design variables and also capable to catch the global optimum solution.

2.4.1. Statement of the problem for the structural strength optimization in adaptive truss structures

An adaptive truss structure, which can modify its configuration by lengthening or shortening some of their members (active elements), is considered for geometry optimization in this study and it is shown in Figure 2.4. The geometry optimization problem for the adaptive truss structures under variable load may be defined mathematically as:

For a given static external load $\boldsymbol{P}$ and angle ψ, find (a_i, l_i) such that the structural strength S_d is maximum subject to

$$a_i \in \aleph,\ 1 \le a_i \le n \tag{2.31}$$

$$l_i \in \Re,\ L_{il} \le l_i \le L_{iu} \tag{2.32}$$

where a_i and l_i are the positions and lengths of the n active elements respectively, L_{il} and L_{iu} are the lower and upper extension limits of each active element. The structural strength may be defined by (Morutso and Shao 1990):

$$S_d = Max\left|\frac{\overline{F}}{\hat{F}(L,\psi)}\right| \tag{2.33}$$

where $\overline{F}$ is the vector of element strength including allowable element forces, $\hat{F}$ is the element force vector due to unit external static load which can be found from finite element analysis of the adaptive structure during optimization procedure.

2.4.2. Application of of the structural strength optimization in adaptive truss structures

The twenty-four-bar adaptive truss structure shown in Figure 2.4 has been optimized to obtain the maximum structural strength under static conditions. It has been considered that the elements 2 to 17 can be chosen as the locations for the active elements. Two different ranges (1.27 and 0.31 m) of the stroke for the active elements have been investigated, and each range has been evaluated with 2, 3 and 4 active elements. The material properties are the same as (Sedhagati et al. 2000, 2001a, b): Young's modulus $E = 7X10^{10}$ N/m^2, Element strength $\overline{F}$ is 1000 N for all the members. The geometrical parameters are: cross-sectional area $a_i = 10^{-4}$ m^2 and $L = 2$ m.

It has been proved (Morutsu and Shao 1990; Sedaghati 2001a) that the critical points for the structural strength are when the angle of load is 0 or 180°. Considering this, the optimum locations have been found using the multi-criterion objective function described as:

$$S_d = Max\left|\frac{\overline{F}}{\hat{F}(L,0)}\right| + Max\left|\frac{\overline{F}}{\hat{F}(L,180)}\right| \tag{2.34}$$

A chromosome of 60 bits for the case of stroke of 1.27m and 44 bits for stroke of 0.31m have been used. The probability of crossover P_c is 0.6, the probability of mutation P_m is 0.05 and the probability of reproduction P_r is 0.4. The final optimum positions are shown in Table 2.2. The Figure 2.5 shows the structural strength for 2, 3 and 4 active elements as a function of the load angle. The Figure 2.6 to 2.11 show the optimum configurations for each case. After the best locations are determined considering (2.34),

the optimum configurations were found for each ψ by solving the geometry optimization problem given in Section 2.33 and it does not have any constraints. In this part, the chromosome has 28 or 20 bits and the above probabilities of crossover, reproduction and mutation are the same as above.

Table 2.2. Optimum location for different stroke and active elements.

Stroke (m)	**Number of active elements**	**Optimum position**
0.31	2	4, 8
	3	4, 8 16
	4	2, 5, 9, 10
1.27	2	4, 8
	3	4, 5, 8
	4	2, 5, 9, 10

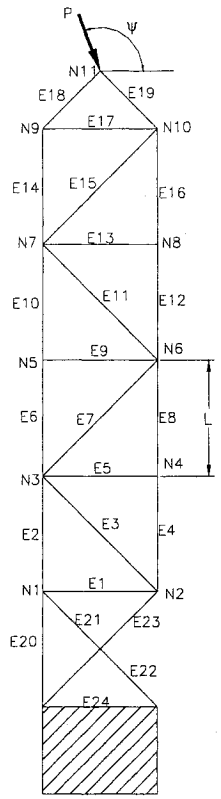

Figure 2.4. The 24-bar plane adaptive truss structures.

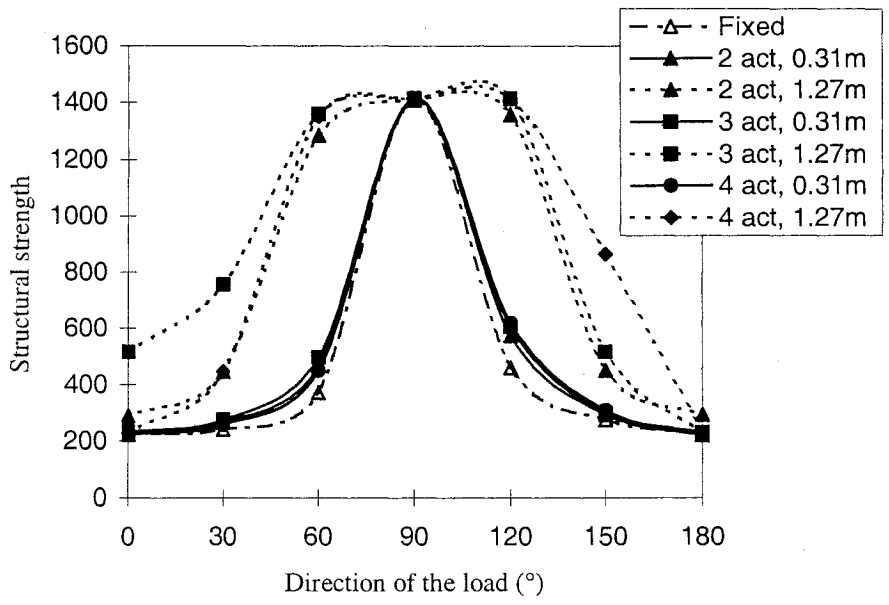

Figure 2.5. Structural strength versus direction of the applied load for the fixed and optimized adapted structure under static load.

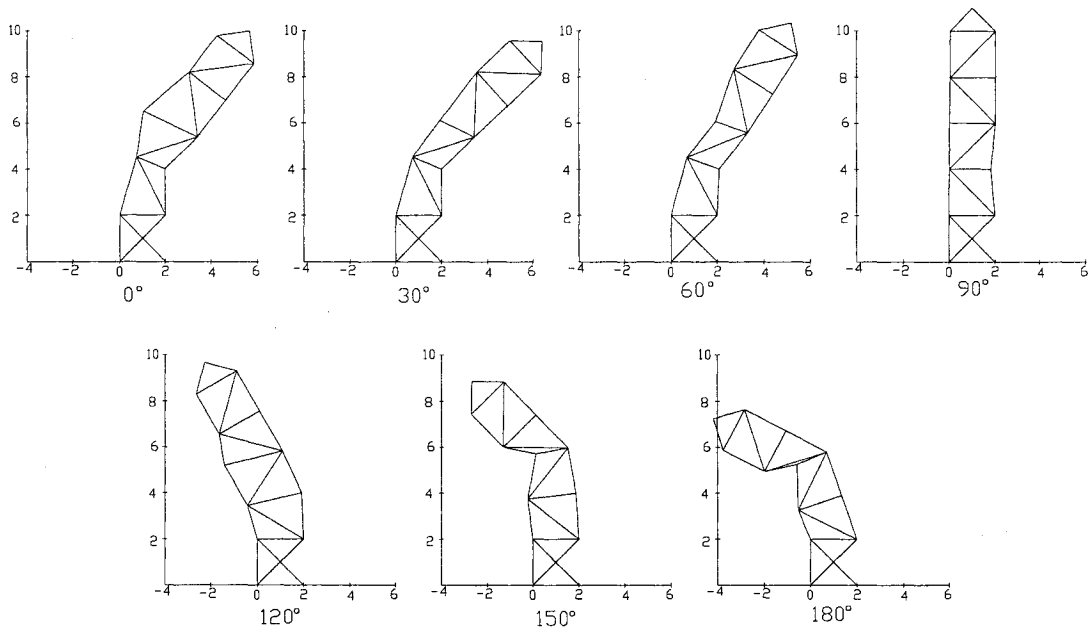

Figure 2.6. Optimal configurations with 4 active elements and maximum stroke of 1.27 m.

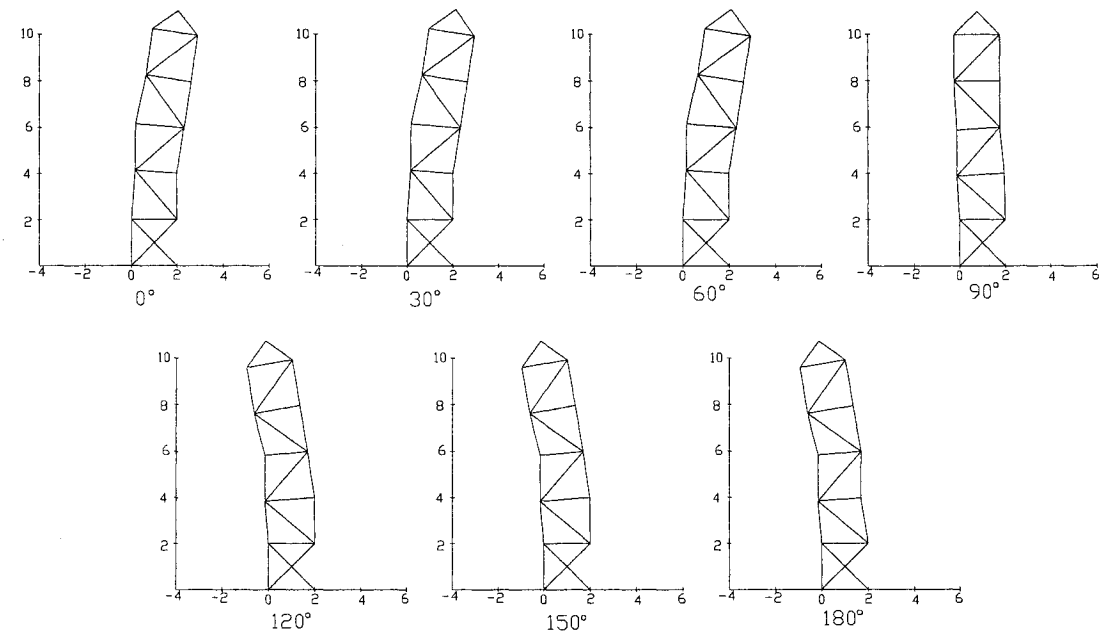

Figure 2.7. Optimal configurations with 4 active elements and maximum stroke of 0.31 m.

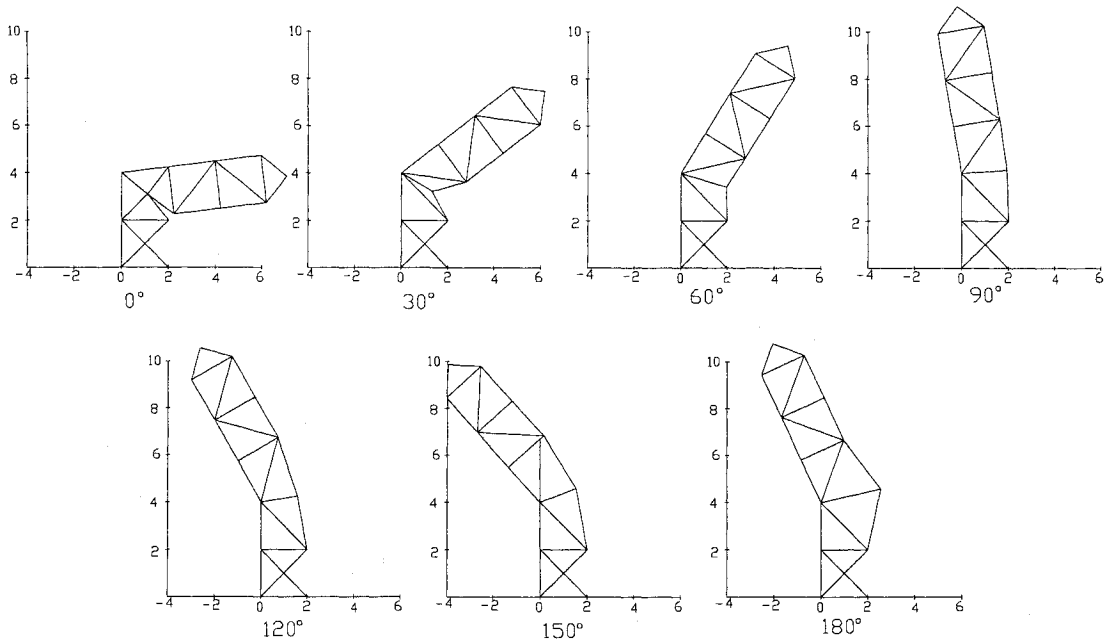

Figure 2.8. Optimal configurations with 3 active elements and maximum stroke of 1.27 m.

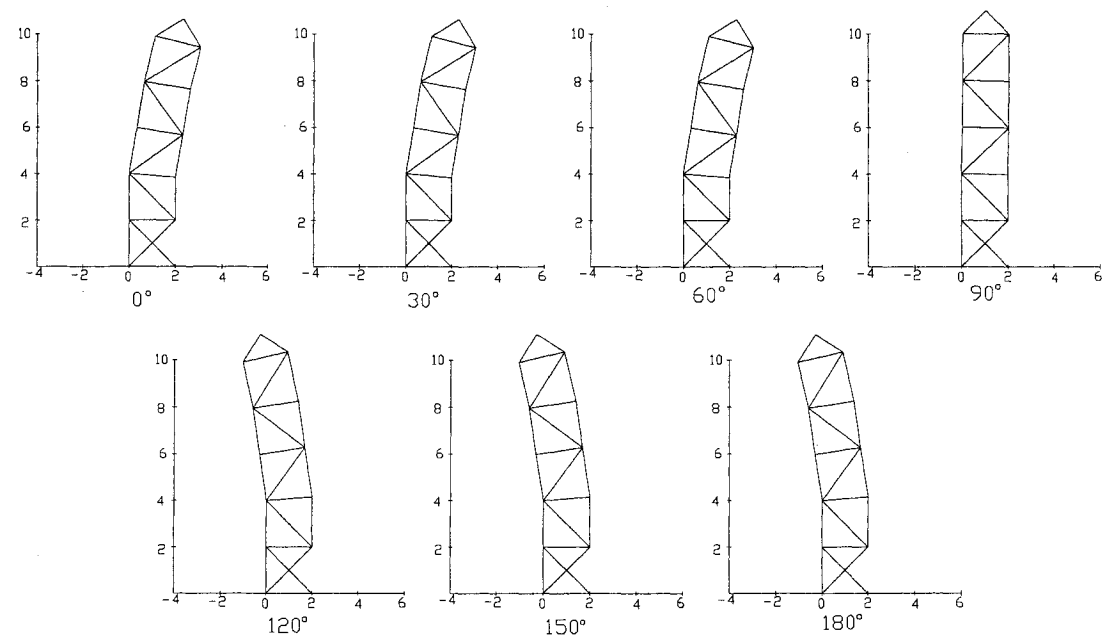

Figure 2.9. Optimal configurations with 3 active elements and maximum stroke of 0.31 m.

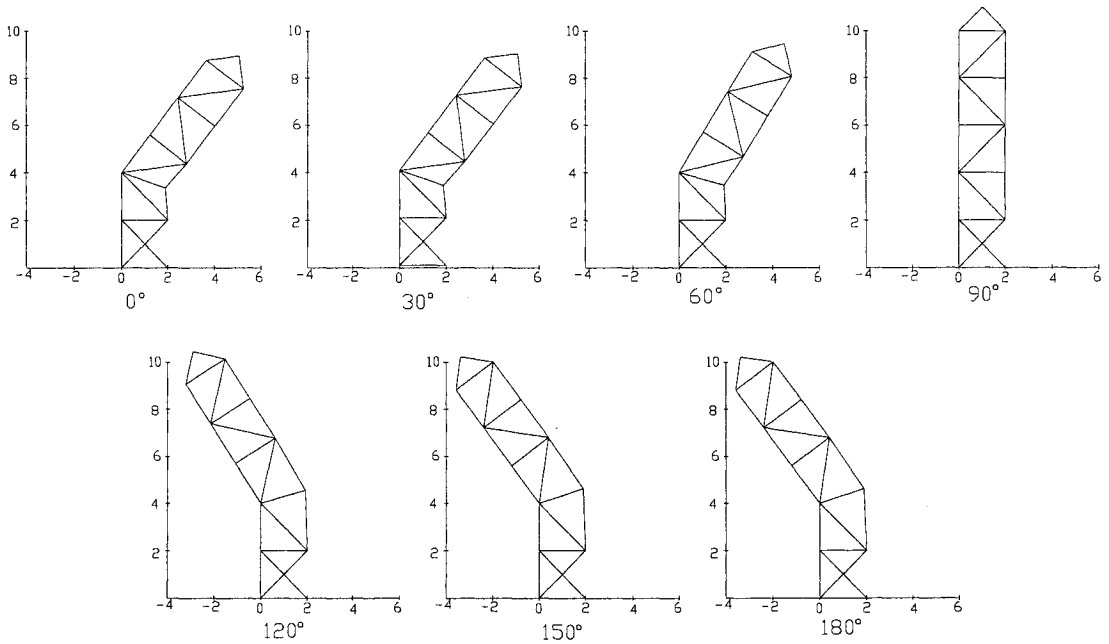

Figure 2.10. Optimal configurations with 2 active elements and maximum stroke of 1.27 m.

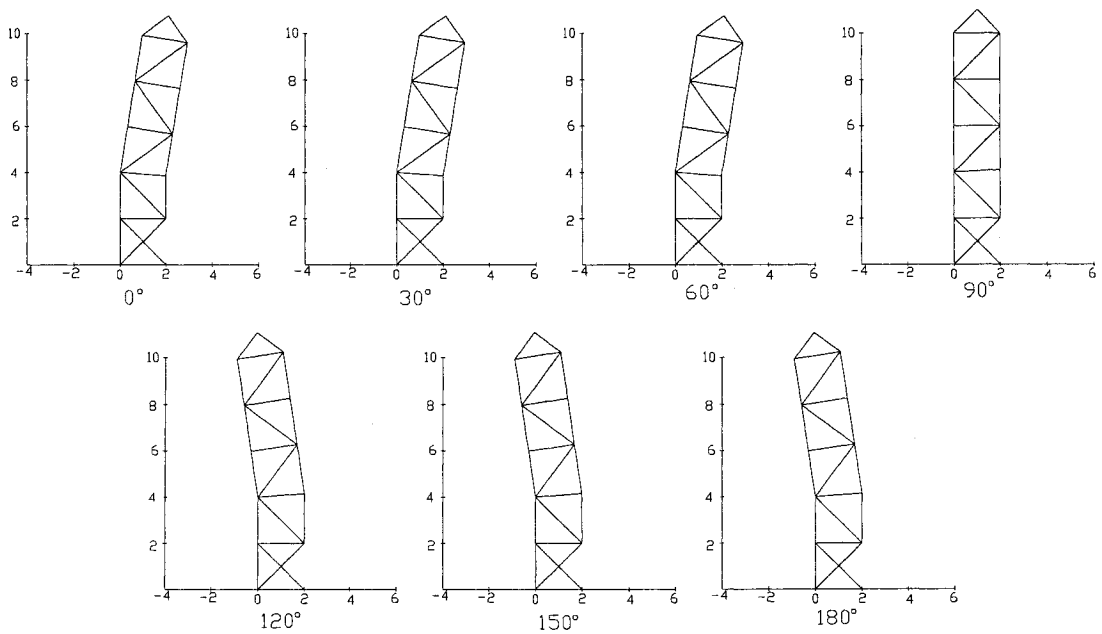

Figure 2.11. Optimal configurations with 2 active elements and maximum stroke of 0.31 m.

From the results, it can be realized that the location of the active elements in an adaptive truss structure plays a critical role in the ability of the structure to adapt itself to changes of the load. It has been shown that the location of actuators or active members depends on the number of the active elements that they should be were in the lower part of the structure. It is also noted that the structural strength is improved significantly using simultaneous optimal placement of actuators and adaptively optimized geometries. The best effect of the active elements is when they are placed in the same triangle in the structure. Furthermore the structural strength is improved when the stroke of the active elements is increased; in fact, large stroke is required to improve the structural strength considerably.

2.5. Topology, size and geometry optimization of the real life structures

Truss structures are widely employed in the industrialized world. They appear in bridges, towers, pylons, roof supports, building exoskeletons or high technology light space structures. This part of the thesis investigates the simultaneous size, geometry and topology optimization of real life large truss structures.

Many large truss structures are constructed from the duplication of some basic structural modules called cells or bays. Here, it is stated that the final optimum design may be reached by optimizing the characteristics of the basic bays instead of optimizing the whole structure through individual elements. Both single and multi-objective functions based on the mass of the structure and the maximum nodal displacement, are considered as the cost functions. In order to have realistic optimal designs, the cross-sectional areas are extracted from the standard profiles according to AISC codes and

practical conditions are imposed to the bays. The design optimization problem is also constrained by the maximum stress, maximum slenderness ratio and the maximum and minimum cross-sectional area of the truss members. To accommodate all these constraints, two different penalty functions are proposed. The first penalty function considers the normalization of violated constraints with respect to the allowable stress or slenderness ratio. The second penalty function is a constant function, which is used to penalize the violations of the slenderness ratio.

An efficient and practical methodology based on the GAs capable of design optimization of realistic truss structures is presented. Generally the design optimization of truss structures generates the design parameters with little or no practical use. For instance the optimum cross-sectional areas of the truss members may not be found on the market, thus imposing high manufacturing cost. Even if the optimization process considers only profiles from the market, the applicability of the final designs is limited due to the involvement of numerous types of profiles and the challenge associated with the assembly of such a structure. Also, generally the optimum design implies many changes of cross-sectional areas at the location of joints, which is not practically recommended. In addition, when the simultaneous optimization of the size and topology of the structure is considered, the optimum structure may include numerous types of elements from different material and geometrical characteristics, which is not feasible from the manufacturing point of view.

In this part, it is considered that the realistic large truss structures are fabricated from the arrangement of the basic bays. Thus, the objective is the optimization of the parameters of the bay. Based on this realistic consideration, the solution space is

drastically reduced and the optimum result can be found efficiently and accurately. Furthermore due to this arrangement, the final optimum design will require few different standard elements, which can be easily found on the market. Thus a final optimum design could be fabricated with low manufacturing cost.

2.5.1. Statement of the problem for topology, geometry and size optimization problem

For this optimization problem both single and multicriteria objective functions are investigated. For the latter, the objective is to minimize both the mass and the maximum nodal displacement and for the former the goal is just minimization of the mass. Thus, the components of the objective function (2.3) may be defined as:

$$f_1(x) = \rho L(x) A \tag{2.35}$$

$$f_2(x) = \max(U(x)) \tag{2.36}$$

subject to:

$$\sigma(x) \leq \sigma(x)_{allow} \tag{2.37}$$

$$\lambda(x) \leq \lambda(x)_{allow} \tag{2.38}$$

$$A_{min} \geq A_i \geq A_{max}; \quad i = 1,...,k \tag{2.39}$$

where $\rho = [\rho_1, \rho_2, ..., \rho_k]$ is the mass density vector; $L(x) = (L_1(x), L_2(x), ..., L_k(x))$ is the length vector; $A = [A_1, A_2, ...A_k]$ is the vector of cross sectional areas; $A_{\min}$ and A_{max} are the vector of lower and upper bound of cross-sectional areas and k is the number of elements. Another constraint regarding the geometry characteristics of the bays or the number of bays will also be specified for each particular problem. The vectors

$\sigma(x)$ and $\lambda(x)$ contain the stress and the slenderness ratio of each element and their respective allowable values are defined in the vectors σ_{allow} and λ_{allow} respectively. $U = [U_1, U_2, ..., U_j]$ is the vector of nodal displacement. It is noted that using FEM nodal displacement vector can be calculated from the equilibrium equation as:

$$U = K^{-1}F \tag{2.40}$$

where K and F are the system stiffness matrix and the nodal force vector, respectively.

To guard against buckling, the stability constraint is considered as part of the design optimization problem. In this study in order to have a sense of real life design practice, the AISC codes (AISC 1989) has been adopted for the relative design specifications. Thus, the allowable tension stress is considered to be $0.6\sigma_y$; the allowable member slenderness ratio is specified to be 300 for tension members and 200 for compression members; to guard against buckling the allowable compression stress σ_i^b of member i may be determined from the following equations according to AISC formulation:

$$\sigma_i^b = \frac{12\pi^2 E}{23\lambda_i^2} \qquad \text{for} \qquad \lambda_i > C \tag{2.41}$$

$$\sigma_i^b = \frac{\left(1 - \frac{\lambda_i^2}{2C^2}\right)\sigma_y}{\frac{5}{3} + \frac{3\lambda_i}{8C} - \frac{\lambda_i^3}{8C^3}} \qquad \text{for} \qquad \lambda_i < C \tag{2.42}$$

where $\lambda_i = L_i / r_i$ is the slenderness ratio, $C = \pi\sqrt{2E/\sigma_y}$, and σ_y, L_i and r_i are the yield stress, the length and the radius of gyration of the cross-section of the member i, respectively.

To convert the constrained problem to unconstrained problem, a penalty function is introduced to the objective function. Penalty functions penalize infeasible solutions by reducing their fitness values in proportion to the violation. In other words, the penalty function is applied whenever the constraints are violated.

Different types of penalty functions have been proposed to handle the constraints. In deterministic methods such as the sequential unconstrained minimization technique (SUMT), the quadratic penalty function is frequently used in order to keep the continuity of the gradients (Pardalos and Rosen 1987). Similar functions in combination with GAs have been applied by Goldberg and Santami (1986) and Galante (1996). In these functions the constraint violation is squared and penalized by a scalar. Simple constants or normalized stresses are used by Deb and Gulati (2001) to penalize the cost function. Sandgren and Cameron (2002) employed the difference and standard deviation between the allowable and the nominal stress and displacement. Nanacorn and Meesomklin (2001) used an adaptive penalty function, which is able to adjust itself during the evolution.

Here different types of penalty functions are considered. The first type of penalty function considers the normalization of violated constraints with respect to the allowable stress or slenderness ratio. The second type of penalty function is a constant function, which is used to penalize the violations of the slenderness ratio. Considering this, the penalty functions may be defined as:

$$p_l(x_i) = \begin{Bmatrix} c_{pl} * (\sigma(x_i) - \sigma_{max}(x_i)) / \sigma_{max}(x_i) & for \ |\sigma(x_i)| > |\sigma_{max}(x_i)| \\ 0 & otherwise \end{Bmatrix} \quad (2.43)$$

$$p_2(x_i)=\begin{cases} c_{p2} * (\lambda(x_i)-\lambda_{max}(x_i))/\lambda_{max}(x_i) & for \ \ \lambda(x_i)>\lambda_{max}(x_i) \\ 0 & otherwise \end{cases} \tag{2.44}$$

$$p_3(x_i)=\begin{cases} c_{p3} & for \ \ \lambda(x_i)>\lambda_{max}(x_i) \\ 0 & otherwise \end{cases} \tag{2.45}$$

where c_{p1}, c_{p2} and c_{p3} are the penalty coefficients. The normalization of the violations allows having large penalty values at the initial stage when the solution is far from the optimum point and small values when the solution is close to the optimum point. The penalty functions in Eqs. (2.43) and (2.44) will be used to penalize the size of the members and Eq. (2.45) will be applied to modify the number of bays. The coefficients c_{p1}, c_{p2} and c_{p3} are used to control the magnitude of the penalty values. To select these values different trials were performed. Big penalty coefficients can lead to slow convergence far from the global optimum. Small penalty coefficients can produce violations of the constraints. The value of the penalty coefficients c_{p1}, c_{p2} and c_{p3} are selected as 6.5, 8 and 1, respectively. For instance, the penalty coefficient of 6.5 means that the algorithm uses the next bigger cross sectional area for each 15% of violation. It is noted that for case of discrete design variables, the penalty functions may require to be rounded.

In this work the proposed methodology considers that the whole truss structures are fabricated from the multiplication of some fundamental bays, which is mainly the case in many real-life truss structures. Thus the design optimization of entire structures is reduced to the design optimization of the bays. This will enable to perform size, topology and geometric optimization of large real-life truss structures with relatively few design variables and thus reduce the computational effort. From the optimization point of view,

this practical arrangement will cause the space solution to be reduced drastically and also cause the convergence to the optimum solution to be faster and more accurate. Since the optimized bays are made of truss elements with profiles available on the market, the fabrication cost would be significantly reduced. Moreover, the optimized bays can be practically used to assemble the whole structures easily, thus reducing the assembling cost drastically and avoiding joint connection problems.

2.5.2. Illustrative examples of optimization of real life structures

To demonstrate the accuracy and efficiency of the proposed methodology three practical 2D and 3D truss structures have been optimized. The objective function is to minimize the weight or minimize both the weight and maximum nodal displacement. Besides the constraints in Eqs. (2.37)-(2.39), structures are also guarded against the local buckling described by Eqs. (2.41) and (2.42). In the problems discussed in this section the material is steel with modulus of elasticity $E = 201 \times 10^3$ MPa, yield stress $\sigma_y = 248.8$ MPa, and density $\rho = 7851$ kg/m^3.

In order to ensure that the final optimum design is practically realizable, the possible cross sectional areas will be selected from the profiles available on the market. Two different groups of selected steel profiles are presented in Table 2.3. The first group comprises only pipes. The second group contains W, S, HP, and L profiles. In both groups the sections are arranged in an ascending order. All the specific properties such as the cross-sectional area, the radius of gyration, the density (mass per unit length) and the moment of inertia of the cross sections could be obtained from the standards (AISC 1989).

In the GAs process a single point crossover with a probability P_c of 0.6 has been used. Consequently, the reproduction operation is conducted as it was explained in the Section 2.3.2.4. It requires to define a probability of reproduction, P_r, which is assumed to be 0.15. Moreover, the probability of mutation P_m, and the initial population n are assumed to be 0.005 and 150, respectively. The values of P_c, P_m are values similar to those found in the literature (Goldbert et Santami 1986; Galante 1986; Prendes et al. 2005). Also different trials were performed to select the appropriate values of P_r and n,

Table 2.3. Selected standard steel profiles from the AISC manual (1989)[1].

Group I	Group II
SP 1/2	L 1x1x1/8, L 1-1/2x1-1/2x1/4
EP 1/2	L 2x2x1/4, L 2-1/2x2-1/2x5/16
SP 3/4,	L 3x2x1/2, L 3x2-1/2x3/8
EP 3/4	L 3x3x1/2, L 3-1/2x3-1/2x3/8
SP 1/2	L 3-1/2x2-1/2x1/2, W 8x10
EP 1	L 4x3x1/2, L 6x3-1/2x3/8
SP 11/4	L 5x3x1/2, L 5x3-1/2x1/2
SP 11/2	L 4x4x5/8, L 5x5x1/2
EP 11/4	W 12x19, L 6x6x1/2
SP 2	L 6x4x5/8, l 7x4x5/8
EP 11/2	L 9x4x9/16, W 14x26
EP 2	W 10x30, W 16x31
SP 21/2	W 14x34, HP 8x36
SP 3	L 8x4x1, W 10x39
EP 21/2	S 12x40.8, HP 10x42
SP 31/2	L 8x6x1, W 18x46
EP 3	W 12x50, L 8x8x1
SP 4	W 14x53, S 18x54.7
EP 31/2	W 21x57, W 16x57
SP 5	HP 13x60, W 24x62
EP 4	W 8x67, W 18x71
SP 6	S 20x75, W 12x79
EP 5	W 14x82, S 20x86
SP 8	W 16x89, W 21x93
EP 6	W 10x100, W 24x103
SP 10	W 14x109, W 18x119
EP 8	W 27x129, W 21x132
SP 12	W 14x145, W 30x146
DEP 6	W 18x158, W 27x161
EP 10	W 33x169, W 24x176
EP 12	W 30x191, W 33x201
DEP 8	W 36x210, W 36x230

[1] SP, ES and DEP are standard, extra strong and double extra strong, respectively.

2.5.2.1. Optimization of a 22-Bar Planar Truss Structure

The 22-bar planar truss structure is shown in Figure 2.12. The structure is fixed at nodes 1 and 2 and the downward force of 49050 N has applied at the last node. This is a benchmark example which is studied by Erbatur (2000) and selected here in order to compare the results of the proposed methodology.

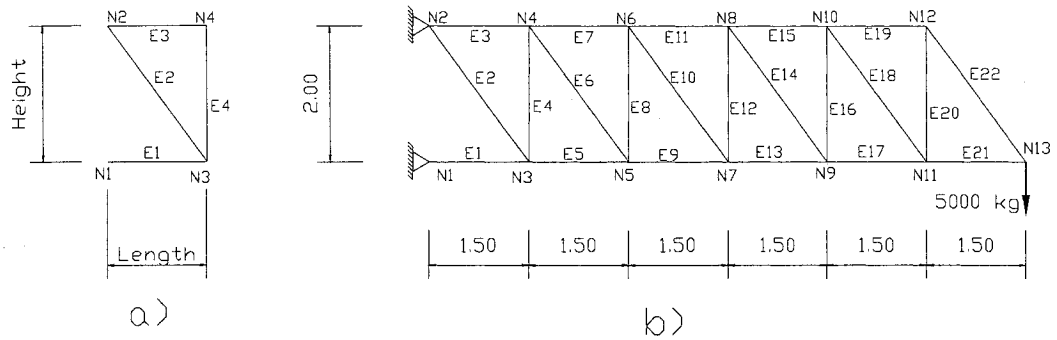

Figure 2.12. a) Basic bay of a statically determinate 22-bar truss; b) Complete structure.

The objective function is to minimize the mass of the structure under stress and slenderness ratio constraints. The allowable compressive stress has been determined using Eqs. (2.41) and (2.42) according to the AISC standards. The possible cross-sectional profiles are selected from the elements of Group I in Table 2.3.

Three different cases have been investigated in this problem. Case I is a size optimization in which the geometry and topology of the structure are assumed to be fixed and the design variables are only the cross-sectional area of the members. A minimum mass of 243.1 kg has been obtained for this case. The optimum results for cross-sectional areas are shown in Table 2.4. It is noted that all constraints have been satisfied in the optimum point. This problem has also been investigated using GAs by Erbatur et al. (2000) and a mass of 248.8 kg has been reported. The true optimum mass is recorded as

238.1 kg. It can be realized that the slightly better optimum solution has been obtained in this study. It is also interesting to note that in this case only 6 optimum profiles are matched with the true optimum profiles; while 17 optimum profiles recorded by Erbatur et al. (2000) are matched with true optimum result. However the optimum mass in this study turns out to be lower than that obtained by Erbatur et al. (2000). This may be due to the fact that structural optimization problems are highly non-unimodal.

In the Case II the number of bays and the height of the structure are also introduced as the design parameters. Increased number of bays reduces the stresses and the buckling effect, however they increase the weight of the structure. It is interesting to note that the minimum mass of 236.7 kg has been obtained in this case, which is about 1.4 kg lower than the true optimum result for the original problem. Also the maximum nodal displacement has been found to be 16% lower than that of case I. The optimum height and the number of bays of the structure have been found to be 2.095 m and 3 m, respectively. Knowing the total length of structure and the number of bays, the length of the individual bay is automatically determined. It is noted that no constraint violation exists at the optimum point.

The iteration history for the average of the population and optimum solution of the evolutionary process in both Cases I and II are shown in Figure 2.13. Improvement of the chromosomes through the process can be realized from this figure.

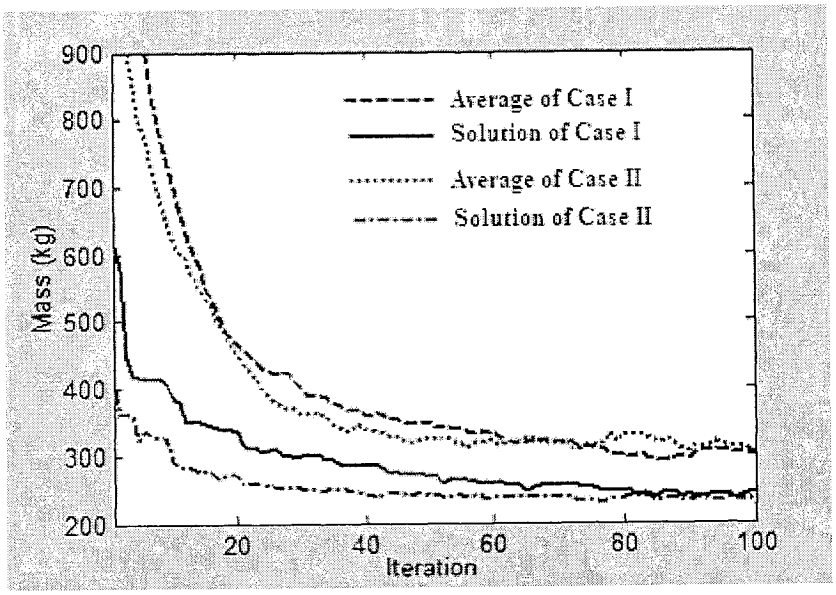

Figure 2.13. Genetic history of the solution and the average for size optimization of 22-bar plane truss for trial I and II.

In the trial III, a single bay has been optimized in order to find the optimum solution of the whole structure. The objective is to minimize the mass of the total structure through the optimization of the parameters of an individual bay. The total structure will then be assembled through the multiplication of this single bay. The design variables are the member's cross-sectional areas, the height and the number of bays. Knowing the length of the total structure, the length of each bay could be automatically determined. These design variables are sufficient to define the size, topology and geometry of the whole structure. The minimum mass of 293 kg has been obtained for this case. The optimum height and length of the bay was found to be 1.69 m and 3 m, respectively. The optimum cross-sectional profiles for elements 1, 2, 3 and 4 for the individual bay shown in Figure 2.12a have been found to be SP-3-1/2, SP-1/2, SP-1/2, EP-1-1/4, respectively, and none of the constraints have been violated.

Table 2.4. Optimum results for 22-bar planar truss structure

Member	Stress, σ Case I $\times 10^8$ Pa	σ_{allow} Case I $\times 10^8$ Pa	λ Case I	True Optimum (Erbatur 2000)	(Erbatur 2000)	Case I	Case II
1	-1.1558	-1.2576	51.8027	SP 3 ½	SP 3 ½	EP 3	SP 4
2	1.4827	1.4928	182.2689	EP 1	EP 1	SP 1 1/4	SP 2
3	-0.7372	-0.8977	100.0510	SP 3	SP 3	SP 2	SP 2
4	1.2984	1.4928	50.9096	SP 2	SP 2	SP 3	EP 2
5	-1.0804	-1.3037	44.0710	SP 3 1/2	SP 3 1/2	SP 3 1/2	EP 3
6	1.4669	1.4928	182.2689	EP 1	EP1 1/2	SP 1 1/4	SP 2
7	-0.7297	-0.8977	100.0510	SP 2 1/2	SP 2 1/2	SP 2	SP 2
8	1.3568	1.4928	62.3602	SP 2	SP 2	SP 2 1/2	SP 1 1/2
9	-1.0344	-1.2631	50.9096	SP 3	SP 3	SP 3	SP 2 1/2
10	1.4526	1.4928	182.2689	EP 1	EP 1	SP 1 1/4	SP 2
11	-0.7231	-0.8977	100.0510	EP 2	SP 2 1/2	SP 2	
12	1.1645	1.4928	77.0955	SP 2	SP 2	EP 2	
13	-1.0138	-1.1894	62.3602	SP 2 1/2	SP 2 1/2	SP 2 1/2	
14	1.4405	1.4928	182.2689	EP 1	EP1 1/4	SP 1 1/4	
15	-0.7176	-0.8977	100.0510	SP 1 1/2	SP 1 1/2	SP 2	
16	1.4334	1.4928	94.7915	SP 2	SP 2	SP 1 1/2	
17	-1.0704	-1.0995	75.0383	SP 2	SP 2	SP 2	
18	1.4307	1.4928	182.2689	EP 1	SP 1	SP 1 1/4	
19	-0.7132	-0.8977	100.0510	EP 3/4	SP 1 1/4	SP 2	
20	1.3188	1.4928	183.9723	SP 2	SP 2	EP 3/4	
21	-0.6482	-0.7828	112.7006	SP1 1/2	SP 1 1/2	EP 1 1/4	
22	1.4894	1.4928	241.8310	EP 1	EP 1 1/2	EP 1	
Mass (kg)				**238.1**	**248.8**	**243.1**	**236.7**

It is noted that although the optimum mass for this case is slightly higher than those in cased I and II, the less number of profiles required to assemble the structure and thus enable an easy fabrication, makes this approach extremely cost effective and

practical. The comparison between these three cases is summarized in Table 2.5. It is clear that case III is computationally significantly more efficient than the other two cases.

Table 2.5. Comparison between different optimization cases for 22-bar planar truss structure.

	Case I	Case II	Case III
Objective function (Kg)	243.1	236.7	293.0
Time (sec)	345	451	91
Analyzed structures	13554	16937	3564
Space solution	1298e33	6.646e35	5.368e8
Bits of chromosome	110	119	29
Number of bays	5	3	3
Number of elements	22	10	10
Iterations	100	100	29
Dispmax(m)	0.0409	0.0343	0.0297
Height (m)	2.0	2.065	1.69

2.5.2.2. Optimization of a Single Lacing Space Truss Structure

In this section, the proposed methodology has been applied to optimize a single-lacing truss structure as shown in Figure 2.14. These kinds of structures are usually used to construct various types of cranes, as shown in Figure 2.15. Practically, the whole structure shown in Figure 2.14b can easily be fabricated by using a basic bay shown in Figure 2.14a. The basic bay has 9 elements. Taking advantage of the symmetry in the structure, it has been assumed that the elements 2 and 3, 4 and 5 and 7and 8 are similar. Thus, six design variables can define the size (cross-sectional area) of the profiles used

for these elements. Geometry and topology of the structure can also be defined by using the width, the height and the number of bays as design variables. As illustrated in Figure 2.14b, the structure is fixed from one side and the forces of 3924 N in X-direction, 7848 N in Y-direction and -78480 N in Z-direction are applied at the end nodes on the other side of structure. The lateral X and Y forces could represent for the inertia forces of the load and wind loads. The constraints are the allowable stress and slenderness ratio which are determined using Eqs. (2.41) and (2.42) according with AISC standards.

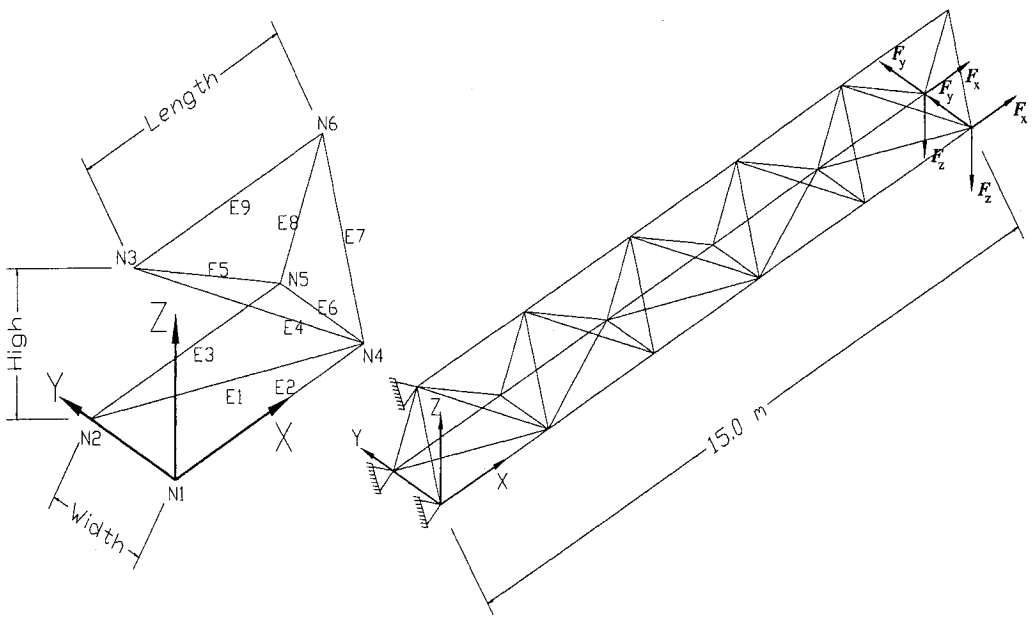

a) b)

Figure 2.14. (a) Description of the basic bay of a Single Lacing Space Truss Structure; (b) Cantilever truss structure with five bays

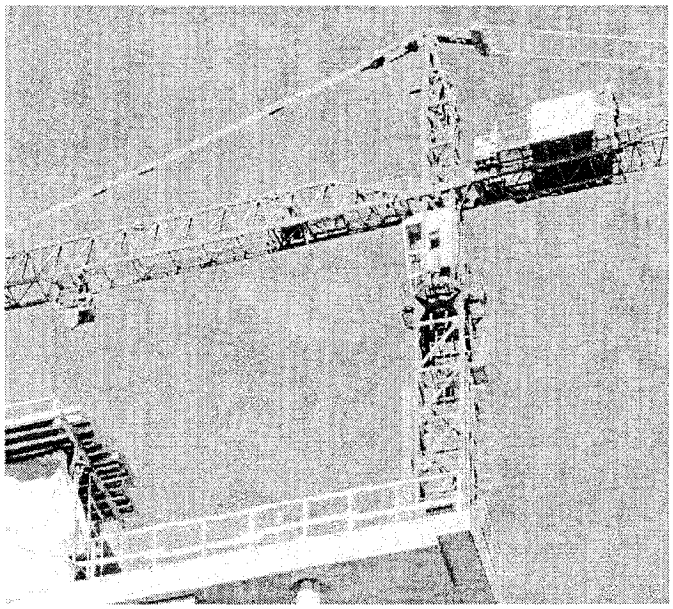

Figure 2.15. A tower crane constructed with the single lacing space truss structures

The direction of the diagonal member E1 is conditioned to change alternatively from one bay to the adjacent bay. Two different cases have been investigated. In Case I, the objective is to minimize the mass of the whole structure through optimization of an individual bay. However in case II, the objective is to simultaneously minimize the mass and maximum nodal displacement. The weighing factor of 20000 has been considered for the displacement component in order to provide the same preference for both displacement and mass. The possible profiles are extracted from the group II of Table 2.3.

A minimum mass of 1677 kg and 2724 kg have been obtained for Cases I and II, respectively. The maximum nodal displacement fore case I and II are 56 mm and 49 mm, respectively. The final optimum design for both Cases recommends 5 bays. The final design for the cross-sectional areas (type of profiles), the height of structure and the number of bays for both cases are given in Table 2.6.

Table 2.6. Results for different cases of optimization of a Single-Lacing Space Truss Structure.

	Case I	Case II
Objective	Mass	Mass + Disp.
Mass(Kg)	1677	2724
Max. disp (m)	0.056	0.049
Stress violations	E3 of 14.9%	E2 of 51%
λ violations	0	0
Time (sec)	1015	1052
Analyzed Struc.	31417	31670
Profiles:		
E1	L 3x2-1/2-3/8	L 3x2-1/2x3/8
E2, E3	W 10x30	W 10x30
E4, E5	L 2-1/2x2-1/2x5/16	L 3x2-1/2x3/8
E6	L 1-1/2x1-1/2x1/4	L 1-1/2x1-1/2x1/4
E7, E8	L 3x3x1/2	L 3-1/2x3-1/2x3/8
E9	L 2-1/2x2-1/2x5/16	W 14x26
Final design	5 bays, width=1.1984 m hight=2.668 m	5 bays, width=1.706 m hight=2.888 m

2.5.2.3. A Double-Layer Grid Space Truss Structure

A double-layer grid structure has been shown in Figure 2.16. This type of structure is commonly used as roof supports as illustrated in Figure 2.17. The basic unit shown in Figure 2.16a has been used to construct by duplication the whole structure shown in Figure 2.16b. The structure supports a load of 50 kg/m^2.

The structure is assumed to have a length of 9 meters in both X and Y directions with equal number of bays on both sides. The objective is to minimize the mass of the whole structure through the optimization of the parameters of the individual bay. The design variables are the cross-sectional areas of the members in a basic bay as shown in Figure 2.16a, which are selected from Group I in Table 2.3. The height of the structure and the number of bays in X or Y directions are evaluated after the optimization is completed. The optimum results have been provided in the Table 2.7. A minimum mass of 1767 Kg has been obtained. The optimum structure consists of 6 bays in each X and Y directions with total of 409 elements and 98 nodes (287 D.O.F).

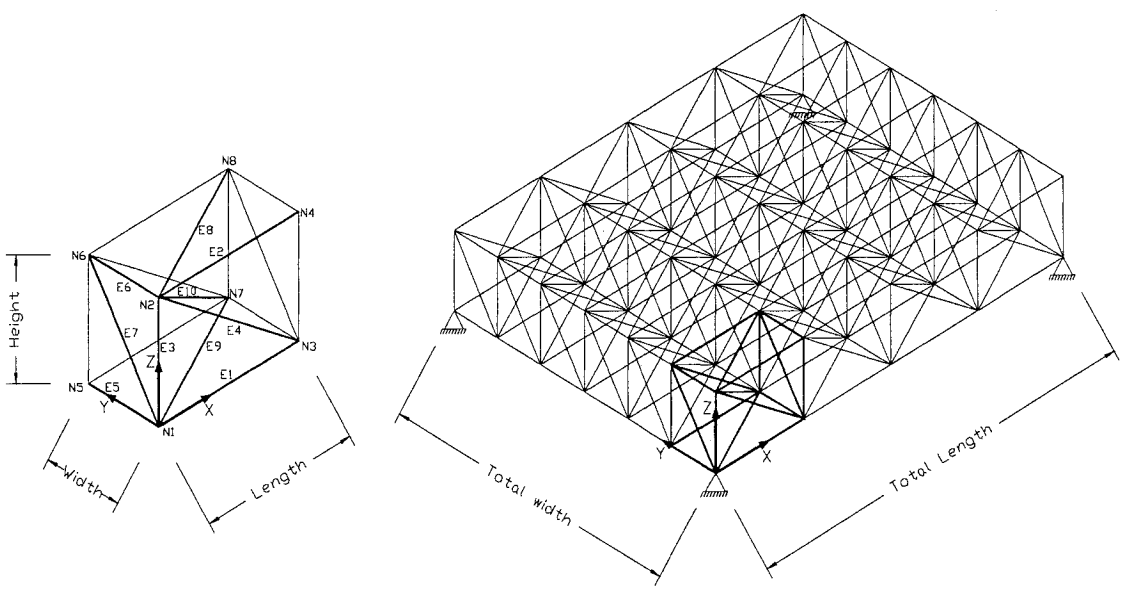

a) b)

Figure 2.16. (a) A single bay considered to construct the double-layer grid 3-D truss structure; (b) Schematic representation of the structure with 4×6 bays.

It is note that the final design is a practical structure with only 10 types of elements, which are available on the market. This will naturally cause drastic reduction in

assembly and fabrication cost of the whole structure. It should be noted that stress constraints have been violated in some members in final design. Although this violation is not significant, it can be easily remedied, using stronger elements for those members. This is possible since the violations and the number of elements violating the stress constraint is small.

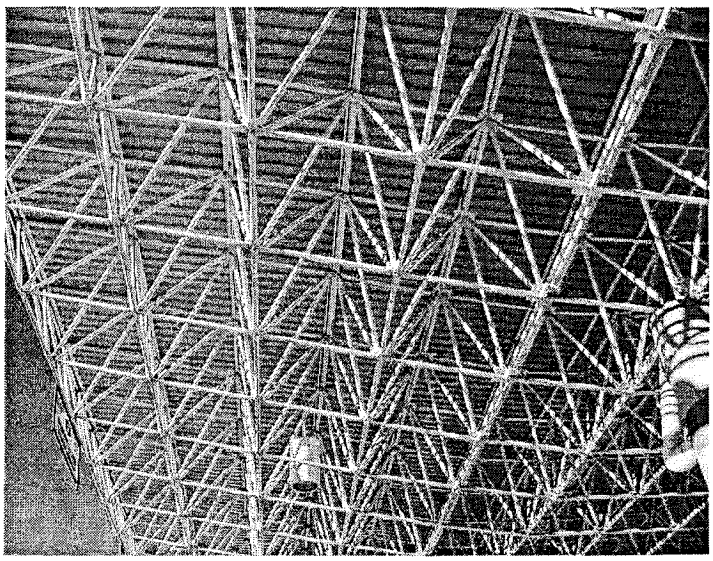

Figure 2.17. Typical application of the structure in roof supports.[2]

Structural problems are usually solved as direct problems. The designer who is facing a problem as any of the above presented in this paper is tempted to produce a configurational structure and work towards accurate evaluating the cross section of each member of the structure. Such an approach significantly limits the capability of producing a topography optimized design. The proposed method based on GAs optimization techniques enables the designer to find the optimal solution from a large map of possible designs.

---

[2] Courtesy of Luis Palomé, Constructor

Most practical large structures have been constructed from the duplication of a basic unit or bay in order to significantly reduce the fabrication and assembling cost. It has been shown that the design parameters of the basic bay could be used to perform the size, geometry and topology optimization of these kinds of structures. This will not only reduce the computational time drastically, but will also generate a realistic and practical optimum structure. In practical design problems usually the size of the members are selected from the standard profiles. This issue has also been incorporated in the proposed approach with introducing two groups of standard profiles.

In order to identify the global optimum the GAs algorithms has been employed as an optimizer. The finite element analysis has also been used to generate the analysis part of the design optimization problem. GAs has proved to be a reliable optimizer for discrete and multi-parametric problems and it has the capability to apply different constrains and penalty functions without any concern regarding the continuity and differentially of the objective function.

Although the GAs has proved to be an excellent tool to find the optimum designs, the experience of the designer play an important role to define some parameters of the optimization process. The design knowledge is essential to define the upper and lower limits for cross-sectional areas of the elements, the number, the length, the height, the width of the bays or even the selection of the set of possible profiles.

Table 2.7. Result for the optimum design of the Double-Layer Grid Truss.

Optimization process	**Variables**	12: height, number of bays and ten for profiles
	Chromosome (Bits)	59
	Load	50 kg/m^2
	Penalty functions	The same as the trial II
	Penalty coefficients	cp_1=6.5, cp_2=8, cp_3=1
Results	**Mass (Kg)**	1767
	Profiles :	E1=SP 3/4, E2=SP 3/4, E3=SP 3/4 E4=EP 1, E5=SP ¾, E6=SP ¾, E7=SP ½, E8=SP 1-1/4, E9=SP 1-1/4, E10=SP 1-1/4
	Stress violations (element and associated bay)	Element 7 bay (1,1) = 11% Element 2 bay (2,1) = 2% Element 2 bay (2,1) = 1.7% Element 6 bay (6,1) = 4.6%
	λ violations	0
	Max. disp. (m)	0.0469
	Bay	6 per side and height of 1.079 m

CHAPTER 3
MODELING THE HYSTERIS BEHAVIOUR OF THE MR DAMPERS

Recently, magnetorheological (MR) dampers have emerged as a potential technology to implement semi-active control in structures and vehicle applications in order to efficiently suppress vibrations. Perfect understanding about dynamic characteristics of such dampers is necessary when implementing MR struts in application. One of the important factors to successfully attain desirable control performance is to have a damping force model that can accurately capture the inherent hysteresis behaviour of MR dampers. In this chapter, a brief description about rheological fluids and MR dampers is provided; then, the most important models are shortly explained. Thus, a methodology to determine the characteristic parameters of the Bouc-Wen model is proposed. Based on the results of the proposed methodology, a new model, which depends on the amplitude, frequency and current excitation, is developed. Both, the methodology and the new model are validated with the experimental data obtained from a commercial MR damper.

3.1. Rheological fluids

Controllable fluids are materials that modify their rheological behaviour due to an applied electric or magnetic field. Typically, this change is manifested when the fluids are sheared by the development of a yield stress that is nonlinear to the magnitude of the applied field (Carlson 2001; Carlson et al. 1996a, b). These materials are commonly

referred to as electrorheological (ER) or magnetorheological (MR) fluids. Their ability to provide simple, quiet, rapid-response interfaces between electronic controls and mechanical systems made them attractive materials for new technological applications. These controllable fluids have the potential to radically change the way electromechanical devices are designed.

ER fluids are materials made of a dielectric base fluid with suspended dielectric particles of size 0.1-100 μm. When the ER fluid is exposed to an external electric field, the particles are polarized since the dielectric constant of suspension particles differs from the dielectric constant of the base fluid. These polarized particles interact and form chain-like or even lattice-like organized structures. Thus, the rheological properties of the suspension change effectively, e.g. the effective viscosity increases dramatically. In conclusion, the viscosity of the electrorheological liquid can be controlled with the electric field strength.

The potential of controllable ER fluids has been recognized since the 1940s when the first ER fluid patent (Winslow 1947) was registered and a paper describing the ER effect written by Willis Winslow (1949) was published. Since then, publications describing the properties, behaviour and application of ER fluids have abounded. ER fluids have been the topic for numerous theses and for many years the imminent, widespread application of ER fluids has been heralded. However, the successful commercialization of ER fluids is not achieved (Carlson et al. 1996) in spite of glowing predictions and the expenditure of sizable sums of R&D money.

The response time of electrorheological fluids is fast in order of 1-10 ms, which in principle enables the use of these liquids in such applications as electrically controlled clutches, valves and active damping devices. Perhaps the most striking application utilizing electrorheological fluids is an artificial muscle made of polymer suspension particles in a polymer gel.

ER fluids routinely exhibit dynamic yield strengths in the range of 2 to 5 kPa for electric fields on the order of 3 to 5 kV/mm and off-state viscosity in the range of 0.20 to 0.30 Pa-s at 25°C (Carlson and Spencer 1996). The maximum strength of a given ER fluid is generally limited by the electric field breakdown strength of the fluid. Operational temperature ranges for ER fluids depend on the type of polarization mechanism used to activate the fluid. Low conductivity, DC, ER fluids polarized by an ionic conduction mechanism are typically operational over the range of 10°C to 90°C. Such fluids have room temperature conductivity such that they require on the order of 5 mA/cm^2 at an electric field of 3 kV/mm. Non-ionic ER fluids are generally usable over a broader temperature range, typically -25°C to + 125°C. While they may exhibit a negligible DC conductivity, such non-ionic fluids are often used with high-frequency AC fields in order to minimize electrophoretic effects. In this case one must be able to provide sufficient non-dissipative, displacement current, perhaps as much as 1-2 mA/cm^2 at 3 kV/mm (RMS), because of the relatively large device capacitance (Carlson et al. 1996; Weiss et al. 1993).

MR fluids, which were developed in the late 1940's by Jacob Rabinow (1948), consist of ferromagnetic particles (in the order of 20-50 microns in diameter) that are

suspended in a carrier fluid. The ferromagnetic particles are often carbonyl particles. Other particles, such as iron-cobalt or iron-nickel alloys, have been used to achieve higher yield stresses from the fluid (Ashour et al. 1996). Fluids containing these alloys are impractical for most applications due to the high cost of the cobalt or nickel alloys. A wide range of carrier fluids such as silicone oil, kerosene, and synthetic oil can be used for MR fluids. The carrier fluid must be chosen carefully to accommodate the high temperatures to which the fluid can be subjected. The carrier fluid must be compatible with the specific application without suffering irreversible and unwanted property changes. The MR fluid must also contain additives to prevent the sedimentation of, and promote the dispersion of, the ferromagnetic particles.

MR fluids exhibit very fast switching (of the order of milliseconds) (Carlson and Spencer 1996) in their rheological properties (elasticity, plasticity, or viscosity) with the application of a magnetic field; thus making them excellent contenders for semi-active devices. MR fluid behaviour is controlled by subjecting the fluid to a magnetic field. The MR effects are often greatest when the applied magnetic field is normal to the flow of the MR fluid. In the absence of a magnetic field, the MR fluid flows freely while in the presence of a magnetic field, the fluid behaves as a semisolid.

Operational temperatures for MR fluids easily span -40°C to +150°C. MR fluids are generally limited by the properties of the carrier fluid used in the formulation rather than the details of the polarization mechanism. Usually, the dynamic yield strengths exhibited by MR fluids is around 50- 100 kPa for applied magnetic fields of 150-250 kA/m (~2-3 kOe) and off-state viscosity of 0.20 to 0.30 Pa-s at 25°C (Carlson and Spencer 1996; Weiss et al. 1993). The ultimate strength of MR fluids is limited by

magnetic saturation. The Table 3.1 gives a comparison of the properties between the ER and MR fluids

Table 3.1.. Comparison of the properties of typical MR and ER fluids (Carlson and Spencer 1996).

Property	MR Fluids	ER Fluids
Max. Yield Stress $\tau^2_{y(field)}$	50 - 100 kPa	2 - 5 kPa
Max. Field	~ 250 kA/m (limited by saturation)	~ 4kV/mm (limited by breakdown)
Viscosity (η_p)	0.1 - 1.0 Pa-s	0.1 - 1.0 Pa-s
Operable Temp. Range	-40 to +150 °C (limited by carrier fluid)	+10 to +90 °C (ionic, DC) -25 to +125 °C (non-ionic, AC)
Stability	Unaffected by most impurities	Cannot tolerate impurities
Response Time	milliseconds	milliseconds
Density	3 - 4 g/cm^3	1 - 2 g/cm^3
$\eta_p / \tau^2_{y(field)}$	10^{-10} to 10^{-11} s/Pa	10^{-7} to 10^{-8} s/Pa
Max. Energy Density	0.1 Joule/cm^3	0.001 Joule/cm^3
Power Supply (typical)	2 - 25 V @ 1 - 2 A(2 - 50 watts)	2 - 5 kV @ 1 - 10 mA (2-50 watts)

where the $\tau^2_{y(field)}$ is the yield stress caused by the applied field and η_p is the field independent plastic viscosity. There are many drawbacks to ER fluids, including relatively small rheological changes and extreme property changes with temperature.

Although power requirements are approximately the same, MR fluids require only small voltages and currents, while ER fluids require very large voltages and very small currents. For these reasons, MR fluids have recently become a widely studied 'smart' fluid.

MR fluid is composed of oil, usually mineral or silicone based, and varying percentages of ferrous particles that have been coated with an anti-coagulant material. When inactivated, MR fluids display Newtonian-like behaviour (Lord Materials Division 1999). When exposed to a magnetic field, the ferrous particles that are dispersed throughout the fluid form magnetic dipoles. These magnetic dipoles align themselves along lines of magnetic flux, as shown in Figure 3.1.

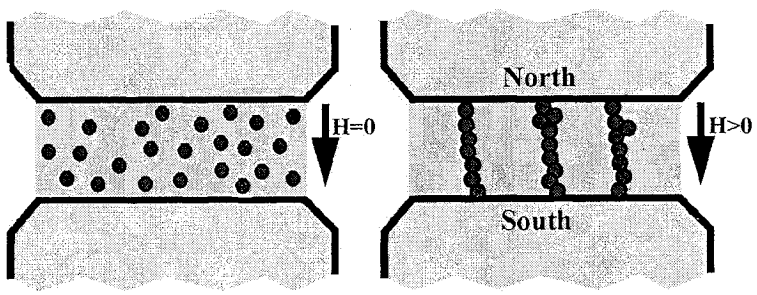

Figure 3.1 MR fluid ferrous particle arrangement in un-energized and energized modes.

The use of MR fluid can be in three different modes, all of which can be applied to MR damper design depending on the damper's intended use. These modes of operation are referred to as the squeeze mode, valve mode, and shear mode.

The squeeze mode is shown in Figure 3.2. A device that uses a squeeze mode has a thin film (on the order of 0.02 inch) of MR fluid that is sandwiched between pole surfaces.

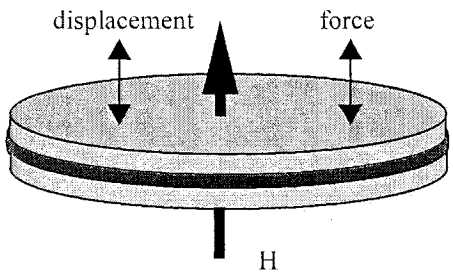

Figure 3.2. MR fluid used in squeeze mode (Yang 2001).

The shear mode is depicted in Figure 3.3. A MR fluid device is said to operate in shear mode when a thin layer (≈0.005 to 0.015 inch) of MR fluid is sandwiched between two paramagnetic moving surfaces. The shear mode is primarily useful for dampers that are not required to provide large forces or for compact clutches and brakes.

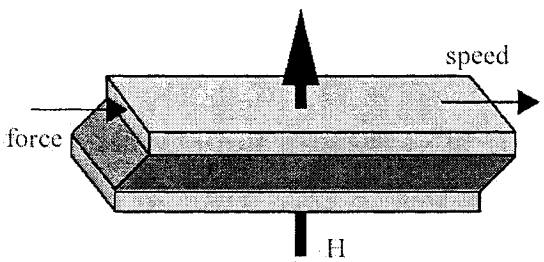

Figure 3.3. MR fluid used in shear mode (Jolly et al. 1999).

The valve mode is the most widely used mode of the operation. An MR device is said to operate in valve mode when the MR fluid is used to impede the flow of MR fluid from one reservoir to another, as is shown in Figure 3.4.

When the MR fluid is under a magnetic field, it also experiences changes in thermal, electrical, and acoustic properties besides the rheological changes. The MR effect is found to be very suitable in the construction of a hydraulic damper. The MR fluid essentially allows one to control the damping force of the damper by replacing mechanical valves commonly used in adjustable dampers. This offers the potential for a

superior damper with little concern about reliability since if the MR damper ceases to be controllable; it simply functions in a passive way.

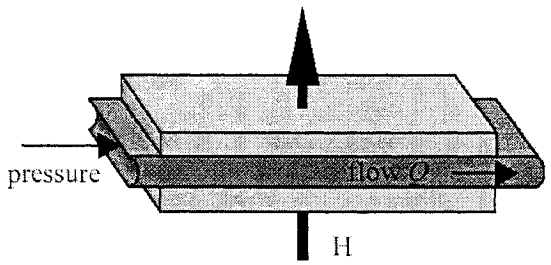

Figure 3.4. MR fluid used in valve mode (Jolly et al. 1999).

3.2. MR dampers

MR dampers are semi-active devices that use MR fluids to construct a versatile damping device. Because the strength of the magnetic field controls the yield stress of the fluid, devices utilizing MR fluid are expected to be applicable for a wide range of situations. A typical MR damper is shown in Figure 3.5. As it can be seen in a MR damper the fluid is transferred from above the piston to below (and vice versa) through the MR valve. The MR valve is a fixed-size orifice with the ability to apply a magnetic field, using an electromagnet, to the orifice volume. This magnetic field results in a change in viscosity of the MR fluid, causing a pressure differential for the flow of fluid in the orifice volume. The pressure differential is directly proportional to the force required to move the damper rod. As such, the damping characteristic of the MR damper is a function of the electrical current flowing into the electromagnet. This relationship allows the damping characteristic of the MR damper to be easily controlled in real time.

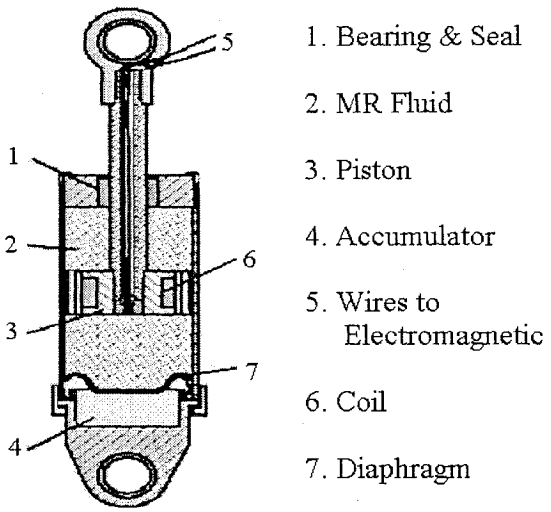

Figure 3.5. Functional configuration of an MR damper.

The accumulator is a pressurized volume of gas that is physically separated from the MR fluid by a floating piston or diaphragm. The accumulator serves two purposes. The first is to provide a volume for the MR fluid to occupy when the shaft is inserted into the damper cylinder. The second is to provide a pressure offset so that the pressure in the low-pressure side of the MR valve does not induce cavitation in the MR fluid by reducing the pressure below the vapour pressure of the MR fluid. Externally the compact design is very similar in size and shape to existing passive vehicle dampers. The only external parts are the two electrical leads for the electromagnet, which are connected to the current source.

There are three main types of MR dampers which are the mono tube, the twin tube, and the double-ended MR damper (El-Auoar 2002). Among these, the mono tube is the most common since it can be easily installed in any orientation and it has a compact size. A mono tube MR damper, shown in Figure 3.5, has only one reservoir for the MR fluid and an accumulator mechanism to accommodate the change in volume that results

from piston rod movement. The accumulator piston or diaphragm provides a barrier between the MR fluid and a compressed gas (usually nitrogen) that is used to accommodate the volume changes that occur when the piston rod enters the housing.

The twin tube MR damper has two fluid reservoirs, one inside of the other. Its configuration is shown in Figure 3.6, in which can be appreciated that the damper has an inner and outer housing, which are separated from each other by a foot valve. The inner housing guides the piston rod assembly, in exactly the same manner as in a mono tubes damper. The volume enclosed by the inner housing is referred to as the inner reservoir and the outer reservoir is the space between the inner and outerhousing. The inner reservoir is filled with MR fluid so that no air pockets exist. To accommodate changes in volume due to piston rod movement, an outer reservoir that is partially filled with MR fluid is used. Therefore, the outer tube in a twin tube damper serves the same purpose as the pneumatic accumulator mechanism in mono tube dampers.

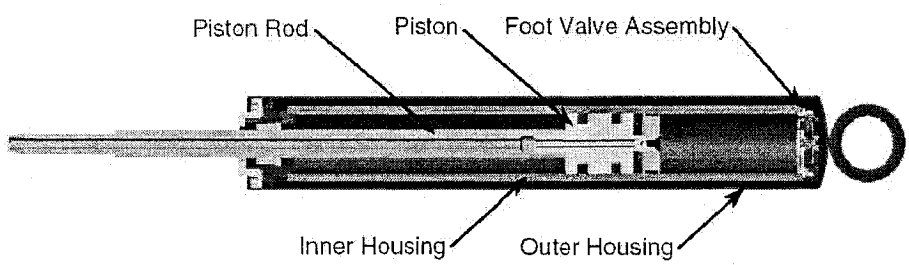

Figure 3.6. Twin tube MR damper (El-Auoar 2002).

The double-ended MR damper, shown in Figure 3.7, has piston rod of equal diameter protrudes from both ends of the damper housing. The double-ended damper does not have accumulator mechanism in view of the fact that there is no change in volume as the piston rod moves relative to the damper body.

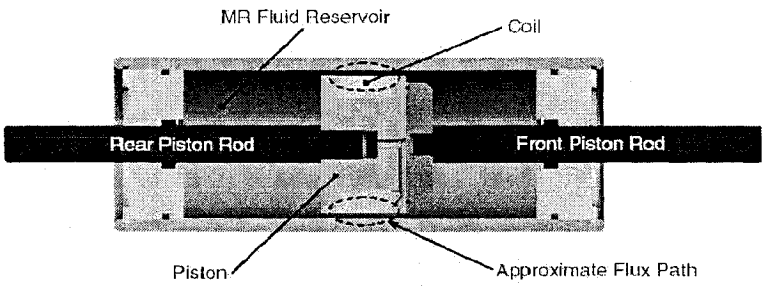

Figure 3.7. Double-ended MR damper (El-Auoar 2002)

In this work, the commercial MR damper RD-1005-3 (Lord Materials Division 2003) manufactured by Lord Corporation is employed to validate the proposed model and later it is embedded in the adaptive structure to reduce the vibration. This MR damper, which configuration is shown in the Figure 3.5, is a compact magnetorheological fluid damper unsurpassed in its combination of controllability, responsiveness, and energy density. As magnetic field is applied to the MR fluid inside the monotube housing, the damping characteristics of the fluid increase with practically infinite precision under 25-millisecond response time. This device is a monotube shock containing nitrogen gas at a high pressure of 300 psi in its accumulator. The Table 3.2 gives a summary of its typical characteristics.

Table 3.2. Characteristics of the MR damper RD-1005-3 from Lord Corporation (Lord Materials Division 2003)

Description	Values
Compressed length	6.1 Inches (155 mm)
Extended length	8.2 Inches (208 mm)
Body diameter	1.63 Inches (41.4 mm)
Shaft diameter	0.390 Inches (10 mm)
Weight	1.8 pounds (800 g)
For installation on pin	0.47 Inches (12 mm)
Electrical characteristics: Input current Input voltage Resistance	 2 amps maximum 12 V DC 5 ohms at ambient temperature 7 ohms at 160° F (70° C)
Damper forces (peak to peak): 2 in/sec at 1 amp 8 in/sec at 0 amp	 >500 pounds (2224 N) <150 pounds (667 N)
Mechanics characteristics: Minimum tensile strength Maximum operating temperature Storage temperature limits	 1000 pounds (4448 N) 160° F (70° C) 212° F to -40° F (100° C to -40° C)
Durability	2 million cycles @ ±0.5 inches (±13 mm), 2 Hz with input current varying between 0 and 0.8 amps
Response time (amplifier & power supply dependent)	< 25 msec –time to reach 90% of max level during a 0 to 1 amp step input @ 2 in/sec (51 mm/sec)

3.3. Hysteresis phenomenon and models

Hysteresis relates to looping graphs which associate two scalar time-dependent quantities other than in terms of a single valued function. Hysteresis is of interest in many different areas: ferromagnetics, superconductivity, spin glasses, semiconductors, economics and physiology, to mention a few. Hysteresis is characteristic of MR dampers because these devices rely on modifications of force-velocity relationships invariably associated with hysteretic behaviour. Loops are created when an input is varied back and forth between two consecutive boundaries. This is not the essence of hysteresis however; it is a particular case of "branching," which occurs at the reversals of an input and where memory has influence over the actual response.

There is no agreement on a general definition of hysteresis. Since the present work is motivated by systems engineering, a black box representation of the system is adopted along with the following definition (Visintin 1991): "At any time t, the output of a system depends not only on the input $y(t)$, but also on its previous trajectory (memory). The input–output relationship is invariant with respect to changes in the time scale (rate independence). When a system has memory and is rate independent, it is said to have hysteresis." From this definition it can be concluded that the response of the structural systems with embedded MR dampers is affected by the hysteresis phenomenon. Furthermore, for control purposes the controlled damping force depends on the hysteresis force.

Different models have been developed to simulate the hysteresis behaviour of controllable fluid devices, which are classified in quasi-static and dynamic models. Yang

(2001) has shown that the quasi-static models are not sufficient to describe the nonlinear damper force-velocity behaviour. Another classification divides the models in two categories: parametric and nonparametric (Smyth et al. 2002). Parametric identification is the most desirable, because if successful, the parameters in a model for the restoring force will have some physical meaning. The nonparametric model may be able to model response behaviour accurately and with considerable flexibility; however, their parameters usually have little or no physical meaning. In this section some of the more important parametric dynamic models are presented.

3.3.1. Bingham model

The Bingham model was proposed by Stanway et al. (1985, 1987). It is based on the stress-strain behaviour of the Bingham viscoplastic model which is often used to describe the behaviour of controllable fluids. The Bingham model consists of a Coulomb friction element placed in parallel with a viscous damper, as it is shown in Figure 3.8. In this model, for nonzero piston velocities $\dot{x}$, the force generated by the device is given by:

$$F = f_c \, sgn(\dot{x}) + c_0 x + f_0 \tag{3.1}$$

where c_0 is the damping coefficient and f_c is the frictional force, which is related to the fluid yield stress. An offset in the force f_0 is included to account for the nonzero mean observed in the measured force due to the accumulator.

For this model, the force-displacement is reasonably well modeled; however, this model does not exhibit the nonlinear force-velocity response behaviour observed in the

data for the case when the acceleration and velocity have opposite signs (or alternatively, when the velocity and the displacement have the same sign) and the magnitude of the velocities are small (Spencer et al. 1997).

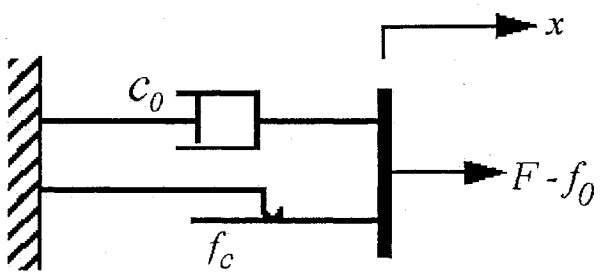

Figure 3.8. Bingham model for controllable fluid dampers (Spencer et al. 1997).

3.3.2. Viscoelastic-plastic model

The viscoelastic-plastic model was proposed by Gamota and Filisko (1991), which is shown in Figure 3.9, is a model based in the Bingham model and combined in series with a standard model of a linear solid (Shames and Cozzarelli 1992). Its governing equations are defined as:

$$\left.\begin{aligned} F &= k_1(x_2 - x_1) + c_1(\dot{x}_2 - \dot{x}_1) + f_0 \\ &= c_0\dot{x}_1 + f_c\, sgn(\dot{x}_1) + f_0 \\ &= k_2(x_3 - x_2) + f_0 \end{aligned}\right\}, \qquad |F| > f_c \tag{3.2}$$

$$\left.\begin{aligned} F &= k_1(x_2 - x_1) + c_1\dot{x}_2 + f_0 \\ &= k_2(x_3 - x_2) + f_0 \end{aligned}\right\}, \qquad |F| \le f_c \tag{3.3}$$

where c_0 is the damping coefficient associated with the Bingham model and k_1, k_2 and c_1 are associated with the linear solid material. It is noted that when $|F| \le f_c$ the Bingham part of the model is static.

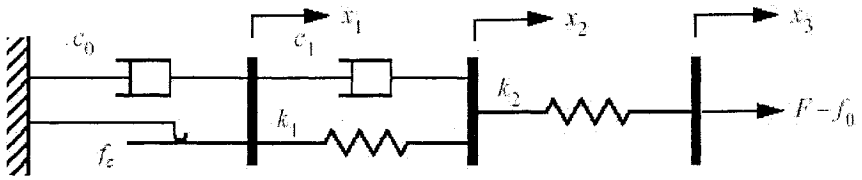

Figure 3.9. Viscoelastic-plastic model (Gamota and Filisko 1991).

3.3.3. Nonlinear hysteretic biviscous model

This model, which is shown in Figure 3.10, was proposed by Wereley et al. (1998). It is an extension of the nonlinear biviscous model having an improved representation of the pre-yield hysteresis.

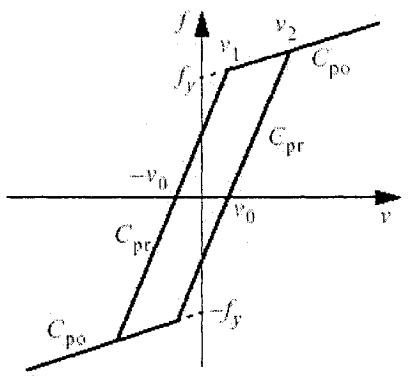

Figure 3.10. Nonlinear hysteretic biviscous model (Wereley and Pang 1998.)

The equations of the nonlinear hysteretic biviscous model can be described as:

$$f = \begin{cases} C_{po}\dot{x} - f_y & \dot{x} \le -\dot{x}_1 & \ddot{x} > 0 \\ C_{pr}(\dot{x} - \dot{x}_0) & -\dot{x}_1 \le \dot{x} \le \dot{x}_2 & \ddot{x} > 0 \\ C_{po}\dot{x} + f_y & \dot{x}_2 \le \dot{x} & \ddot{x} > 0 \\ C_{po}\dot{x} + f_y & \dot{x}_1 \le \dot{x} & \ddot{x} < 0 \\ C_{pr}(\dot{x} + \dot{x}_0) & -\dot{x}_2 \le \dot{x} \le \dot{x}_1 & \ddot{x} < 0 \\ C_{po}\dot{x} - f_y & \dot{x} \le -\dot{x}_2 & \ddot{x} < 0 \end{cases} \tag{3.4}$$

where the decelerating and accelerating yield velocity $\dot{x}_1$ and $\dot{x}_2$ are given by

$$\dot{x}_1 = \frac{f_y - C_{pr}\dot{x}_0}{C_{pr} - C_{po}} \text{ and } \dot{x}_2 = \frac{f_y + C_{pr}\dot{x}_0}{C_{pr} - C_{po}} \tag{3.5}$$

3.3.4. Bouc-Wen model

The Bouc-Wen model was initially formulated by Bouc (1971) as an analytical description of a smooth hysteretic model and later generalized by Wen (1976). The Bouc-Wen model shown in Figure 3.11 is one of the models that is numerically tractable and has been extensively used to characterize the hysteresis phenomenon in MR dampers, since it possesses the force-displacement and force-velocity behaviour, which resembles that of the real life MR dampers. The total damping force in the Bouc-Wen model can be represented by:

$$F\left(x(\tau), \dot{x}(\tau),\ 0 \le \tau \le t; t\right) = c_0\,\dot{x} + k_0\,x + \alpha\,z \tag{3.6}$$

where z is an evolutionary shape variable described by the first order differential equation as follows:

$$\dot{z} = -\gamma|\dot{w}||z|^{(n-1)}z - \beta\dot{w}|z|^n + A\dot{w} \tag{3.7}$$

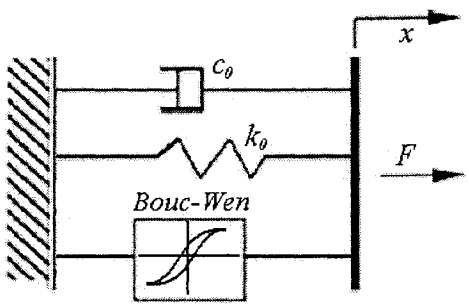

Figure 3.11. Bouc-Wen model.

where w is a generic variable the parameters c_0, k_0, α, β, γ, n and A are called shape or characteristics parameters of the Bouc-Wen model which are functions of current excitation, amplitude and frequency of vibration and can control the linearity in the unloading and the smoothness of the transition from the pre-yield to the post-yield region.

3.3.5. Phenomenological model

The phenomenological model shown in Figure 3.12, is based on the Bouc-Wen hysteresis model and is proposed by Spencer et al. (1997). A dashpot with damping coefficient of c_1 is added in series to produce the roll-off behaviour observed in the experimental data at low velocities and a spring k_1 is put in parallel to simulate the nominal damper force due to the accumulator.

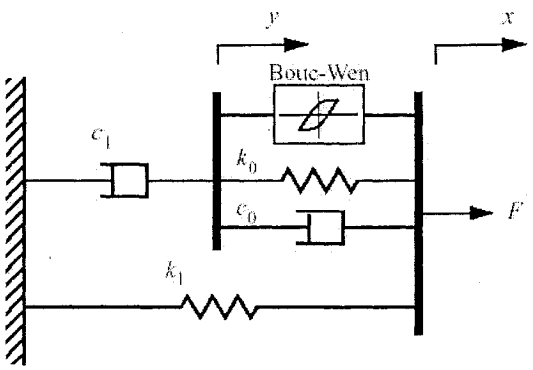

Figure 3.12. Phenomenological model (Spencer et al. 2000.)

The total force can be written as

$$f = c_1\dot{y} + k_1(x - x_0) \tag{3.8}$$

where z and y are governed by the following equations:

$$\dot{z} = -\gamma|\dot{x} - \dot{y}|z|z|^{(n-1)} - \beta(\dot{x} - \dot{y})|z|^n + A(\dot{x} - \dot{y}) \tag{3.9}$$

$$\dot{y} = \frac{1}{c_0 + c_1}\{\alpha z + c_0\dot{x} + k_0(x - y)\} \tag{3.10}$$

in which c_0 and k_0 are the viscous damping and stiffness parameters at large velocities, respectively and x_0 is the initial displacement of the spring k_1.

3.3.6. Phenomenological model considering the shear thinning and inertial effects

This model is also based on the Bouc-Wen model and the damper response analysis and it was proposed by Yang (2001). In the model, the stiction and inertia effect is simulated by adding a mass m and the MR fluid shear thinning effect is considered by defining a mono-decreasing function $c(\dot{x})$ to describe the damping coefficient as it is illustrated in Figure 3.13.

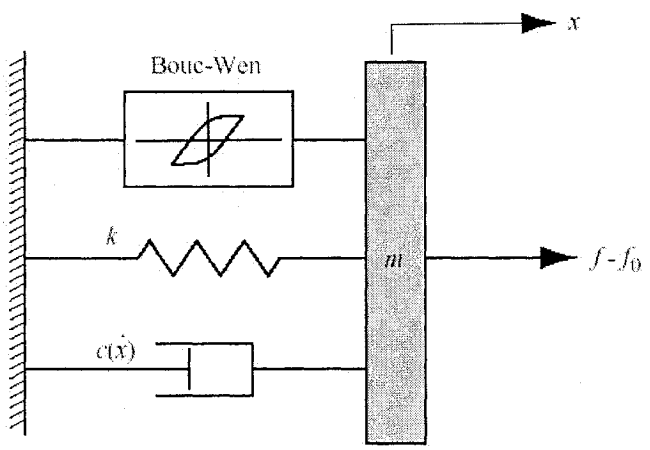

Figure 3.13. Phenomenological model considering MR fluid stiction phenomenon, as well as inertial and shear thinning effects.

In this model, the damping force is determined by:

$$f - f_0 = \alpha z + kx + c(\dot{x})\dot{x} + m\ddot{x} \tag{3.11}$$

where the evolutionary variable is governed by

$$\dot{z} = -\gamma|\dot{x}|z|z|^{(n-1)} - \beta\dot{x}|z|^n + A\dot{x} \tag{3.12}$$

and the post-yield damping coefficient function is defined by

$$c(\dot{x}) = a_1 e^{-(a_2|\dot{x}|)^p} \tag{3.13}$$

here, k is the accumulator stiffness and the MR fluid compressibility, f_0 represents the friction force due to seals and measurement bias and a_1, a_2 and p are constants.

3.3.7. LuGre model

The LuGre model, proposed by Canudas et al. (1995), describes reasonably well all the dynamic effects of friction, such as the pre-sliding displacement, the frictional lag, the Stribeck effect, which occur in the so-called "low-velocity" and the "pre-sliding regions. The LuGre model considers the dynamic effects of friction as arising out of the defection of bristles which model the asperities between two contacting surfaces. The friction force is given by

$$f = a_0 z + a_1 \dot{z} + a_2 \dot{x} \tag{3.14}$$

where z denotes the average deflection of the bristles, which is not measurable, and it is determined by

$$\dot{z} = \dot{x} - \alpha(x,\dot{x})|\dot{x}|z \tag{3.15}$$

the constants a_0, a_1 and a_2 are friction parameters that represent the stiffness of bristles, damping coefficient and viscous coefficient. The nonlinear friction characteristic function $\alpha(x,\dot{x})$ is a finite positive function that can be chosen to describe different friction effects. The parameterization of $\alpha(x,\dot{x})$ to characterize the Stribeck effect is given by

$$\alpha(x,\dot{x}) = \frac{a_0}{f_0 + (f_s - f_c)e^{-(\dot{x}/x_s)^2}} \tag{3.16}$$

where f_c is the Coulomb friction level, f_s is the level of the stiction force and $\dot{x}_s$ is the constant Stribeck velocity.

One drawback of the parametric models presented in this section is that for all of them the parameters are found by trial and error or by running any optimization procedure to minimize the difference between the simulation and the experimental data. Since the limits for the parameters are unknown, the search space is significantly large and the error is not unimodal function. This leads to the optimization procedure to be trapped in a local optimum. Another problem with the models is that the final solution is valid only for single excitation conditions; thus, as the excitation condition changes the characteristic parameters should be re-evaluated.

In the next section, the aforementioned problems are alleviated by proposing an efficient methodology to directly find the characteristic parameters and by developing a new model which depends on the current, the amplitude and the excitation frequency. It is stated that many of the errors shown in the published paper comes mainly from the not-properly selected parameters. It will be shown that using the proposed methodology and Bouc-Wen model, it is possible to simulate the hysteresis phenomenon inherited in accurately for MR dampers accurately and efficiently.

3.4. Proposed methodology to identify the constant parameters of the Bouc-Wen model

The Bouc-Wen model presented in the Section 3.3.4 is a suitable dynamic model, which has been used extensively by different researchers to simulate the hysteresis phenomenon realized in a MR damper. However one of the main problems in this model is the evaluation of its seven characteristic parameters. Trial and error or some optimization techniques such as Sequential Quadratic Programming (SQP) have already been applied to determine these parameters in such a manner that the error between experimental and simulation results be minimized (Choi et al. 2001; Spencer et al. 1997; Yang 2001; Yao et al. 2002). Combination of such sets of parameters could be significantly large and usually no unique and exact solution exists. In other words since the search space solution is a large domain, the final solution cannot reasonably match with the real hysteresis phenomenon. Thus, some considerable differences have been reported between the generated simulations and the experimental data (Choi et al. 2001; Spencer et al. 1997; Yang 2001; Yao et al. 2002). In consequence, the Bouc-Wen model has been criticized due to its inherent difficulties in predicting the essential parameters (Wang et al. 2003).

In this section a reliable methodology to find the appropriate characteristic parameters of the Bouc-Wen model is proposed in order to accurately and efficiently characterize a MR damper. Generally two main aspects should be considered in order to generate a hysteresis loop realized in the MR damper using the Bouc-Wen model. The first is the accuracy of the model to predict the response and the second is the computational time required to estimate the model's characteristics parameters. Both

aspects are improved using the proposed methodology, which has been validated through the data obtained from the laboratory tests performed on the MR-damper RD-1005-3 from Lord Corporation (Lord Materials Division 2003). The results obtained from the proposed methodology also show that the estimated parameters have linear or exponential relationship respect the current excitation of the damper.

The total damping force in the Bouc-Wen model is given by the Eq. (3.6). In this equation, the first term describes the force associated with viscous dissipation, the second term represents the linear force portion due to the compressed gas in the accumulator and the last term is the evolutionary force due to the hysteresis portion of the total restoring force. A typical hysteresis curve and its Bouc-Wen components are illustrated in Figure 3.14.

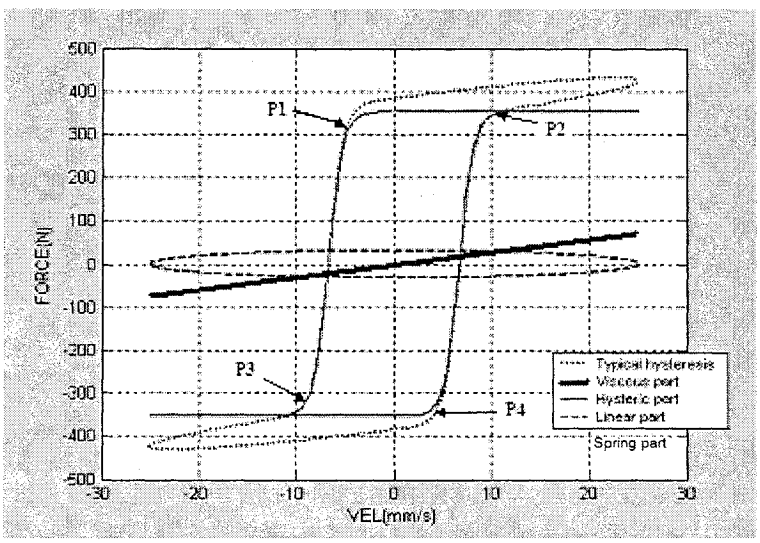

Figure 3.14. Typical hysteresis curve and its Bouc-Wen components.

Depending on the sign of z and $\dot{x}$, Eq. (3.7) can be represented in the following forms:

$$\frac{dz}{dw} = A - (\gamma + \beta)z^n \qquad for\ z \geq 0;\ \dot{w} \geq 0$$

$$\frac{dz}{dw} = A - (\gamma - \beta)z^n \qquad for\ z \geq 0;\ \dot{w} < 0 \tag{3.17}$$

$$\frac{dz}{dw} = A + (-1)^{n+1}(\gamma + \beta)z^n \qquad for\ z < 0;\ \dot{w} < 0$$

$$\frac{dz}{dw} = A + (-1)^{n+1}(-\gamma + \beta)z^n \qquad for\ z < 0;\ \dot{w} \geq 0$$

Optimization or trial and error techniques are the most common methods used to estimate the characteristic parameters of the Bouc-Wen model that characterize the hysteric behaviour of the MR damper. However due to infinite solution space, these techniques demands high computational cost to generate the required parameters which still cannot characterize the hysteresis behaviour of the MR damper accurately. In this work, the required parameters have been determined by considering the individual effect of each term of Eq. (3.6) over the hysteresis curve. It is demonstrated that it is possible to extract some information from the experimental data in order to obtain directly the values of the characteristics parameters without using any method to match the experimental data with simulation results.

The effect of parameter n over the shape of the hysteresis loop has been described by Spencer (1995). He concludes that as n increases, the radius of curvature decreases in the vicinity of the transitions points P1 and P3 known as the transition velocity points as shown in Figure 3.14. Considering n = 2 (Choi et al. 2001; Spencer et al.1997; Yao et al. 2002) and solving differential equations presented in Eq. (3.17), the following analytical solutions can be obtained:

$$z = \frac{\sqrt{AB}}{B}\tan\left(\sqrt{AB}(w + c)\right) \qquad for\ \ B < 0 \tag{3.18}$$

$$z = \frac{\sqrt{AB}}{B}\tanh\left(\sqrt{AB}(w+c)\right) \qquad for \quad B>0 \tag{3.19}$$

where B represents the parameter that multiply the evolutionary variable, z, in Eq. (3.17) (for instance B is equal to $-(\gamma+\beta)$ and $-(\gamma-\beta)$ for the first and second equation in Eq. (3.17), respectively and so on) and c is the integration constant which can be determined from the experimental data.

In order to generate the hysteresis part due to the evolutionary variable shown in Figure 3.14 (force-velocity behaviour) which is normally realized in real life MR damper, one should replace the w by $\dot{x}$ in Eqs. (3.18) and (3.19):

$$z = \frac{\sqrt{AB}}{B}\tan\left(\sqrt{AB}(\dot{x}+c)\right) \qquad for \quad B<0 \tag{3.20}$$

$$z = \frac{\sqrt{AB}}{B}\tanh\left(\sqrt{AB}(\dot{x}+c)\right) \qquad for \quad B>0 \tag{3.21}$$

In this work an efficient and accurate methodology has been proposed to find the required six parameters (c_0, k_0, α, β, γ, and A) of the Bouc-Wen model in order to closely fit the response of the Bouc-Wen model to the experimentally measured response of the MR damper. The methodology is based on the effect of each above parameters on the hysteresis loop.

According to Figure 3.14, one can realize that the typical hysteresis phenomenon experienced in MR dampers composed of three building block curves representing viscous, spring and hysteresis behaviour of the Bouc-Wen Model. The straight-line is the viscous effect, the dashed line is the spring effect due to the pressurized gas and the

continuous line is the hysteresis effect caused by evolutionary variable represented by the first, second and third terms in Eq. (3.6), respectively.

Let us first evaluate the characteristics parameter c_0. It is clear from Figure 3.14 that the viscous part of the Bouc-Wen model can be extracted from the typical hysteresis loop where its centerline reaches to maximum velocity. In other words the viscous damping factor is the slope of the centerline of the hysteresis loop in the maximum velocity point. For practical experimental data, the slope of the centerline in maximum velocity point may be well approximated by the following equation:

$$c_0 = \frac{F_{ku} + F_{kl} - F_{iu} - F_{il}}{2*(\dot{x}_k - \dot{x}_i)} \tag{3.22}$$

where $\dot{x}_k$ and $\dot{x}_i$ represent velocities at two different points i and k in the vicinity of the maximum velocity, F represents the forced obtained from the experiment and the indices u and l refers to the upper and lower part of the hysteresis loop. It is noted that in order to reduce errors due to small variations in the experimental data, the average values of force at different points close to i and k has been used.

As mentioned before, the second term in Eq. (3.6) represents the spring effect due to the pressurized gas. Typical hysteresis loops for different spring constants; k_0, have been shown in Figure 3.15. A close examination of Figure 3.15 reveals that the spring constant is zero where the force in upper and lower curves of the hysteresis loop coincides in the region I. Moreover as the spring constant increases, the openness of the hysteresis loop becomes more pronounced in that region. It is clear from Figure 3.14 and

Figure 3.15 that an elliptical relationship exists between the force due to the spring part and the velocity for harmonic excitation. Thus, the constant k_0 may be expressed by:

$$k_0 = \frac{\dot{x}_{\max}(F_{iu} - F_{il})}{2\sqrt{\dot{x}_{\max}{}^2 x^2 - x^2 \dot{x}_k{}^2}} \tag{3.23}$$

where $\dot{x}_{\max} = \omega x_{\max}$ is the maximum velocity and x is the amplitude of the excitation displacement.

The effect of parameter β on the typical hysteresis curve has been shown in Figure 3.16. It is noted that as the parameter β increases, the radius of curvature (smoothness of the curve) decreases in the vicinity of the points P1 and P3.

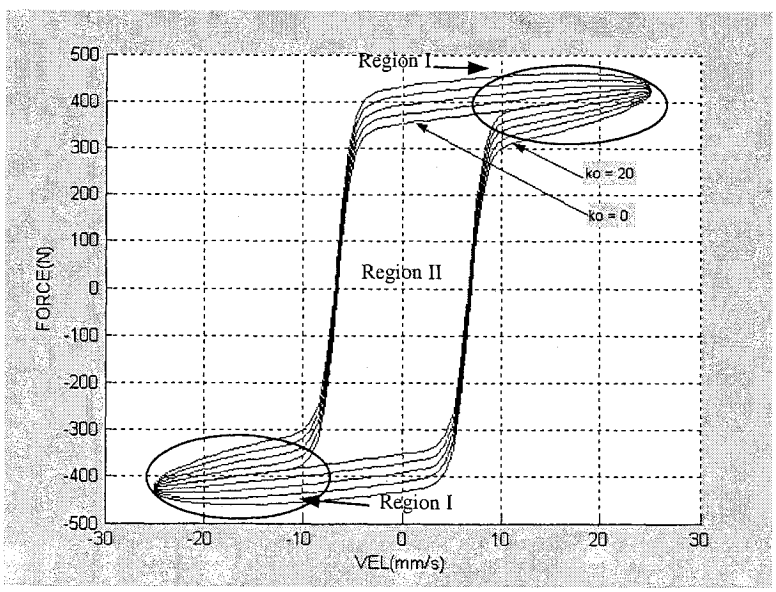

Figure 3.15. Effect of the constant k_0 on the hysteresis loop of the Bouc-Wen model for $k_0 = 0, 5, 10, 15, 20$.

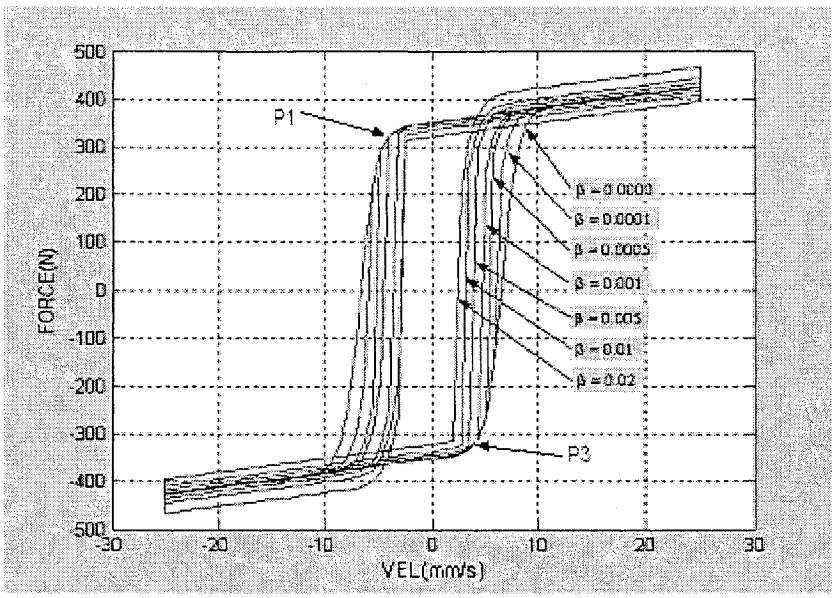

Figure 3.16 The effect of the constant β over the hysteresis shape.

Considering this, the hysteresis phenomenon in MR dampers can be better approximated by assuming $\beta = 0$. Considering this Eq. (3.20) and(3.21) may be re-formulated as:

$$z = \frac{\sqrt{A\gamma}}{\gamma}\tanh\left(\sqrt{A\gamma}(\dot{x} + c_1)\right) \qquad for \ \ (z < 0,\ x < 0) \ \ or \ \ (z \geq 0,\ x < 0) \tag{3.24}$$

$$z = \frac{\sqrt{A\gamma}}{\gamma}\tanh\left(\sqrt{A\gamma}(\dot{x} + c_2)\right) \qquad for \ \ (z \geq 0,\ x \geq 0) \ \ or \ \ (z < 0,\ x \geq 0) \tag{3.25}$$

where again c_1 and c_2 are the integration constants. It is noted that Eqs. (3.24) and (3.25) can be used to define the lower and upper hysteric loop due to the evolutionary variable , respectively. Different combinations of the constant parameters A and γ can define the amplitude of the curve and the velocity at the point where the evolutionary variable is zero. In other words, these two variables can describe the shape of the evolutionary variable z. From the experimental data the hysteresis loop for the evolutionary force versus velocity can be established using Eq. (3.6). Then, the points $(F_{z0}, \dot{x} = 0)$ and

$(F_z = 0, \dot{x}_{z0})$ which are the evolutionary forces at zero velocity and the velocity at the zero evolutionary force can be extracted for each of the upper and lower part of the hysteresis loops. It is noted that the evolutionary force can be described by:

$$F_z = \alpha z \tag{3.26}$$

where z is the evolutionary variable. Assuming $A = 1$ and substituting evolutionary variable z from Eq. (3.24) into Eq. (3.26), the integration constant can be determined using the coordinate point $(F_{z0}, \dot{x} = 0)$:

$$c_1 = \frac{1}{\sqrt{\gamma}} \text{a}\tanh\left(\frac{F_{z0}}{F_{z\max}}\right) \tag{3.27}$$

where

$$F_{z\max} = \frac{\alpha}{\sqrt{\gamma}} \tag{3.28}$$

is the evolutionary force at maximum velocity or simply maximum evolutionary force.

It is noted that $F_{z\max}$ can be calculated from experimental data using the following equation:

$$F_{z\,max} = F_{max} - c_0 \dot{x}_{max} \tag{3.29}$$

where F_{max} is the maximum total hysteresis force.

Considering Eqs. (3.24), (3.26) and (3.27) and using the coordinate point $(F_z = 0, \dot{x}_{z0})$, the parameter γ may be determined by solving the following equation:

$$0 = F_{z\,max} \tanh\left(\sqrt{\gamma}\left(\dot{x}_{z0} + \frac{1}{\sqrt{\gamma}} \text{a}\tanh\left(\frac{F_{z0}}{F_{z\,max}}\right)\right)\right) \tag{3.30}$$

Knowing the parameter γ, now the parameter α can be easily calculated using Eq. (3.28). Finally, the integration constants are substituted in Eqs (3.24 and 3.25) to obtain the evolutionary variable, and subsequently evolutionary force.

To summarize, the characteristic parameters have been estimated using Eqs. (3.22, 3.23, 3.28 and 3.30) based on the experimental results.

3.5. Validation of the proposed methodology

The above proposed methodology is applied to simulate the hysteresis behaviour of the MR damper RD-1005-3 manufactured by Lord Corporation. Multiple experiments for different excitation conditions are performed in laboratory. The data is acquired and further these data is employed to obtain key information and determine directly the characteristic parameters using the proposed methodology.

3.5.1. Description of the experiment

MR fluid is kind of smart material, which can be made by mixing fine particles into liquid with low viscosity. Upon the presence of high magnetic field, these fine particles will be formed into chain-like fibrous structures. When the magnetic field strength reaches a certain value, the MR fluid becomes solidified and creates high yield stress; conversely, the MR fluid can be liquefied once more by removal of the magnetic field. The change of process is very quick, less than a few milliseconds, and can be easily controlled. Due to these characteristics, the MR fluid has been highly used in recent controlled semi-active dampers.

The MR damper is generally defined as being a controlled semi-active damper which its damping force can be changed continuously using minimal power requirement, unlike a fully active control actuator (can add energy to the system or remove from the system) which requires a large power supply. The semi-actively controlled MR fluid dampers offer rapid variation in damping properties in a reliable fail-safe manner, since they continue to provide adequate damping, of a passive manner, in the event of a control hardware malfunction (Carlson and Sproston 2000). The schematic representation of the cylindrical type of MR damper has been shown in Figure 3.5.

The characterization test was specifically conducted on a MR damper model RD-1005-3 manufactured by Lord Corporation, which is shown in Figure 3.5. This is a compact magnetorheological fluid damper unsurpassed in its combination of controllability, responsiveness, and energy density, which can be applicable to an adaptive space truss structures or a middle-sized passenger vehicle. In this MR damper the viscous and shear properties of the MR fluid are controlled by the applied magnetic field, which is a function of the excitation current. A DC current of maximum 2 A is used as command signal as well as the input for the coils. The electric resistance of the coil varies from 5 Ω at ambient temperature to 7 Ω at 70° C and for an input voltage of 12 V DC.

The characterization of the MR damper consists of different laboratory tests to acquire the force-velocity and force-displacement curves for different current excitations. To perform testing, the MR damper is mounted on an electrohydraulic vibration exciter from one side and on a fixed inertial frame through a force transducer from other side. The instantaneous velocity and displacements were measured by the installation of an

LVT and LVDT sensors respectively. The force, velocity and displacement data, acquired through a data acquisition board, are used to provide on-line displays of hysteretic force-velocity characteristics. The current excitation is provided by a dual regulated DC power supply. In order to assure that the test is accomplished within the range of 30±10 ° C, a thermocouple was also installed on the damper body.

The hysteresis phenomenon in the MR damper was evaluated under harmonic excitations in the frequency range of 0.1 to 15 Hz. The limit of 15 Hz was selected to operate the MR damper in safe conditions; moreover, this range covers the fundamental natural frequency, which is the most important one. Many experiments have been performed for different combination of current excitations (0.00, 0.25, 0.50, 0.75, 1.00, 1.25 and 1.50 A) and strokes (2.5, 6.35, 12.7 and 19.05 mm). The amplitudes for displacement excitations at higher frequencies were limited to lower values to ensure that the damper was operating within safe velocity limits.

3.5.2. Comparison of the simulation and experimental results

The methodology explained in Section 3.4 is applied to find the characteristic parameters of the Bouc-Wen model for different current excitations, frequencies and amplitudes and to simulate the hysteresis behaviour of the MR-damper RD-1005-3 from Lord Corporation. The sample estimated parameters for the frequency of 5 and10 Hz and amplitudes of 19.05 and 6.35 mm respectively are tabulated in Table 3.3. Naturally, each set of parameters can characterize the hysteresis behaviour of the tested MR damper under specific excitation conditions. The experimental data is the same obtained by Wang et al. (2003).

Table 3.3. Final results for the Bouc-Wen model parameters under frequency excitation 5 and 10 Hz and amplitudes of 19.05 and 6.35 mm respectively.

	A		α (N/m)		γ (m^{-2})		c_0 (Ns/m)		k_0 (kg/s^2)		F_{z0} (N)	
	Amplitude (mm)											
Current (Amp)	6.35	19.05	6.35	19.05	6.35	19.05	6.35	19.05	6.35	19.05	6.35	19.05
0.00	1	1	82	1196	280	1400	257	1023	1085	3758.4	1.3	7.1
0.25	1	1	1514	3853	277	1335	358	912	1681	3769.0	66.8	49.4
0.50	1	1	3091	7368	276	1300	497	1226	3119	4733.5	162	126
0.75	1	1	4259	10926	273	1250	559	1377	3510	6101.2	229	205
1.00	1	1	4635	11514	272	1200	617	1444	4262	6532.7	256	214
1.25	1	1	5147	11210	269	1165	614	1684	4387	7771	269	238
1.50	1	1	5382	13302	267	1100	647	1831	5477	7747.9	287	237

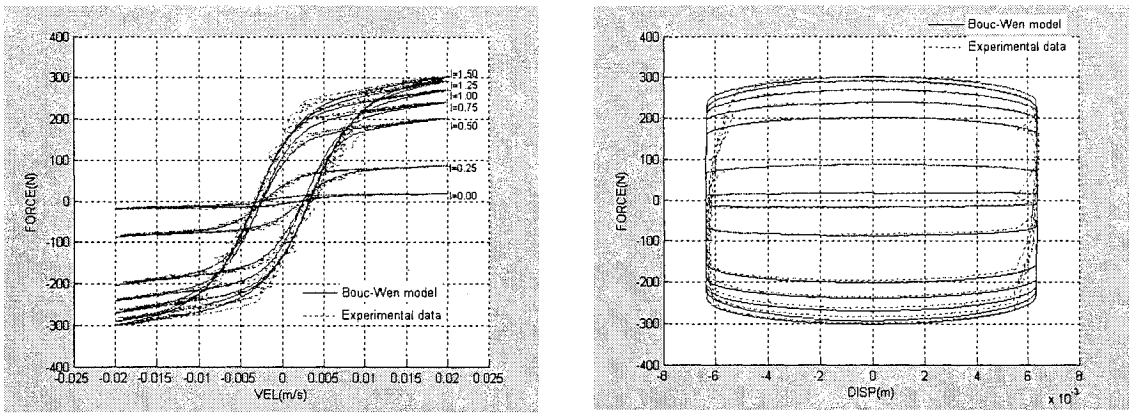

(a) 0.5 Hz and amplitude of 6.35 mm

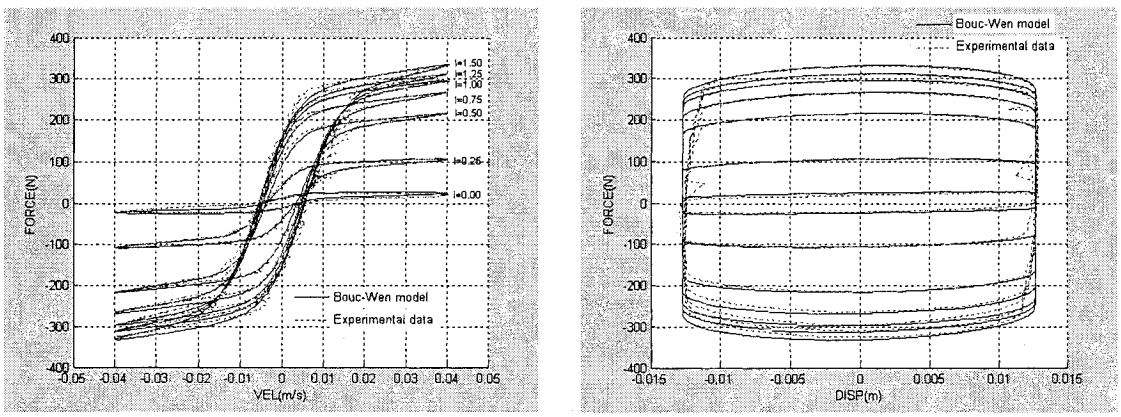

(b) 0.5 Hz and amplitude of 12.7 mm

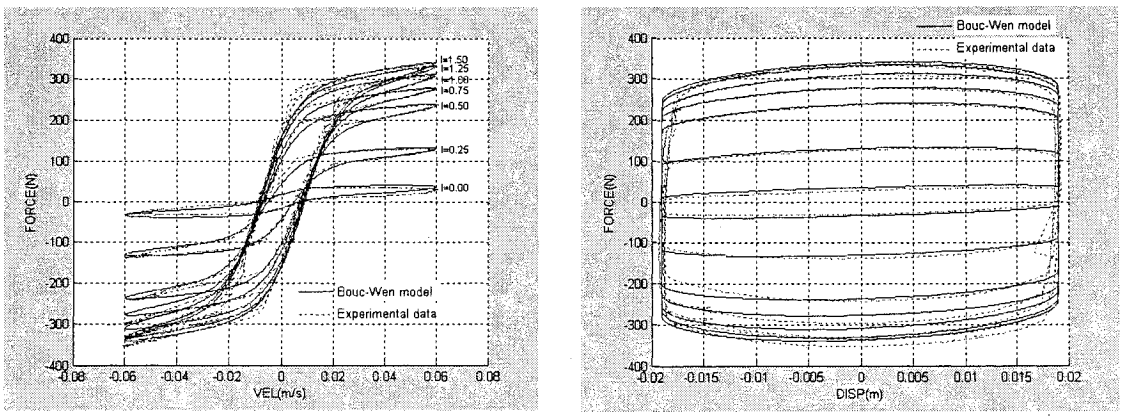

(c) 0.5 Hz and amplitude of 19.05 mm

Figure 3.17. Comparison between the experimental data and the Bouc-Wen model with proposed estimated parameters for current excitations of 0.00, 0.25, 0.50, 0.75, 1.00, 1.25 and 1.50 A

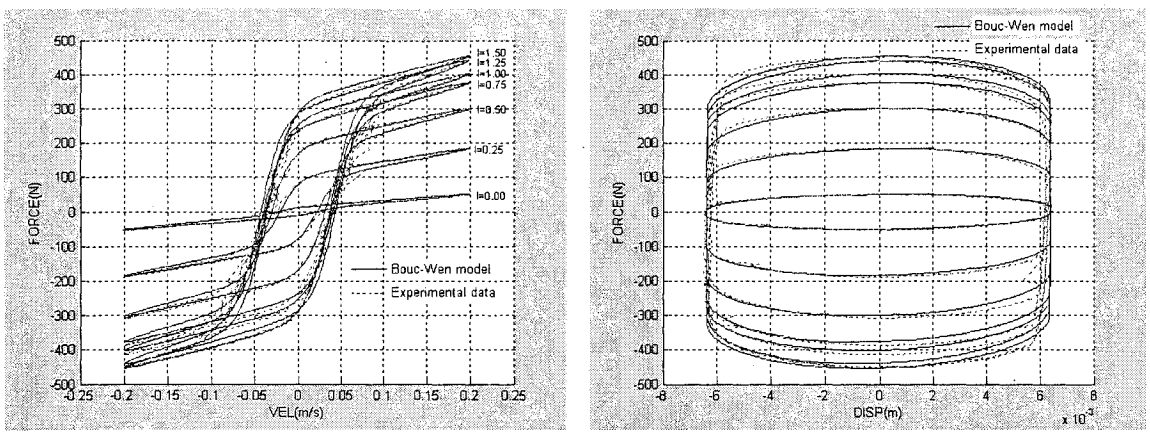

(d) 5.0 Hz and amplitude of 6.35 mm

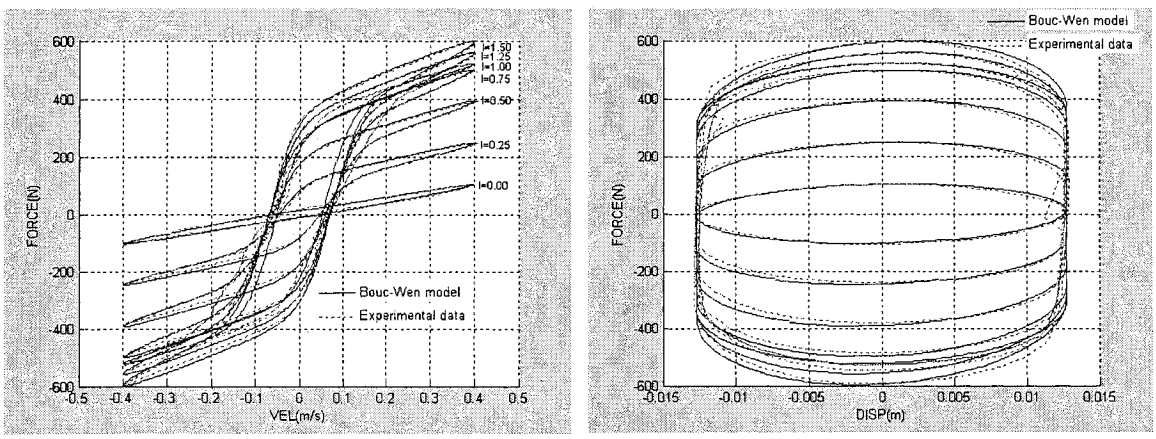

(e) 5.0 Hz and amplitude of 12.7 mm

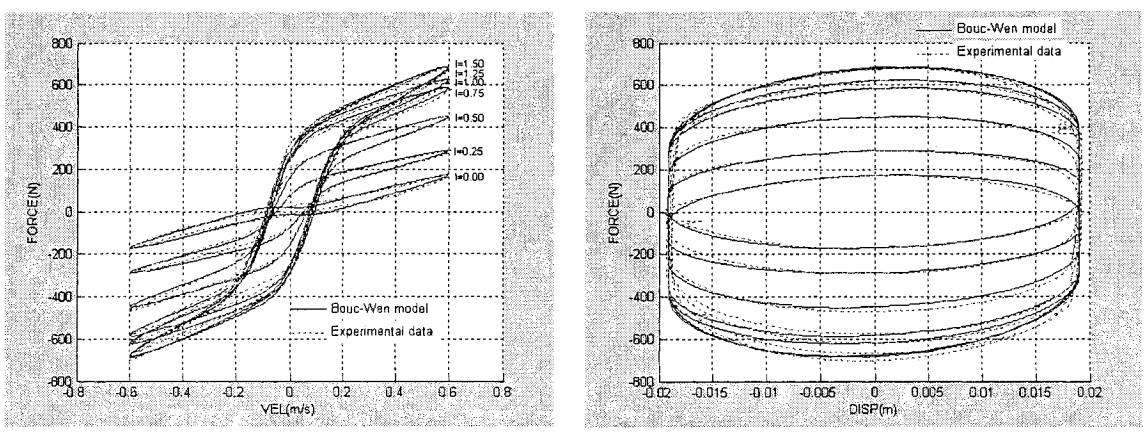

(f) 5.0 Hz and amplitude of 19.05 mm

Figure 3.17. (Continued.)

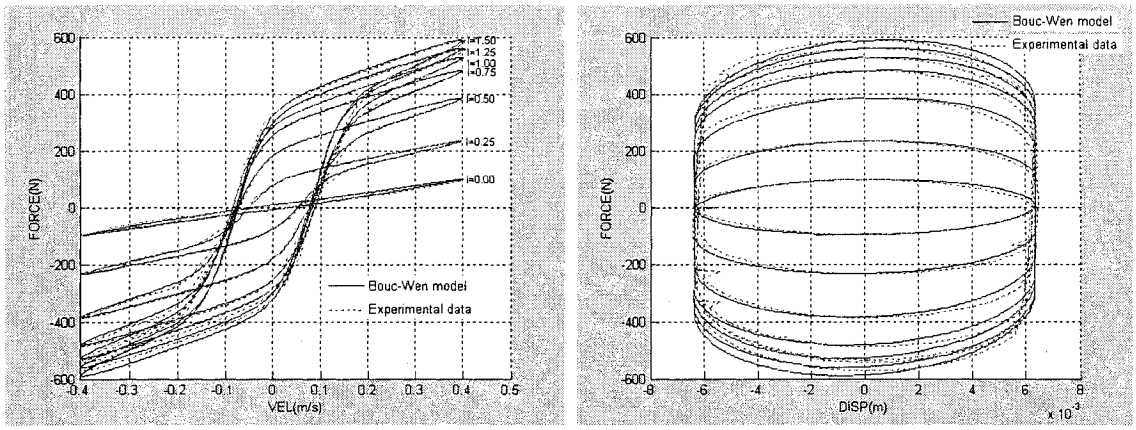

(g) 10.0 Hz and amplitude of 6.35 mm

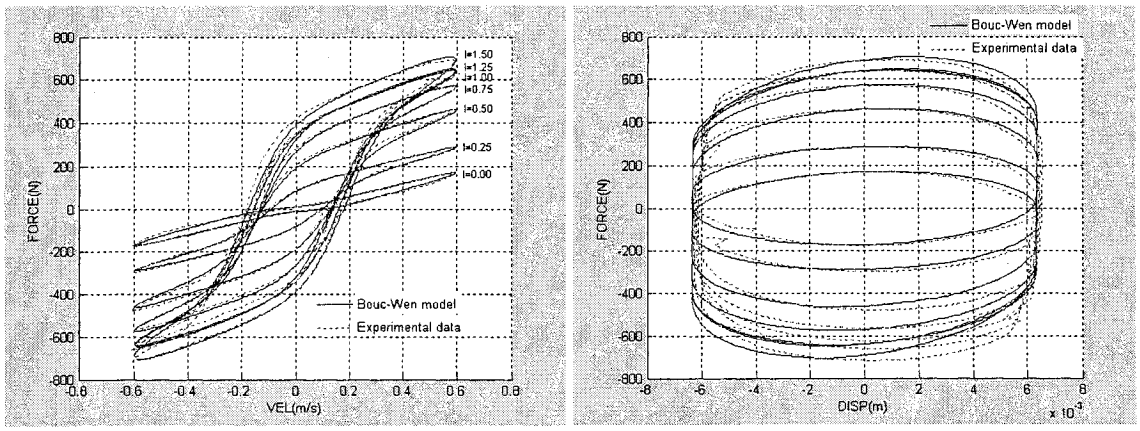

(h) 15.0 Hz and amplitude of 6.35 mm

Figure 3.17. (Continued.)

Having determined the required six characteristic parameters of the Bouc-Wen model, the Eqs. (3.6, 3.24 and 3.25) are employed to simulate the hysteresis phenomenon of the MR damper. The simulation results (force versus velocity and force versus displacement) and their comparison with experimental data for the frequency range of 0.5, 5.0, 10.0 and 15.0 Hz and amplitudes of 6.35, 12.70 and 19.05 mm are illustrated in Figures 3.17 a-h. The examination of these figures reveals that excellent agreement exists between the results obtained by using the proposed methodology to find the characteristic parameters of the Bouc-Wen model and the experimental data.

The above mentioned approach can be applied to find the characteristic parameters of the Bouc-Wen model for different current excitations, frequencies and amplitudes and to simulate the hysteresis behaviour of the MR-damper. Naturally, each set of parameters can characterize the hysteresis behaviour of the tested MR damper under specific excitation conditions.

The sample variation of the estimated parameters versus the current excitation for the frequency of 5.0 Hz and amplitude of 6.35 mm has been shown in Figure 3.18. It can be realized that the estimated characteristics parameters c_0, α, and F_{z0} tend to follow a linear pattern for low excitation currents and an exponential pattern for higher value of currents. These parameters reach to a saturation point for high excitation currents. This coincides with the saturation experienced by MR dampers for high currents. It can also be realized that the parameters γ and k_0 trend to vary linearly with respect to the current excitation. This behaviour has also been observed for other frequencies and amplitudes.

Figure 3.19 demonstrates a sample relationship between the maximum hysteresis force and the amplitude of excitation for a given frequency of 5 Hz and different current excitation. Figure 3.20 shows the behaviour of the hysteresis force as a function of the excitation frequency for given amplitude of 6.35 mm and different current excitation.

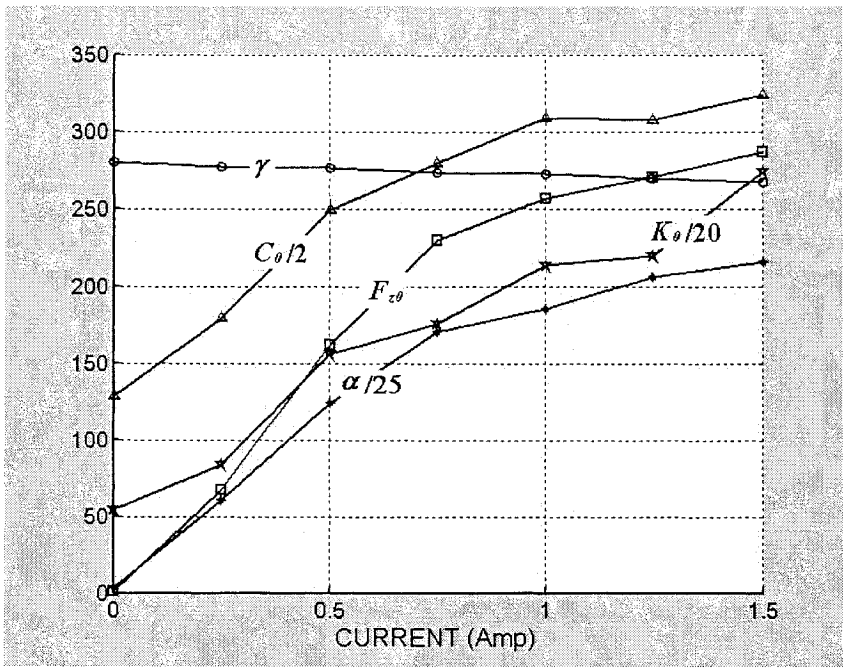

Figure 3.18. The characteristic parameters c_0, k_0, α, and γ and the evolutionary force at zero velocity, F_{z0}, versus the current excitation for the frequency of 5 Hz and amplitude of 6.35 mm

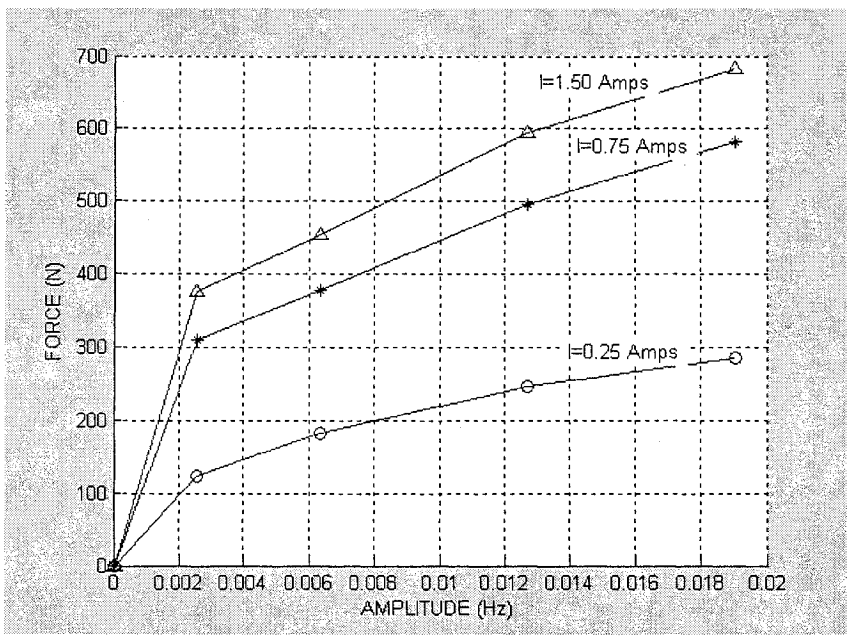

Figure 3.19. Hysteresis force as function of the amplitude excitation for frequency of 5 Hz and different current excitations.

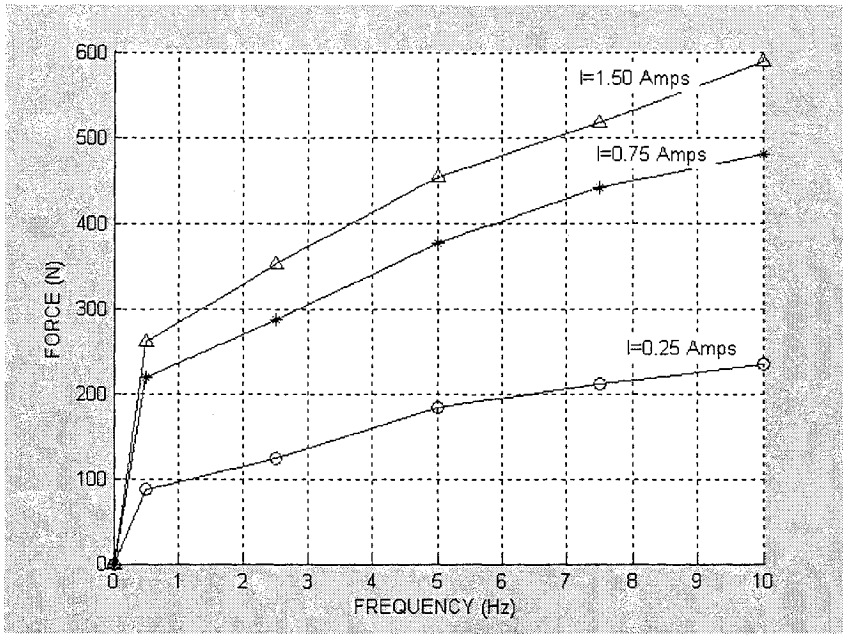

Figure 3.20. Hysteresis force against the frequency excitation for amplitude of 6.35 mm and different current excitations.

It is noted that the magnitude of the hysteresis force increases sharply for small values of the frequency and then it grows gradually for higher values of frequency. Similar trend can be observed for the variation of the hysteresis force with respect to the amplitude.

3.6. New current, frequency and amplitude dependent Bouc-Wen model

The semi-actively controlled MR fluid dampers offer rapid variation in damping properties in a reliable fail-safe manner using very low power requirements. Their characteristics made them ideal for semi-active control in structures and vehicle applications in order to efficiently suppress vibration. To take advantage of their exceptional characteristics, a high fidelity model is required for vibration suppression strategies. Perfect understanding about the dynamic characteristics of such dampers is necessary when implementing MR struts in applications. Different models have been

proposed to simulate the hysteresis phenomenon of MR dampers. The Bouc-Wen model has been extensively used to simulate the hysteresis behaviour of MR dampers. However, considerable differences still exist between the simulation and experimental results. Moreover the characteristic parameters in the traditional Bouc-Wen model are not dependent on the frequency, amplitude and current excitations; therefore, the estimated parameters can characterize the behaviour of the tested MR damper under specific excitation conditions and must be again revaluated if different combination of excitation parameters is desired. This can be extremely cumbersome and computationally expensive. In this section a new hysteresis model based on the Bouc-Wen model is developed to better characterize the hysteresis phenomenon of the MR damper.

In the simple Bouc-Wen model the current, frequency and magnitude of excitation are not considered as variables; therefore, the characteristic parameters must be estimated for each different set of current, frequency and magnitude, which can be extremely cumbersome and computationally expensive. In this study a new model based on the Bouc-Wen model has been proposed to incorporate the current, frequency and amplitude excitation as variables in order to accurately and efficiently characterize the hysteresis behaviours of the MR damper.

As it was shown in Figure 3.18, parameters c_0, k_0, α and are all function of current excitation. Thus Eq. (3.6) has been reformatted to consider the current dependency of theses variables. Moreover, close examination of Figure 3.19 and 3.20 reveal that the hysteresis force increases rapidly for small frequencies and amplitudes and then increases gradually as the frequency or amplitude become larger. Parabolic functions

with exponents lower than one may describe such kind of behaviour. Considering this, the Bouc-Wen model in Eq. (3.6) has also been modified to incorporate the variation of the Hysteresis force versus amplitude and frequency of excitation.

Based on the above rationale the modified Bouc-Wen model incorporating the current, frequency and amplitude excitation as variables may be reformulated as below:

$$F(x(\tau),\dot{x}(\tau),I,\omega,x,0\le\tau\le t;t)=(d_1\omega^{d_2})(d_3 x_{\max}^{d_4})[c_0(I)\dot{x}+k_0(I)x+\alpha(I)z] \tag{3.31}$$

where ω is the frequency of the excitation, $d_1,\ldots,d_4$ are constants and z is the evolutionary variable defined by the following differential equation:

$$\dot{z}(I)=\gamma(I)\dot{x}|z|^{(n-1)}z-\beta(I)\dot{x}|z|^n+A(I)\dot{x} \tag{3.32}$$

where as mentioned in Section 3.4, $A(I)$ and $\beta(I)$ assumed to be one and zero, respectively.

As it was concluded in Section 3.5.2 a linear relationship exists between the current excitation and the parameters γ and α. Also, a close examination of the results revealed that the characteristic parameters c_0, k_0 and F_{z0} vary linearly for low current excitation and exponentially for high current excitations. Considering this observation, the following relationships are proposed:

$$\begin{aligned} c_0(I)&=c_1+c_2(1-e^{-c_3(I-I_c)}) \quad for\ I>I_c \\ c_0(I)&=c_4+\frac{c_4-c_1}{I_c}I \qquad\quad for\ I\le I_c \end{aligned} \tag{3.33}$$

$$k_0(I)=k_1+k_2 I \tag{3.34}$$

$$\alpha(I)=\alpha_1+\alpha_2(1-e^{-\alpha_3(I-I_c)}) \quad \text{for } I>I_c \tag{3.35}$$

$$\alpha(I) = \alpha_1 + \frac{\alpha_4 - \alpha_1}{I_c} I \qquad for\ I \le I_c$$

$$\gamma(I) = \gamma_1 - \gamma_2 I \tag{3.36}$$

$$F_{z0}(I) = F_{z01} + F_{z02}(1\text{-}e^{-F_{z03}(I-I_c)}) \qquad \text{for } I > I_c$$

$$F_{z0}(I) = F_{z04} + \frac{F_{z04} - F_{z01}}{I_c} I \qquad for\ I > I_c \tag{3.37}$$

where 16 constant parameters c_1, c_2, c_3, c_4, k_1, k_2, α_1, α_2, α_3, α_4 γ_1, γ_2, F_{z01}, F_{z02}, F_{z03} and F_{z04} relates the characteristic shape parameters to current excitation and should be specified in a way to better characterize the behaviour of MR dampers. I_c is the critical current in which the characteristics parameter change their linear behaviour in low velocity to exponential behaviour in high velocity. For this particular MR damper the critical current was found to be nearly 0.25 A.

Now using these current dependent parameters the evolutionary variable in Eqs. (3.18) and (3.19) may be updated to the following form:

$$z(I) = \frac{1}{\sqrt{\gamma(I)}} \tanh\left\{\sqrt{\gamma(I)}\left[\dot{x} + \frac{1}{\sqrt{\gamma(I)}} a \tanh\left(\frac{F_{z0}(I)\sqrt{\gamma(I)}}{\alpha(I)}\right)\right]\right\} \quad for \begin{cases} (z<0,\ x<0)\ or \\ (z \ge 0,\ x<0) \end{cases} \tag{3.38}$$

$$z(I) = \frac{1}{\sqrt{\gamma(I)}} \tanh\left\{\sqrt{\gamma(I)}\left[\dot{x} + \frac{1}{\sqrt{\gamma(I)}} a \tanh\left(-\frac{F_{z0}(I)\sqrt{\gamma(I)}}{\alpha(I)}\right)\right]\right\} \quad for \begin{cases} (z \ge 0,\ x \ge 0)\ or \\ (z<0,\ x \ge 0) \end{cases} \tag{3.39}$$

3.6.1. Comparison of the simulation and experimental results of the new model

As explained in Section 3.6, the constant parameters have been estimated so that the simulated hysteresis loop can be well matched with its counterpart experimental results. The experimental data is the same obtained by Wang et al. (2003). For the MR damper RD-1005-3 from Lord Corporation, the 20 parameters introduced in Section 3.4

are estimated as: $c_1 = 358\,\text{Ns/m}$, $c_2 = 280\,\text{Ns/m}$, $c_3 = 2.4\,\text{A}^{-1}$, $c_4 = 230\,\text{Ns/m}$, $k_1 = 1085\,\text{N/m}$, $k_2 = 2928\ \text{N/A-m}$, $\alpha_1 = 1514\,\text{N/m}$, $\alpha_2 = 4200\,\text{N/m}$, $\alpha_3 = 2.2\,\text{A}^{-1}$, $\alpha_4 = 82\,\text{N/m}$ $\gamma_1 = 280\,\text{m}^{-2}$, $\gamma_2 = 8.66\,\text{m}^{-2}\text{A}^{-1}$, $d_1 = 5.08\,\text{m}$, $d_2 = 0.333$, $d_3 = 0.251\,\text{s/rad}$, $d_4 = 0.351$ $F_{z01} = 67\,\text{N}$, $F_{z02} = 250\,\text{N}$, $F_{z03} = 1.9\,\text{A}^{-1}$ and $F_{z04} = 1.32\,\text{N}$.

It is interesting to note that the above constant parameters are valid for any desired set of current, frequency and amplitude of excitation. In other words the model can predict the hysteresis behaviour of MR damper under any excitation conditions without any re-evaluation of the characteristic parameters for those conditions. This is not the case for the traditional Bouc-Wen model in which the characteristics parameters have to be identify for each set of current, amplitude and frequency of excitation used in experimental test.

Figure 3.21 illustrates a sample of hysteresis force versus time generated by the simulation using proposed model and experiment for the frequency of 10 Hz, amplitude of 6.35 mm and three current excitations of 0.25, 0.75 and 1.25 A. As it can be seen the proposed model can accurately predict the hysteresis force at all times.

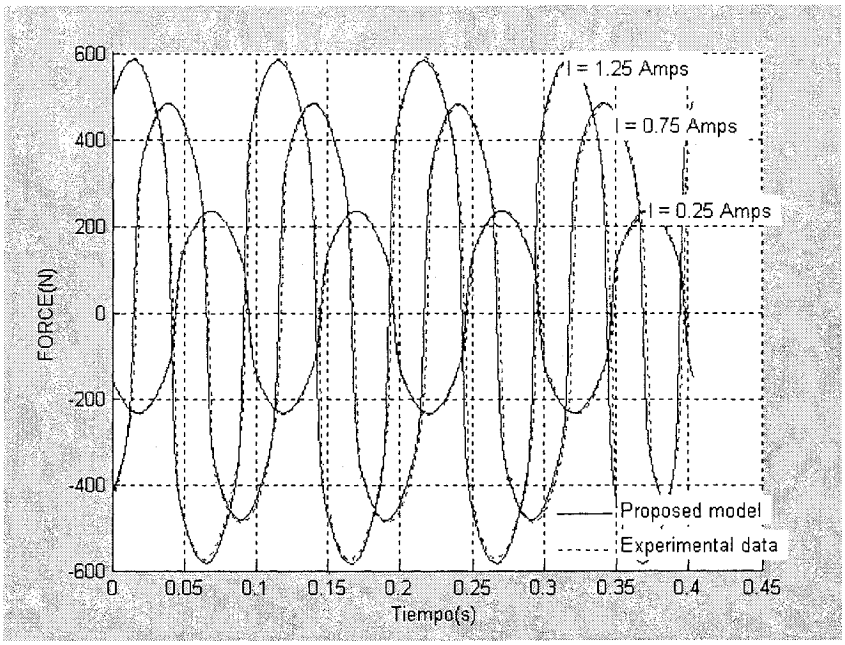

Figure 3.21. Hysteresis force versus time generated by the experimental data and the proposed model for different current excitations.

The simulation results for hysteresis force versus velocity and hysteresis force versus displacement conducted using the proposed model and their comparison with the experimental data for different combination of current, frequency and amplitude excitation are also illustrated in the Figure 3.22 show the results for the frequency of 5 and 10 Hz at different level of current excitation. The amplitude in both frequencies is considered to be 6.35 mm. Moreover, the simulation and experimental results for different level of frequencies at specified current and amplitude of excitations and for different level of amplitudes at specified current and frequency of excitations are shown in Figures 3.23 and 3.24, respectively.

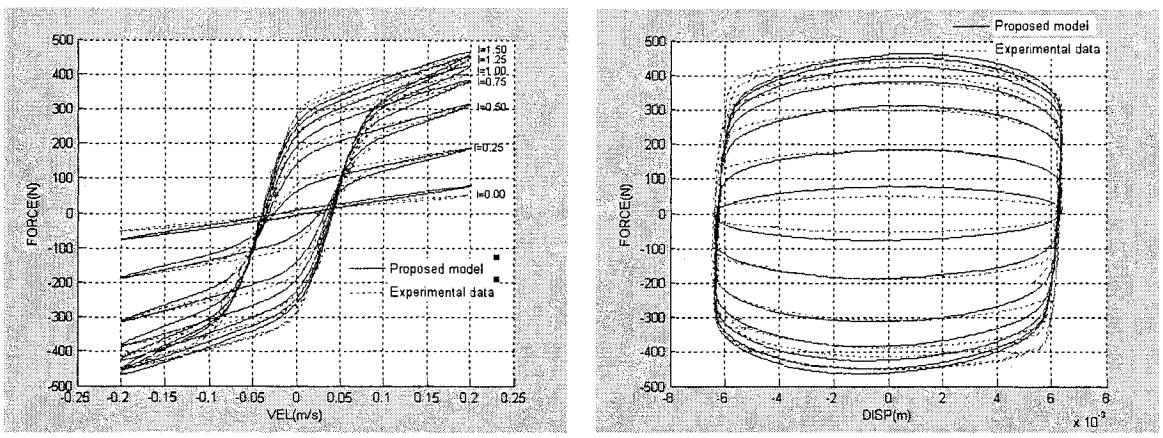

(a) 5.0 Hz and amplitude of 6.35 mm

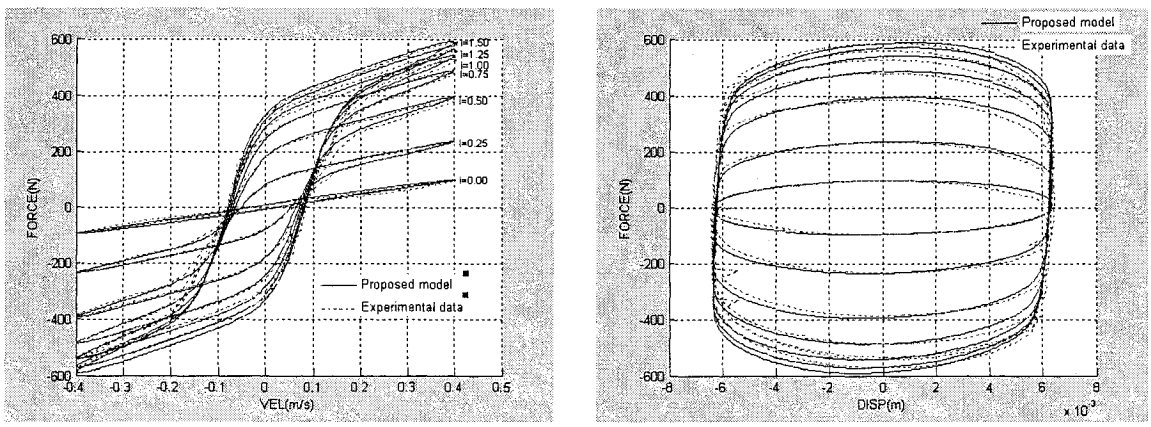

(b) 10.0 Hz and amplitude of 6.35 mm

Figure 3.22. Comparison between the experimental data and the proposed model for the current excitations of 0.00, 0.25, 0.50, 0.75, 1.00, 1.25 and 1.50 A

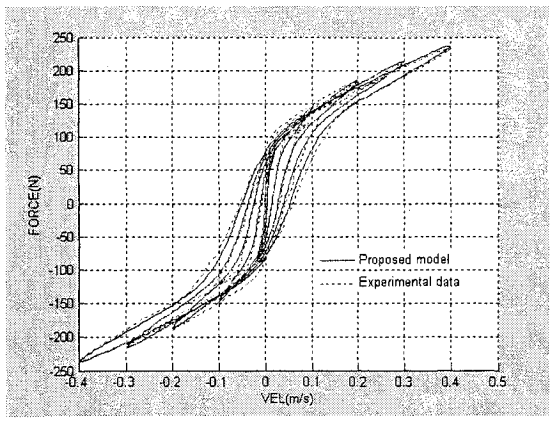

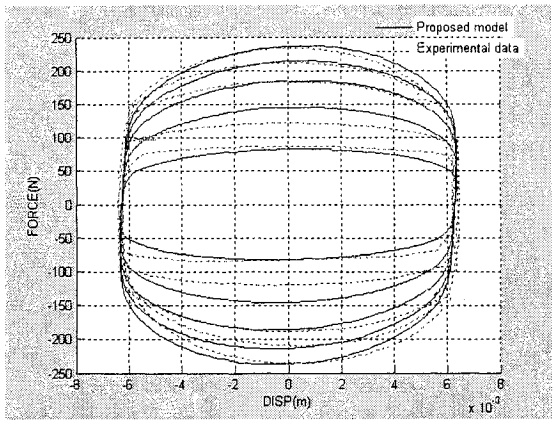

(a) I = 0.25 Amps and amplitude of 6.35 mm

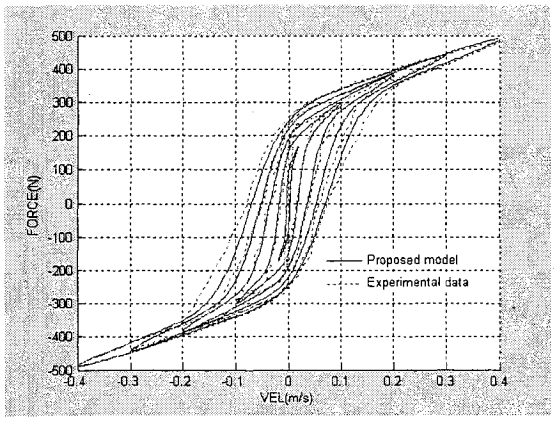

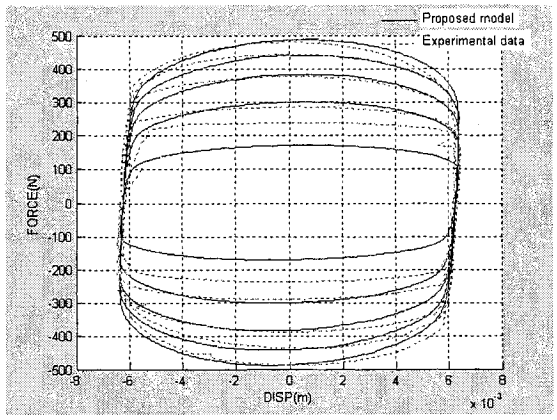

(b) I = 0.75 Amps and amplitude of 6.35 mm

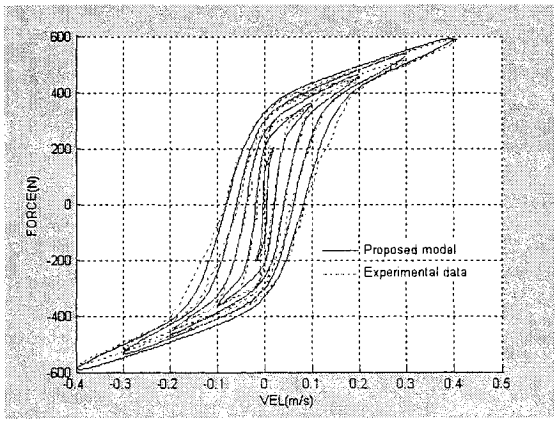

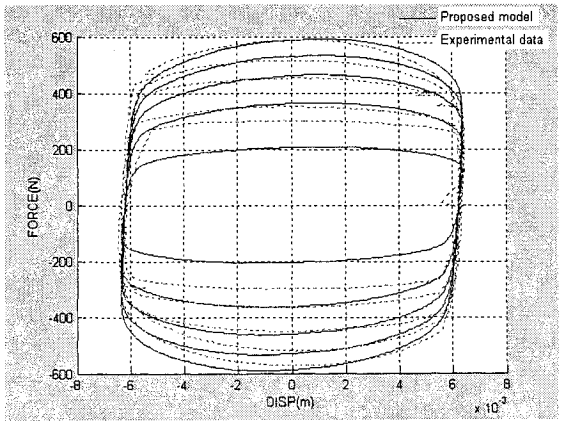

(c) I = 1.5 Amps and amplitude of 6.35 mm

Figure 3.23. Comparison between the experimental data and the proposed model for the frequency excitations of 0.25, 2.5, 5.0, 7.5 and 10.0 Hz from inside to outside loop.

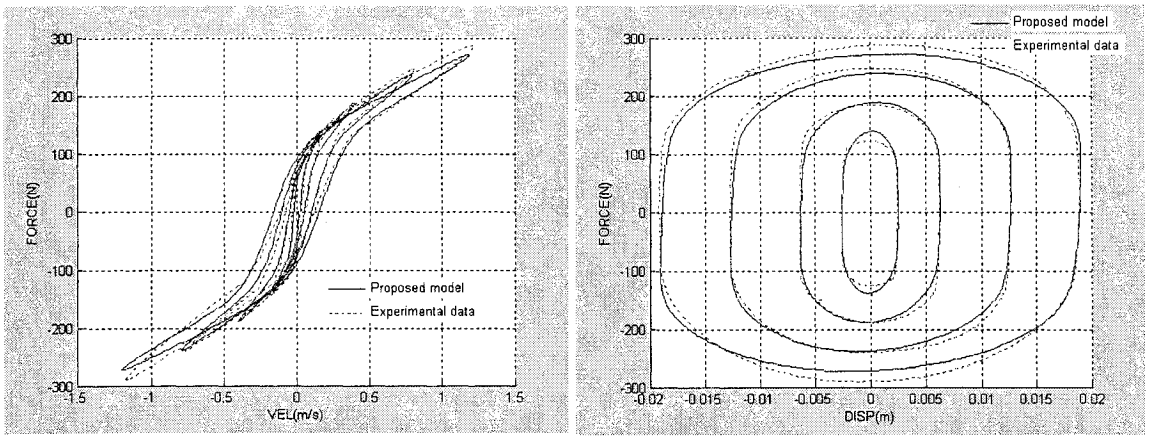

(a) I = 0.25 Amps and frequency of 5 Hz

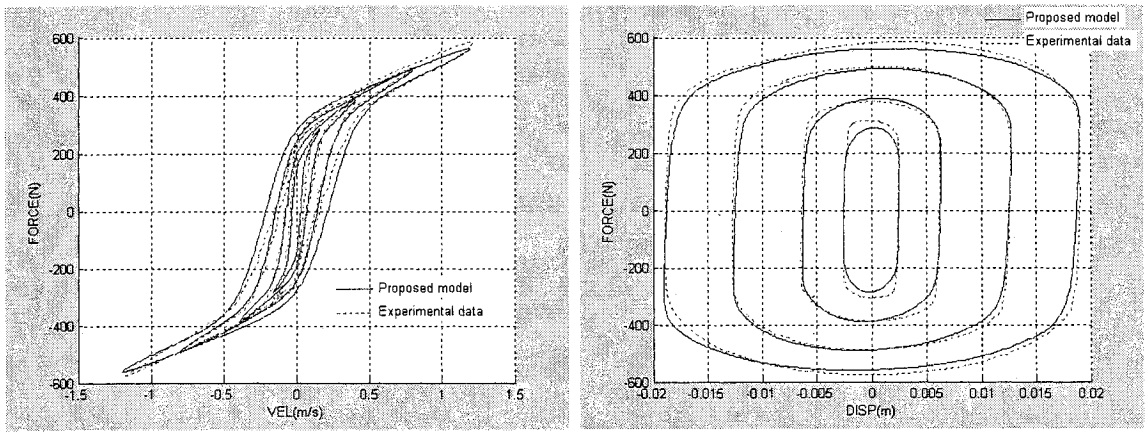

(b) I = 0.75 Amps and frequency of 5 Hz

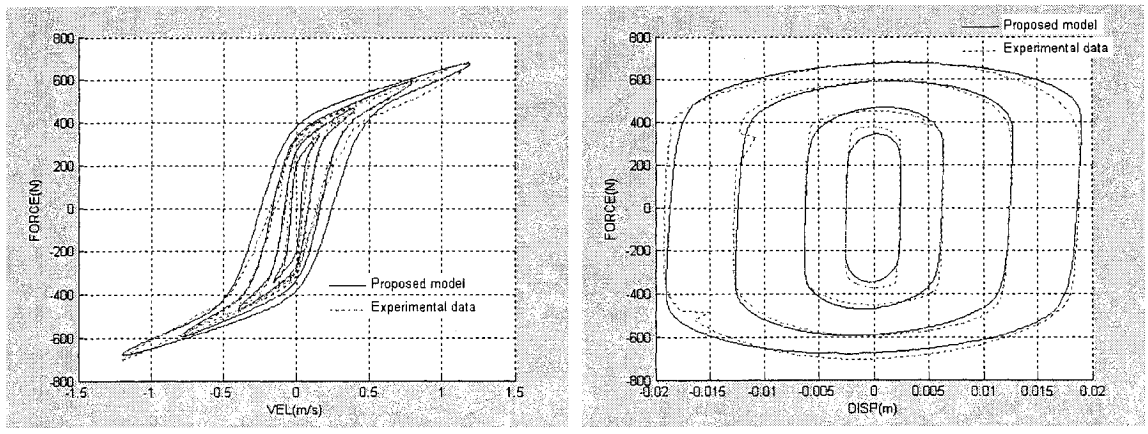

(c) I = 1.5 Amps and frequency of 5 Hz

Figure 3.24. Comparison between the experimental data and the proposed model for the amplitude excitations of 2.54, 6.35, 12.7 and 19.05 mm from inside to outside loop.

The examination of the above figures reveals that very good agreement has been established between the simulation and experimental results for any combinations of current, frequency and amplitude excitations thus confirming that the proposed model is able to predict the hysteresis force in MR dampers accurately and efficiently.

3.6.2. Error analysis of the new model

In addition to the graphical evidence of the effectiveness of the proposed model, a quantitative analysis of the errors for different excitation conditions has been accomplished. The normalized errors between the predicted and experimental force in time, displacement and velocity domain can be effectively expressed as:

$$E_t = \sqrt{\frac{\int_0^T (F_{\exp} - F)^2 dt}{\int_0^T (F_{\exp} - \mu_{\exp})^2 dt}} \tag{3.40}$$

$$E_x = \sqrt{\frac{\int_0^T (F_{\exp} - F)^2 \left|\frac{dx}{dt}\right| dt}{\int_0^T (F_{\exp} - \mu_{\exp})^2 \left|\frac{dx}{dt}\right| dt}} \tag{3.41}$$

$$E_{\dot{x}} = \sqrt{\frac{\int_0^T (F_{\exp} - F)^2 \left|\frac{d\dot{x}}{dt}\right| dt}{\int_0^T (F_{\exp} - \mu_{\exp})^2 \left|\frac{d\dot{x}}{dt}\right| dt}} \tag{3.42}$$

where $F_{\exp}$ represents the measured or experimental force , F is the predicted or simulated force which is calculated by Eq. (3.31), $\mu_{\exp}$ is the mean value of the experimental force during the period T. A sample of normalized errors for the frequency amplitude of 10 Hz, amplitude of 6.35 mm and different current excitations are provided

in Table 3.4. The error results are also compared with the minimum error reported by Spencer et al. (1997).

Table 3.4. Normalize errors in time, displacement and velocity domain for 10 Hz and amplitude of 6.35 mm.

	Current (Amps)							(Spencer et al.1997)
	0.0	**0.25**	**0.50**	**0.75**	**1.00**	**1.25**	**1.50**	
E_t	0.1511	0.1275	0.1023	0.0962	0.0965	0.1095	0.0850	0.167
E_x	0.1002	0.0656	0.0555	0.0513	0.0532	0.0641	0.0535	0.0585
$E_{\dot{x}}$	0.2246	0.1782	0.1390	0.1306	0.1312	0.1465	0.1126	0.135

It can be realized that an acceptable error exists between the simulated and measured hysteresis forces experienced in the MR damper.

It is noted that in the proposed model, the characteristic parameters are function of the current, frequency and amplitude excitation. Thus the hysteresis force of the MR damper can be easily evaluated for any desired combination of the frequency, amplitude and current excitations without any revaluation of these characteristics parameters. This is not the case for the simple or traditional Bouc-Wen model in which the characteristic parameters are valid only for a specific excitation. The ability of the proposed model to predict the hysteresis force for any excitation condition can make it ideal for the semi-active control applications.

The application of Magneto Rheological (MR) dampers in semi-active control has received significant attention in the recent years due to the rapid variation in their damping properties in a reliable fail-safe manner and low power requirements. One of the

important factors to successfully attain desirable control performance is to have a damping force model, which can accurately capture the inherent hysteresis behaviour of MR dampers. It was shown that the characteristics parameters of the Bouc-Wen model obtained by the application of the proposed methodology follow specific patterns in which some characteristics parameters vary linearly with respect to the current excitation in whole region and others tend to follow a linear pattern for low excitation currents and to follow an exponential pattern for higher value of currents. It was also demonstrated that the magnitude of the hysteresis force increases rapidly for small values of the frequency and then grows gradually for higher values of frequency. Similar trend was also observed for the variation of the hysteresis force with respect to amplitude. Based on these observations, a new model based on Bouc-Wen model has been proposed in which the current, frequency and amplitude of excitation have been incorporated as variables.

It was demonstrated that an excellent agreement exist between the simulated results generated by the proposed model and the experimental results. Error analysis demonstrates that acceptable errors exist between the predicted and measured force confirming that proposed model is reliable and capable to predict the hysteresis force accurately and efficiently at any excitation conditions.

One of the main advantages of the proposed model is that it can be used for situations where the excitation conditions are changing. Therefore, it is possible to practically apply the proposed model in semi-active control applications such as automotive suspension systems and adaptive structures. Moreover since terms of stiffness, damping and evolutionary forces are separated in the total hysteresis damping force, one can easily formulate the damping force in matrix format which is suitable for

the finite element analysis. It is noted that two aspects should be considered in the application of the proposed model to simulate the transient response of the structure with embedded MR dampers. First, the input frequency to the hysteresis model is considered as the fundamental natural frequency of the structure. Second, the amplitude of the excitation should be approximated by a relation that uses the instant displacement, velocity and acceleration for transient problems, as explained in Section 4.7. This approximation can introduce some errors in the calculation of the hysteresis force.

CHAPTER 4
MATHEMATICAL MODELING OF SEMIACTIVE STRUCTURES

In this chapter the finite element model of the MR damper, proposed in the Chapter 3, is developed. Subsequently the nonlinear dynamic finite element model of a space truss structure embedded with the MR damper is created and its local and global nonlinear matrix formulation is obtained. In the global matrix formulation it is considered a proportional damping to simulate the structural damping. The insertion of the MR damper in the structure converts the system into nonlinear system. To solve the nonlinear problem the powerful unconditionally stable Newmark time integration technique is reformulated and combined with the Newton Raphson method to get the dynamic response of the system. Finally the experimental study has been carried out to validate the mathematical model.

4.1. Finite element model of the passive bar element

The test space truss structure is an assemblage of bar through bolt coupling and connection nodes as shown in Figure 4.1. Thus, the objective of this section is to propose a FEM model that accurately describes the behaviour of the bar elements that include the attached nodes and bolt couplings. For this purpose, a truss element containing three members as shown in the Figure 4.2 is developed. The element is shown in its local coordinates with end nodes N1 and N2. The middle member of the element, E2,

represents the tube whose physical characteristics are known. The adjacent members E1 and E2 are proposed to simulate the node and the bolt connection.

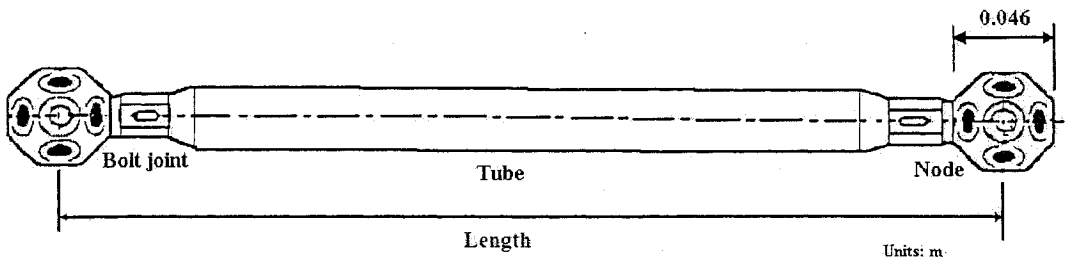

Figure 4.1. Typical assembly of a bar element.

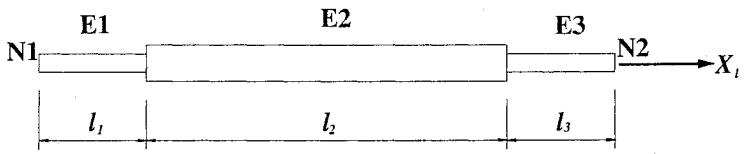

Figure 4.2. Finite element of a passive bar element.

The stiffness for each section is determined by:

$$k_i = \frac{E_i l_i}{A_i} \tag{4.1}$$

where the cross sectional area A_i for each section is computed by:

$$A_i = \frac{\pi}{4}\left(D_i^2 - d_i^2\right) \tag{4.2}$$

here, D_i and d_i represent the exterior and interior diameter of the i^{th} member. Thus, the equivalent stiffness and mass of the proposed bar can be calculated by:

$$k_{eq}^{-1} = \frac{k_1 k_2 + k_1 k_3 + k_2 k_3}{k_1 k_2 k_3}; \quad m_{eq} = m_1 + m_2 + m_3 \tag{4.3}$$

Considering this, the stiffness and lumped mass matrices for the complete bar element in local coordinates may be described by:

$$\left[K_{eq}^{(e)}\right] = \begin{bmatrix} k_{eq} & -k_{eq} \\ -k_{eq} & k_{eq} \end{bmatrix}; \quad \left[M_{eq}^{(e)}\right] = \begin{bmatrix} \frac{m_{eq}}{2} & 0 \\ 0 & \frac{m_{eq}}{2} \end{bmatrix} \tag{4.4}$$

As explained in Chapter 2, the local elemental stiffness and mass matrices can be transformed to the global coordinates using the rotational or transformation matrix using the following relations:

$$[K]^g = [R]^T \left[K_{eq}^{(e)}\right][R]; \quad [M]^g = [R]^T \left[M_{eq}^{(e)}\right][R] \tag{4.5}$$

Once the transformation has been performed, the matrices can be assembled properly to obtain the system stiffness and mass matrices. The global damping matrix will be developed in the next section following the Wilson's Theory.

4.2. Finite element model of the bar element with MR damper

In this section the finite element model for the element that contains the MR damper is proposed. First, the matrix formulation is obtained just for the MR damper and then it is included in the model of the whole element. Assuming that the mass of the MR damper can be equally lumped at its both ends, the finite element model for MR damper is obtained by applying the Second Newton's Law to the masses shown in Figure 4.3 as follow:

$$\begin{cases} c_0(\dot{x}_j - \dot{x}_i) + k_0(x_j - x_i) + \alpha z - F_0 = \dfrac{m_{MR}}{2}\ddot{x}_i \\ c_0(\dot{x}_i - \dot{x}_j) + k_0(x_i - x_j) - \alpha z + F_0 = \dfrac{m_{MR}}{2}\ddot{x}_j \end{cases} \tag{4.6}$$

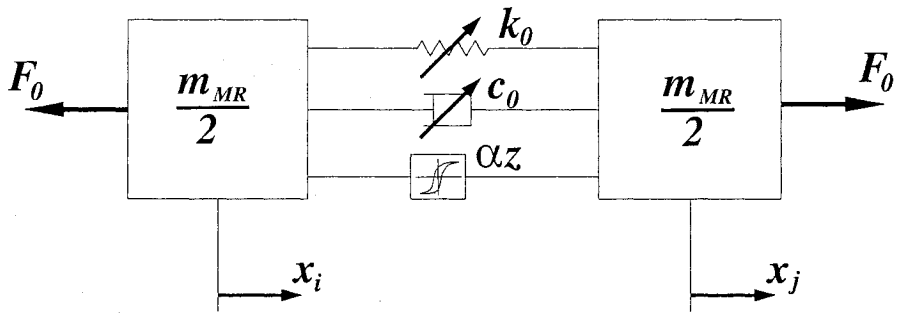

Figure 4.3. Lumped mass representation of an MR damper bar element.

where m_{MR} is the mass of the MR damper which is considered as lumped mass. k_0 is the time dependent stiffness due mainly to the effect of gas accumulator in the MR damper, c_0 is the time dependent viscous damping coefficient, αz is the evolutionary force and F_0 is initial force required to install the MR damper in its initial position. The equations to determine the stiffness, damping and evolutionary force were obtained in Section 3.6.

Writing Eqs. (4.6) in matrix form, we can obtain:

$$\begin{bmatrix} \frac{m_{MR}}{2} & 0 \\ 0 & \frac{m_{MR}}{2} \end{bmatrix} \begin{Bmatrix} \ddot{x}_i \\ \ddot{x}_j \end{Bmatrix} + \begin{bmatrix} c_0 & -c_0 \\ -c_0 & c_0 \end{bmatrix} \begin{Bmatrix} \dot{x}_i \\ \dot{x}_j \end{Bmatrix} + \begin{bmatrix} k_0 & -k_0 \\ -k_0 & k_0 \end{bmatrix} \begin{Bmatrix} x_i \\ x_j \end{Bmatrix} = \begin{bmatrix} 1 & 0 \\ 0 & 1 \end{bmatrix} \begin{Bmatrix} \alpha z \\ -\alpha z \end{Bmatrix} + \begin{bmatrix} 1 & 0 \\ 0 & 1 \end{bmatrix} \begin{Bmatrix} -F_0 \\ F_0 \end{Bmatrix} \tag{4.7}$$

or

$$[M_{MR}]\{\ddot{x}\}+[C_0]\{\dot{x}\}+[K_0]\{x\}=[I]\{F_z\}+[I]\{F_0\} \tag{4.8}$$

where $\{x\}$, $\{\dot{x}\}$ and $\{\ddot{x}\}$ are the vector of nodal displacement, velocity and acceleration for the MR damper respectively. $[M_{MR}]$ is the lumped mass matrix, $[C_0]$ is the damping matrix, $[K_0]$ is the stiffness matrix, $\{F_z\}$ is the hysteresis force vector and $\{F_0\}$ is the vector of initial force.

Similarly, the mass and stiffness of the MR damper can be transformed to global coordinates for assembling purposes. It is noted that the damping coefficient c_0 is significantly larger than the typical structural damping of the bars; thus, the structural damping may be ignored. The global damping matrix $[C_0]$ of the bar element with MR damper can also be obtained by transforming the local damping matrix using the rotational matrix as:

$$[C_0]^g = [R]^T [C^{(e)}][R]; \tag{4.9}$$

which can be properly assembled in similar way to the stiffness and mass matrices to obtain the system damping matrix of the MR damper bar element. It is convenient to remark that the global damping matrix $[C_0]^g$ is a matrix with time dependent coefficients.

Further, the FEM for the bar element that contains the MR damper is proposed. The bar element consists of five individual members as it is shown in Figure 4.4. The end elements, E1 and E5, are simulating the node and bolt connections and the elements E2

and E4 are the bar members employed to couple the middle element representing the MR damper to the end connection members.

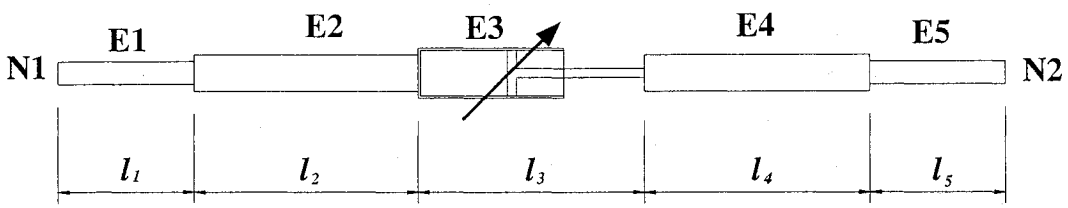

Figure 4.4. Finite element model for the MR damper bar element.

Considering this, the equivalent stiffness and mass may be written as:

$$k_{eq}^{-1} = \frac{k_2k_0k_4k_5 + k_1k_0k_4k_5 + k_1k_2k_4k_5 + k_1k_2k_0k_5 + k_1k_2k_0k_4}{k_1k_2k_0k_4k_5}; \tag{4.10}$$

$$m_{eq} = m_1 + m_2 + m_{MR} + m_4 + m_5$$

where $k_0 = k_3$ is stiffness of the MR damper

Finally the stiffness and mass matrices for passive members with MR damper are obtained by substituting the Eqs. (4.10) into the Eqs. (4.4) and (4.5). It is to remark that the stiffness matrix for the MR damper bar element has time dependent coefficients due to nonlinearly of the controllable damper.

4.3. Derivation of the damping matrix

The synthesis of damping in structural systems and machines is extremely important if a model is to be used in predicting transient responses, transmissibility, decay time or other characteristics in design and analysis that are dominated by energy dissipation. In this section the damping matrix is derived to be included in the FEM

formulation. Although the damping effects in structural problems are clear, the characterization of the damping is still under development. However some approaches have been proposed with good accuracy. Pilkey (1998) provides a complete description of the different approaches to determine the damping matrix.

In this work a proportional damping methodology is adopted (Hasselman 1972; Wilson 1976). In proportional damping, the damping matrix $[C]$ is assumed to be proportional to the mass matrix $[M]$ or to the stiffness matrix $[K]$ or combination of both according to the Rayleigh's proportional damping. These kinds of proportional damping can be stated mathematically as:

$$[C]=\alpha[M],\ [C]=\beta[K] \text{ or } [C]=\alpha[M]+\beta[K] \tag{4.11}$$

where α and β are constant parameters.

To accomplish this, it is first required to obtain the eigenvalues and eigenvectors of the undamped free vibration system to establish the modal matrix. The equation of motion for undamped free vibration can written as:

$$[M]\{\ddot{x}\}+[F]\{x\}=\{0\} \tag{4.12}$$

Assuming harmonic solution, the solution of the Eq. (4.12) can be described as:

$$\{x\}=\{\varphi\}\sin\omega(t-t_0) \tag{4.13}$$

where $\{\varphi\}$ is a amplitude vector, t is the time variable, t_0 is a time constant, and ω is the frequency of vibration of the system. Substituting the Eq. (4.13) into (4.12), the generalized eigenproblem is stated as:

$$[K]\{\varphi\}=\omega^2[M]\{\varphi\} \tag{4.14}$$

in which $\{\varphi\}$ and ω are the eigenvector and eigenvalue respectively. A system with n degrees of freedom has n solutions for eigenproblem which can be represented in matrix form as:

$$[K][\Phi]=[M]\{\Phi\}[\Omega]^2 \tag{4.15}$$

where $[\Phi]$ is called modal matrix containing n column eigenvectors and $[\Omega]^2$ is a diagonal matrix with the eigenvalues ω_i^2 on its diagonal as follow:

$$[\Phi]=[\{\varphi_1\},\{\varphi_2\},...,\{\varphi_n\}];\quad [\Omega]^2=\begin{bmatrix}\omega_1^2 & 0 & \cdots & 0\\ 0 & \omega_n^2 & \cdots & 0\\ \vdots & \vdots & \ddots & \vdots\\ 0 & 0 & \cdots & \omega_n^2\end{bmatrix} \tag{4.16}$$

with $0<\omega_1<\omega_2<\ldots<\omega_n$. The eigenvectors are called M-normalized when

$$[\Phi]^T[M][\Phi]=[I] \tag{4.17}$$

Noew Eqs. (4.14) and (4.17) yields:

$$[\Phi]^T[K][\Phi]=[\Omega]^2 \tag{4.18}$$

Unlike the mass and stiffness matrices, in general, the damping matrix cannot be constructed from element damping matrices, and its purpose is to approximate the overall energy dissipation during the system response.

Let us assume that the governing differential equations of motion in finite element form can be written as:

$$[M]\{\ddot{x}\}+[C]\{\dot{x}\}+[K]\{x\}=\{F\} \tag{4.19}$$

To decouple the Eq. (4.19), the following linear transformation can be used:

$$[x]=[\Phi]\{p\} \tag{4.20}$$

where $\{p\}$ is referred to as modal coordinates.

Now substituting Eq. (4.20) into(4.19) and multiply both sides from left by $[\Phi]^T$ and using the properties of M-normalized eigenvector described in Eqs. (4.17) and (4.18) yields:

$$[I]\{\ddot{p}\}+[\Phi]^T[C][\Phi]\{\dot{p}\}+[\Omega]^2\{p\}=[\Phi]^T\{F\} \tag{4.21}$$

It is observed that the matrices of the first and third left terms of in the Eq. (4.21) are diagonal matrices because of orthogonality relation between the eigenvectors and mass $[M]$ and stiffness $[K]$ matrices. However the second term $[\Phi]^T[C][\Phi]$ does not usually reduce to a diagonal matrix. Now using proportional damping concepts formulated in Eq. (4.11), one is able to diagonalize the second term.

While considering Eq. (4.21) it is common practice to assume the second term has the form:

$$[\Phi]^T[C][\Phi]=2[\Omega][\zeta] \tag{4.22}$$

where the modal damping ratio matrix $[\zeta]$ is represented by:

$$[\zeta]=\begin{bmatrix} \zeta_1 & 0 & \cdots & 0 \\ 0 & \zeta_2 & \cdots & 0 \\ \vdots & \vdots & \ddots & \vdots \\ 0 & 0 & \cdots & \zeta_n \end{bmatrix} \tag{4.23}$$

This has been successfully employed and recommended (Wilson 2002; Heverly II et al. 2001; Bath and Wilson 1976) to simulate the damping effects of structural systems. In most vibrational problems, it is immaterial whether the modal damping $2\zeta_i\omega_i$ in Eq. (4.22) is based upon $[C]$ being proportional to $[M]$ or $[K]$ or a combination of both as in Rayleigh's proportional damping. Thus, from a practical point of view, the damping factor ζ_i and the undamped natural frequency ω_i can be interpreted as being the properties that are inherent in the system. Furthermore, typical values and characteristics of the damping ratio ζ_i for various types of structures are available from experimental studies. Knowing this the damping matrix $[C]$ in Eq. (4.22) can be determined with respect to modal damping factors and undamped natural frequencies as:

$$[C]=2[\Phi]^{-T}[\Omega][\zeta][\Phi] \tag{4.24}$$

4.4. Solution of governing differential equations of motion

As it has been described above, one the system mass, stiffness and damping matrices are identified; the governing equations of motion can be established as provided in Eq. (4.19). If system has n degrees of freedom (Dofs), then the n coupled governing equations of motion should be solved simultaneously to obtain the response of the system which can be computationally extensive if the number of Dofs is large. In practical finite element analysis, the most effective time domain methods are the direct time integration

technique and the mode superposition method (Bath and Wilson 1976). The solution of the system can be obtained efficiently in frequency domain when the system is exposed to single-harmonic excitations as the response has the same frequency. When the system is linear it is possible to apply the mode superposition method using modal transformation matrix to convert the original system into a set of linearly uncoupled equations which can be solved individually. Among the direct integration methods the most popular and powerful in structural dynamic analysis is the Newmark's method. With selection of suitable controlling parameters, the Newmark's method is unconditionally stable for any desired time steps. Furthermore, this method can easily be extended to solve the nonlinear problems which is the case when the MR damper is embedded in the structure. This requires an iterative process at each time step in order to balance the system equations. In this section the frequency domain, the mode summation method and the Newmark's techniques, will be briefly explained. The Newmark's method will then be reformulated efficiently in order to solve the nonlinear systems.

4.4.1. Frequency domain response due to single harmonic excitation

This method is based on the method of undetermined coefficients which assume that the response of the systems due to a harmonic excitation follows the same frequency of the excitation. The differential equations governing the motion of Dofs system with structural damping subject to a single-frequency harmonic excitation can be written as:

$$[M]\{\ddot{x}\}+[C]\{\dot{x}\}+[K]\{x\}=\mathrm{Im}\{F\}e^{i\omega t} \tag{4.25}$$

where $\{F\}$is a n-dimensional vector of force amplitude which could be complex if the phase of each generalized force is not the same as:

$$F_i = f_i e^{i\phi} \tag{4.26}$$

The solution of Eq. (4.25) is assumed to be harmonic in the form of:

$$\{x(t)\} = \mathrm{Im}\left(\{U\}e^{i\omega(t)}\right) \tag{4.27}$$

where $\{U\}$is a n-dimensional vector of displacement amplitude. Substitution of Eq. (4.27) into Eq. (4.25) leads to:

$$\left(-\omega^2[M]+i\omega[C]+[K]\right)\{U\} = \{F\} \tag{4.28}$$

Finally the solution of Eq. (4.28) is obtained by

$$\{U\} = \left(-\omega^2[M]+i\omega[C]+[K]\right)^{-1}\{F\} \tag{4.29}$$

4.4.2. Mode superposition method

This method as described in Section 4.3 decouples the finite element equations of motion by using a modal transformation matrix which consists of the free vibration mode shapes of the finite element system. This method is computationally more efficiently than the direct integration methods; however, it is not applicable for nonlinear problems because the superposition principle employed to obtain the solution of the set governing of differential equations is not valid in this case (Kelly 2000).

As explained in Section 4.3, the finite element system equations are decoupled using the eigenvector modal matrix $[\Phi]$. This matrix represents a transformation matrix that change the original coordinates $\{x\}$ called generalized coordinates to a new reference called principal or modal coordinates $\{p\}$. Using the linear transformation

relation given in Eq. (4.20) and orthonormal properties of eigenvectors, the governing coupled equation of motion can be decoupled as:

$$[\tilde{M}]\{\ddot{p}\}+[\tilde{C}]\{\dot{p}\}+[\tilde{K}]\{p\}=\{\tilde{F}\} \tag{4.30}$$

where

$$[\tilde{M}]=[\Phi]^T[M][\Phi];\quad [\tilde{C}]=[\Phi]^T[C][\Phi];\quad [\tilde{K}]=[\Phi]^T[K][\Phi];\quad \{\tilde{F}\}=[\Phi]^T\{F\} \tag{4.31}$$

where $[\tilde{M}]$, $[\tilde{C}]$ and $[\tilde{K}]$ are the modal mass, damping and stiffness matrices and $\{\tilde{F}\}$ is modal force vector. The relation between generalized and normal coordinates is rewritten as :

$$[x(t)]=[\Phi][p(t)] \tag{4.32}$$

Since the system of equations given in Eq. (4.30) is uncoupled, each equation has the following form:

$$\ddot{p}_j(t)+2\omega_j\xi_j\dot{p}_j(t)+\omega_j^2 p_j(t)=f_j(t),\qquad j=1,\ldots,n \tag{4.33}$$

with

$$f_j(t)=\{\varphi_j\}^T\{F(t)\} \tag{4.34}$$

the initial conditions in the principal coordinates are determined using the Eq. (4.32) and the M-normalized property represented by Eq. (4.17) as follow:

$$p_j(0)=\{\varphi_j\}^T[M]\{x(0)\} \text{ and } \dot{p}_j(0)=\{\varphi_j\}^T[M]\{\dot{x}(0)\} \tag{4.35}$$

The solution of Eq. (4.33) can be calculated using an integration scheme or by evaluating the Duhamel integral as:

$$p_j(t)=\frac{1}{\varpi_j}\int_0^t f_j(\tau)e^{-\xi_j\omega_j(t-\tau)}\sin\varpi_j(t-\tau)d\tau+e^{-\xi_j\omega_j t}\left(\alpha_j\sin\varpi_j t+\beta_j\cos\varpi_j t\right) \tag{4.36}$$

where the damped natural frequency is determined by:

$$\varpi_j=\omega_j\sqrt{1-\xi_j^2} \tag{4.37}$$

for the case of free vibrations the solution may be simplified as:

$$p_j(t)=A_j e^{-\xi_j\omega_j t}\sin\left(\varpi_j t-\theta_j\right) \tag{4.38}$$

where A_j and θ_j are constants which are determined from the initial conditions. Once the solution in modal coordinates has been obtained, the relation (4.32) can be used to obtain the result in generalized coordinates.

4.4.3. Newmark's method

In direct time integration methods, the equations of motion are integrated using a numerical step-by-step procedure. The term "direct" meaning that prior to the numerical integration, no transformation of the equations into a different form is carried out. New time integration methods and their properties have been investigated for different researchers. In practical application, the computational cost, accuracy, stability, damping of high and low frequencies, and type of inertia matrices are the main features in the selection of suitable time integration methods.

Among direct time integration techniques, the Newmark's method (Newmark 1959) is very popular. It is a single step integration implicit method that attempts to satisfy the differential equation of motion at time $t+\Delta t$ after the solution at time t is found. In order to illustrate the application of this family of numerical integration methods, let us consider the solution of the linear dynamic equilibrium Eqs. (4.19) written in the following form:

$$[M]\{\ddot{x}\}_{t+\Delta t}+[C]\{\dot{x}\}_{t+\Delta t}+[K]\{x\}_{t+\Delta t}=\{F\}_{t+\Delta t} \tag{4.39}$$

where the mass matrix $[M]$, the damping matrix $[C]$ and the stiffness $[K]$ are defined at time t. Thus, the Eq. (4.39) is only satisfied if the matrices do not change during the interval Δt. Using the truncated Taylor's series, the displacement and velocity vectors can be approximated in the form:

$$\{x\}_{t+\Delta t}=\{x\}_t+\Delta t\{\dot{x}\}_t+\frac{\Delta t^2}{2}\{\ddot{x}\}_t+\beta\Delta t^3\{\dddot{x}\}_t \tag{4.40}$$

$$\{\dot{x}\}_{t+\Delta t}=\{\dot{x}\}_t+\Delta t\{\ddot{x}\}_t+\gamma\Delta t^2\{\dddot{x}\}_t \tag{4.41}$$

Considering that the acceleration is linear; then, it may be represented by:

$$\{\dddot{x}\}_{t+\Delta t}=\frac{(\{\ddot{x}\}_{t+\Delta t}-\{\ddot{x}\}_t)}{\Delta t} \tag{4.42}$$

The standard form of Newmark equations are obtained by substituting the Eq. (4.42) into Eqs. (4.40) and (4.41) as:

$$\{x\}_{t+\Delta t}=\{x\}_t+\Delta t\{\dot{x}\}_t+\left(\frac{1}{2}-\beta\right)\Delta t^2\{\ddot{x}\}_t+\beta\Delta t^2\{\ddot{x}\}_{t+\Delta t} \tag{4.43}$$

$$\{\dot{x}\}_{t+\Delta t}=\{\dot{x}\}_t+(1-\gamma)\Delta t\{\ddot{x}\}_t+\gamma\Delta t\{\ddot{x}\}_{t+\Delta t} \tag{4.44}$$

These Equations together with Eq. (4.39) are used iteratively, for each time step, for each displacement DOF of the structural system. Wilson (1962) formulated the Newmark's method in matrix notation, added stiffness and mass proportional damping, and eliminated the need for iteration by introducing the direct solution of equations at each time step. For this, the Eqs. (4.43) and (4.44) are rewritten as:

$$\{\ddot{x}\}_{t+\Delta t} = b_1(\{x\}_{t+\Delta t} - \{x\}_t) + b_2\{\dot{x}\}_t + b_3\{\ddot{x}\}_t \tag{4.45}$$

$$\{\dot{x}\}_{t+\Delta t} = b_4(\{x\}_{t+\Delta t} - \{x\}_t) + b_5\{\dot{x}\}_t + b_6\{\ddot{x}\}_t \tag{4.46}$$

where the constants b_i are defined by:

$$b_1 = \frac{1}{\beta \Delta t^2},\ b_2 = \frac{1}{\beta \Delta t},\ b_3 = \beta - \frac{1}{2} \tag{4.47}$$

$$b_4 = \gamma \Delta t b_1,\ b_5 = 1 + \gamma \Delta t b_2,\ b_6 = \Delta t(1 + \gamma b_3 - \gamma)$$

Now substituting $\{\dot{x}\}_{t+\Delta t}$ and $\{\ddot{x}\}_{t+\Delta t}$ from Eqs. (4.45) and (4.46) into Eq. (4.39) yield the following suitable form:

$$\begin{aligned}(b_1[M] + b_4[C] + [K])\{x\}_{t+\Delta t} = \{F\}_{t+\Delta t} + [M](b_1\{x\}_t + b_2\{\dot{x}\}_t + b_3\{\ddot{x}\}_t) \\ + [C](b_4\{x\}_t + b_5\{\dot{x}\}_t + b_6\{\ddot{x}\}_t)\end{aligned} \tag{4.48}$$

or it is simply rewritten as:

$$[\hat{K}]\{x\}_{t+\Delta t} = \{\hat{F}\} \tag{4.49}$$

where

$$[\hat{K}] = b_1[M] + b_4[C] + [K] \tag{4.50}$$

is called the effective stiffness matrix or pseudo stiffness matrix and the effective load vector can be defined by:

$$\{\hat{F}\} = \{F\}_{t+\Delta t} + [M](b_1\{x\}_t + b_2\{\dot{x}\}_t + b_3\{\ddot{x}\}_t) + [C](b_4\{x\}_t + b_5\{\dot{x}\}_t + b_6\{\ddot{x}\}_t) \tag{4.51}$$

Note that for a linear structural problem with constant properties, the pseudo stiffness matrix $[\hat{K}]$ and the constants b_i are calculated only once. It is noted that Newmark's method is unconditionally stable if:

$$2\beta \geq \gamma \geq \frac{1}{2} \tag{4.52}$$

when $\beta = \frac{1}{4}$ and $\gamma = \frac{1}{2}$, the method is called the constant-average acceleration method (Weaver and Johnston 1987).

In nonlinear problems where $[M]$, $[C]$ or $[K]$ are time variant, the system becomes nonlinear and a state of dynamic equilibrium given in Eq. (4.39) will generally not be achieved at time $t + \Delta t$. For this type of problems, the Newmark's method is modified to accommodate an iterative process in each step or in some of the steps. For nonlinear systems it is convenient to write the equations of motion in the incremental form. The incremental displacement, velocity and acceleration vectors at time $t + \Delta t$ and iteration $(i+1)^{th}$ required to achieve equilibrium may be written as:

$$\{\delta x\}^{i+1} = \{x\}_{t+\Delta t}^{i+1} - \{x\}_{t+\Delta t}^{i} \tag{4.53}$$

$$\{\delta \dot{x}\}^{i+1} = \{\dot{x}\}_{t+\Delta t}^{i+1} - \{\dot{x}\}_{t+\Delta t}^{i} \tag{4.54}$$

$$\{\delta \ddot{x}\}^{i+1} = \{\ddot{x}\}_{t+\Delta t}^{i+1} - \{\ddot{x}\}_{t+\Delta t}^{i} \tag{4.55}$$

Substituting Eqs. (4.45) and (4.46) into Eqs. (4.55) and (4.54) respectively, the incremental acceleration and velocity vector can be reduced to the following form:

$$\{\delta \ddot{x}\}^{i+1} = b_1 \{\delta x\}^{i+1} \tag{4.56}$$

$$\{\delta \dot{x}\}^{i+1} = b_4 \{\delta x\}^{i+1} \tag{4.57}$$

The system equations in incremental form of motion for the $(i+1)^{th}$ interval may be written as:

$$[M]\{\delta \ddot{x}\}^{i+1} + [C]^i_{t+\Delta t}\{\delta \dot{x}\}^{i+1} + [K]^i_{t+\Delta t}\{\delta x\}^{i+1} = \{\delta F\}^i \tag{4.58}$$

Now considering Eqs. (4.56) and (4.57), Eq. (4.58) can be simplified to the following form:

$$[\hat{K}]^{i+1}\{\delta x\}^{i+1} = \{\delta F\}^i \tag{4.59}$$

where the updated stiffness matrix is determined by

$$[\hat{K}]^{i+1} = [K]^i_{t+\Delta t} + b_1[M] + b_4[C]^i_{t+\Delta t} \tag{4.60}$$

It is noted that the mass matrix remains constant during $t + \Delta t$ since the model for the MR damper proposed in the Section 3.6.1 modifies only the damping and the stiffness matrices. The right term in the above Eq. (4.59) is the unbalance force vector which is the difference between the forces at time $t + \Delta t$ before and after the matrices C and K are updated. It can be expressed as:

$$\{\delta F\}^i = \{F\}_{t+\Delta t} - [M]\{\ddot{x}\}^i_{t+\Delta t} - [C]^i_{t+\Delta t}\{\dot{x}\}^i_{t+\Delta t} - [K]^i_{t+\Delta t}\{x\}^i_{t+\Delta t} \tag{4.61}$$

The Figure 4.5 illustrates the proposed Newmark procedure formulated for nonlinear system. The above incremental form is embedded into the Newmark algorithm in order to ensure that the equilibrium equations are held at each time interval.

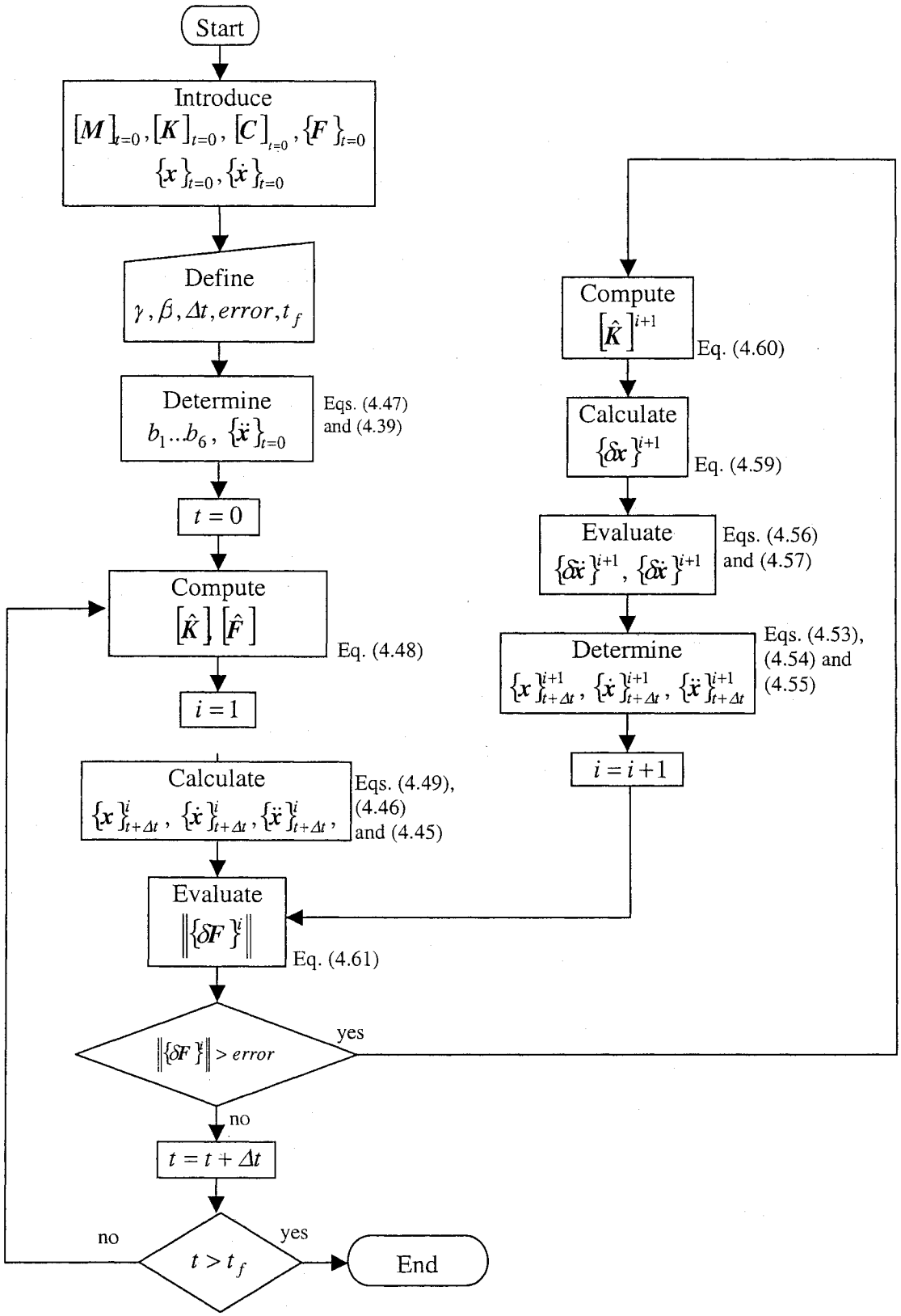

Figure 4.5. Newmark's method with iterative process for nonlinear systems

For nonlinear dynamic structural; analysis, it is found that the constant average-acceleration method is stable and yields enough accuracy. Although this method works accurately, it is not as efficient as the mode superposition method for linear system problems (Wilson 2002; Bathe and Wilson 1976).

4.5. Description of the experiment

In this section the proposed model for the MR damper and its corresponding finite element model is validated with a 3-D structure is exposed to different excitations. The structure is a aluminium truss space assembled from the commercial available hardware Meroform M12 manufactured by MERO. Figure 4.1 and Figure 4.6 show the details of the frame nodes and elements that are used to build the structure. The nodal joint design allows the structure to be assembled into numerous configurations in any of three orthogonal directions, thereby providing structures with variety of configurations. The elements are aluminium tubes with screwed solid steel end connectors, which when tightened into the node also clamp the tube by means of an internal compression fitting. Thus, any element member can be replaced without disassembling the whole structure. This feature allows installing the MR damper easily in any required location.

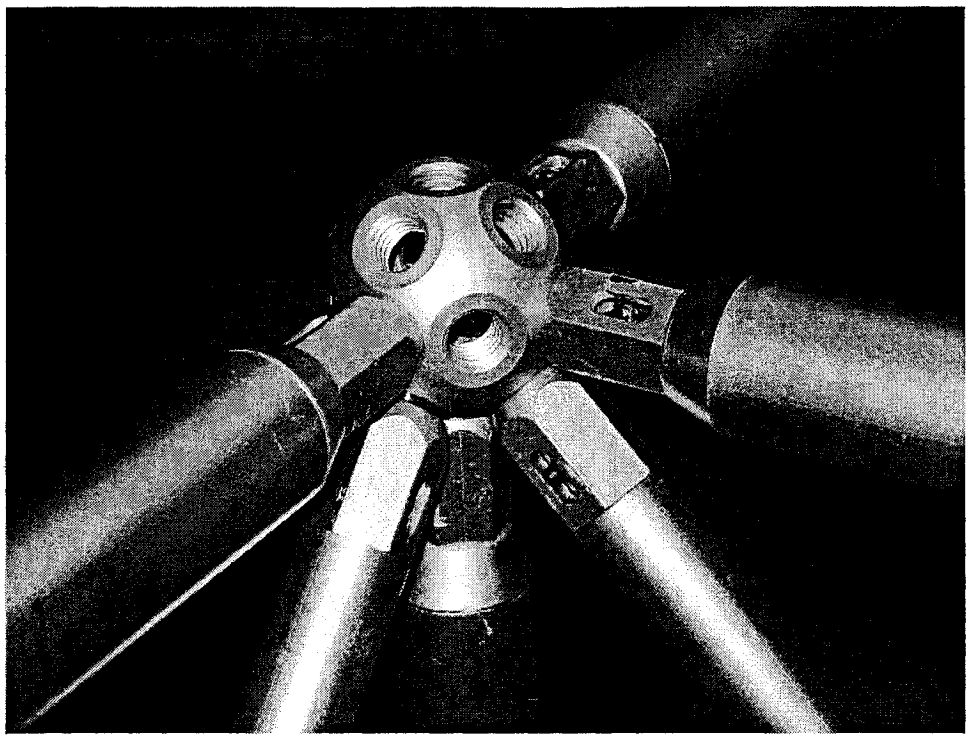

Figure 4.6. Details of a typical space truss spherical node.

Figure 4.7 shows the complete geometric configuration of the test article with the associated node numbers. It consists of a four-bay space truss structure. Each assembled bay is a 0.707 cube shaped structure. A correct assemblage is important because of the fact that the joint connections exhibit some level of flexibility. It is evident that the flexibility is severely affected by the tightening torque. Accordingly, to have a consistent assembling procedure in order to reduce the joint modeling errors, the space structure has been assembled at an optimum tightening torque of 22.6 N m (Zaher 2002).

The structure is mounted on a hydraulic shaker through a cross-type fixture as shown in Figure 4.8. A mass of 1.44 kg has been attached to the free nodes 3, 4, 7, 8, 9-12 and a mass of 2.88 to the free nodes of 13-20. The nodes 1, 2, 5 and 6 are fixed to the shaker.

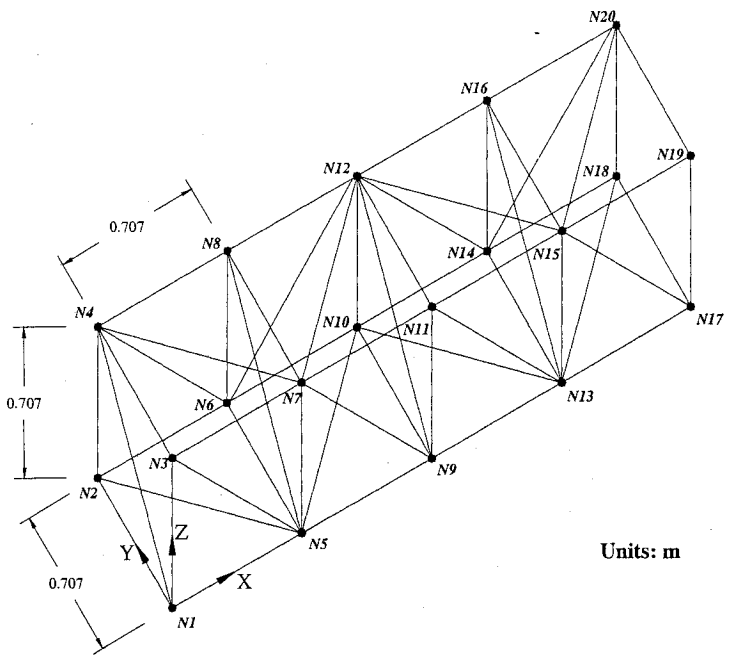

Figure 4.7. Schematic 4-bay space truss structure.

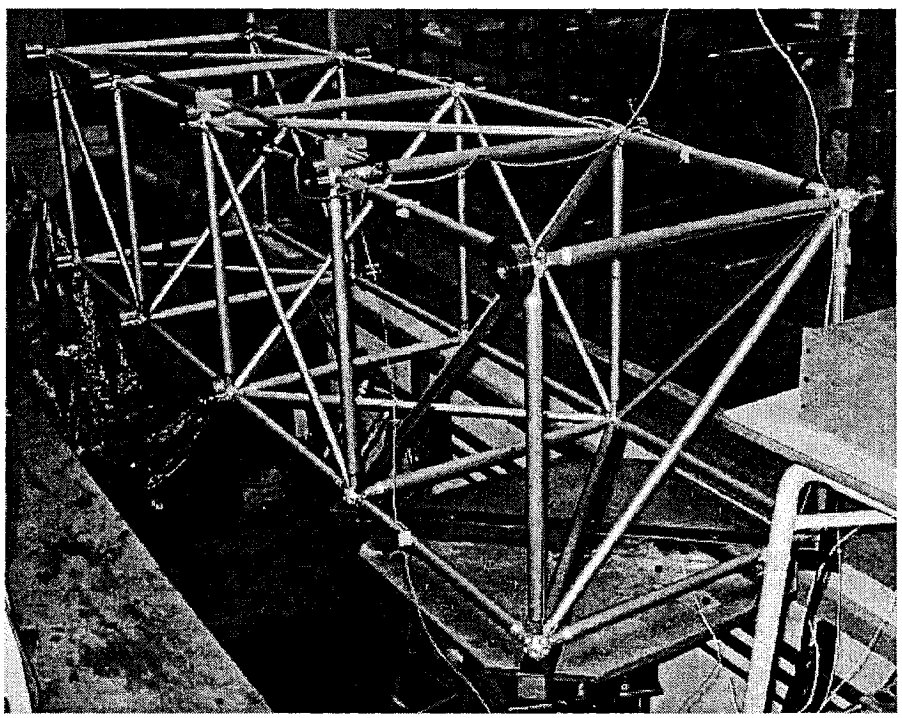

Figure 4.8. Set-up of the experimental test.

In Figure 4.9 shows the schematic description of the experimental setup. The structure is mounted on four points on a hydraulic shaker. The step, harmonic and random vibration signals are introduced to the shaker through signal generator. Two accelerometers are properly instrumented to measure the input and output accelerations. The first accelerometer (input) is mounted on the plate that supports the structure and the second (output) is located on the structure at node 19. The signals from accelerometers are properly amplified and then fed into the Signal Analyzer unit to obtain the transmissibility spectrum in the frequency domain.

The MR damper has been embedded into the structure between the nodes 8 and 12. The relative velocity between two ends of MR damper is obtained by the Linear Velocity Transducer (LVT) sensor which is installed in parallel with the MR damper. The signal from LVT is then filtered and introduced to the PC where a control strategy using the Simulink Toolbox of MATLAB has been developed. The output signal from the control is fed into a Power Amplifier Circuit to provide the controlled current excitation (current maximum value of 1.5 A) to the MR damper.

The connectivity for each element of the structure is provided in the Table 4.1 which is used to construct the FEM matrices of the structure.

The nominal physical properties of the structural components including lumped masses are listed in Table 4.2.

Table 4.1. Connectivity of the structure

Element Number	**Node 1**	**Node 2**	**Element Number**	***Node 1***	**Node 2**
1	1	5	29	11	15
2	2	6	30	12	16
3	3	7	31	9	11
4	4	8	32	10	12
5	1	3	33	9	10
6	2	4	34	11	12
7	1	2	35	9	12
8	3	4	36	13	11
9	1	4	37	14	12
10	5	3	38	10	13
11	6	4	39	12	15
12	2	5	40	13	17
13	4	7	41	14	18
14	5	9	42	15	19
15	6	10	43	16	20
16	7	11	44	13	15
17	8	12	45	14	16
18	5	7	46	13	14
19	6	8	47	15	16
20	5	6	48	13	16
21	7	8	49	13	19
22	5	8	50	14	20
23	5	11	51	13	18
24	6	12	52	15	20
25	5	10	53	17	19
26	7	12	54	18	20
27	9	13	55	17	18
28	10	14	56	19	20

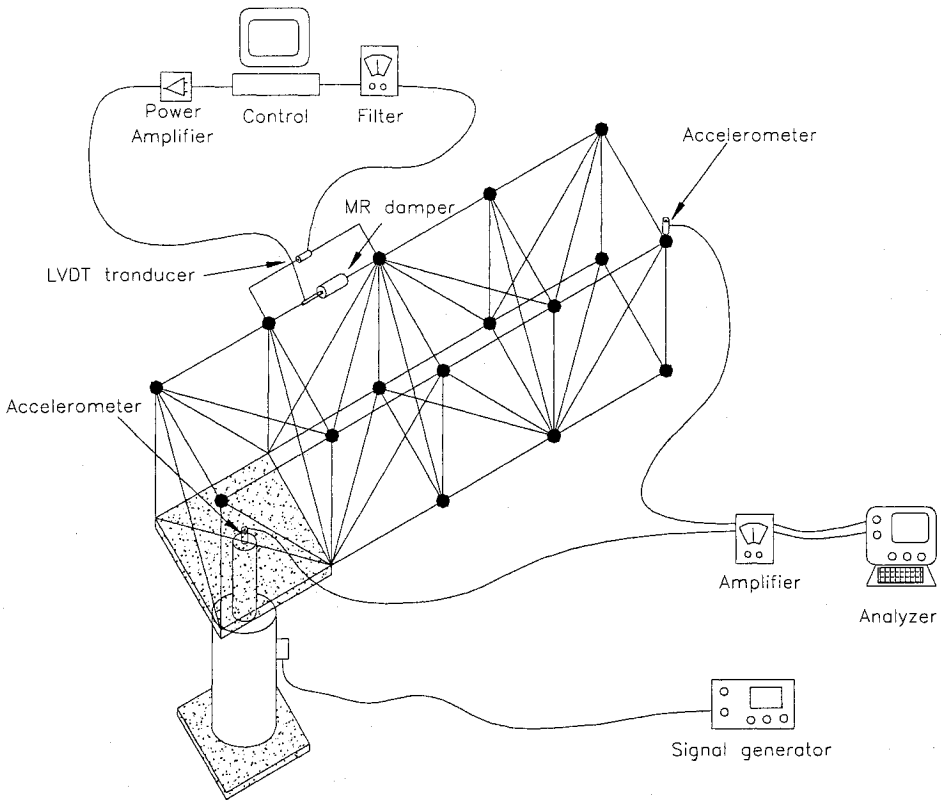

Figure 4.9. Schematic set-up of the test.

Table 4.2. Physical properties of the frame components

Component	**Dimension (mm)**	**Cross-sectional Area (mm2)**	**Weight (Kg)**
Lumped mass	-	-	1.44
Aluminum node	Φ 46	-	80
X, Y and Z-bar element	707x30x1.5	134.3	350
Diagonal member	1000x22x1.0	65.97	275

4.6. Validation of the proposed finite element bar model of the passive bar

In this section the response of the structure obtained using the finite element analysis of the proposed model is compared with that obtained in experimental test. For this purpose, the 3-D structure with 56 elements and four bays is mounted on the hydraulic shaker and it is excited with different signals inputs. Different experiments were performed to validate the finite element model proposed in the Section 4.3. In the first experiment the structure was excited under random vibration and the input and output responses were measured using accelerometers installed in the plate that supports the structure and at the node 19 respectively. Both accelerometers were properly installed in order to measure the Z-direction acceleration. The element 17 is removed and later replaced by the MR damper for subsequent experiments.

Table 4.3. Propeties of the finite element bar elements

Property	**E1, E3 (connections)**	**E2 (bars)**
Young's modulus (N/m^2)	67e9 (Aluminium)	67e9 (Aluminium)
Density (Kg/m^3)	2700	2700
Exterior Diameter (m)	0.011	0.030 (X,Y, Z directions) 0.022 (diagonals)
Thickness (m)	0.00035	0.0015 (X,Y, Z directions) 0.001 (diagonals)
Length (m)	0.064	0.579 (X,Y, Z directions) 0.872 (diagonals)

As previously mentioned in the finite element model of the bar elements the bolt connections and the half of the node are represented by the equivalent bars E1 and E3.

Their equivalent physical properties as well as the properties of the E2 are provided in the Table 4.3.

The transmissibility, defined as the ratio of output and input magnitude accelerations, in Z-axis obtained from the experimental test and finite element model for the structure without MR damper is presented in the Figure 4.10. The fundamental damped natural frequency is found to be 9.10 Hz. As it can be realized there is an excellent agreement between the simulation and the experimental results.

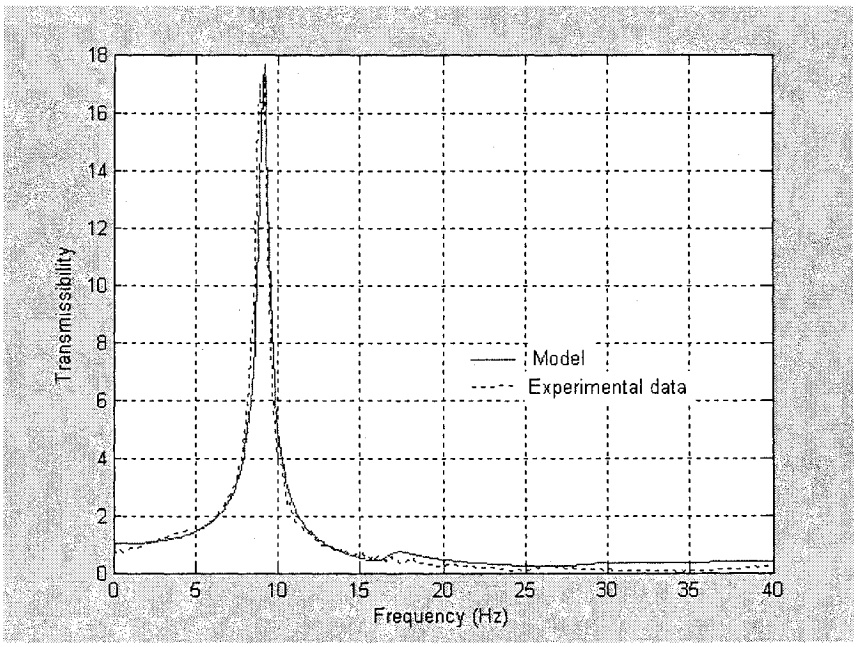

Figure 4.10. Comparison of the transmissibility in Z-axis between the input excitation and the output at 29-node obtained from experiment.

The proportional damping approach explained previously was applied to determine the damping matrix. It was considered a damping ratio of 0.16% for all the modes of vibration to match the transmissibility amplitude of the model with the experimental data. When proportional damping is applied, it is found that the higher frequencies are damped more than those modes with lower frequencies. The natural

frequencies of the structural systems are usually greatly separated and the effect of the higher modes in the response of the system is found to be negligible (Kelly 2000; Wilson 2002). The Newmark's method was applied to obtain the transient response with time increment of 0.004 s. The control parameters are selected as $\beta = 0.25$ and $\gamma = 0.5$ in order to have unconditional stability. The Figure 4.11 shows the comparison of the Z-acceleration response at node 19 between the test and the simulation. In this experiment the structure is excited with a step function with amplitude of 0.00254 m and then released until it reaches the equilibrium point.

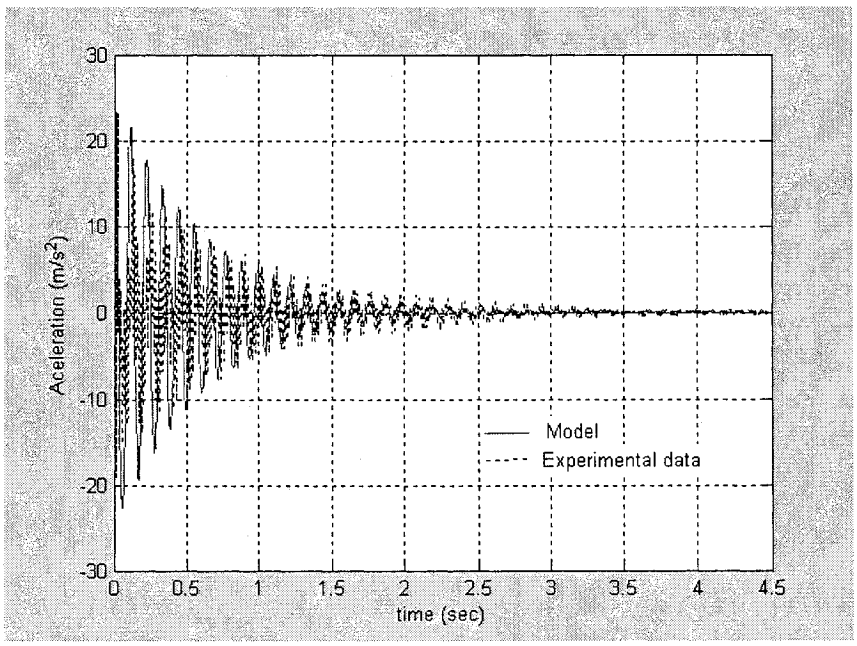

Figure 4.11. Comparison of the Z-acceleration for the structure at node 19 under step excitation.

The second experiment consists of exciting the structure under a harmonic excitation with frequency of 2.5 Hz and amplitude excitation of 0.004 m. Figure 4.12 presents the comparison between the experimental data and the model response at node

19. It is noted that the Newmark's method was employed to obtain the harmonic response with a time increment of 0.0025 s.

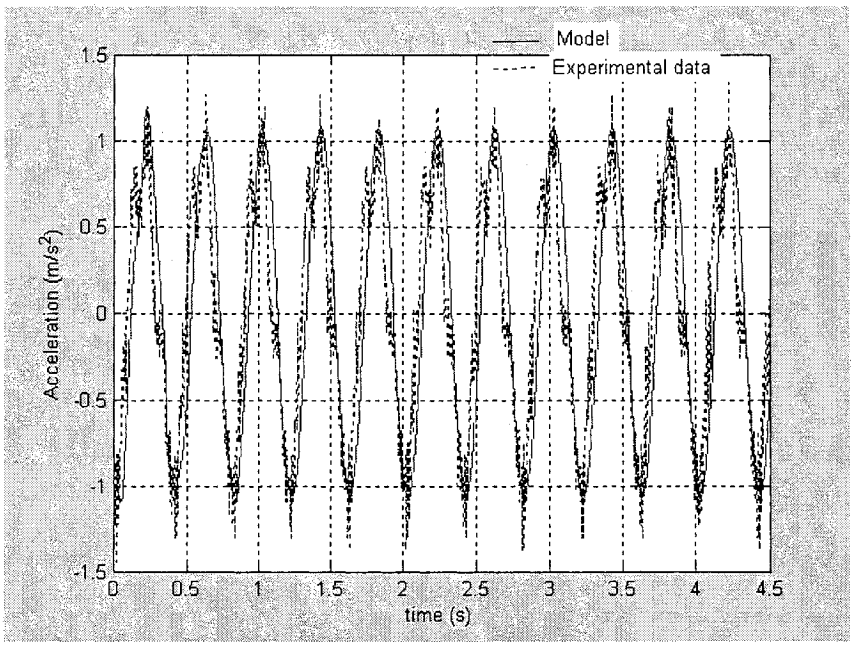

Figure 4.12. Z-acceleration response under harmonic excitation at the node 29.

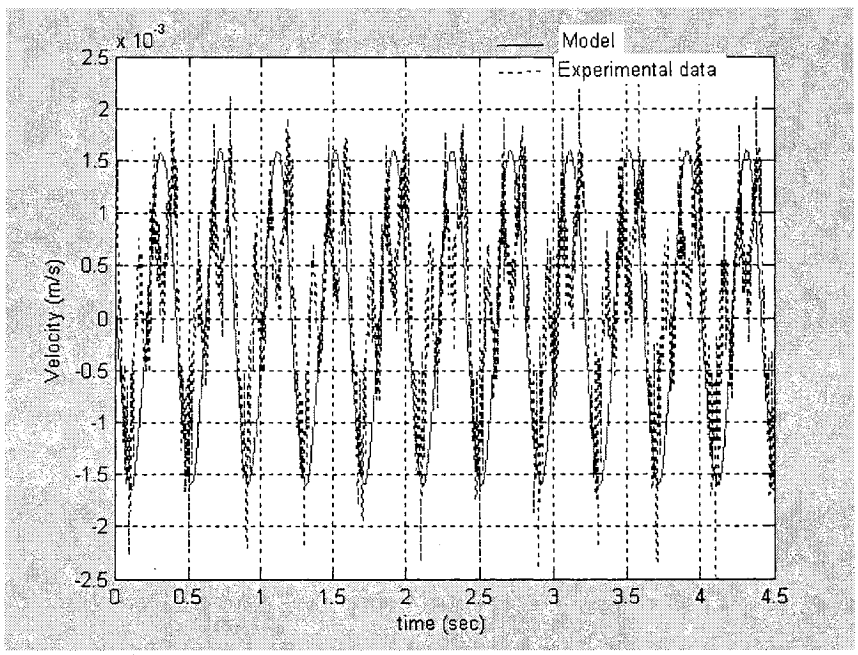

Figure 4.13. Comparison of the relative velocity between the nodes 8 and 12.

For the same experiment, the relative velocity between the nodes 8 and 12, the position where the MR damper will be installed, was measured. Figure 4.13 shows this relative velocity obtained for the simulation and experimental results.

As it can be observed the FEM with three elements proposed to simulate each bar element of the structure reproduce accurately the response under different excitations. It has been noted that the proportional damping can precisely reproduce the response for the lower frequencies which are the more important for structural systems.

4.7. Validation of the proposed finite element model for the MR damper bar element

Now the finite element of the MR damper bar proposed in Section 4.2 is validated. The model response is compared with the data extracted from the laboratory tests. As previously discussed the proposed model for the MR damper bar contains five elements. The physical properties for the connecting elements E1 and E5 are the same as those for E1 and E3 provided in Table 4.3. The E2 and E4 are solid bars of Aluminium with diameter of 0.012 m and length of $0.18l$ and 0.200 m respectively. The MR damper was installed in the middle position as E3; thus, an initial compressed force is considered in the model. The model proposed in the Section 3.6 is used to simulate the hysteresis force experienced in the MR damper. Thus, the values that characterize the MR damper response are similar to those obtained in that section. This requires information regarding the maximum displacement x_{max} and excitation frequency ω information as inputs. For transient problems the excitation frequency was considered to be the first natural frequency. It is noted that the response is mainly dominated by the first fundamental

mode as it can be observed from Figures 4.10 and 4.11. For the case of harmonic excitation, the frequency employed for the MR model is the same as that of the input excitation.

The instant maximum velocity is approximated using information obtained from instant displacement, x, velocity, $\dot{x}$ and acceleration, $\ddot{x}$, as (Wang et al. 2003):

$$\dot{x}_{\max} = \sqrt{\dot{x}^2 + x\ddot{x}} \tag{4.62}$$

Using Eq. (4.62) the maximum displacement can be obtained as:

$$x_{\max} = \dot{x}_{\max} / \omega \tag{4.63}$$

Since the inclusion of the MR damper into the space structure converts the linear system into nonlinear, the solution of the model is obtained using the Newmark's method reformulated for nonlinear problems as explained in Section 4.4. The time increment applied to acquire the transient response is 0.0025 s and 0.0095 s for harmonic excitation. This time integration method was complemented with an inner iterative process to solve the non-linearity of the problem due to the nonlinear MR model and maintain the equilibrium between the forces at any time step.

Figures 4.14 -16 show the comparison between the model response and the experimental data due to a step excitation of 0.0254 m for excitation currents of 0.0, 0.75 and 1.50 Amps. As it can be observed the vibration is damped out fast when the current excitation becomes larger. Examination of the results reveals that the fundamental natural frequency of the structures increases insignificantly from 9.10 Hz when the MR damper is not installed to 9.13 Hz when MR damper is installed with not current excitation. The fundamental natural frequency of the structure with embedded MR damper increases

lager current excitation. The first natural frequencies are found to be 10.06 and 10.38 Hz for 0.75 and 1.5 Amps respectively and excellent agreement with those obtained from experimental test.

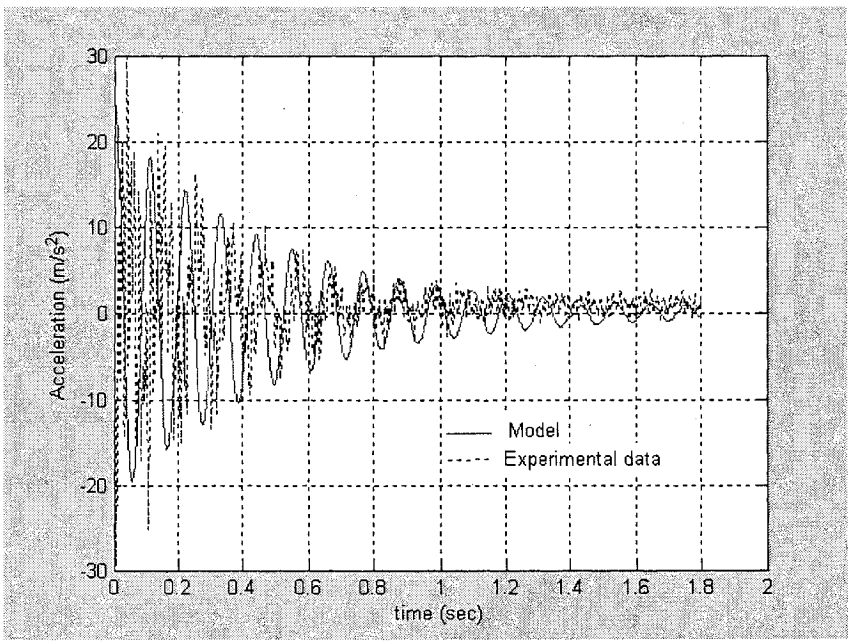

Figure 4.14. Comparison of the relative acceleration at node 19 with current excitation of 0.0 Amps.

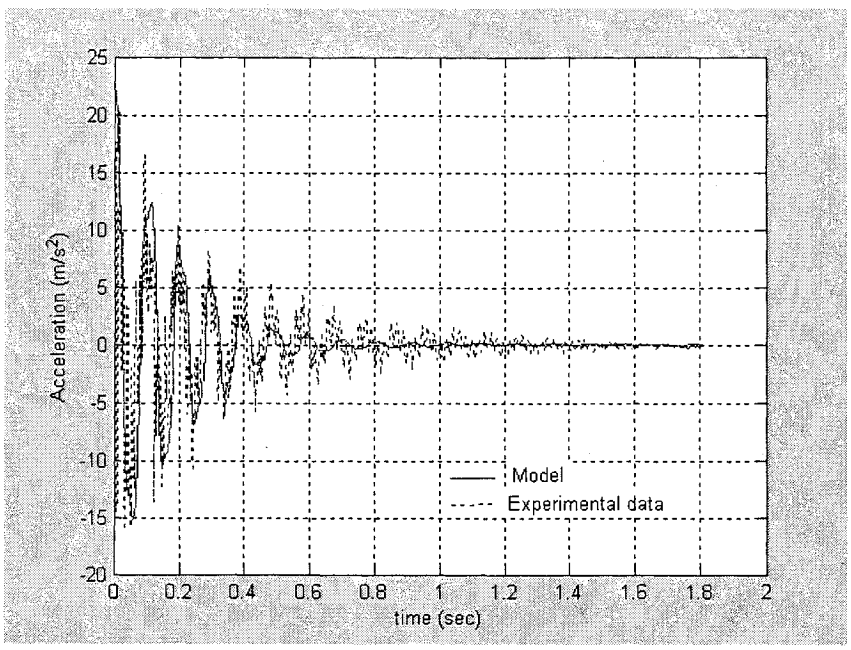

Figure 4.15. Comparison of the relative acceleration at node 19 with current excitation of 0.75 Amps.

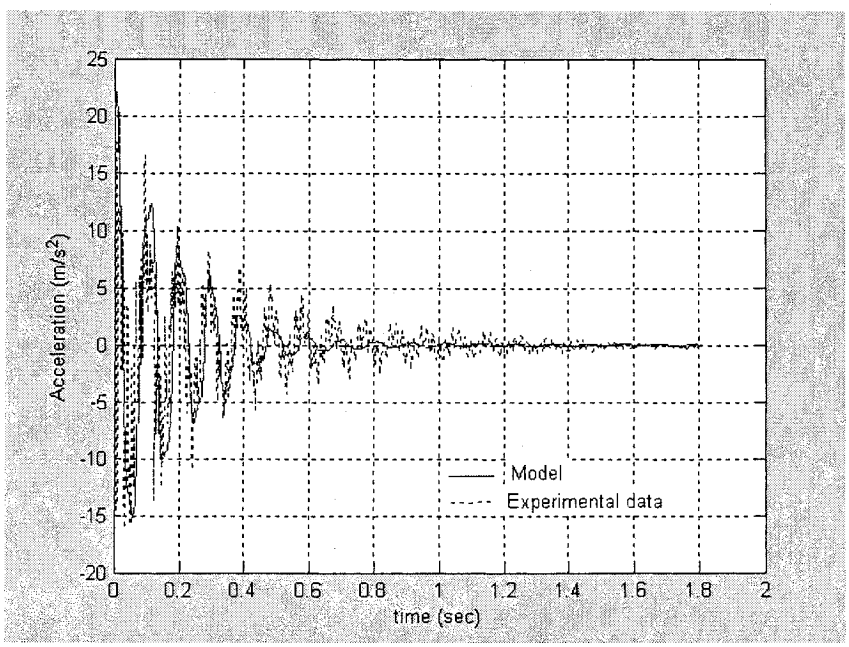

Figure 4.16. Comparison of the relative acceleration at node 19 with current excitation of 1.50 Amps.

The next experiment consists of exciting the structure under harmonic excitation with frequency of 2.5 Hz and amplitude of 0.004 m. The current excitation for the MR damper is 1.5 Amps. The comparison between the experimental data and the proposed model is shown in Figure 4.17. The experimental data was obtained from the accelerometer installed at node 19.

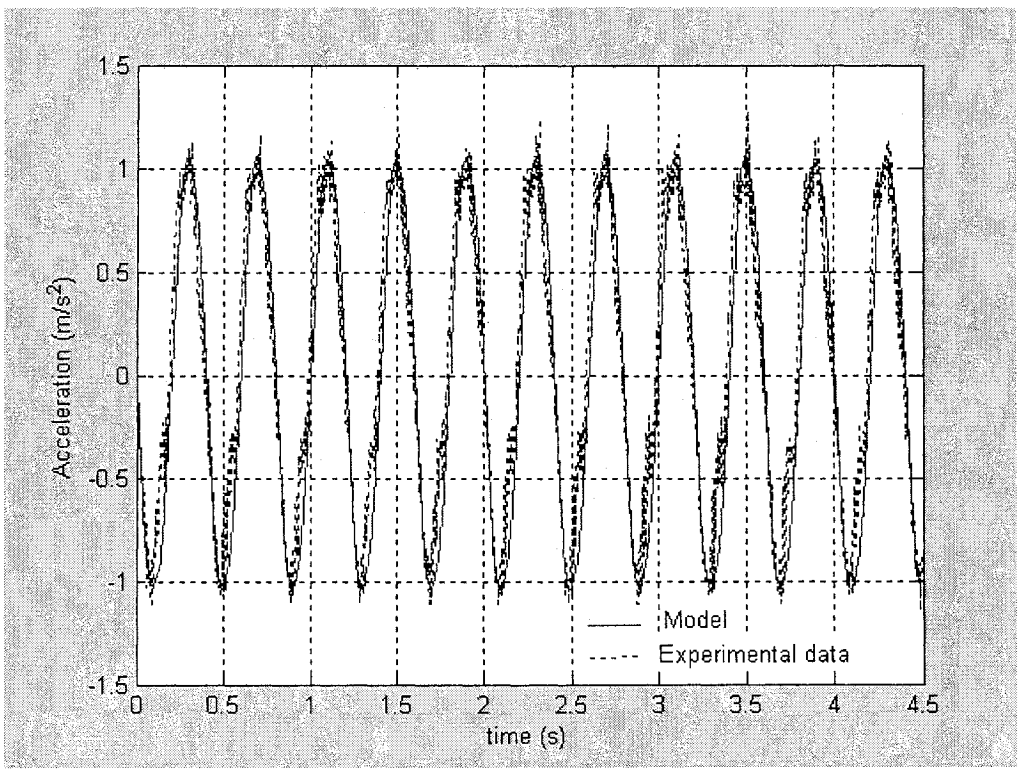

Figure 4.17. Comparison of the acceleration at node 19 under harmonic excitation of 2.5 Hz with excitation current of 1.50 Amps.

The relative velocity measured by the LVT installed at both ends of the MR damper is also extracted and compared with the theoretical results as shown in Figure 4.18.

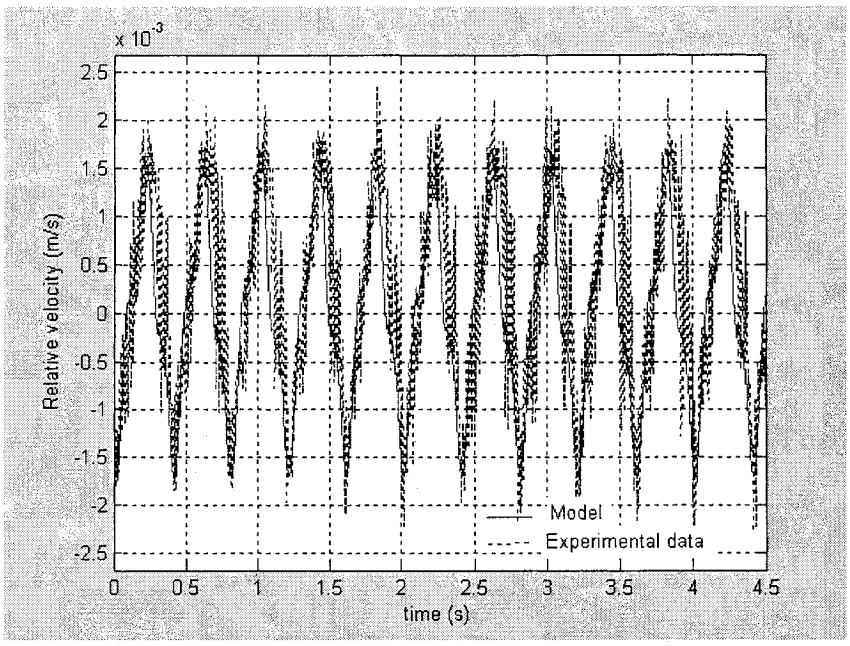

Figure 4.18. Comparison of the relative velocity at both ends of the MR damper under harmonic excitation of 2.5 Hz and excitation current of 1.50 Amps.

As it can be observed, a good agreement exists between the experimental data and the proposed models of the structure and the MR damper. It can also be realized from the figures that the amplitude and the fundamental natural frequency of the response has been well predicted by the model. Thus finite element model proposed for the element bar and the MR damper bar can be applied with confidence to predict the response of the structure for variable excitation conditions.

CHAPTER 5

THE PERFORMANCE EVALUATION OF THE PASSIVE AND SEMIACTIVE DAMPING IN VIBRATION SUPPRESSION OF DISCRETE STRUCTURES

The vibration suppression in structural systems can be accomplished by passive, active and semiactive ways. The passive manner mainly includes the installation of heavy, viscoelastic damping devices to mitigate the damaging effects of the vibration. Although these devices have proved effectiveness for specific conditions, they have the drawback that they cannot adapt themselves to changing environments. Another much cheaper passive manner is through optimum design of the structure so that it has intrinsic passive vibration characteristics.

Active systems can adapt themselves to different loading conditions and to suppress different vibrational modes of the structure; however, the high cost, the large external sources, the instability due to the injected energy and the preference by traditional technology have limited its applications. On the other hand, the semiactive system is a safe and trust manner system to suppress the structural vibration as it can adapt itself to changing environments while not requiring large external sources. In this chapter the passive and semi active suppression of vibrations are explored. The passive suppression has been achieved efficiently trough the redesigning of the structure so that it can intrinsically damp out the vibration. The optimum design of the structure to minimize

the vibrational energy is achieved using Genetic Algorithms (GAs). Moreover, the implementation of a Magnetorheological (MR) damper to reduce the vibration is performed in passive and semiactive manner. Furthermore, the optimum placement of the MR damper is investigated. Finally, semiactive strategy is implemented to improve the performance of the structure and to achieve a lengthening effect on the MR damper.

5.1. Passive reduction of vibrations in structures via optimum shape

Traditional techniques to reduce vibration are to increase the mass and/or damping; however, the former is normally in violation with design goals, and the latter is the most regularly applied passive technique. Another recent developed way is to apply active control to produce countervibrations in order to reduce vibration (Anthony et al. 2000b). Alternatively the vibration transmission can be reduced by dynamically isolating the structure where it is practically applicable. The problem of minimization of vibrations of structures subjected to periodic loading is also of great importance since many sources of vibrations are periodic forces due to rotating components (Jog 2002). In this part the different shapes of the structures are explored to reduce the transmitted vibration in the structures due to an external excitation.

The minimization of the vibration can be made locally or on the whole structure. Here the objective function is to minimize the total vibration. In order to have more robust final optimum designs, the optimization is performed over a range of frequencies that includes the lower natural frequencies which are the most important components in the total structural response. Therefore, the objective function is to minimize the total

vibration represented by the performance index f over a range of frequencies which can be mathematically expressed as:

Minimize

$$f(\boldsymbol{x},\omega) = \int_{\omega_0}^{\omega_f} \{\boldsymbol{x}\}^T [\boldsymbol{W}] \{\boldsymbol{x}\} d\omega \tag{5.1}$$

subject to:

$$a_i \leq x_i \leq b_i \tag{5.2}$$

where $[\boldsymbol{W}]$ is a prescribed weighting matrix associated with nodal displacement $\{\boldsymbol{x}\}$, and a_i b_i are lower and upper limits for the search space which are taken from nodal coordinates of the original structure. The purpose of weighting function is to emphasize certain portions of the structure.

The optimization process is applied to the structure shown in Figure 4.7 which is the original structure. The structure is fixed at nodes N1, N2 and N6 and excited harmonically at N5 in Z-direction with amplitude of 0.005 m. A range of frequencies between 0 to 40 Hz is evaluated to determine the objective function. It is assumed that the design nodes are N7, N8,..., N16. Two cases are studied. In the first case it is assumed that the limits for search space are +/- 0.16 m from the original coordinates. In the second case the limits are expanded to +/- 0.32m. The effect of the probability of reproduction employed in the evolutionary process is also investigated. It was assumed the identity matrix as the weighting matrix.

Optimum solutions have been obtained using GAs. The parameters used in GAs process and optimum results for both cases 1 and 2 are provided Table 5.1. The effectiveness of GAs can be realized as the number of analyzed structures is much lower that the design space in both cases. For example, for Case 1 the number of analyzed structures using GAs is 3750 compared to 1.427e45 possible solutions. Total vibration for both cases is very small compared with the original structure. The performance vibration function for the original to structure is 1.4429 m^2-Hz compared to 0.2925 m^2-Hz and 0.0306 m^2-Hz for the Case 1 and Case 2, respectively.

Table 5.1. Parameters and results of the GAs process

Parameter	**Case 1**	**Case 2**
Space solution	1.427e45	1.532e54
Probability of crossover and mutation	0.8 and0.005 respectively	0.8 and0.005 respectively
Probability of reproduction	0.2	0.2, 0.5 and 0.8
Initial population	50	50
Bits of the chromosome	150	180
Analysed structures	3750	3750
CPU time (s)	1281	1316
Solution (m^2-Hz)	0.2925	0.0306

The history evolution of the best chromosome is shown in Table 5.1. For the reproduction operation of GAs, the methodology proposed in the Section 2.3.2.4. has been applied. The result shows how the probability of reproduction can control the rate of convergence. The proper selection of the probability of reproduction allows to avoid the situations where the chromosomes becomes clones very fast due to of the existence of a

very good element or the opposite case where the convergence is very slow when the population becomes homogeneous.

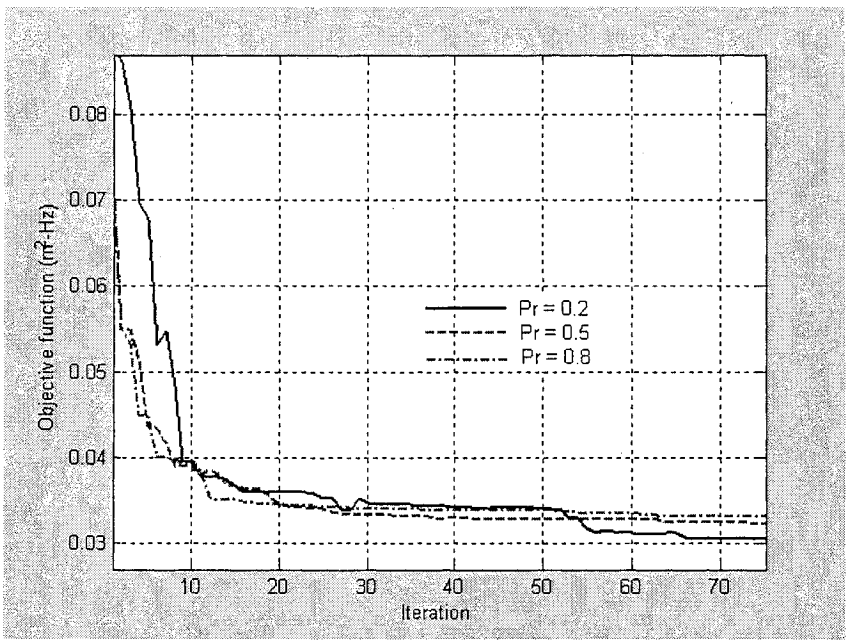

Figure 5.1. Optimum solution history for different probability of reproduction $P_r = 0.2$, 0.5 and 0.8 in Case 2.

The original and final coordinates of design nodes for Case 1 and 2 are tabulated in Table 5.2. The corresponding final optimum configuration of the structure for Cases 1 and 2 are shown in Figure 5.2 and Figure 5.3 respectively.

Table 5.2. Coordinates of the design nodes for the original and the optimum structures (m)

Node		X	Y	Z	Node		X	Y	Z
7	**Original**	0.707	0	0.707	12	**Original**	1.414	0.707	0.707
	Case 1	0.827	-0.150	0.557		**Case 1**	1.554	0.807	0.587
	Case2	1.027	-0.090	0.407		**Case2**	1.664	1.007	0.487
8	**Original**	0.707	0.707	0.707	13	**Original**	2.121	0	0
	Case 1	0.557	0.577	0.867		**Case 1**	2.011	0.060	-0.060
	Case2	0.407	0.737	0.407		**Case2**	2.181	0.270	0.210
9	**Original**	1.414	0	0	14	**Original**	2.121	0.707	0
	Case 1	1.514	-0.14	-0.15		**Case 1**	1.971	0.607	0
	Case2	1.384	0.050	-0.110		**Case2**	2.241	0.457	0.290
10	**Original**	1.414	0.707	0	15	**Original**	2.121	0	0.707
	Case 1	1.404	0.687	0.110		**Case 1**	2.201	0.140	0.557
	Case2	1.164	0.967	-0.010		**Case2**	2.141	-0.300	0.597
11	**Original**	1.414	0	0.707	16	**Original**	2.121	0.707	0.707
	Case 1	1.264	0.090	0.867		**Case 1**	2.011	0.667	0.557
	Case2	1.664	0.070	0.917		**Case2**	2.321	0.807	0.977

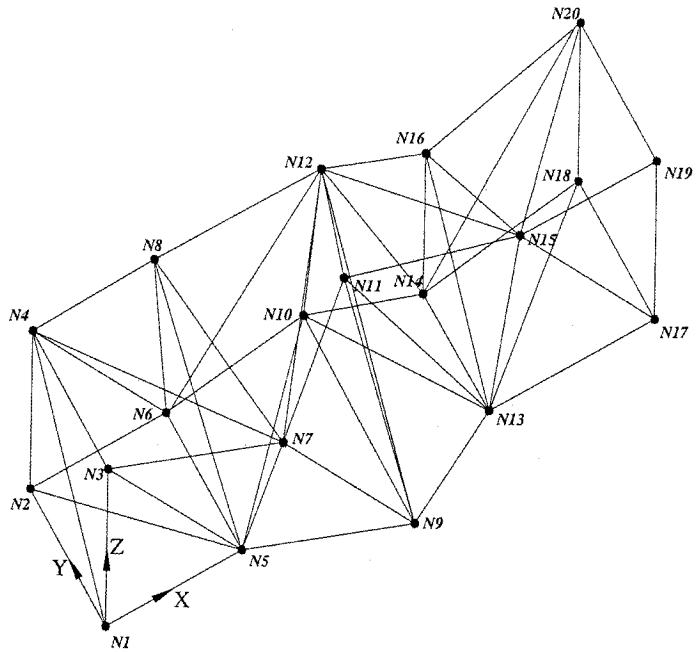

Figure 5.2. Final optimum configuration of the structure for Case 1.

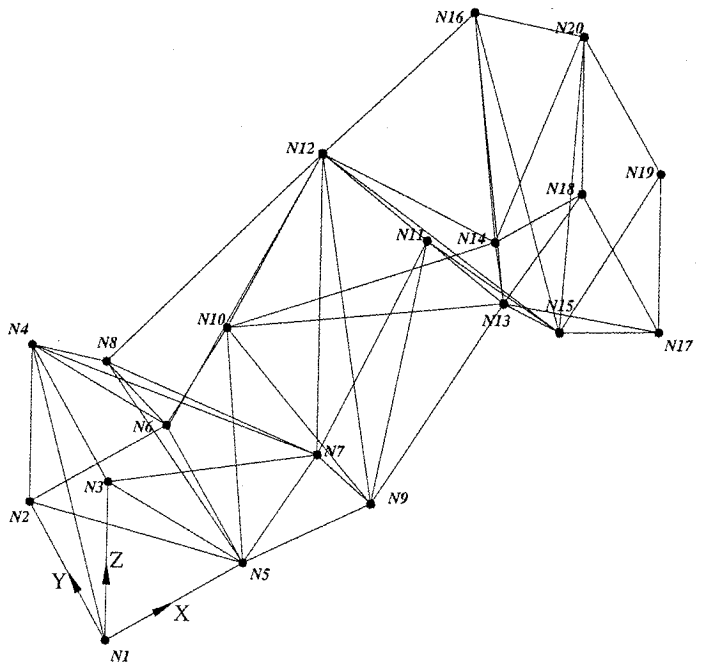

Figure 5.3. Final optimum configuration of the structure for Case 2.

The variation of the performance vibration function versus frequency is shown in Figure 5.4. As it can be realized, the performance function has reduced drastically for optimized structures (Cases 1 and 2) in comparison to the original structure. Performance of optimized structures with respect to original structure may be better visualized in Figure 5.5 where the transmissibility has been shown for original and optimized structures.

The transmissibility is defined as the ratio of the norm of nodal acceleration of node 19 to the norm of the nodal input acceleration of node 5, which can be represented by:

$$Transmissibility = \frac{\|\ddot{x}_{19}\|}{\|\ddot{x}_{5}\|} \tag{5.3}$$

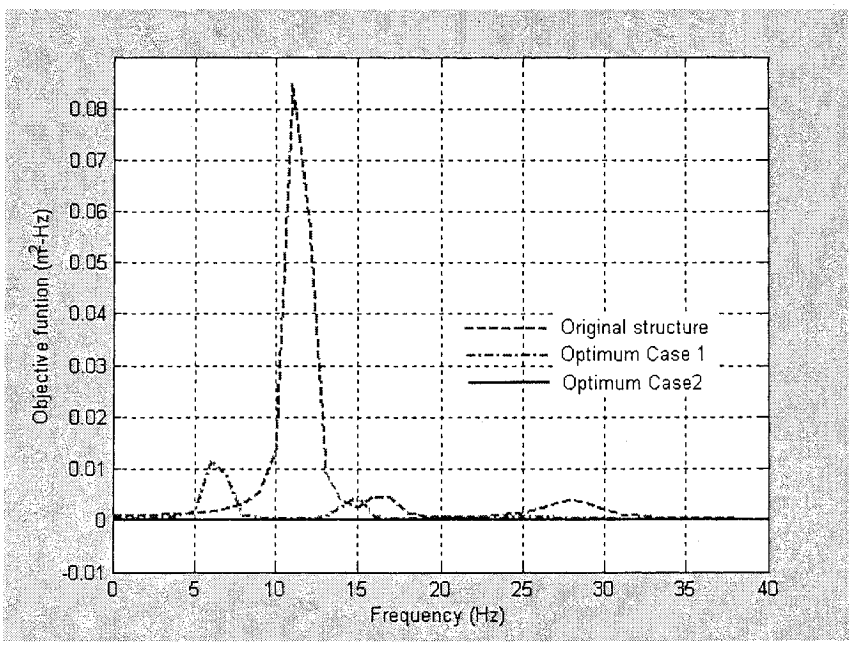

Figure 5.4. Performance function versus frequency range.

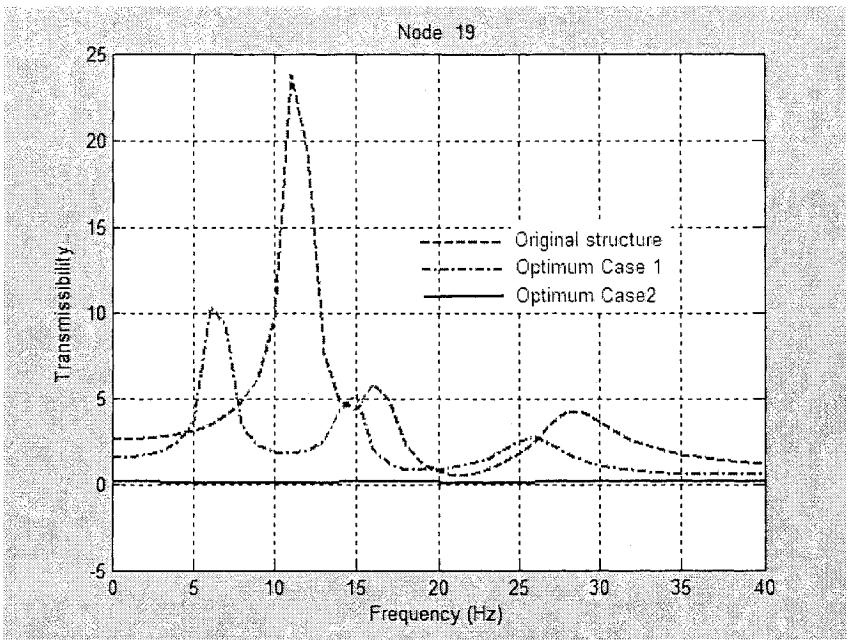

Figure 5.5. Transmissibility of the vibration for the original and optimized structures.

It is observed that optimally shaped structures reduce drastically the vibration transmission in structural system. It is noted that the final optimum structures may not be practically realizable due to other design restrictions. Considering Figure 5.5, it should be noted that at zero frequency, the transmissibility for the original and optimized structures are not 1 as one may be expected. The reason is that the structure is fixed at nodes N1, N2, N6 and vibrated harmonically at node N5. At zero frequency, a displacement applied at node N5 will cause a different displacement at node N19 and it can be realized that the ratio of the norm of these two displacements is not equal to unity. To conclude, the traditional periodic design is particularly bad design with respect to the transmission of vibrational energy. The periodicity of the structure, whilst being on favourable aesthetic grounds, allows similar frequency components, that would propagate relatively unimpeded through one bay section, through all the bay sections. This study shows that

with geometry optimization of the structure, it is possible to have optimized structure with intrinsic passive vibration filtration characteristics.

5.2. Passive reduction of vibrations in structures via MR dampers

The controllable fluids dampers can work in semiactive or passive manner by controlling or keeping constant the current excitation. In this part the passive application of MR dampers to reduce the vibration is investigated.

To measure the effectiveness of the MR damper to suppress the vibration, a performance index is defined. The following displacement part of performance index frequently used in control for the Linear Quadratic Regulator has been employed (Qu et al.; 2002):

$$f(\boldsymbol{x},t) = \int_{t_0}^{t_f} \{\boldsymbol{x}\}^T [W] \{\boldsymbol{x}\} dt \tag{5.4}$$

This performance index, which will be referenced as total vibration, can be applied to measure the global vibration of the whole structure if all the components of the displacement vector, $\{\boldsymbol{x}\}$, are considered or to measure the local vibration if only the components of the interested nodal displacement are considered. Here, both global and local vibration and compared.

Simulations for three different positions of the MR damper are accomplished. The selected positions are lower horizontal, upper horizontal and diagonal elements numbered as 14, 17 and 24 respectively. For each position, the response of the system for each current excitation of 0.0, 0.75 and 1.5 A and under step and harmonic load applied on the

nodes 1, 2, 5 and 6 has been studied. All simulations were obtained using Newmark's method with time increment of 0.0004 s for transient case and 0.00125 s for harmonic case.

Figures 5.6-5.8 show the Z-displacement response of node 19 under step input when the MR damper located at positions of elements 14, 17 and 24. Table 5.3 presents the local and global performance index values calculated for interval time of 2 s for each position of the MR damper.

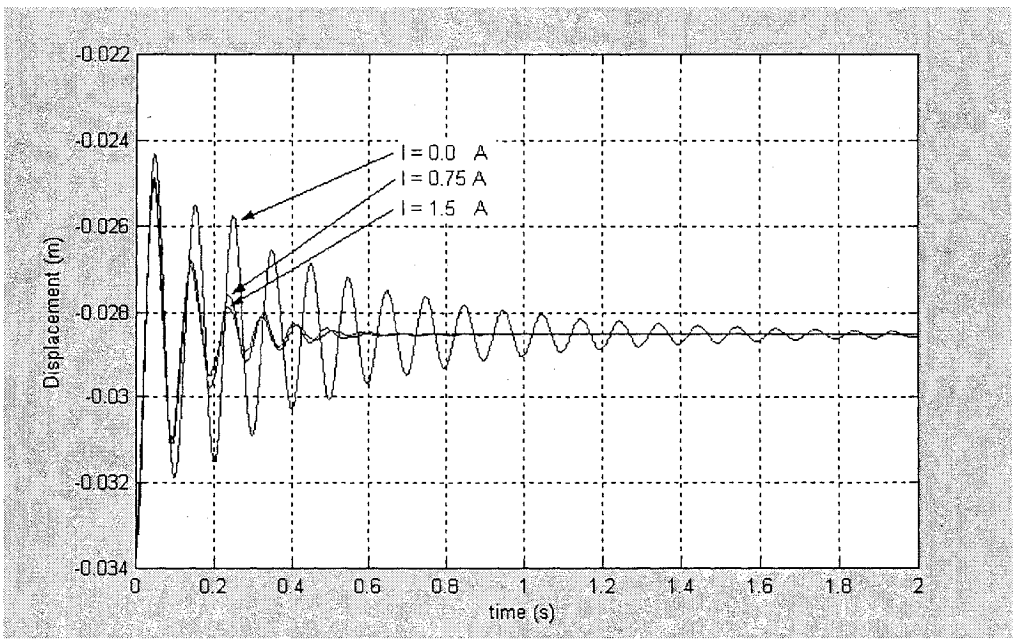

Figure 5.6. Z-displacement response of node 19 with MR damper located at element 14 under step input.

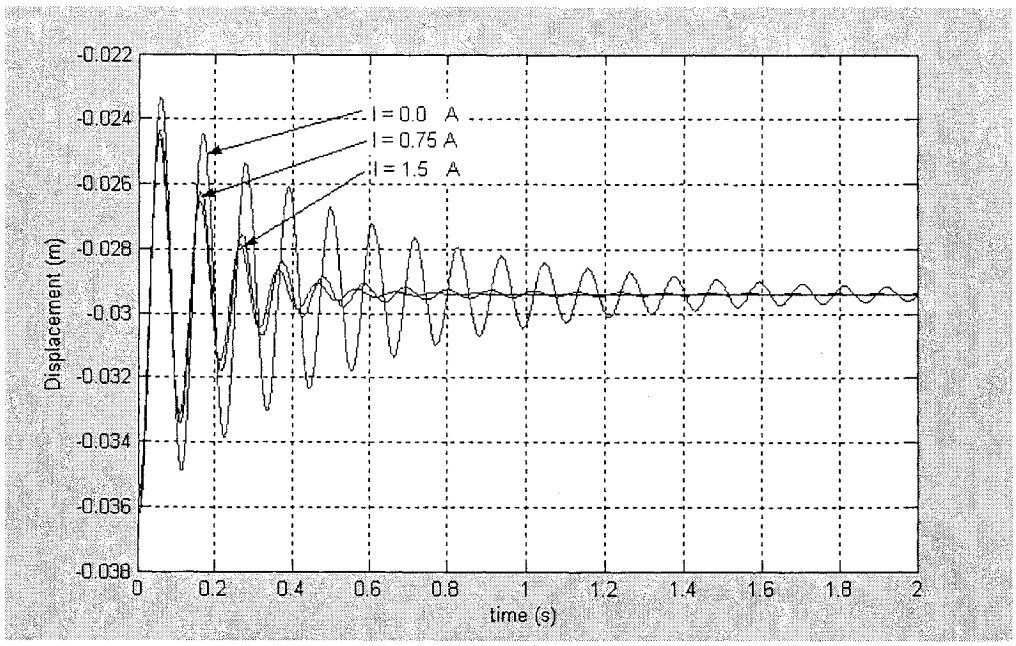

Figure 5.7. Z-displacement response of node 19 with MR damper located at element 17 under step input.

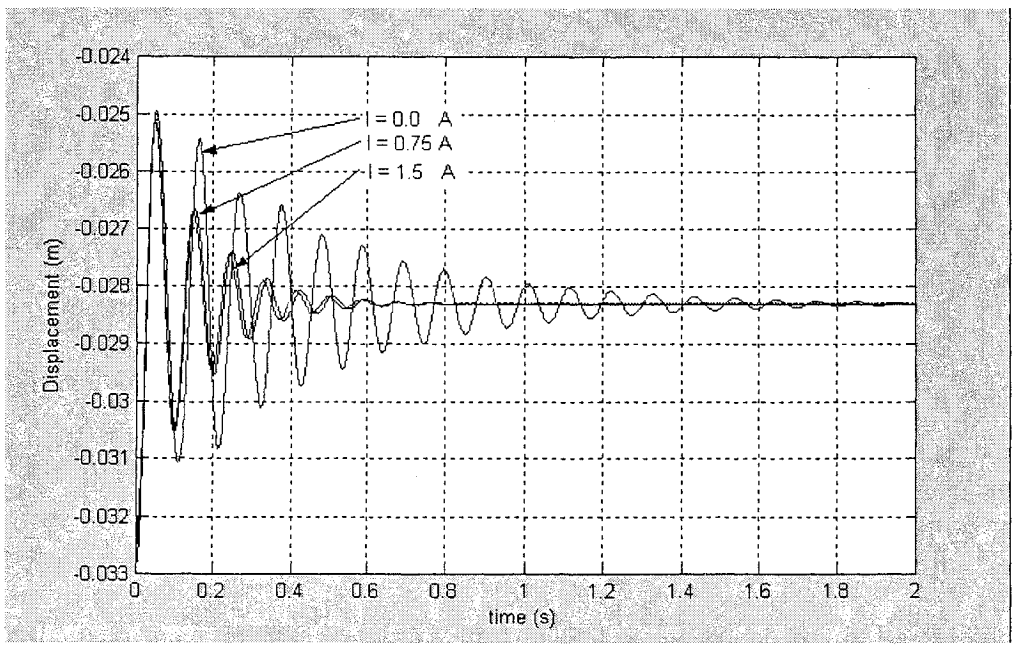

Figure 5.8. Z-displacement response of node 19 with MR damper located at element 24 under step input.

Table 5.3. Global and local vibration and for the node 19 under step excitation

Current (A)	Position 14		Position 17		Position 24	
	Global	**Node 19**	**Global**	**Node 19**	**Global**	**Node 19**
0.0	5.179e-3	14.812e-4	5.211e-3	24.285e-4	5.192e-3	15.751e-4
0.75	5.170e-3	5.032e-4	5.181e-3	9.5333e-4	5.173e-3	5.878e-4
1.50	5.167e-3	4.563e-4	5.178e-3	7.729e-4	5.172e-3	5.477e-4

As it can be observed, the position of the MR damper plays a very important role in vibration suppression of the structure. The results suggest that among the three positions analysed, the position 14 is the ideal for the installation of the MR damper as it causes the lowest performance index. Moreover, it can be realized that current excitation of 1.5 A has the lowest local and global vibration values.

Figure 5.9-5.11 show the Z-displacement of node 19 under harmonic excitation with frequency of 7.5 Hz and amplitude of 0.0127 m for three levels of current excitation and the three selected positions of the MR damper. The global and local vibration for each MR damper position under harmonic excitation are also tabulated in Table 5.4.

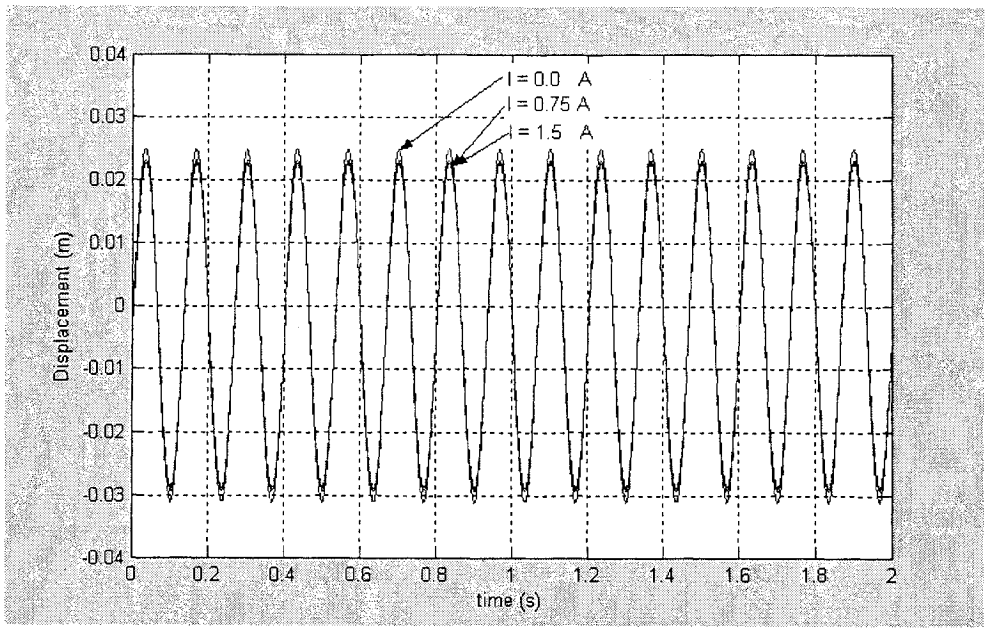

Figure 5.9. Z-displacement response of node 19 with MR damper at position 14 under harmonic excitation.

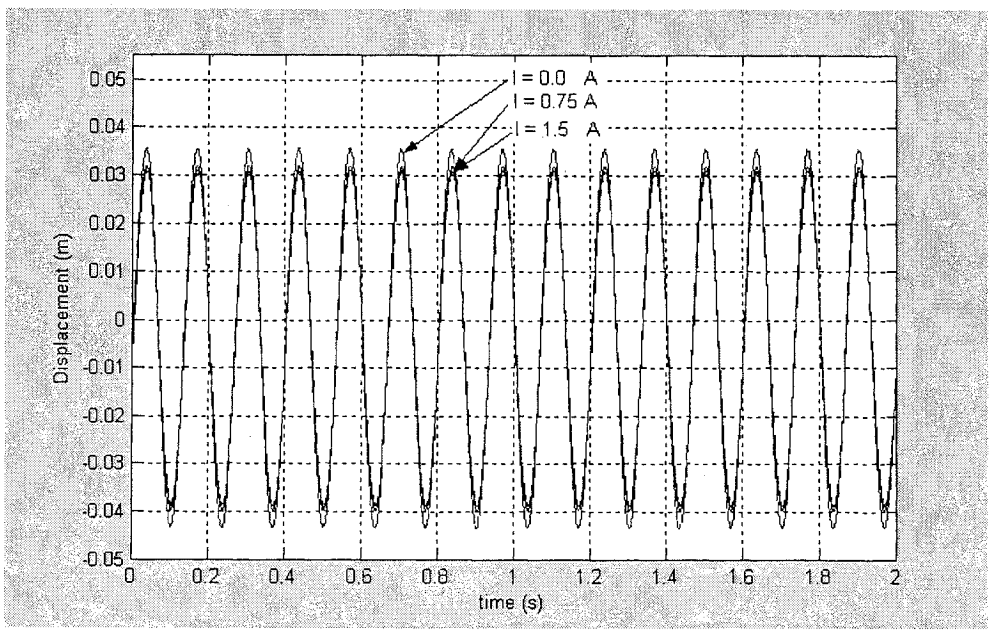

Figure 5.10. Z-displacement response of node 19 with MR damper at position 17 under harmonic excitation.

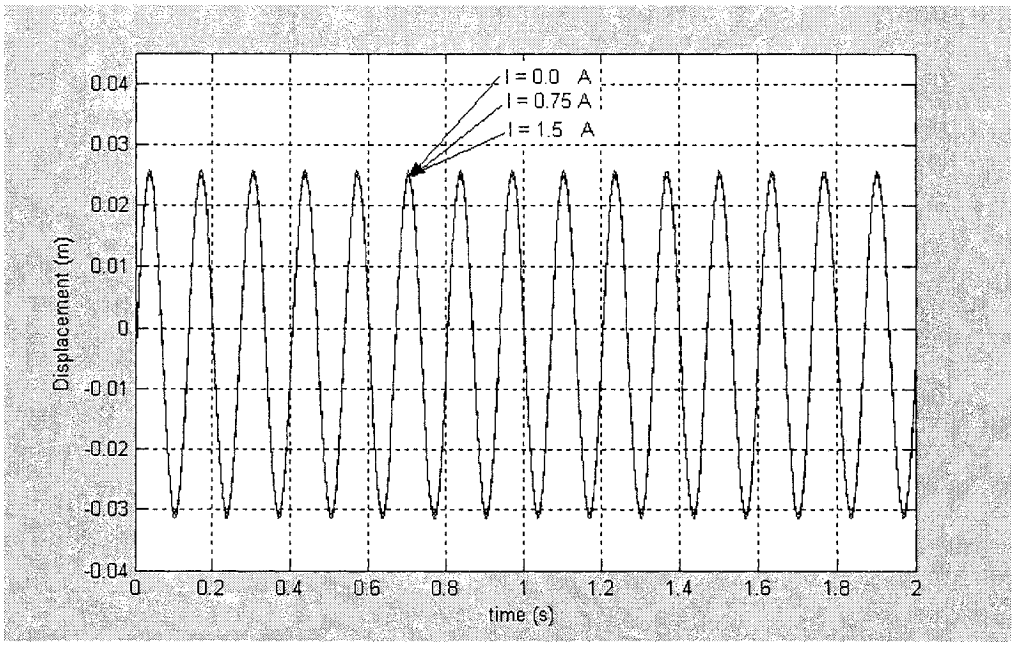

Figure 5.11. Z-displacement response of node 19 with MR damper at position 24 under harmonic excitation.

Table 5.4. Global and local vibration for the node 19 under harmonic excitation.

Current (A)	**Position 14**		**Position 17**		**Position 24**	
	Global	**Node 19**	**Global**	**Node 19**	**Global**	**Node 19**
0.00	2.114e-3	20.661e-3	6.263e-3	36.371e-3	4.212e-3	26.481e-3
0.75	1.799e-3	18.234e-3	4.875e-3	31.671e-3	3.806e-3	24.977e-3
1.50	1.7233-3	17.599e-3	4.517e-3	30.346e-3	3.739e-3	24.730e-3

Close examination of the results reveals that the position 14 with an excitation current of 1.5 is the best condition for the analysed cases under harmonic excitation which is similar to that of previous case for step excitation. It is concluded that the effectiveness of the MR damper heavily depends on its location. Thus, it is very

important to find the optimum location of the MR dampers in design optimization of semiadaptive structures for vibration suppression.

5.3. Semiactive reduction of vibrations in structures through MR dampers – performance evaluation

Semiactive devices can control the state of systems such that their inherent damping characteristics are enhanced. Using semiactive approach, vibration is suppressed by passive energy dissipation mechanisms. Therefore, systems are always stable even with improper selection of control logic due to, for example, lack of exact information about the dynamic characteristics of the structure (Onoda et al.; 1997).

In this section a strategy has been proposed to evaluate the reduction of the vibration in discrete structures through MR dampers. The proposed strategy employ the absolute velocity at the end of the MR damper in local coordinates and the hysteresis force experienced by the MR damper. It assigns maximum current when the both velocity and hysteresis force have the same sign and zero when the sign of both is different. This proposed strategy can be stated as:

$$\begin{cases} I_{\max} & \text{when} \quad \dot{x}_j F_z > 0 \\ I_{\min} & \text{when} \quad \dot{x}_j F_z \leq 0 \end{cases} \tag{5.5}$$

Different simulations are carried out to validate the proposed strategy. First, the structure is excited with harmonic excitation. The amplitude and frequency of the excitation are selected to be 0.0127 m and 7.5 Hz, respectively. The position of element 15 is chosen for installation of the MR damper. The simulations were performed using

the Newmark's method with time increment of 0.0015 s. The absolute Z-displacement response of node 19 has been obtained for three different cases namely response by the proposed vibration suppression strategy, response for 0.0 A and response for 1.5 A constant current. The responses for harmonic excitation are compared in Figure 5.12. The relative displacement of the MR damper is plotted for three cases in Figure 5.13. The variation of MR damper stiffness k_0 and damping c_0 with and without strategy of suppression is demonstrated in Figures 5.14 and 5.15 respectively. As it can be realized using the proposed strategy, the vibration has drastically reduced.

The hysteresis loops with and without proposed strategy of suppression for the case of harmonic excitation are shown in Figure 5.16. It can be appreciated how the strategy modifies the hysteresis loop by giving maximum current excitation when velocity at the end of the MR damper has the same sign of the hysteresis force and assuming minimum current otherwise.

The transient response of the structure using the proposed strategy under step input is also investigated. The structure is excited with the step input of 0.0254 m. The absolute Z-response of node 19 for the three cases is shown in Figure 5.17. The relative displacement of the MR damper is also shown in Figure 5.18. The variation of the MR damper stiffness k_0 and damping c_0 are also shown in Figures 5.19 and 5.20, respectively and the hysteresis loops for transient response for all three cases are shown in Figure 5.21

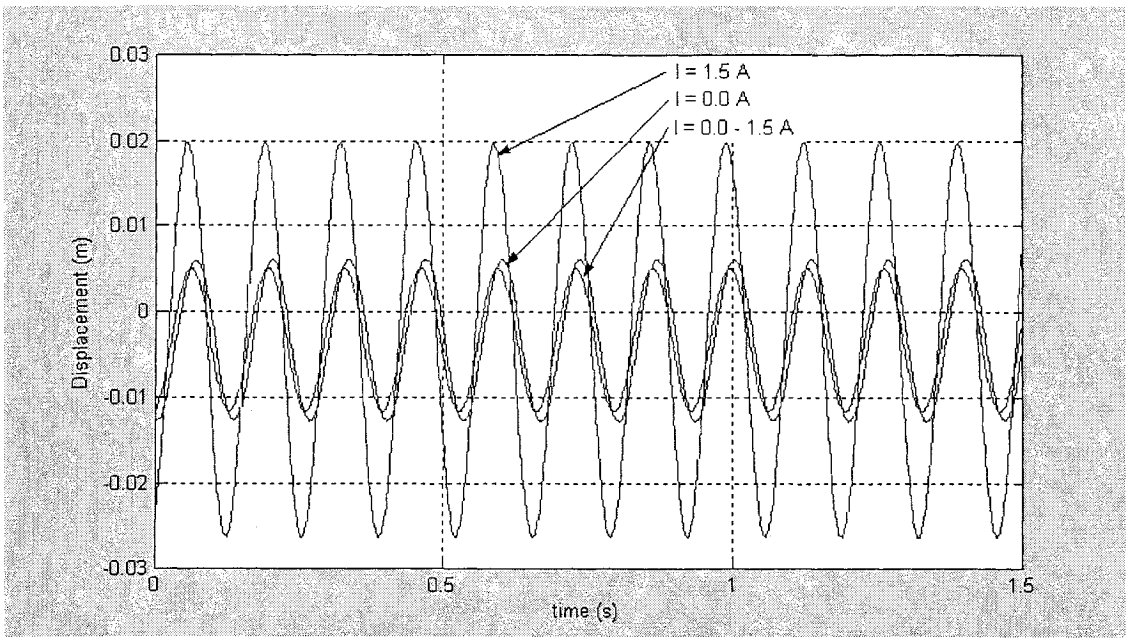

Figure 5.12. Absolute Z-displacement of node 19 under harmonic excitation with and without proposed strategy of suppression.

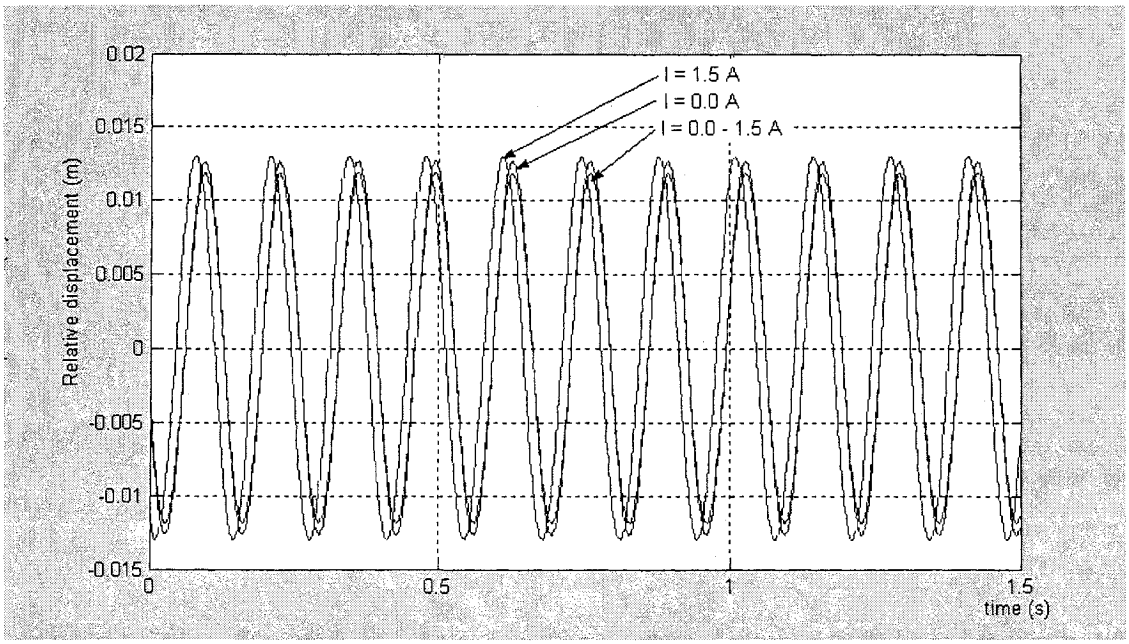

Figure 5.13. Relative displacement of the MR damper with and without proposed strategy of suppression.

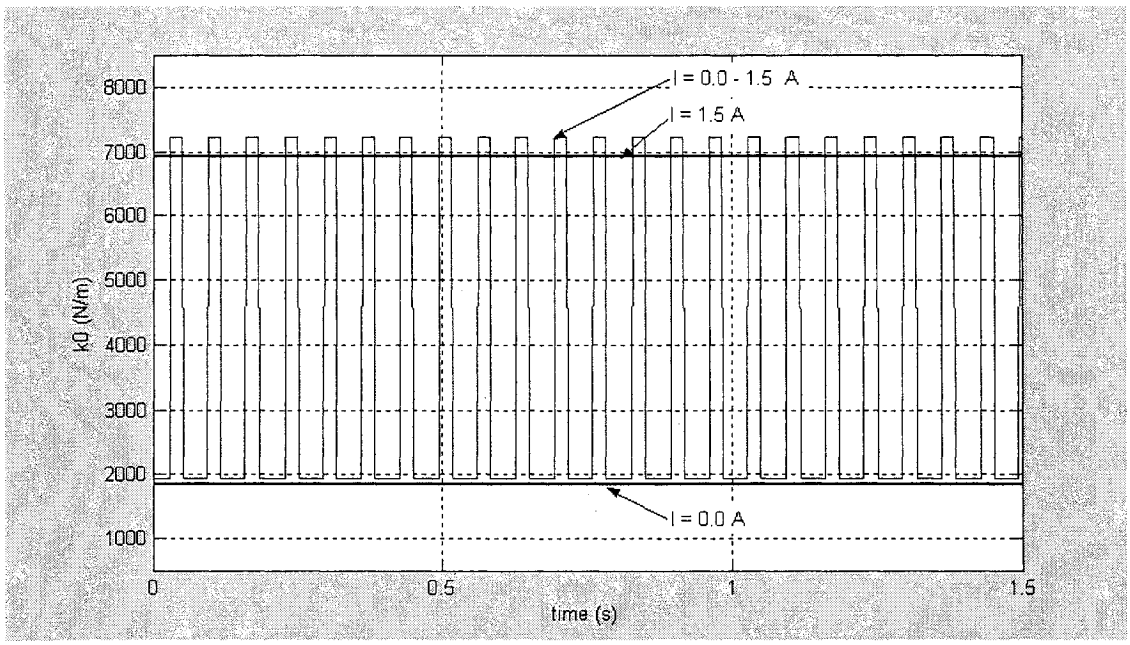

Figure 5.14. MR damper stiffness under harmonic excitation with and without proposed strategy of suppression.

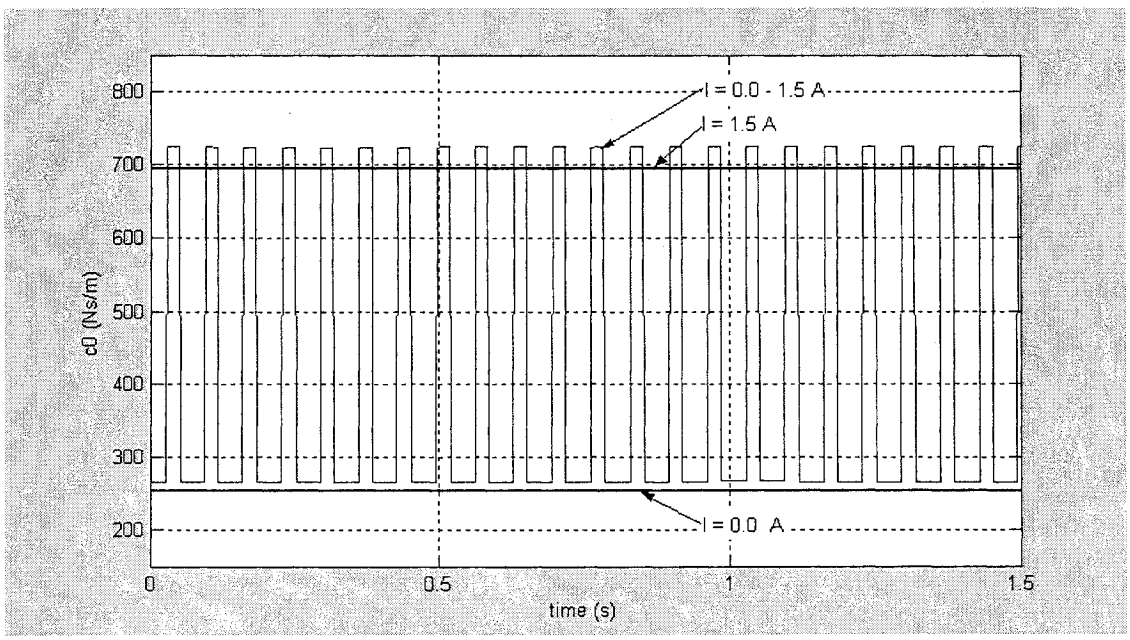

Figure 5.15. MR damper damping under harmonic excitation with and without proposed strategy of suppression.

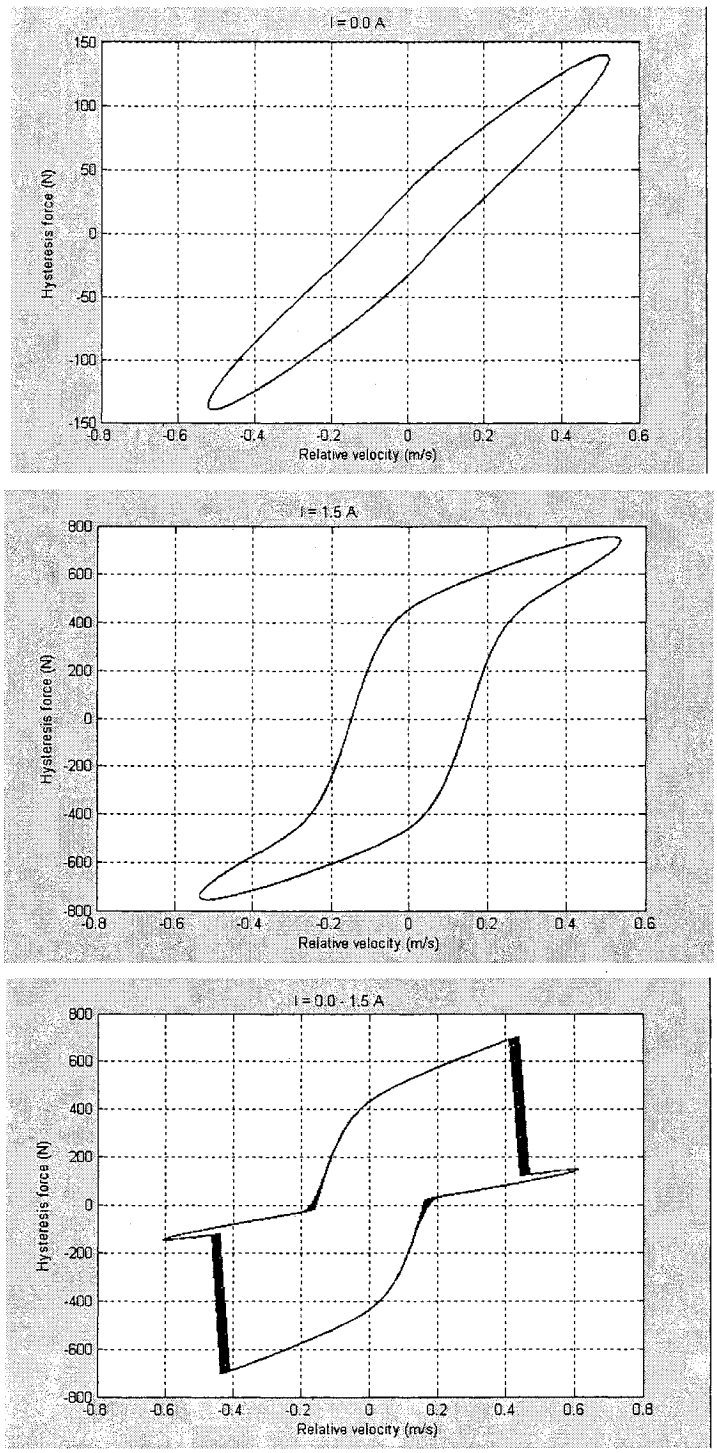

Figure 5.16. Hysteresis force of the MR damper with harmonic excitation with and without proposed strategy of suppression.

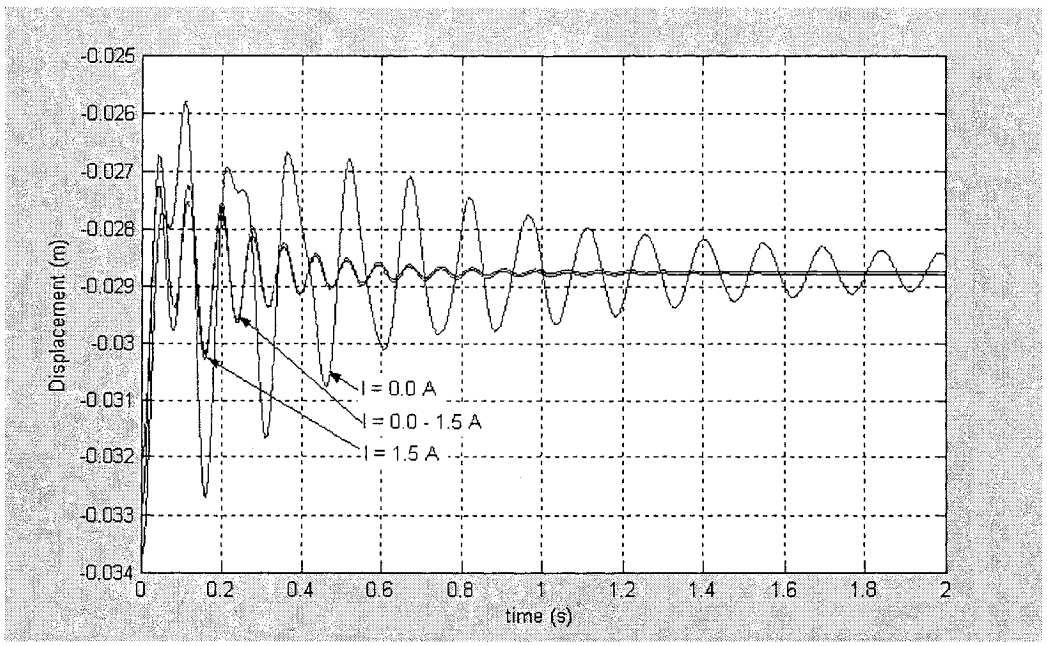

Figure 5.17. Absolute Z-displacement of node 19 under step excitation with and without proposed strategy of suppression.

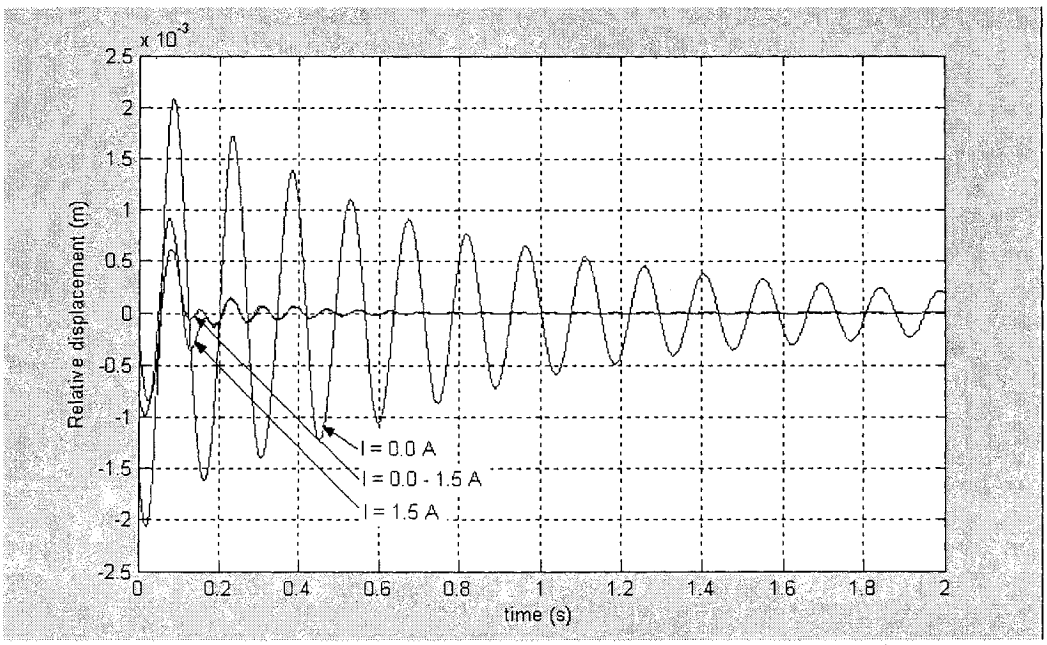

Figure 5.18. Relative displacement of MR damper under step excitation with and without proposed strategy .

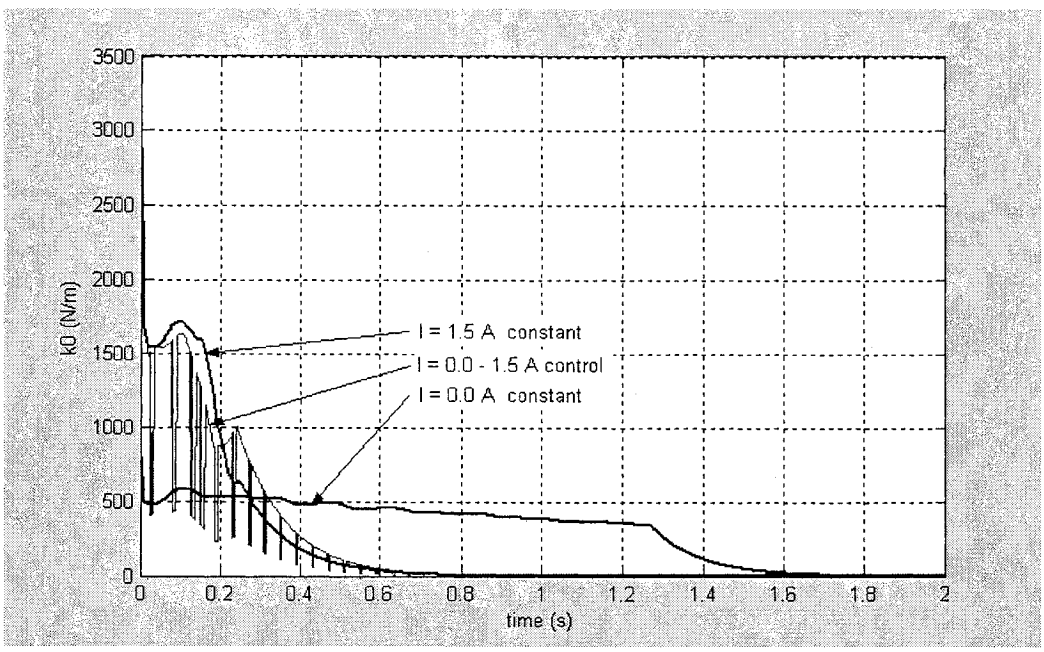

Figure 5.19. MR damper stiffness under step excitation for with and without strategy of proposed suppression.

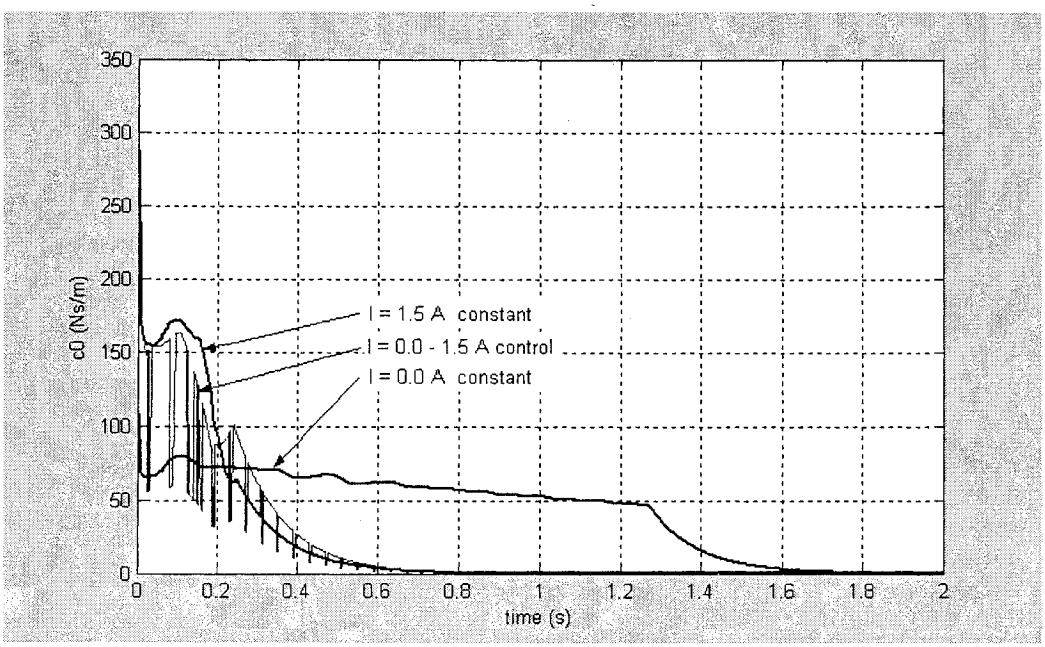

Figure 5.20. Damping coefficient under step excitation with and without strategy of proposed suppression.

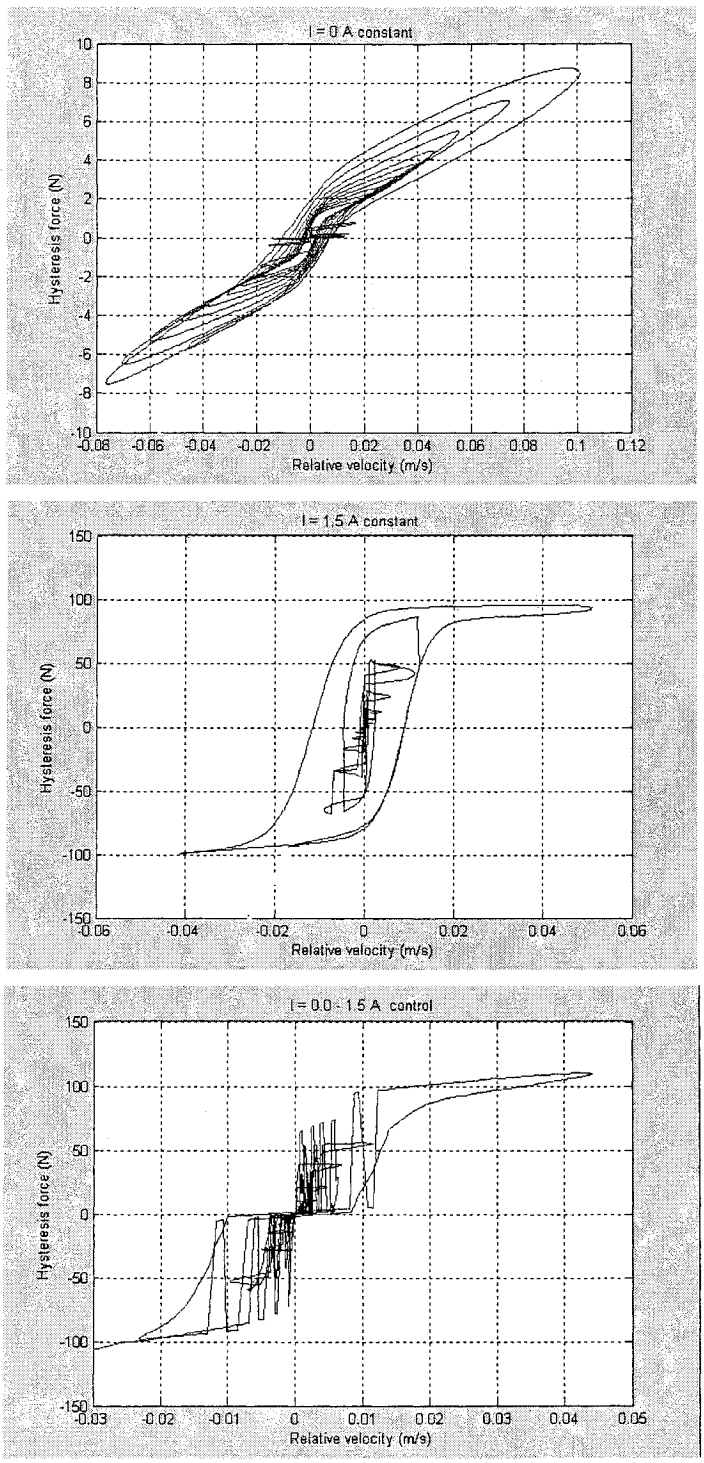

Figure 5.21. Hysteresis force of the MR damper under step excitation with and without proposed strategy of suppression.

The performance index for with and without proposed strategy of suppression cases under harmonic and transient excitations are presented in Table 5.5. The global and local vibration (node 19) was obtained during a period of 3 s for the harmonic excitation and 2 s for the transient response.

Table 5.5. Total vibration of the whole structure and node 19.

	I = 0.0 A		**I = 1.50 A**		**I = 0.0 – 1.50A**	
	Global	Node 19	Global	Node 19	Global	Node 19
Harmonic	0.0156	0.0013	0.0201	0.0020	0.0125	0.0011
Transient	0.0052	0.0028	0.0051	0.00055	0.0051	0.00047

The results show that the proposed strategy of suppression can improve the performance of the structure. 20% reduction of global vibration is observed between the case of 0.0 A and the case with strategy of suppression under harmonic excitation. This reduction is 15% for local vibration at node 19. For the vibration transient response, a significant vibration reduction has been achieved for the case with the proposed strategy. 15% vibration reduction has been obtained using the proposed strategy in comparison to case of 1.5 A and this vibration reduction is increased to 80% if it is compared with case of 0.0 A.

5.4. Optimum position of MR dampers to reduce the vibrations

In this part, the optimum position of the MR damper is investigated. As it was stated in the Section 5.2, the optimum location of the controllable fluid damper affects considerably the index performance of the vibration reduction. The assumed index performance measures the local vibrations and is defined by the Eq. (5.4). The feasible

design space solution considers only 51 possible locations for the MR damper since the five positions for the elements are attached to plate of shaker are discarded. From the previous simulations it was noted that the best results occurs for the maximum current in transient cases, thus, maximum current of 1.5 A is considered for all the cases. Since the feasible design space solution is small it was decided to evaluate all the possible positions instead of using an optimization algorithm. Table 5.6 presents only the best ten positions of the MR damper.

Table 5.6. Local vibration of the node 19 for differen locations of the MR damper for transient response

	Position	**Local vibration (m^2s)**		**Position**	**Local vibration (m^2s)**
1	14	0.4562e-3	**5**	22	0.7348 e-3
2	15	0.5303 e-3	**7**	21	0.7351 e-3
3	24	0.5477 e-3	**8**	19	0.7359 e-3
4	16	0.6754 e-3	**9**	9	0.7365 e-3
5	25	0.7324 e-3	**10**	13	0.7379 e-3

Examination of Table 5.6 shows that the position 14 is the optimum position as performance index vibration is the lowest for this case.

5.5. Application of MR dampers as translational actuator using semiactive strategy

As it has been shown, the hysteresis force of the MR damper is modified by modifying the excitation current of the MR damper. In this section possible application of MR dampers as a translational actuators or lengthening effect is explored. It is intended to show that the MR damper can use the vibration energy to modify its length for

actuation purposes. The MR damper, with an appropriate current excitation strategy, can not only act as dissipative energy element but also as active element which can modify its length. In order to better understand the structural problem, a simplified model is presented in Figure 4.2. In this scheme, it is assumed that the MR damper is in equilibrium position; therefore, the initial force considered in the MR damper model is zero.

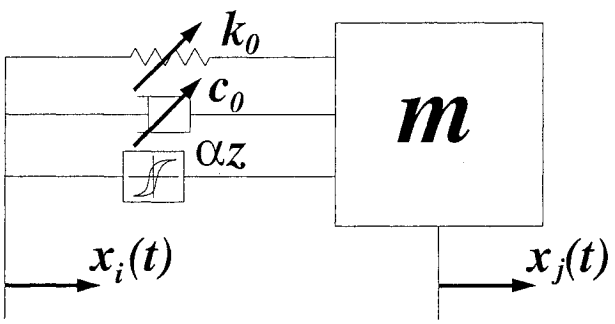

Figure 5.22. Schematic representation of the MR damper with input excitation x_i.

The strategy proposed to achieve the desired effect is based on the relative velocity between both ends of the MR damper. For the lengthening effect, the strategy assigns maximum current excitation when the relative velocity is negative and zero current when the relative velocity is positive. This strategy can be stated as:

$$\begin{cases} I_{\max} & \text{when} \quad (\dot{x}_j - \dot{x}_i) < 0 \\ I_{\min} & \text{when} \quad (\dot{x}_j - \dot{x}_i) \geq 0 \end{cases} \tag{5.6}$$

when the MR damper is allowed to lengthen and can be state as:

$$\begin{cases} I_{\min} & \text{when} \quad (\dot{x}_j - \dot{x}_i) < 0 \\ I_{\max} & \text{when} \quad (\dot{x}_j - \dot{x}_i) \geq 0 \end{cases} \tag{5.7}$$

when the MR damper is allowed to shorten.

The simulation has been performed for different excitation conditions to observe their effect on the final results. For all the cases, the proposed mathematical model of the MR damper discussed in the Section 3.6. has been used and the solution in time domain was obtained using the modified Newmark method for nonlinear systems presented in the Section 4.4.3. The time increment of 0.002 s was selected and the mass m is 200 kg. The minimum and maximum excitation current is zero and 1.5 A respectively.

Figure 5.23 shows the lengthening effect of the MR damper under harmonic excitations with frequency of 2.5 Hz and amplitude of 0.00635, 0.0127, 0.01905 and 0.0254 m. It is noted that the relative displacement grows until it reaches the steady state point about which the MR damper oscillates. The equilibrium length and output amplitude of the MR damper for harmonic excitation with different amplitudes are provided in Table 5.7.

Figure 5.24 shows the hysteresis force for an excitation with amplitude of 0.00635 m and frequency of 2.5 Hz. It is noted that the hysteresis curve is shifted up when the proposed strategy is applied to the MR damper. Similar effect is observed for larger amplitudes excitations. The maximum and minimum values of the hysteresis force in steady state for the four amplitude excitations are provided in Table 5.7.

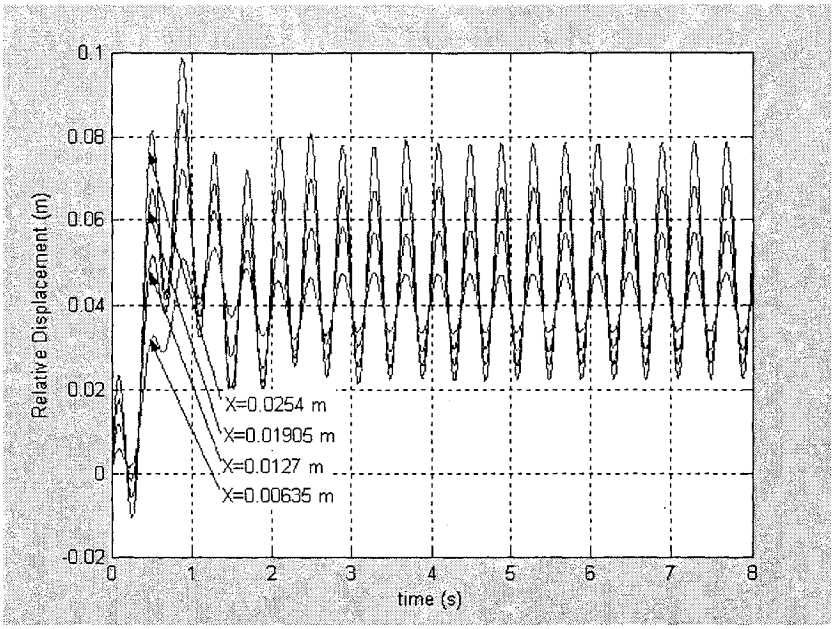

Figure 5.23. Relative displacement of the MR damper under amplitude excitations of 0.00635, 0.0127, 0.01905 and 0.0254 m and frequency of 2.5 Hz.

The variation of the MR damper damping due to the proposed strategy is presented in Figure 5.25 for amplitude excitation of 0.00635 m and frequency of 2.5 Hz. The results shows that the magnitude of the damping coefficient switches from 207 to 76.5 Ns/m periodically and the same phenomenon happens to the MR damper stiffness as shown in Figure 5.26. The maximum and minimum values for the MR damper stiffness and damping for different amplitude excitation is presented in Table 5.7.

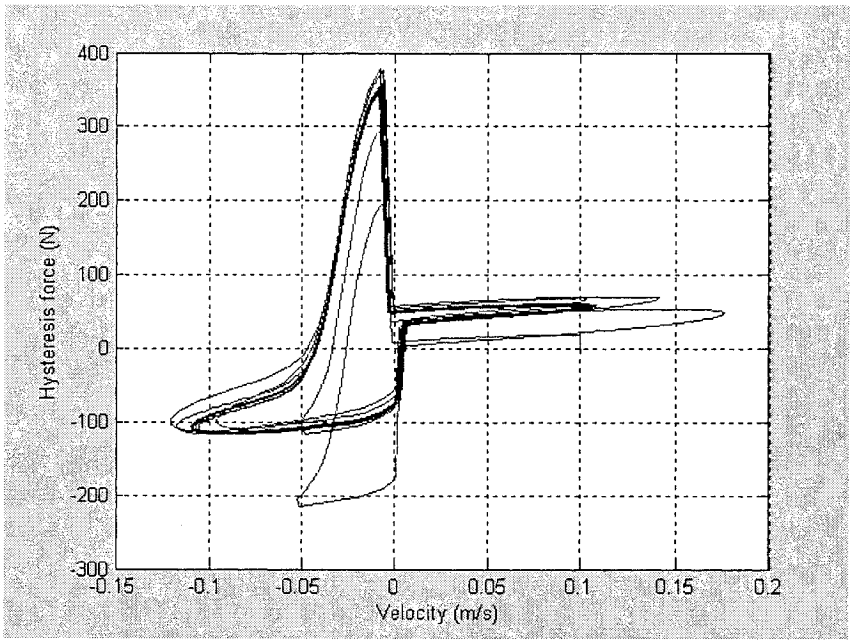

Figure 5.24. Hysteresis curve of the MR damper under amplitude excitation of 0.0127 m and frequency of 2.5 Hz.

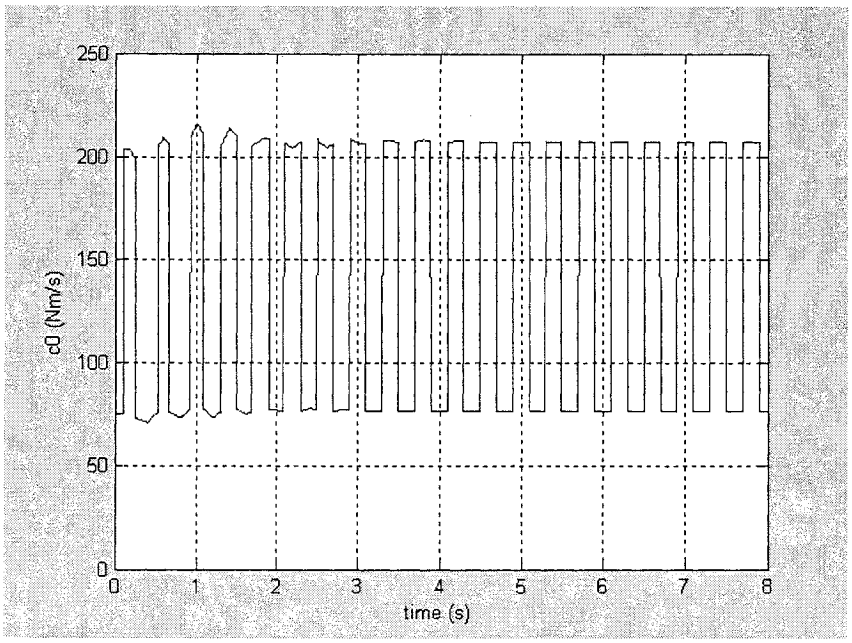

Figure 5.25. Damping in time domain of the MR damper under amplitude excitations of 0.00635 m.

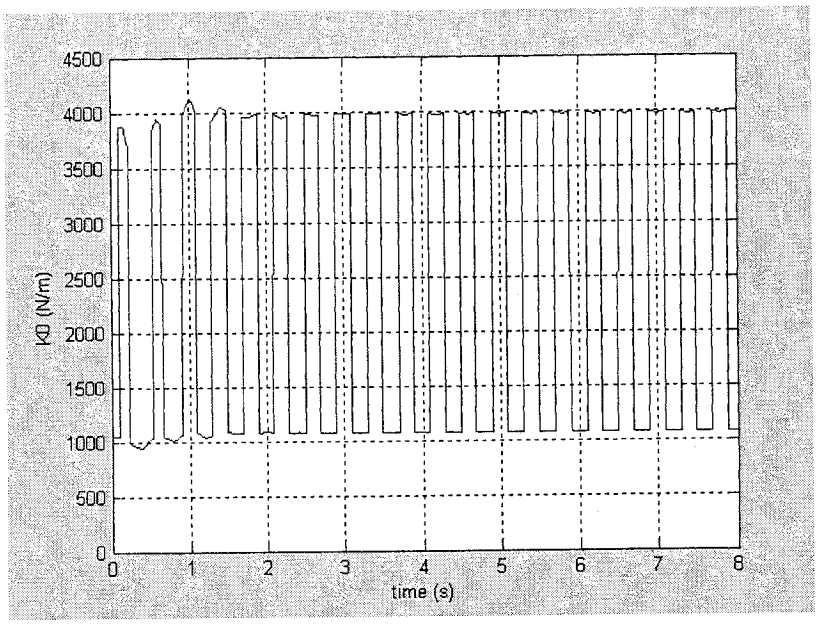

Figure 5.26. Stiffness in time domain of the MR damper under amplitude excitation of 0.00635 m.

Now the lengthening effect of the MR damper under different frequency excitations is explored. The frequency excitations of 1.0, 2.5, 5.0 and 7.5 Hz are considered. The amplitude excitation for all the cases is fixed at 0.00127 m. Figure 5.27 shows the output response for the harmonic excitation with frequencies of 1.0 and 5.0 Hz and amplitude of 0.0254. Table 5.8 provide the damping, stiffness, hysteresis force, equilibrium length and output amplitude of MR damper for harmonic excitation with amplitude of 0.0127 m and different frequencies. It is observed that for higher frequencies the equilibrium length becomes larger. This is due to the fact that the hysteresis force depends on the frequency excitation as it was shown in the Section 3.6.

Table 5.7. Values for the translational effect of the MR damper under different amplitude excitation and frequency of 2.5 Hz

		Amplitude excitation (m)			
		0.00635	**0.0127**	**0.01905**	**0.0254**
c_0 (Ns/m)	max	398	502	576	635
	min	147	186	213	234
k_0 (N/m)	max	3976	5023	5760	6350
	min	1073	1355	1555	1715
F_z (N)	max	353	360	380	405
	min	-115	-285	-422	-553
Equilibrium length (m)		0.0403	0.0433	0.0470	0.0505
Amplitude output (m)		0.0019	0.0032	0.0046	0.0059

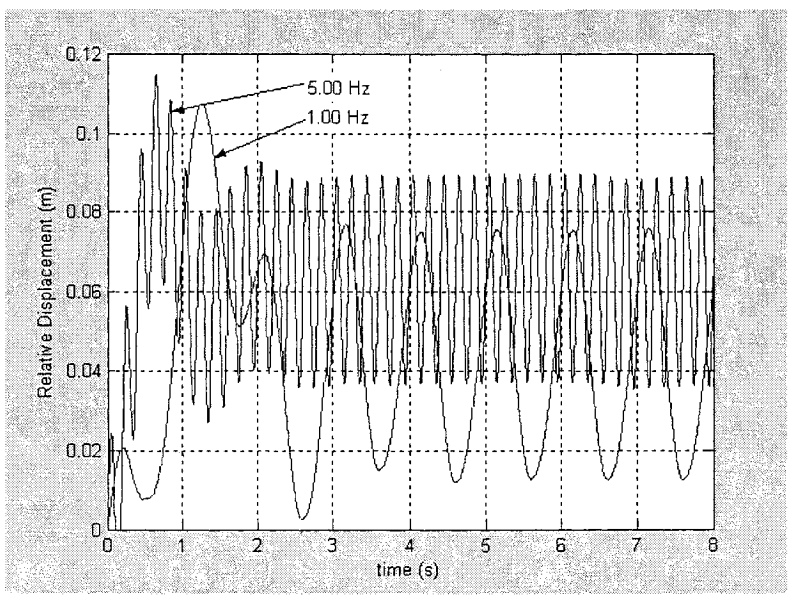

Figure 5.27. Relative displacement of the MR damper under frequency excitations of 1.0 and 5.0 Hz and amplitude of 0.0254 m.

Table 5.8. Values for the translational effect of the MR damper under different frequency excitations and amplitude of 0.0127 m.

		Frequency excitation (Hz)			
		1.0	**2.5**	**5.0**	**7.5**
c_0 (Ns/m)	max	478	635	795	912
	min	180	234	293	336
k_0 (N/m)	max	4800	6350	7945	9113
	min	1300	1715	2140	2456
F_z (N)	max	295	405	505	600
	min	-320	-553	-970	-1440
Equilibrium length (m)		0.0442	0.0505	0.0587	0.0758
Amplitude output (m)		0.0207	0.0059	0.0025	0.0016

When the MR damper is installed in the structural system, the effect of the structural stiffness and damping should be considered. Figure 5.28 shows a simplified model with structural stiffness k and damping c added to the MR damper model shown in Figure 5.22. In this part, some simulations are performed to evaluate the effect of the structural stiffness on the lengthening effect of the MR damper. To accomplish this, four different values of stiffness 0, 1000, 10000 and 100000 N/m were considered. The structural damping c is neglected since it is small compared with the damping of the MR damper

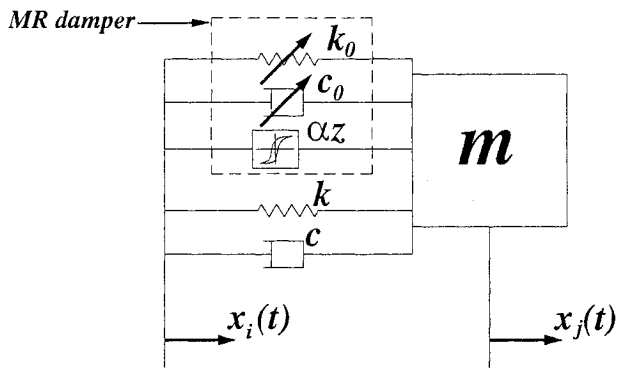

Figure 5.28. Schematic representation of a MR damper with an additional structural stiffness and damping.

Figure 5.29 shows the lengthening effect for zero and 1000 N/m structural stiffness under harmonic excitation with frequency of 2.5 Hz and amplitude of 0.0254m. The complete results are tabulated in Table 5.9. It is observed that the lengthening effect is seriously affected by the structural stiffness. In fact equilibrium length decreases from 0.0505 to 0.0026 m for zero and 100000 N/m structural stiffness, respectively.

Further the proposed strategy is applied to modify the length of the MR damper located at position 17 of the structure presented in the Section 4.5. The structure is harmonically base-excited at different frequencies and amplitude of 0.0508 m.

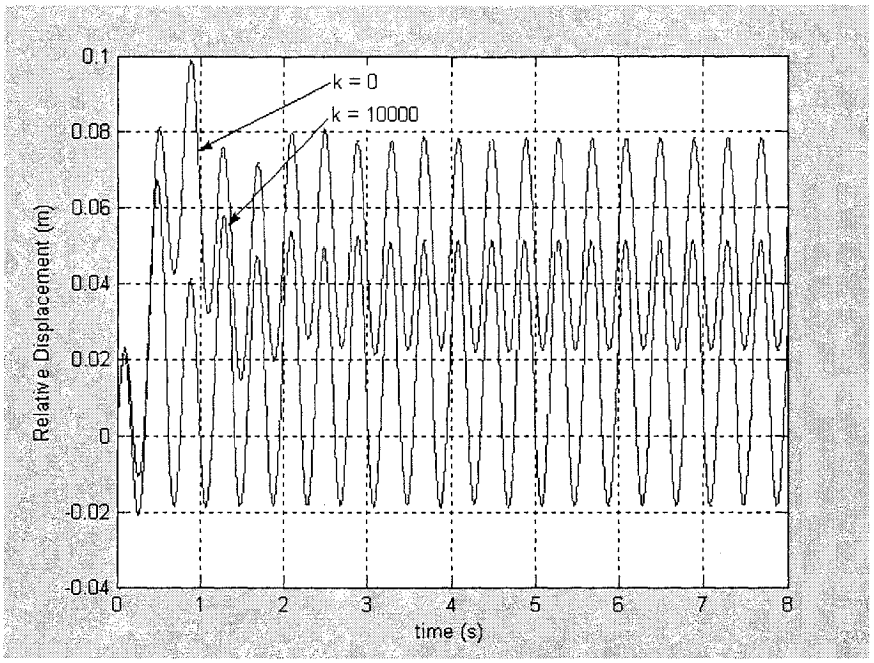

Figure 5.29. Translational effect of the MR damper for different structural stiffness k.

Table 5.9. Values for the translational effect of the MR damper for different structural stiffness uncer excitation frequency of 2.5 Hz and amplitude of 0.0254 m

		Structural stiffness (N/m)			
		0	**1000**	**10000**	**100000**
c_0 (Ns/m)	max	635	639	684	588
	min	234	236	253	217
k_0 (N/m)	max	6350	6385	6835	5880
	min	1715	1725	1845	1590
F_z (N)	max	405	390	374	310
	min	-553	-580	-729	-525
Equilibrium length (m)		0.0505	0.0405	0.0165	0.0026
Amplitude output (m)		0.0059	0.0067	0.0139	0.0469

Figure 5.30 shows the input excitation and the response calculated in the Z-direction of the node 19 for an excitation of 5 Hz. The relative displacement experienced by the MR damper is presented in Figure 5.31. The Effect of the proposed strategy over the hysteresis loop can be appreciated and compared with the not control hysteresis loop in Figure 5.32. The variation of the damping and stiffness of the MR damper in time domain due to the proposed strategy can be seen in Figures 5.33 and 5.34 respectively. Table 5.10 summarizes all the results of the simulations for the three different cases of excitation with frequency of 5 Hz with and without the proposed strategy and excitation with frequency of 7.5 Hz with the proposed strategy. Examination of the results reveals that that the lengthening effect is very small in the real structure

As it can be observed the equilibrium length of MR damper increases from 0.0 to 0.0005 m for 5 Hz frequency excitation with constant current of 1.5 A and the proposed strategy, respectively, which is negligible with respect to equilibrium length of the MR damper when the structural stiffness is not considered. Also as the frequency increases from 5 Hz to 7.5 no significant increment in steady state point of the MR damper is observed.

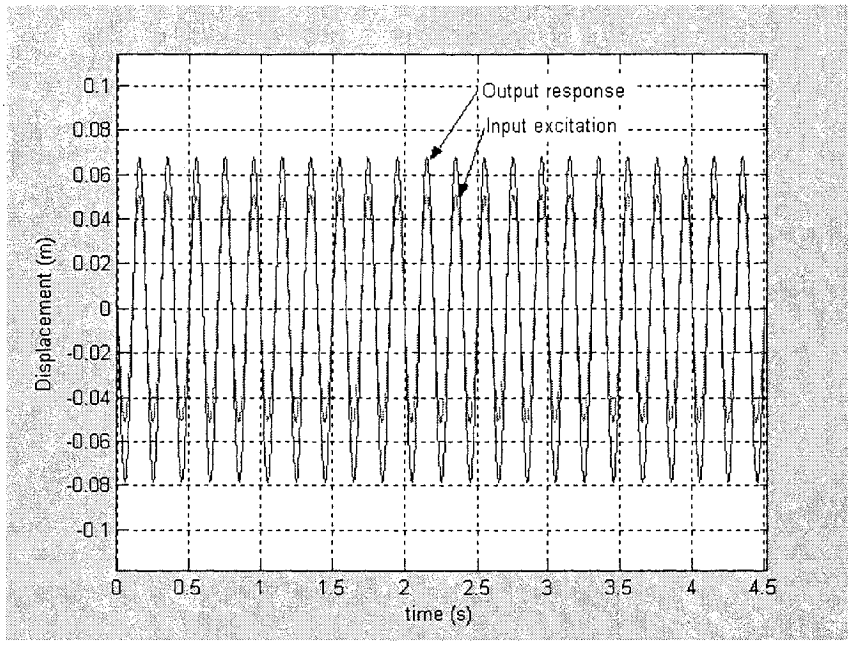

Figure 5.30. Z-displacement response of node 19 for an excitation of 5Hz with the proposed strategy.

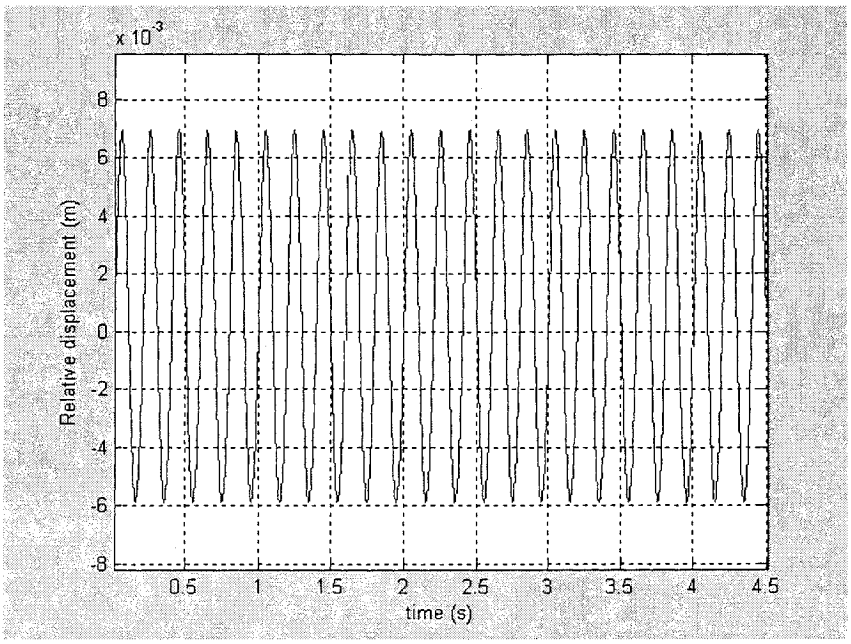

Figure 5.31. Relative displacement of the MR damper for input excitation with frequency of 5 Hz with the proposed strategy.

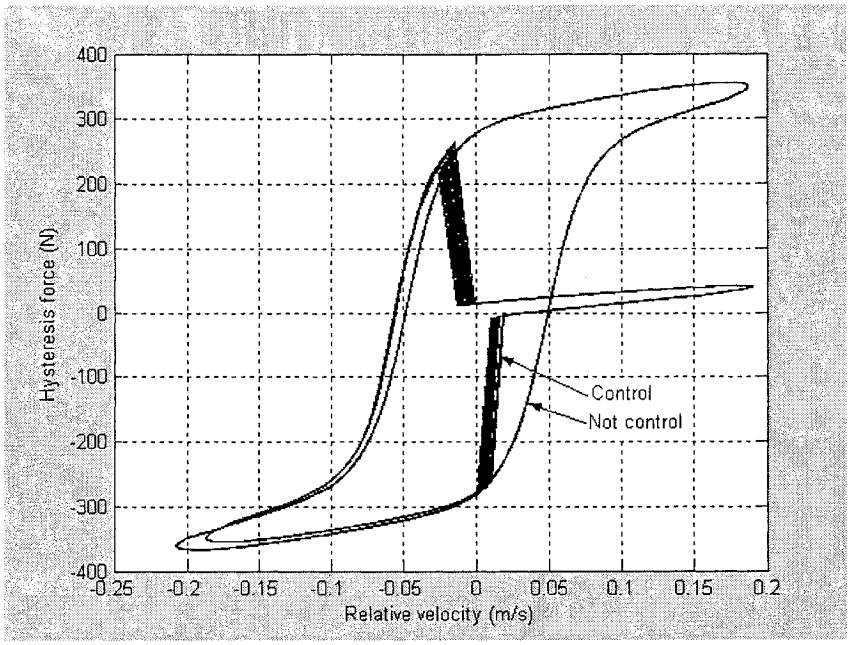

Figure 5.32. Hysteresis force with and without the strategy with current excitation of 1.5 Amps.

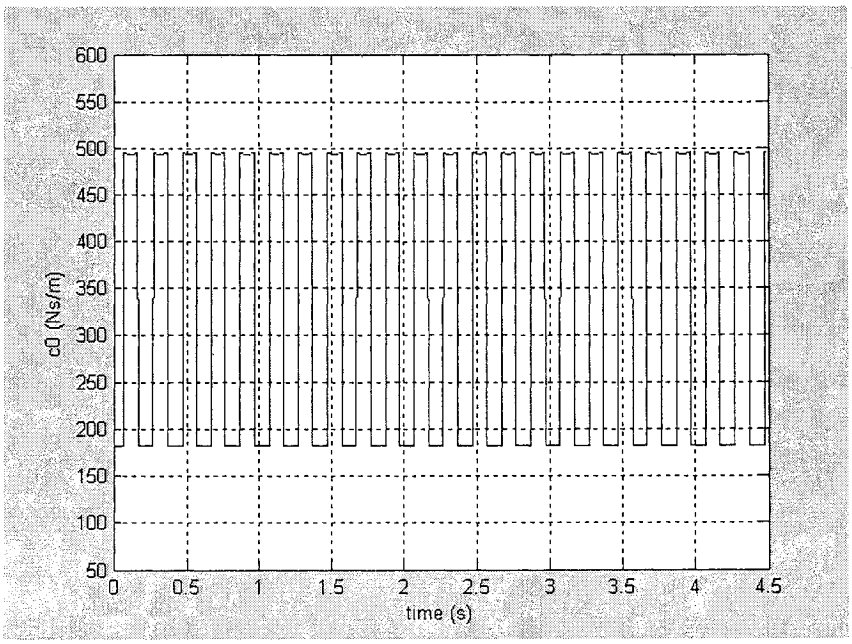

Figure 5.33. Damping of the MR damper for the proposed strategy case and excitation of 5.0 Hz..

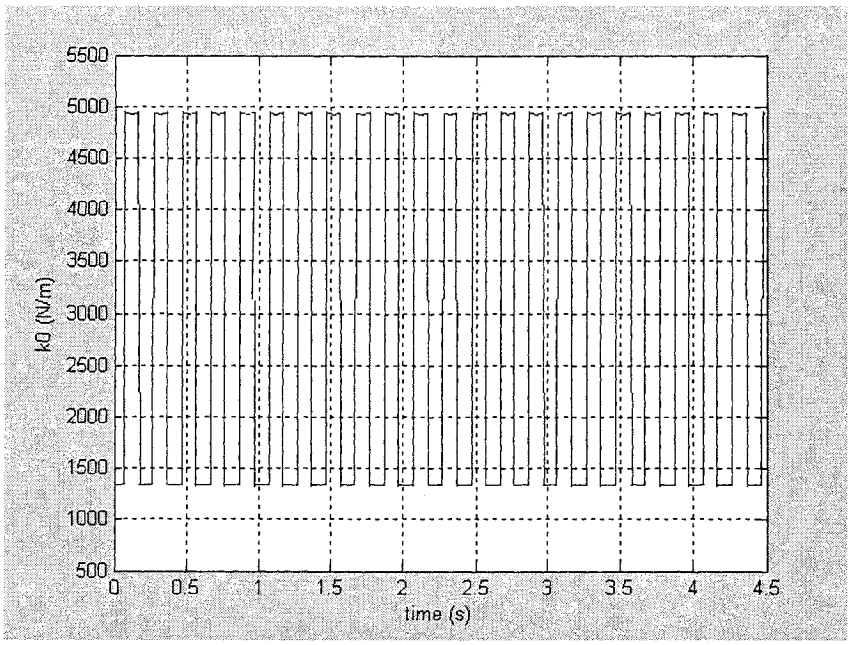

Figure 5.34. Stiffness of the MR damper for proposed strategy case and excitation of 5.0 Hz.

The lengthening effect caused by a proper strategy was proved in this section. It was shown that the magnitude of the equilibrium length depends on the frequency and magnitude of the excitation. Unfortunately, a significant practical limitation is the structural stiffness. It was shown that the lengthening effect is pronounced well for systems with small structural stiffness; however, when the MR damper is implemented in a real structure, the lengthening effect is small due to the stiffness of the structure. Furthermore, it is noted that structure requires large excitation in order to achieve the lengthening effect.

Table 5.10. Values for the translational effect of the MR damper for different structural stiffness and amplitude of 0.0508 m

		Excitation		
		5 Hz (constant)	**5 Hz (without proposed stratefy)**	**7.5 Hz (without proposed stratefy)**
c_0 (Ns/m)	max	484	494	933
	min	484	183	344
k_0 (N/m)	max	4844	4935	9330
	min	4844	1336	2513
F_z (N)	max	355	250	660
	min	-355	-367	-1745
Equilibrium length of the MR damper(m)		0	0.00053	0.0011
Z- equilibrium output (m)		-0.0041	-0.0055	-0.0059
Z-amplitude output (m)		0.0721	0.0735	0.151

CHAPTER 6
CONCLUSIONS AND FUTURE WORK

6.1. Conclusions

The present thesis constitutes an in-depth fundamental and experimental investigation in structural design optimization and vibrations suppression of adaptive structures. New mathematical modelling and optimization algorithms have been developed and integrated into a structural analysis and optimization tool to study the static and dynamic response of the system. From the design optimization prospective, an efficient and practical methodology to find the simultaneous size, geometry and topology optimization has been developed. For vibration suppression point of view, application of magnetorheologic (MR) damper to suppress vibration in space discrete structures and also a new concept of MR damper have been introduced. Meanwhile a new strategy has been developed for an efficient vibration suppression. The proposed mathematical models are finally validated with experimental study.

The nature of studied structural optimization problems is highly nonlinear and non-convex and many local optimum points exist. Gradient based techniques such as modern Sequential Programming Techniques have some deficiencies to handle these types of problems. Furthermore, the existence of discrete variables makes then inappropriate techniques for specific problems. The main disadvantage of the gradient based techniques is that they may get trapped in local optimum, without having a

mechanism to climb out of the local optimum. Considering this, these methods may fail to discover a more global optimum solution. To alleviate this problem and also due to discrete nature of the optimization problem, Genetic Algorithms (GAs) combined with finite element method has been used to analyse and optimize the structural systems. Reproduction operation is one of the most critical steps in the optimization process of GAs. The roulette-wheel selection is usually applied to give higher chance to individuals with higher fitness values. However, the drawbacks of this technique is that a very good element may lead to have clones early far from the optimum point or a uniform population may make the convergence slow. One contribution of this work was to propose a new approach which can solve the previous drawbacks. In the proposed approach a probability of reproduction, which can control the rate of convergence, has been developed. The proposed modified GAs has been employed in the solution of practical structural design optimization problems.

GAs was applied to find the optimum solution for constraint structural problems with discrete and continuous variables. First, the optimum position and actuator action for adaptive structures under varying load has been studied. The advantage of GAs with respect to the published works based on the gradient based methods is that the maximum actuator action can be specified and the position of the actuator can be included as design variable. Second, a new methodology is proposed to find the optimum design of real life structures. This methodology considers that the whole structure is built with the repetition of single bays. This will cause the number of design variables to be reduced drastically; thus, reducing the computational time and the search space solution significantly. Furthermore, the final design respects the AISI standards and uses few commercial

profiles which makes it more cost effective. The final optimum solution was found using proposed improved GAs with multicriteria objective function. Appropriated penalty function has been introduced to convert the constrained problem into the unconstrained problem. The final results were validated with those available in the literature.

In this study, application of semiactive control using MR dampers to suppress the vibration of space discrete structure has been studied. A methodology to find the characteristic parameters of the Bouc-Wen model in an attempt to better characterize the hysteresis phenomenon of MR dampers has been proposed. It was shown that the relations to determine directly the characteristic parameters of the Bouc-Wen model can be derived from the key information of the experimental data. The proposed methodology avoids applying any optimization method to match the model with experimental curves and thus eliminate the possible errors from the optimization procedure. The proposed methodology has been validated against experimental results and excellent agreement has been found.

From the derived characteristic parameters and their variation with current excitation, it was shown that these parameters vary linearly or exponentially with respect to current excitation. Furthermore, it was observed that the hysteresis force for the MR damper is also sensible to the amplitude and the frequency of the excitation and it was found that parabolic curves could describe that phenomenon. All these relations were incorporated in a new nonlinear model for the MR damper which includes the current, amplitude and frequency excitation as input variables. An error analysis was performed to validate the proposed model against the experimental data and very good agreement was found making the proposed model reliable for the semiactive control application.

Subsequently, the MR damper was incorporated to the structure in order to suppress the vibrations. To accomplish this, a finite element model for the passive bar element was proposed. The element consists of a truss element with three members to simulate the node bolt connection of the test structure. Next, the finite element model of the MR damper has been developed and its correspondent local and global matrix formulations have been derived. To solve the finite element formulation with embedded MR damper, the unconditional stable time integration Newmark method was modified by adding an inner iterative process to overcome the nonlinearity and to assure the equilibrium forces in each time step. To find the proportional damping ratio and to validate the proposed finite element model for the passive and MR damper bars, a space discrete structure with four bays was fabricated and tested on a hydraulic shaker. The good agreement between the experimental and simulation results validates the proposed finite element for the bar and MR damper bar.

The developed finite element model was then employed to study the performance of the vibration suppression strategy in structural systems. First, the passive vibration reduction through optimum shape was investigated. It was shown that it is possible to redesign the load bearing structure so that it has intrinsic passive vibration suppression characteristics. In order to ensure robust final designs, the global vibration over a range of frequencies was considered. GAs were applied to find the final optimum design to reduce the global vibration. It was concluded that the structures with repetitive bays are structure with high vibration transmission characteristics. Also, it was shown that the structures with small perturbations in their nodal configurations can significantly reduce the transmissibility. However, it may not always represent a practical solution.

The passive application of MR damper to reduce the vibration in structures was also studied. The response of the structure with different constant current excitations and MR damper positions was simulated. It was concluded that the effectiveness of the MR damper is highly influenced by not only the current excitation but also it its location. Also it was observed that the local vibration in comparison to the global vibration is a better performance index to characterize the effectiveness of the MR damper. The optimum location of the MR damper in order to maximize its effectiveness in the vibration reduction was also studied.

Finally, two semiactive vibration suppression strategies were proposed. First, a strategy was developed to improve the performance of the MR damper to reduce the vibration. This strategy considers the signs of the absolute velocity of one end of the MR damper in local coordinates and the hysteresis force. If the hysteresis force is in phase with the velocity, maximum current is applied otherwise minimum current is assumed. This semiactive vibration suppression strategy was applied and compared with the cases were the MR damper is working in passive way. It was observed that the proposed strategy reduces the local and global vibration. Second, a proposed semiactive vibration suppression strategy has been used to generate an translational effect on the MR damper. The concept involves the removal of the vibration energy from the structure to produce a translational action. For this objective, the vibration suppression strategy assumes maximum current when the relative velocity of the MR damper is positive and zero current excitation when the relative velocity is negative and viceverse to achieve the opposite effect. The influence of the frequency and amplitude excitation as well as the structural stiffness over the lengthening effect was also studied. It was proved that the

proposed strategy can produce the actuation effect. However, it was shown that the structural stiffness has significant influence on the actuation effect of the MR damper makes its application limited.

6.2. Recommendations for future work

The research work presented in this dissertation is intended to contribute in the developing of design optimization methodologies and suppress vibration strategies in structural systems. It is expected that this study accelerate the implementation of design optimization in practical designs. Also, it is expected that the present dissertation motivates the study and the practical implementation of MR dampers to reduce the vibration in large scale structures and mitigate damages and dangerous situations. Some recommendations are stated for further research in the topics of optimum design and implementation of MR damper:

In this study a new methodology to optimize the structures from the repetition of individual bays was proposed. Although the final designs are practical, the possible commercial application has yet some limitations. For instance, tapered structures or sometimes the inevitable shape changes due to physical restrictions may be required. It is recommended to complement the proposed methodology with all practical cases and develop a robust design optimization algorithm to handle large scale problems.

It is known that the time response of MR dampers is large compared with other active actuators such as piezoelectric actuators. This is a challenging area for material researchers and designers. From material point of view, it is recommended to improve the rheological properties of rheologic fluids as well as thickening phenomenon of the MR

fluids which is a strong limitation of an extended application in areas such as automobile suspensions. From design perspective, it is recommended to develop new designs to reduce the response time of the controllable devices since the effectiveness of semiactive control highly depends on the time response of the MR damper

The proposed model has proved to describe accurately the hysteresis behaviour of the MR damper and was applied to predict successfully the structural response when it is embed in a structure. It would be interesting to incorporate the semiactive control application of the proposed model in car suspensions models in order to improve their ride performance.

The proposed semiactive strategy has proved to reduce the vibration; however, the robustness of such control requires further study. Furthermore, the existing nonlinear feedback control should be implemented with the proposed MR damper model and their effectiveness be evaluated on the semiactive vibration control of structural systems in order to fully utilize the capabilities of these unique devices.

REFERENCES

AISC, (1989). Manual of Steel Construction: Allowable stress design, American Institute of Steel Construction, 9th ed. Chicago.

Akbay, Z. and Aktan, H. M. (1995). "Abating earthquake effects on buildings by active slip brace devices." *Shock Vibration*, 2:133-142.

Akbay, Z. and Aktan, H. M. (1991). "Actively regulated friction slip devices." *Proceedings 6th Can. Conference on Earthquake Engineering*, 3:367-374.

Akbay, Z. and Aktan, H. M. (1990). "Intelligent energy dissipation devices." *Proceedings 4th U. S. National Conference on Earthquake Engineering*, 367-374.

An, J. and Kwon, D. (2003). "Modeling of a magnetorheological actuator including magnetic hysteresis." *Journal of Intelligent Material Systems and Structures*, 14:541-550.

Anthony, D. K. (2001). "Robustness of optimal design solutions to reduce vibration transmission in a lightweight 2-d structure, part III: using both geometric redesign and the application of active vibration control." *Journal of Sound and Vibration*, 245(3):417-431.

Anthony, D. K. and Elliot, S. J. (2000a). "Robustness of optimal design solutions to reduce vibration transmission in a lightweight 2-d structure, part II: application of active vibration control techniques." *Journal of Sound and Vibration*, 229(3):529-548.

Anthony, D. K., Elliot, S. J. and Keane, A. K. (2000b). "Robustness of optimal design solutions to reduce vibration transmission in a lightweight 2-d structure, part I:

geometric design." *Journal of Sound and Vibration*, 229(3):505-528.

Anthony, D. K., Elliot, S. J. and Keane, A. K. (2000). "Robustness of Optimal Design Solutions to Reduce vibration Transmission in a Lightweight 2-D structure." *Journal of Sound a Vibration*, 229(3):505-528.

Aprile, A., Inaudi, J. A. and Kelly, J. M. (1997). "Evolutionary model of viscoelastic dampers for structural applications." *Journal of Engineering Mechanics*, 123:551-560.

Arora, J. S. (1989). *Introduction to Optimum Design*, McGraw-Hill, New York.

ASCE (1997) *Guide to Structural Optimization*, ASCE Manuals and Reports on Engineering Practice No. 90.

Ashour, O., Rogers, C.A., and Kordonsky, W. (1996). "Magnetorheological fluids: materials, characterization, and devices." *Journal of Intelligent Material Systems and Structures*, 7:123-130.

Bathe, K. J. and Wilson, E. L. (1976). *Numerical Methods in Finite Element Analysis*, Prentice Hall.

Baumann, B. and Kost, B. (2005). "Structure assembling by stochastic topology optimization." *Computers and Structures*, in press.

Bouc, R. (1971). "Modèle mathématique d'hystérésis." *Acustica*, 24:16-25.

Buckle, I. G. and Mayes, R. L. (1990). "Seismic isolation history, application and performance - a would view." *Earthquake Spectra*, 6:161-201.

Canudas, C., Olsson, H., Åmstrom, K. J. and Lischinsky, P. (1995). "A new model for control of systems with friction.' IEEE Transactions on Automatic Control, 40(3): 419-425.

Carlson, J. D. (2001). "What makes a good mr fluid?" *Journal of Intelligent Material Systems and Structures*; 13: 431-435.

Carlson, J. D., Catanzarite, D. M., and St. Clair, K. A. (1996a). "Commercial magnetorheological fluid devices." *International Journal of Modern Physics B*,

10(23-24): 2857-2865.

Carlson, J. D. and Spencer Jr., B. F. (1996a). "Magnetorheological fluid dampers for semi-active seismic." *Control Proceedings of the 3rd International Conference of Motion and Vibration Control*, 3:35-40.

Carlson, J. D. and Sproston, J. L. (2000). "Controllable fluids in 2000-status of ER and MR fluid technology." *Actuator 2000, 7th International Conference on New Actuator.* Bremen, Germany, 126-130.

Chan, E. (1997). *Optimal Design of Buildings Structures using Genetic Algorithms,* Ph. D. Dissertation, California Institute of Technology, Pasadena, California.

Chang, C. C., and Roshke, P. (1998). "Neural network modeling of a magnetorheological damper." *J. Intelligent Material Systems and Structures*, 9:755-764.

Chang, C.C.,Asce, M. and Zhou L. (2002). "Neural network emulation of inverse dynamics for a magnetorheological damper." *Journal of Structural Engineering*, 128(2):231-239.

Chen, G., Bruno, R., and Salama, M., (1994). "Optimal placement of active/passive members in truss structures using simulated annealing." *AIAA Journal,* 32:1327–1334.

Choi, S. B., Lee, S. K. and Park, Y. P. (2001) "A hysteresis model for the field-dependent damping force of a magnetorheological damper." *Journal of Sound and Vibration*, 245(2):375-383.

Coello, C. A. (2000). "An Updated Survey of GA-Based Multiobjective Optimization." *ACM Computing Surveys*, 32(2):109-143.

Colajanni, P. and Papia, M. (1997). "Hysteretic characterization of friction-damped braces." *Journal of Structural Engineering*, ASCE, 123:1020-1028.

Deb, K. and Gulati, S. (2001). "Design of truss-structures for minimum weight using genetic algorithms." *Finite Elements in Analysis Design*, 37:447-465.

Dyke, S. J., Spencer Jr., B. F., Quast, P., Sain, M. K., and Carlson, J. D. (1996a).

"Modeling and control of magnetorheological dampers for seismic response reduction." *Smart Materials and Structures*, 5:565-575.

Dyke, S. J., Spencer Jr., B. F., Quast, P., Sain, M. K., and Carlson, J. D. (1996b). "Seismic response reduction using magnetorheological dampers." *Proceedings IFAC World Congress,* Int. Fed. Of Automatic Control, L:145-150.

Ehrgott, R. and Masri, S. F. (1992). "Modeling the oscillatory dynamic behaviour of electrorheological materials in shear." *Smart Materials and Structures*, 1:275-285.

El-Aouar, W. H. (2003). *Finite Element Analysis Based Modeling of Magneto Rheological Dampers*, M. C. Thesis, Virginia Polytechnic Institute and State University, Virginia.

Erbatur, F., Hasançebi, O., Tütüncü, I. and Kiliç, H. (2000). "Optimal design of Planar and Space Structures with Genetic Algorithms." *Computers & Structures*, 75:209-224.

Feng Q. and Shinozuka, M. (1990). "Use of a variable damper for hybrid control of bridge response under earthquake." *Proceedings U. S. Nat. Workshop on Struc. Control Res.* USC Publ., CE-9013.

Feng, Q., Shinozuka, M., and Fujii, S. (1993). "Friction-controllable sliding isolated systems." *Journal of Engineering Mechanics*, ASCE, 119:1845-1864.

Filiatrault, A., Trembaly, R. and Kar, R. (2000). ' Performance evaluation of friction spring seismic damper." *Journal of Structural Engineering.*, ASCE, 126:491-499.

Fleming, P. J. and Purshouse, R. C. (2002). "Evolutionary algorithms in control systems engineering: a survey." *Control Engineering Practice*, 10:1223-1241.

Fogel, D. B. (1995). *Evolutionary Computation: Toward a New Philosophy of Machine Intelligence*, IEEE Press, Piscataway, NJ.

Galante, M. (1996). "Genetic algorithms as an approach to optimize real-world trusses." *International Journal for Numerical Methods in Engineering*, 39:361-382.

Gamota, D. R. and Filisko, F. E. (1991). "Dynamic mechanical studies of

electrorheological materials: moderate frequencies." *Journal of Rheology*, 35(3): 399-425.

Gavin, H. P., Hanson, R. D. and Filisko, F. E. (1996). "Electrorhelogical dampers, part 1: analysis and design." *J. Applied Mech.,* ASME, 63:669-675.

Gavin, H. P., Hanson, R. D. and Filisko, F. E. (1996). "Electrorhelogical dampers, part 2: testing and modeling." *J. Applied Mech.,* ASME, 63:676-682.

Goldberg, D. E. (1989). *Genetic Algorithms In Search, Optimization, And Machine Learning*, Addison-Wesley Publishing Company, Inc.

Goldberg, D. E. and Deb, K. (1991). "A comparative analysis of selection schemes used in genetic algorithms." *Foundations of Genetic Algorithms*, San Mateo, CA, 69-93.

Goldberg, D. E. and Santami, M. P. (1986). "Engineering optimization via genetic algorithm." *Proceedings of the Ninth Conference on Electronic Computation, ASCE*, New York, 471-482

Hafka, R. T. and Grandhi, R. V. (1986) "Structural Shape Optimization -a survey." *Comp. Meth. in Mech. & Eng*, 57:91-106.

Haroum, M. A., Pires, J. A. and Won, A. (1994). "Active orifice control in hybrid liquid column dampers." *Proceedings 1st World Conference on Structural Control*, FA1:69-78.

Hasselman, T. K. (1972). "A method of constructing a full modal damping matrix from experimental measurements." *AIAA Journal*, 10:552-527.

Herverly II, D. E., Wang, K. W. ad Smith, E. C. (2001). "An optimal actuator placement methodology for active control for helicopter airframe vibrations." *Journal of the American Helicopter Society*, 251-256.

Herverly II, D. E., Wang, K. W. and Smith, E. C. (2002). "Optimal actuator placement and active structure design for control of helicopter airframe vibrations." *American Helicopter Society 58th Annual Forum, Montreal,* Canada, June, 11-13.

Heyman, J. (1956) "Design of beams and frames for minimum material consumption." *Quarterly of Applied Mathematics*, 8:373-381.

Holland, J. H., (1975). *Adaptation In Natural And Artificial Systems*, Ann Arbor, MI: The University of Michigan Press.

Housner, G. W., Bergman, L. A., Caughey, T. K., Chassiakos A. G., Claus, R. O., Masri, S. F., Skelton, R. E., Soon, T. T., Spencer Jr., B. F. and Yao, T. P. (1997). "Structural control: past, present and future" *Journal of Engineering Mechanics*, 123(9):897-971.

Inaudi, J. A. (1997). "Modulated homogeneous friction: a semi-active damping strategy." *Earthquake Engineering and Structures Dynamics*, 26:361-376.

Jansen, L. M. and Dyke, S. J. (2000). "Semi-active control strategies for MR dampers: comparative study." *Journal of Engineering Mechanics*, ASCE, 126(8):795-803.

Jimenez, R. and Alvarez, L. (2002). "Real time identification of structures with magnetorheological dampers." *Proceedings of the 41st IEEE*, Las Vegas Nevada, USA, 1017-1022.

Johnson, E. A., Baker, G. A., Spencer Jr., B. F. and Fujino, Y. (2002). "Semiactive damping of stay cables." *Journal of Engineering Mechanics*, ASCE, 1-4.

Jolly, M. R., Bender, J. W., and Carlson, J.D., (1999). "Properties and applications of commercial magnetorheological fluids." *Intelligent Material Systems and Structures,* 10(1), 5.

Kamath, G. M. and Wereley, N. M. (1996). "A nonlinear viscoelastic-plastic model for electrorheological fluids." *Smart Materials and Structures*, 6:351-359.

Keane, A. J. (1995). "Passive vibration control via unusual geometries: the application of genetic algorithm optimization to structural design." *Journal of Sound and Vibration,* 185 (3):441-453.

Keane, A. J. and Bright, A. P. (1996). "Passive vibration control via unusual geometries: experiments on model aerospace structures." *Journal of Sound and Vibration,*

190(4):713-719.

Kelly, S. G. (2000). *Fundamental of Mechanical Vibrations*, Mc Graw Hill.

Kida, Y., Kawamura, H., Tani, A. and Takizawa, A. (2000). "Multi-objective optimization of spatial truss structures by genetic algorithm." *Department of Architecture and Civil Engineering, Kobe University*, Japan. 15:133-139.

Kirsh, U. (1989) "Optimal topologies of structures." *Applied Mechanics Reviews*, 42(8):223-238.

Kwon, W. and Bang, H. (1996). *The Finite Element Method using Matlab*, CRC Press, New York.

Lammering, R. Jia, J. and Rogers, C. A. (1994). "Optimal placement of piezoelectric actuators in adaptive truss structures." *Journal of Sound and Vibration*, 171:67-85.

Lee, D. Y., and Wereley, N. M. (2000). "Analysis of electro- and magneto-rheological flow mode dampers using Herschel-Bulkley model." *Proceedings SPIE Smart Structure and Materials Conference*, Newport Beach, California, 3989:244-252.

Levy. R., Marianchik, E., Rutenberg, A. and Segal, F. (2000). "Seismic design methodology for friction damped braced frames." *Earthquake Engineering and Structural Dynamics,* 29:1405-1421.

Liu, X., Begg, D. W., and Matravers, D. R. (1997). "Optimal topology/actuator placement design of structures using SA." *Journal of Aerospace Engineering*, 11:119-125.

Lord Material Division (1999). "Designing with mr fluids." *Lord Corporation Tomas Lord Research Center, Cary, N. C.*

Lord Materials Division. (2003). "Rheonetic RD-1005-3 MR damper, Product bulletin." *Lord Corporation.*, http://www.rheonetic.com/pdf/RD_1005_3_ 2003_19_1.pdf .

Lou, J. Y. K., Lutes, L. D. and Li, J. J. (1994). "Active tuned liquid damper for structural control." *Proceedings 1st World Conference on Structural Control*, TP1:70-79.

Makris, N. Burton, S. A., Hill, D. and Jordan, M. (1996). " Analysis and design of ER damper for seismic protection of structures." *Journal of Engineering Mechanics*, 122:1003-1011.

Miyazaki, M. and Mitsusaka, Y. (1992). "Design of a building with 20% or greater damping." *Proceedings 10th World Conference on Earthquake Engineering*, Madrid, 4143-4148.

Morutsu, Y. and Shao, S. (1990). "Some approaches to the optimal adaptive geometries intelligent truss structures." *First Jointly US/Japan Conference on Adaptive Structures*, Hawaii US, Nov. 13-15, 743-771.

Murphey, T. W. and Hinkle, J. D. (2003). "Some performance trends in hierarchical truss structures." *American Instute of Aeronautics and Astronatics*, 1919:1-15.

Nagarajaiah, S., Sahasrabudhe S. and Iyer, R. (2000). "Seismic response of sliding isolated bridges with MR dampers." *Proceedings of the American Control Conference*, Chicago, Illinois, 4437-4441.

Nanakorn, P. and Meesomklin, K. (2001). "An adaptive Penalty function in genetic algorithms for structural design optimization." *Computers & Structures*, 79:2527-2539.

Newmark, N. M. (1959). "A method of computation for structural dynamics." *Proc. A.S.C.E.*, 8:67-94.

Onoda, J., Oh, H. U., Minesugi, K. (1998). "Semi-active vibration suppression of truss structures by electro-rheological fluid." *46th International Astronautical Congress*, Oslo, Norway, 40(11):771-779.

Onoda, J., Ung, H. O. and Minesugi, K. (1997). "Semi-active vibration suppression of truss structures by electro-rheological fluid." *46th International Astronautical Congress*, October 2-6, Oslo, 40(11):771-779.

Osyczka, A. (1985) "Multicriteria Optimization for Engineering Design." *In Gero JS Editor. Design optimization, New York, Academic Press*, 193-227.

Qu, W. L., Xu, Y. L. and Lv, M. Y. (2002). "Seismic response control of large-span machinery building on top of ship lift towers using ER/MR moment controllers." *Engineering Structures*, 24:517-527.

Pardalos, P.M. and Rosen, J. B (1987). *Constrained global optimization: algorithms and applications*, Berlin, New York, Springer-Verlag.

Patten W. N. (1999). "Field test of an intelligent stiffener for bridges at the I-35 Walnut Creek bridge." *Earthquake Engineering and Structures Dynamics*, 28:109-126.

Patten W. N. (1998). "The I-35 Walnut Creek Bridge: and intelligent highway bridge via semi-active structural control." *Proceedings 2nd World Conference on Structures Control*, 1:427-436.

Pilkey, D. F. (1998). *Computation of Damping Matrix for Finite Element Model Updating*, Ph. Thesis, Virginia Polytechnic Institute and State University, U.

Phillips, R. W. (1969). *Engineering Applications of Fluids with a Variable Yield Stress*, Ph. D. Thesis, University of California, Berkeley, California.

Prendes-Belen, M. B., Bello-Garcia, A. and Coz-Garcia, J. J. (2005) "A modified elitist genetic algorithm applied to the design optimization of complex steel structures." *Journal of Constructional Steel Research*, 61:265-280.

Qu, W. L., Xu, Y. L. and Lv, M. Y. (2002). "Seismic response control of large-span machinery building on top of ship lift towers using ER/MR moment controllers." *Journal of Engineering Structures*, 24:517-527

Sedhagati, R., Suleman, A., Dost, S. and B. Tabarrok (2001a). "Optimum design of adaptive truss structures using the integrate force method." *CMES*, 2(2): 259-271.

Rabinow, I. (1948). "The magnetic fluid clutch." *AIEE Transactions*, 67:1308-1305.

Rao, S. S. (1999). *The Finite Element Method in Engineering,* Butterworth-Heinemann.

Rao, S. S., Pan, T. and Venkayya, V. P. (1991). "Optimal placement of actuators in actively controlled structures using genetic algorithms." *AIAA Journal*, 29:942-953.

Rajeev, S. and Krishnamoorthy, C. S. (1997) "Genetic Algorithms-Based Methodologies for Design Optimization of Trusses." *Journal of Structural Engineering*, 123(3):350-358.

Ramallo, J. C., Johnson, E. A. and Spencer Jr., B. F. (2002). "`Smart` base isolation systems." *Journal of Engineering Mechanics*, ASCE, 128(10):1088-1099.

Rozvany, G. I. N. (1989). *Structural design via Optimality Criteria*, Kluwer Academic Publishers.

Rutenbar, A. (1989). "Simulated annealing algorithms: an overview." *IEEE Circuits and Devices Magazine*, 19-26.

Sakai, C., Ohmori, H. and Sano, A. (2003). "Modeling of MR damper with hysteresis for adaptive Vibration Control." *Proceedings of the 42nd IEEE Conference on Decision and Control*, Maui, Hawaii, 3840-3845.

Sandgren, E. and Cameron, T. M. (2002). "Robust Design optimization of Structures through consideration of variation." *Computers & Structures*, 80:1605-1613.

Sarma, K. C. and Adeli, J. (2000). "Fuzzy genetic algorithm for optimization of steel structures." *Journal of Structural Engineering*, 126(5):596-604.

Sedaghati, R., Suleman, A., Dost, S. and Tabarrok, B. (2001b) "Optimum design of adaptive truss structures using the integrated force method." *CMES*, 2:259-271.

Sedaghati, R., Tabarrok, B., Suleman, A. and Dost, S. (2000). "Optimization of adaptive truss structures using the finite element force method based on complementary energy." *Transactions of the CSME*, 24:263-271.

Shames, I. H. and Cozzarelli, F. A. (1992). *Elastic and Inelastic Stress Analysis*, Prentice Hall, Englewood Cliffs, NJ.

Simmerman, D. D. (1993). "A darwinian approach to the actuator number and placement problem with non-negligible actuator mass." *Mechanical Systems and Signal Processing*, 7(4):363-374.

Smyth, A. W., Masri, S. F., Kosmatopuolos, W. B. and Chassiakos, A. G. (2002).

"Development of adaptive modeling techniques for nonlinear hysteretic systems." *International Journal of Non-Linear Mechanics*, 37(8):1435-1451.

Soh, C. K. and Yang, Y. (2000). "Genetic programming-based approach for structural optimization." *Journal in Computing in Civil Engineering*, 14(1):687-809.

Soon, T. T. and Constantinou, M. C. (1994). *Passive and Active Structural Vibration Control in Civil Engineering,* Springer-Verlag Wien, New York.

Soong, T. T. and Dargush, G. F. (1997). *Passive Energy Dissipation Systems in Structural Engineering*, John Wiley and Sons Inc, New York.

Soong, T. T. and Spencer Jr., B. F. (2002). "Supplemental energy dissipation: state-of – art and state-of-pratice." *Engineering Structures*, 24:243-259.

Spencer, Jr. B. F. (1986). *Reliability of Randomly Excited Hysteretic Structures*, Springer-Verlag, Berlin.

Spencer Jr., B. F. Sain, M. K. (1997). "Controlling buildings: A new frontier in feedback." *Control Systems*, IEEE, 7(6):19-35.

Spencer, Jr. B. F., Dyke, S. J., Sain, M. K. and Carlson J. D. (1997). "Phenomenological model for a magnetorheological damper." *Journal of Engineering Mechanics, American Society of Civil Engineers,* 123:230-252.

Spencer Jr., B. F., Johnson, E. A. and Ramallo, J. C. (2000). "'Smart'isolation for seismic control," *JSME International Journal: Special Isue on Frontier of Motion and Vibration Control*, Series C, 43(3):704-707.

Stanway, R. Sproston, J. L. and Stevens, N. G. (1985). "Non-linear identification of an electrorheological vibration damper." *IFAC Identification and System Parameter Estimation*, 195–200.

Stanway, R., Sproston, J. L. and Stivens, N. G. (1987). "Non–linear modeling of an electrorheological vibration damper." *J. Electrostatics*, 20:167-184.

Stelzer, G. J., Schulz M. J., Kim, J. and Allemang, R. J. (2003). "A magnetorheological semi-active isolator to reduce noise and vibration transmissibility in automobiles."

Journal of Intelligent Material Systems and Structures, 14:743-765.

Symans, M. D. and Constantinou, M. C. (1997). "Seismic testing of a building structure with semi-active fluid damper control system." *Earthquake Engineering and Structures Dynamic*, 26:757-777.

Symans, M. D., Constantinou, M. C., Taylor, D. P. and Garnjost, K. D. (1994). "Semi-active fluid viscous dampers for seismic response control." *Proceedings 1st World Conference on Structures and Control*, FA4:3-12.

Taylor, D. P. and Constantinou, M. P. (1996). "Fluid dampers for applications of seismic energy dissipation and seismic isolation." *Proceedings 11th World Conference on Earthquake Engineering,* Acapulco, Mexico.

Turner, M. J., Clough, R. W., Martin, H. C. and Topp, L. J. (1956). "Stiffness and deflexion analysis of computer structures." *Journal of Aeronautical Science*, 23:805-824.

Tzou, H. S. and Anderson, G. L. (1992). *Intelligent Structural Systems*, Kluwer Academic Publishers.

Uang,C-M., and Bertero, V. V. (1988). "Use of energy as a design criterion in earth-quake-resistant design." *Report No. UCB/EERC-88/18,* University of California, Berkeley.

Umesha, P. K., Venuraju, M. T., Hartmann, D. and Leimbach, K. R. (2005). "Optimal design of truss structures using parallel computing." *Struc. Multidisc. Optim*, 29:285-297.

Vanderplaats, G. N. (1984). *Numerical Optimization Techniques for Engineering Design*, McGraw-Hill, New York.

Venkaya, V. B. (1971). "Design of optimum structures." *Computers and Structure,* 1:265-309.

Vinogradov, O. and Pivovarov, I. 1986. "Vibrations of a system with non-linear hysteresis." *Journal of Sound and Vibration*, 111(1):145-152.

Visintin, A. (1991). *Differential models of hysteresis*, Springer-Verlag, 1991.

Wada, A. Huang, Y. H. and Iwata, M. (1999). "Passive damping technology for buildings in Japan." *Progress in Structures, Engineering and Materials*, 2:1-15.

Wang, X. and Gordaninejad, F.(2000). "Study of field-controllable, electro- and magneto-rheological dluid dampers in flow mode using Herschel-Bulkley theory." *Proceedings SPIE Smart Structure and Materials Conference*, Newport Beach, California, 3989:232-243.

Wang E. R., Ma X. Q., Rakheja S. and Su C. Y. 2003. "Modelling the hysteric characteristics of a magnetorheological fluid damper," *Proc. Instn. Mech. Engrs. Part. D.: J. Automobile Engineering*, 217(7):537-550(14).

Weaver W. Jr. and Johnston, P. R. (1987). *Structural Dynamics by Finite Elements*, Prentice Hall.

Weiss, K. D., Duclos, T. G., Carlson, I. D., Chrzan, M. I. and Margida A. I. (1993). "High strength magneto- and electro-rheological fluids." *Society of Automotive Engineers,* Paper no. 932451.

Wen, Y. K. (1976). "Method of random vibration of hysteretic systems." *Journal of Engineering Mechanics division, ASCE*, 102(EM2):249-263.

Wereley, N. M. and Pang, L. (1998). "Nondimensional analysis of semi-active electrorheological and magnetorheological dampers using approximate parallel plate models." *Smart Materials and Structures*, 7:732-743.

Wereley, N. M., Pang, L. and Kamath, G. M. (1998). "Idealized hysteresis modeling of electrorheological and magnetorheological dampers." *J. Intelligent Material Systems and Structures*, 9:642-649.

Wilson, E. L. (1962). "Dynamic response by Step-By-Step Matrix Analysis." *Proceedings of Symposium on the Use of Computers in Civil Engineering*, October 1-5, Lisbon, Portugal.

Wilson, E.L. (2002): *Three Dimensional Static and Dynamic Analysis of Structures, A*

Physical approach with Emphasis on Earthquake Engineering, Computers and Structures, Inc., Berkeley, California, USA

Winslow, W. M. (1949). "Induced fibrillation of suspensions." *Journal of Applied Physics*, 20:1137-1140.

Winslow, W. M. (1947). "Method and means for translating electrical impulses into mechanical force." *U. S. Patent* 2,417,850.

Xie, Y. M. and Steven, G. P. (1997). *Evolutionary structural optimization*, Springer-Verlag, London.

Xu, X. and Agrawal, S. K. (2000). "Linear time-varying dynamic systems optimization via higher-order method: a sub-domain approach." *Journal of Vibrations and Acoustics*, 122:31-35.

Xu, Y. L., Qu, W. L. and Ko, J. M. (2000). "Seismic response control of frame structures using magnetorheological/electrorheological dampers." *Earthquake Engineering and Structural Dynamics*, 29:557-575.

Xu, Z. D., Shen Y. P. and Guo Y Q. (2003). "Semi-active control fo structures incorparated with magnetorheological dampers using neural networks." *Smart Materials and Structures*, 12:80-87.

Yalla, S. K. and Kareem, A. (2001). "Modeling TLDs using impact characteristics: experiments and system identification." *Earthquake Engineering and Structures Dynamics*, submitted.

Yan, Y. J. and Yam, L. H. (2002a). "Optimal design of number and locations of actuators in active vibration control of a space truss." *Institute of Physics Publishing*, 11:496-503.

Yan, Y. J. and Yam, L. H. (2002b). "A synthetic analysis on design of optimum control for an optimized intelligent structure." *Journal of Sound and Vibration*, 249(4):775-784.

Yang, G. (2001). *Large-Scale Magnetorheological Fluid Damper for Vibration*

Mitigation: Modeling, Testing and Control, Ph. D. Dissertation, University of Notre Dame, Indiana.

Yang, G., Jung, H. J. and Spencer Jr., B. F. (2001a). "Dynamic model of full-scales MR dampers for civil engineering applications." *Proceedings US-Japan Workshop on Smart Structures for Improved Seismic Performance in Urban Region*, Seattle, WA.

Yang, G., Spencer Jr. B. F., Jung, J. H. and Carlson, D. (2004). "Dynamic modeling of large-scales magnetorheological damper systems for civil engineering applications." *Journal of Engineering Mechanic,* ASCE, 130(9):1107-1114.

Yang, G., Spencer Jr., B. F., Carlson, J. D. and Sain, M. K. (2001b). "Dynamic modeling and performance considerations on full-scale MR fluid dampers." *Proceedings* 8^{th} *International Conference on Structural Safety and reliability*, Newport Beach, CA.

Yang, G., Spencer Jr., B. F. Carlson, J. D., and Sain, M. K. (2002). "Large-scale MR fluid dampers: modeling, and dynamic performance considerations." *Engineering Structures*, 24(3):309-323.

Yang, Y. and Soh, C. K. (2002). "Automated optimum design of structures using genetic programming." *Computers and Structures*, 80:1537-1546.

Yao, G. Z., Yap, F. F., Chen, G., Li, W. H. and Yeo, S. H. (2002). "MR-damper and its application for semi-active control of vehicle suspension system." *Mechatronics,* 12:963-973.

Yi, F. and Dyke, S. J. (2000). "Structural control systems: performance assessment." *Proceedings of American Control Conference*, Chicago, IL.

Ying, Z. G., Ni, Y. Q. and Ko, J. M. (2005). "Semiactive optimal control of linearized systems with multi-degree of freedom." *Journal of Sound and Vibration*, 279:373-388.

Yoshida, O. and Dyke, S. J. (2003). "Response control in full scale irregular buildings using MR dampers." *ASCE Journal of Structural Engineering*, in review.

Yoshioka, H., Ramallo, J. C. and Spencer Jr., B. F. (2001). "`Smart` base isolation strategies employing magnetorheological dampers." *Journal of Engineering Mechanics*, ASCE,128(5):540-551.

Zaher, M. S. (2002). *An integrated vibration-based structural health monitoring system*, Ph. Thesis, Carleton University, Ottawa, Canada.

Zhang, J. and Roshke, P. N. (1999). "Active control of a tall structure excited by wind." *Journal of Wing and Industrial Aerodynamics*, 83:209-223.

Zhu, W. Q., Luo, M. and Dong, L. (2004). "Semi-active control fo wind excited building structures using MR/ER dampers." *Journal of Probabilistic Engineering Mechanics*, 19:279-285.